Sandia National Laboratories	Document type Team report	SAND2017-0031R
	Information RESTRICTED	Number of pages 13 Number of appendices

Document title

IRIS III Benchmark – Team report

Subtitle

IRIS III tests

Document objectives

To give further details on modeling than requested in the Excel sheets

To analyze the results and draw any conclusion with respect to the vibration modeling purpose

Contributors :	
1	Christopher Jones
2	Joshua Hogancamp
3	Gullermo Mata
4	Peter Coffin
5	

Calculation code or Software used (including version number) :	
Modal analysis	Sierra Salinas, 4.42.1
Impact analysis	Sierra Solid Mechanics, 4.42.1

Team Name : Sandia National Laboratories	IRIS III Benchmark – IRIS III tests

Sandia National Laboratories is a multi-mission laboratory managed and operated by Sandia Corporation, a wholly owned subsidiary of Lockheed Martin Corporation, for the U.S. Department of Energy's National Nuclear Security Administration under contract DE-AC04-94AL85000.

1. IRIS III modeling

1.1 Modal analysis

1.1.1 Finite element mesh

The finite element mesh for use in the IRIS 3 Modal Calculations was identical to the mesh used for impact calculations. The description presented here is duplicated below for the impact calculation description.

The Modal Analysis mesh contained 772,704 nodes and 718,953 elements. The concrete in the mock-up was modeled using a coarse finite element mesh, and the impact face and corners of the concrete where slabs met were refined by a factor of 27.

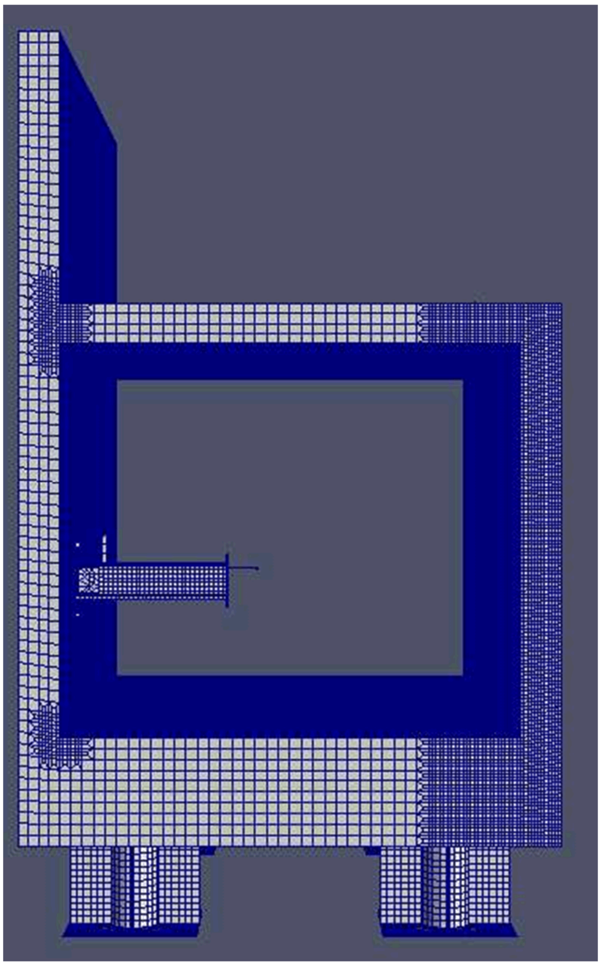

Figure 1: IRIS 3 Mockup Mesh

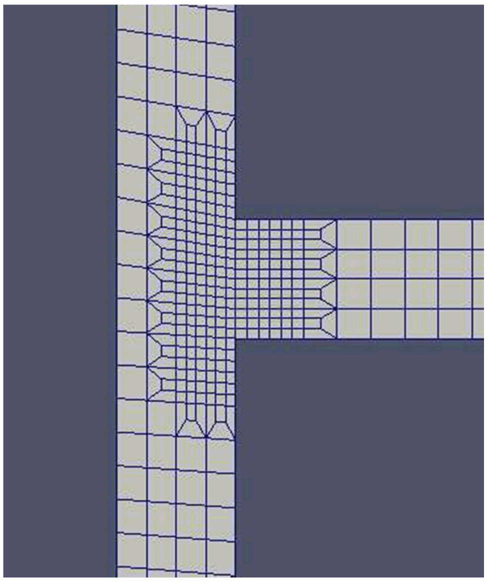

Figure 2: Localized Refinement at intersections

The rebar inside the concrete was modeled as a 6 degree of freedom beam elements with a cylindrical cross-section; the rebar elements were embedded into the concrete, and explicit contact was turned off for the rebar elements to avoid simulation instability.

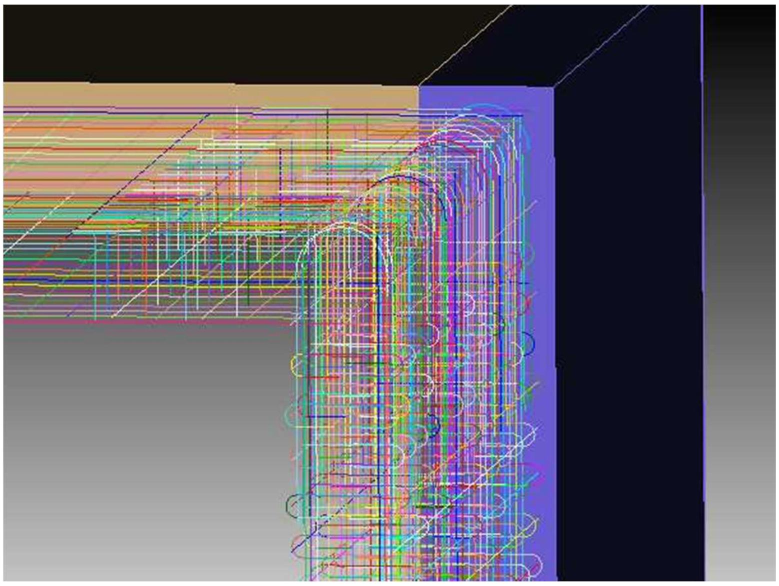

Figure 3: Embedded Rebar Modeled with Beam Elements

All rebar in the structure was initially meshed at approximately 30 mm per element, and the rebar in the impact face was refined by a factor of 2 (15 mm per element).

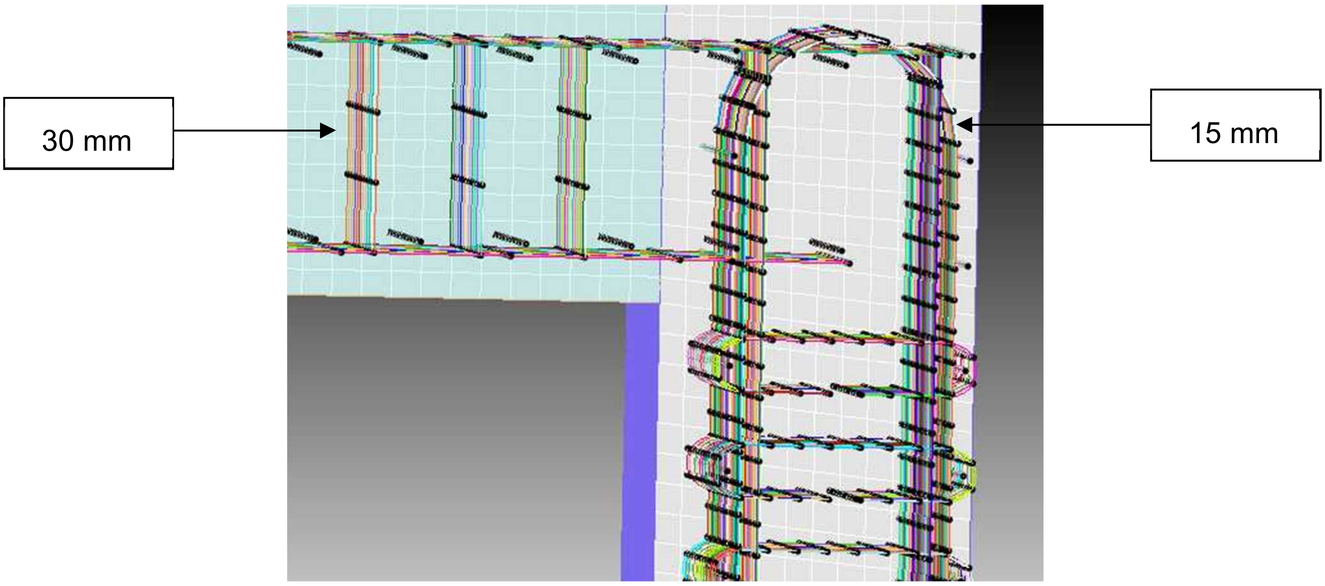

Figure 4: Refined Rebar on the Impact Face

The supports and the anchor plates were removed for the modal analysis and the base of the concrete mockup where the support pedestals would have attached, were fixed in space.

1.1.2 Material modeling and parameters

For the constitutive modeling in the modal analyses, only the linear elastic material behavior was considered. Each material in the mockup had a separate constitutive relationship, as show in Table 1.

Table 1: Materials for modal analyses

Material Name	Material Model	Material Application	Young's Modulus (GPa)	Poission's Ratio	Density (kg/m^3)
S355 Steel	Elastic	Supports (pipe and webbing)	200	0.333	7850
500B Steel 1		6mm diameter rebar			
500B Steel 2		8mm and 10mm diameter rebar			
Generic steel*		Anchor rods, I-beams, I-beam supporting plates (connect the I-beams to the concrete)			
Concrete		Concrete	29.67	0.222	2255

*This steel was given properties similar to S355 steel but without multiple stages in the elastic regime.

1.1.3 Boundary conditions modeling

Unlike the impact simulations presented below, the support pipes were not modeled for the modal analysis, nor was the supporting foundation. The concrete mockup was fixed in space at the locations where the support pipes would connect.

1.1.4 Solver

The modal analysis was performed with the Sandia National Laboratories code, Sierra Salinas. Salinas is a general purpose structural dynamics code capable of massive parallelization and can operate in the time and frequency domains. Salinas utilizes the Trillinos Solver package which has a number of solvers including several for linear algebra and Eigen-analysis. For these simulations, the generalized Dryja, Smith, Widlund or GDSW solver was utilized.

1.2 Impact analysis

1.2.1 Missile modeling

1.2.1.1 Loading method and main assumptions

The missile was modeled explicitly using 2D finite element shell elements that were extruded to the appropriate thickness. The missile tube was modeled as a hollow cylinder of steel with a thickness of 1.89 mm. The tip of the missile that impacts the wall was modeled as a hollow steel hemisphere with a thickness of 3.00 mm. The rear end of the missile was modeled as a circle that extruded into the missile to whatever length was necessary to make the mass of the entire missile 50.1 kg. The missile steel was modeled using a multi-linear elastic plastic model that dictated the behavior of the missile steel at strains up to 165%, ensuring that the simulation remained stable during the extreme deformation of the missile. The missile was given an initial velocity (of either 90 m/s or 170 m/s) and allowed to impact the mock-up at the specified location; it should be noted that the impact location is above the plane that contains the pseudo-equipments. The missile for 90 m/s simulations was initially meshed with a relatively coarse mesh, and the nose and region of deformation was refined by a factor of 16. The missile for 90 m/s had a total length of 2125 mm.

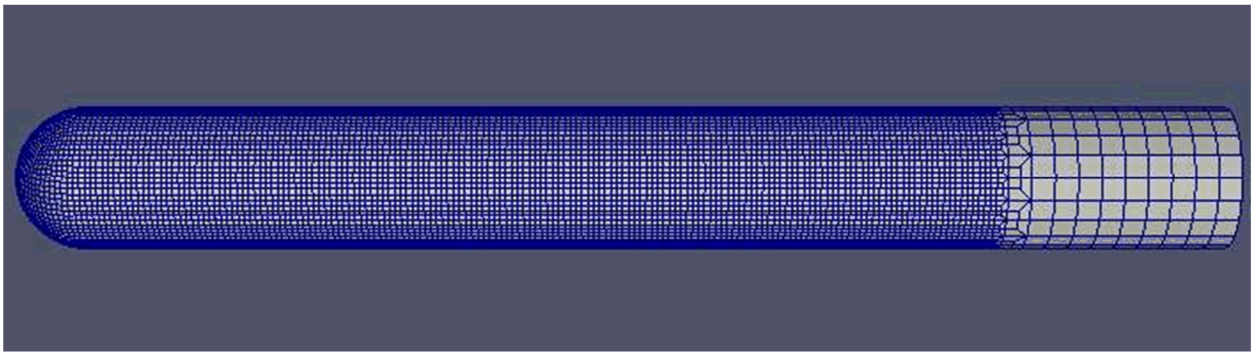

Figure 5: Meshed Geometry for the 90 m/s Impact

The missile for 170 m/s simulations was refined throughout the entire volume and given a total length of 2525 mm since it was expected to have a larger crush length. The plug in the rear of the missile had a different length for each missile so that the total mass for each missile was 50.1 kg.

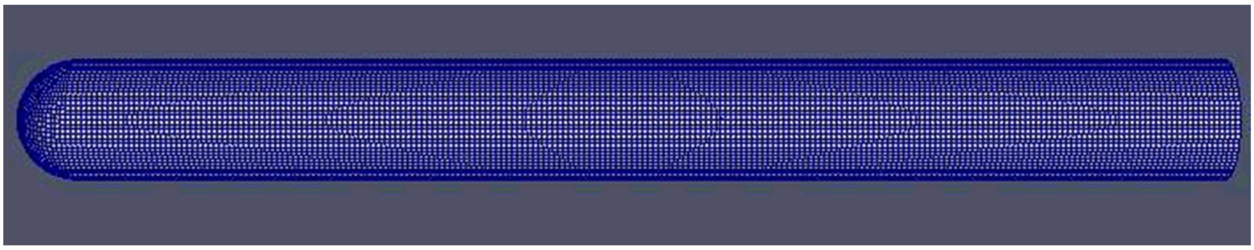

Figure 6: Meshed Geometry for the 170 m/s Impact

1.2.1.2 Force-time history on a rigid plane target

Both missiles (90 m/s and 170 m/s) were simulated to impact a rigid plane target, and the forces on the plane target were summed to obtain the force-time history.

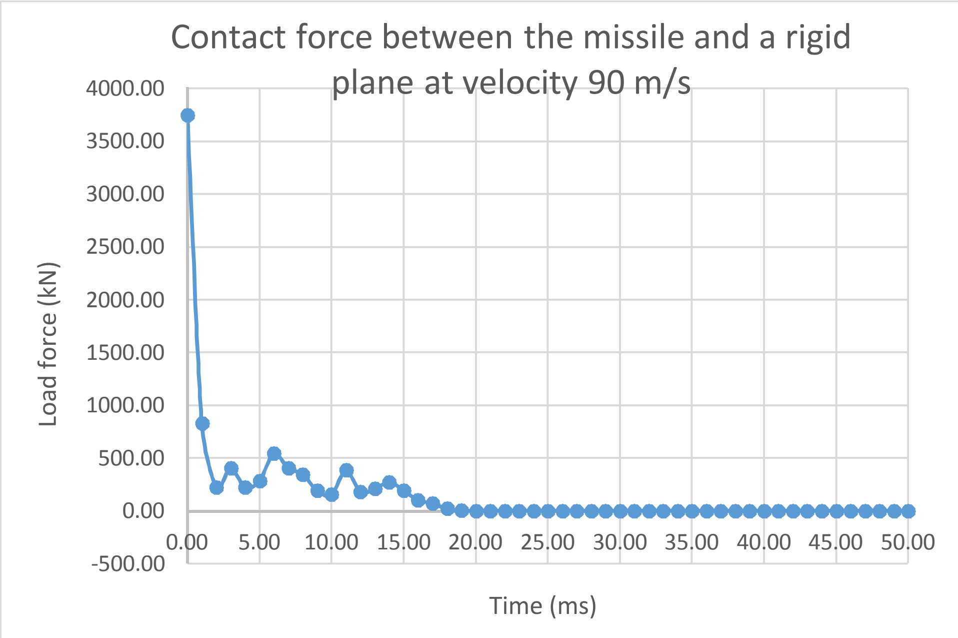

Figure 7: Contact Force versus Time for the 90 m/s Impact

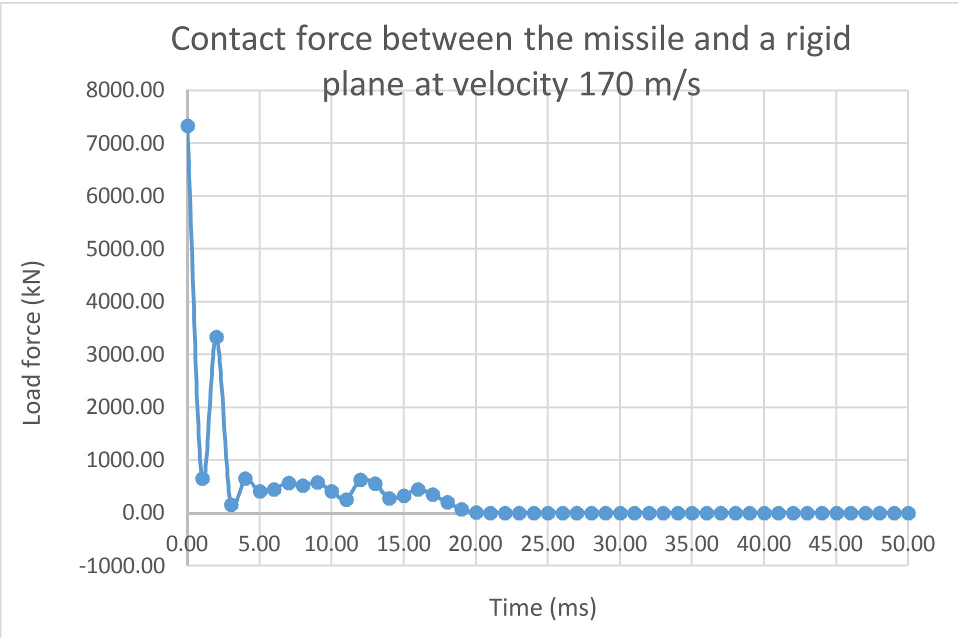

Figure 8: Contact Force versus Time for the 170 m/s Impact

1.2.2 Mock-up modeling

1.2.2.1 Finite element mesh

The simulation with the 90 m/s missile contained 772,704 nodes and 718,953 elements. The simulation with the 170 m/s missile contained 778,584 nodes and 724,833 elements owing to the refined missile meshing scheme mentioned above. The concrete in the mock-up was modeled using a coarse finite element mesh, and the impact face and corners of the concrete where slabs met were refined by a factor of 27.

The rebar inside the concrete was modeled as a 6 degree of freedom beam elements with a cylindrical cross-section; the rebar elements were embedded into the concrete, and explicit contact was turned off for the rebar elements to avoid simulation instability.

All rebar in the structure was initially meshed at approximately 30 mm per element, and the rebar in the impact face was refined by a factor of 2 (15 mm per element).

The supports and the anchor plates were modeled as 2D shells that were extruded to their proper thicknesses. The anchor rods that connected the supports to the concrete were modeled as beam elements that were embedded into the concrete and fixed to the anchor plates.

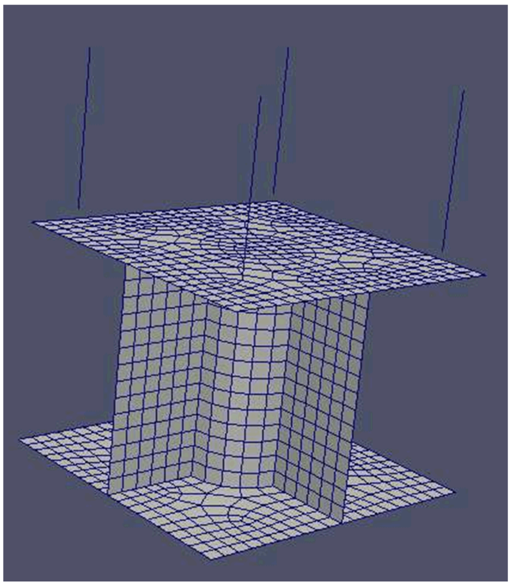

Figure 9: Support Pedestals Used for the Impact Simulations

Element death was applied only when the Jacobian of the elements passed below 0.05. The ensured that elements that were severely distorted were removed from the simulation before causing convergence difficulties. Typically, elements with a Jacobian that passed below 0.05 were already severely damaged and were not contributing to overall structural integrity, so deleting these elements had no significant negative effects on the simulation.

1.2.2.2 Material modeling

The materials used in the simulations in this project are listed in Table 2. The steel model properties were selected to best match the given steel information. The missile steel (EN1.4404) was assumed to be identical to 316L stainless steel and nominal 316L properties were utilized. The concrete data was constructed by fitting the provided data from the IRIS-2 project and altering the behavior for the different f'_c failure strength for IRIS-3. This modification was based on analyst judgement and should be considered a significant source of uncertainty for the pre-test predictions.

Table 2: Material Models

Material Name	Material Model	Material Application
S355 Steel	Multilinear elastic plastic	Supports (pipe and webbing)
500B Steel 1	Elastic plastic	6mm diameter rebar
500B Steel 2	Elastic plastic	8mm and 10mm diameter rebar
316L Stainless Steel	Multilinear elastic plastic	Missile
Generic steel*	Elastic plastic	Anchor rods, I-beams, I-beam supporting plates (connect the I-beams to the concrete)
Concrete	Holmquist Johnson Cook concrete	Concrete
*This steel was given properties similar to S355 steel but without multiple stages in the elastic regime.		

1.2.2.3 Boundary conditions modeling

The nodes of the structure that are in contact with the 'ground' were considered fixed in all directions.

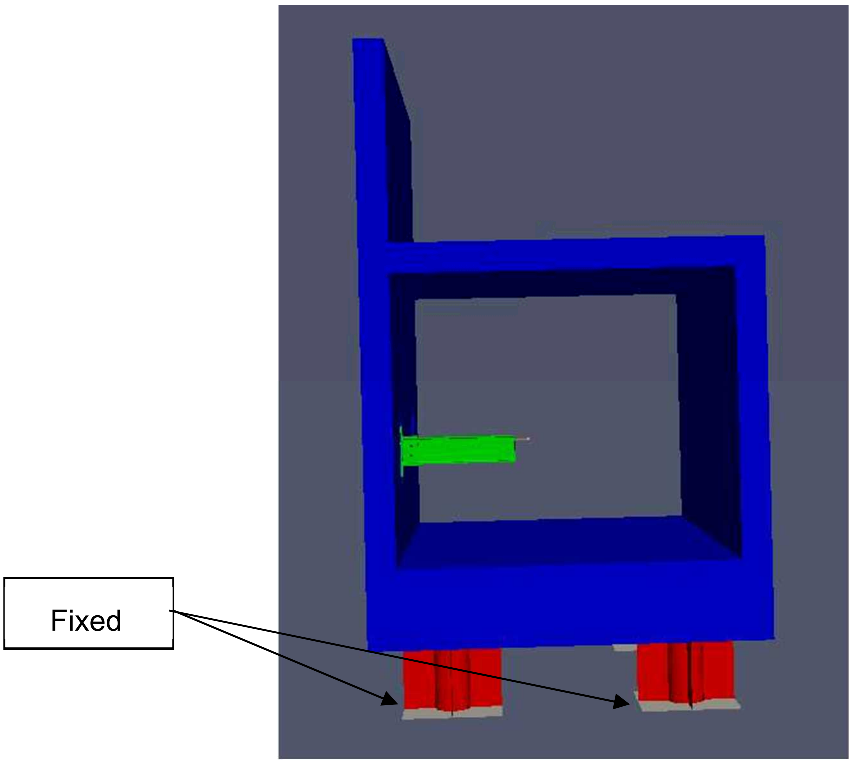

Figure 10: Schematic Illustrating the Boundary Conditions Used for the Impact Simulations

1.2.2.4 Damping

No damping was included in the model.

1.2.2.5 Pseudo-Equipments modeling

The two I-beam connections (bolted vs. welded) were modeled differently in these simulations. The welded connection I-beam was modeled as a set of beam elements that with a cross-section representative of an IPE140 section and was 700 mm long (600 mm for the beam and another 100 mm to reach the middle of the pseudo-equipment). The end of the beam elements connected to the anchor plate was fixed in all directions and against all rotations, simulating a perfectly rigid connection. The pseudo-equipment attached to the welded connection I-beam was modeled as a single spherical point mass of 61 kg at the end of the beam. The bolted connection I-beam and the angle steel connecting the I-beam to the anchor plate was 600 mm long and was explicitly modeled using 3D finite elements. The angle steel, anchor plate, and I-beam had explicit bolt holes, but no bolts were used. The bolt holes were rigidly fixed together at the contact point which was believed to be a conservative estimate based on separate simulations. The following bolt-hole trial simulations were conducted and are listed in order of most to least conservative:

- Completely rigid connection of I-beam end surfaces to anchor plate
- Completely rigid connection of 1) I-beam bolt holes to angle steel bolt holes, and 2) angle steel bolt holes to anchor plate bolt holes
- Bolted connection with axial prestressing on bolt
- Bolted connection with no prestressing on bolt

The pseudo-equipment on the I-beam with the bolted connection was modeled as a circle extruded to a cylinder rigidly attached to the free end of the I-beam; the cylinder had the same dimensions and mass as shown in the drawings.

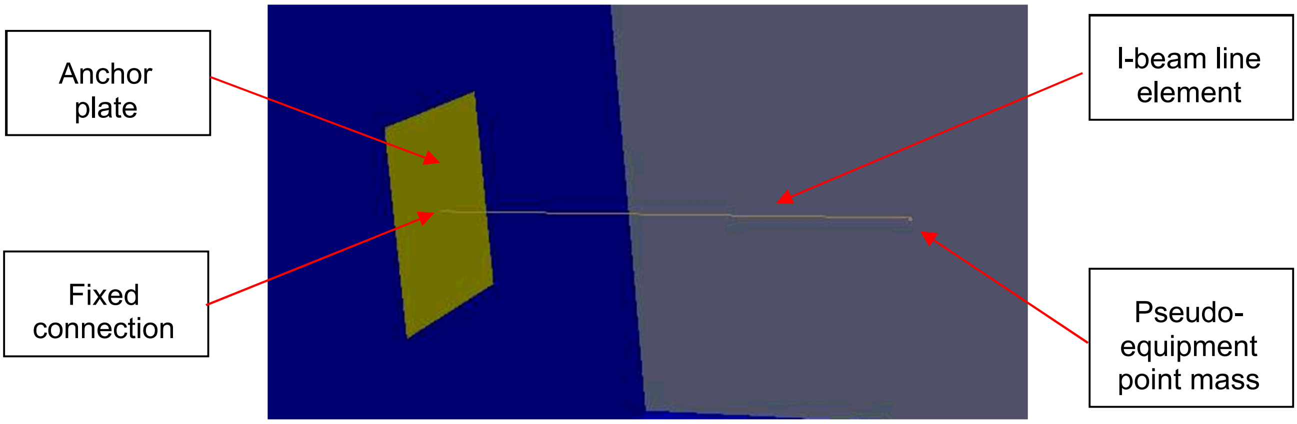

Figure 11: Representation of the "Welded" Beam

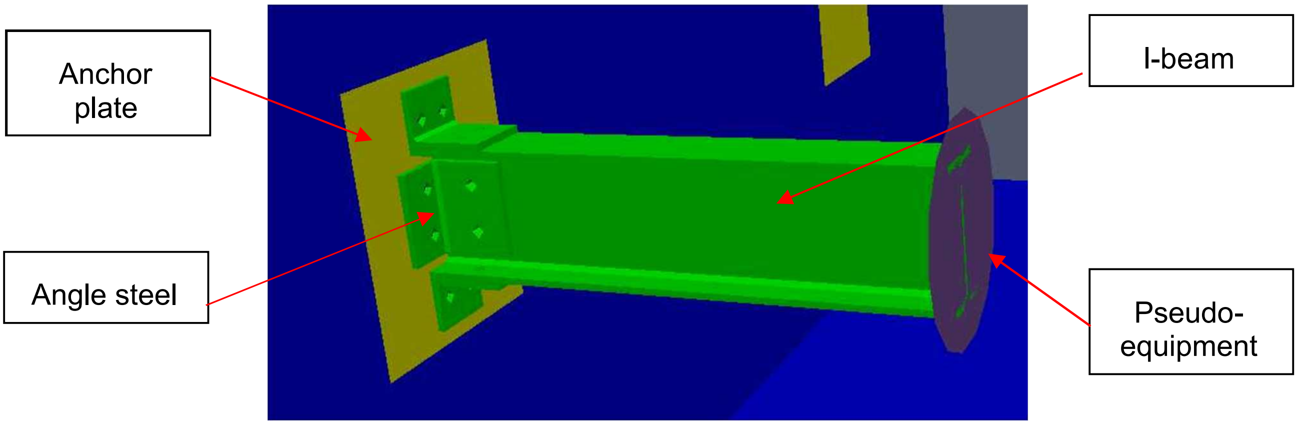

Figure 12: Representation of the "Bolted" Beam

1.2.3 Computation

1.2.3.1 Solver

Sierra solid mechanics utilizes the Trillinos solver package, both developed and maintained at Sandia National Laboratories. For the impact simulations, an explicit time integration scheme was utilized and therefore no "solver" was utilized.

1.2.3.2 Calculation step(s) and duration

A summarized section of output from the Sierra SM log file is reproduced below.

Table 3: Sample output from the Sierra SM impact calculations

STEP	SIMULATION TIME	TIME STEP	CRITICAL TIME STEP ELEMENT ID	KE	IE	EE	ERROR %	HE	CPU TIME	REAL TIME
0	0.00E+00	5.56E-07	718145	2.08E+11	-1.75E-13	2.08E+11	-5.88E-14	0.00E+00	7.55E+00	7.01E-01
100	5.56E-05	5.56E-07	718145	2.08E+11	-1.63E-10	2.08E+11	-5.88E-14	2.68E-11	2.00E+01	1.32E+01
200	1.11E-04	5.56E-07	718145	2.08E+11	-2.48E-10	2.08E+11	-5.88E-14	3.81E-11	3.24E+01	2.56E+01
300	1.67E-04	5.56E-07	718145	2.08E+11	-3.08E-10	2.08E+11	-5.88E-14	4.58E-11	4.48E+01	3.80E+01
400	2.22E-04	5.56E-07	718144	2.08E+11	1.44E+07	2.08E+11	2.54E-03	1.78E+06	5.71E+01	5.03E+01
500	2.78E-04	5.56E-07	718144	2.07E+11	3.25E+08	2.07E+11	2.88E-02	9.22E+06	9.08E+01	8.79E+01
600	3.33E-04	5.56E-07	718144	2.07E+11	8.20E+08	2.07E+11	4.05E-02	9.72E+06	1.04E+02	1.01E+02
700	3.89E-04	5.56E-07	718145	2.06E+11	1.52E+09	2.07E+11	5.07E-02	1.07E+07	1.16E+02	1.14E+02
800	4.45E-04	5.56E-07	718145	2.05E+11	2.44E+09	2.07E+11	6.09E-02	1.15E+07	1.29E+02	1.27E+02
900	5.00E-04	5.56E-07	718144	2.04E+11	3.55E+09	2.07E+11	6.83E-02	1.49E+07	1.42E+02	1.39E+02
1000	5.56E-04	5.56E-07	718145	2.02E+11	4.85E+09	2.07E+11	7.50E-02	1.50E+07	1.55E+02	1.52E+02

1.2.3.3 Time step, CPU time, CPU configuration

The simulation with the 90 m/s missile had a critical time step of 6.175e-07 seconds and ran for 47.5 hours on 96 processors. The simulation with the 170 m/s missile had a time step of 5.027e-07 seconds and ran for 96.0 hours on 96 processors. In both cases, the actual calculation time step is derived from the critical time step multiplied by 0.9 to improve stability (e.g. 6.175e-07 x 0.9 = 5.56e-07).

1.2.3.4 Post-processing

The output frequency of the simulations was 1.0e-4 seconds (or 0.1 ms). The basic units of the simulation were mm-seconds, so post-processing was required to change the units to meters. All visual post processing was performed with Paraview.

2. IRIS III results: modal analysis

The modal analysis results obtained from Sierra – Salinas are shown below in Figure 13 through Figure 32. For all the figures presented the visualization scaling factor was selected for each result since the calculated displacement magnitude varied widely between modes. Also note that the calculated modes were not screened in any way for mass, so the first 20 modes are presented to include modes with more mass associated.

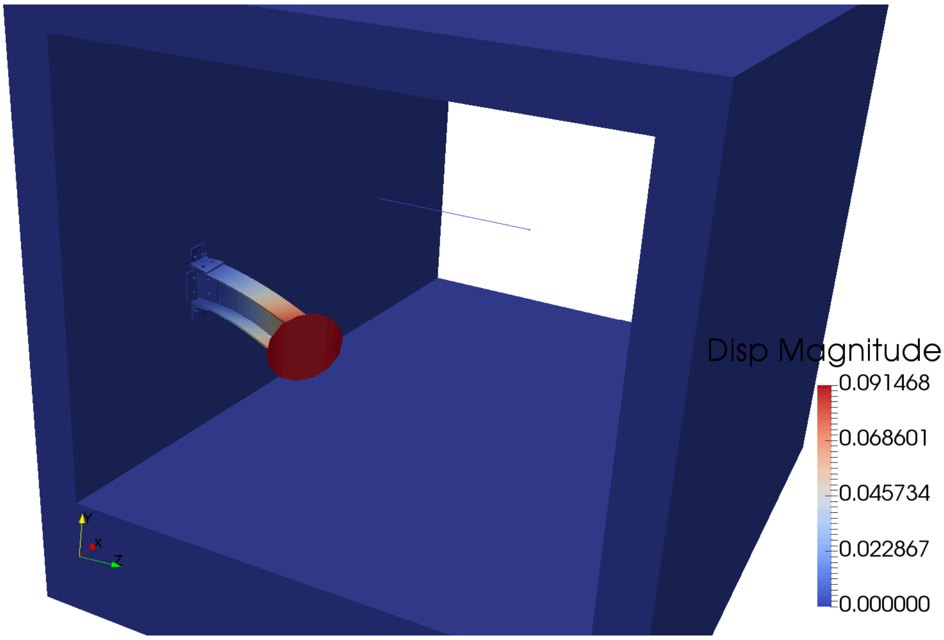

Figure 13: Mode 1 (11.09 Hz)

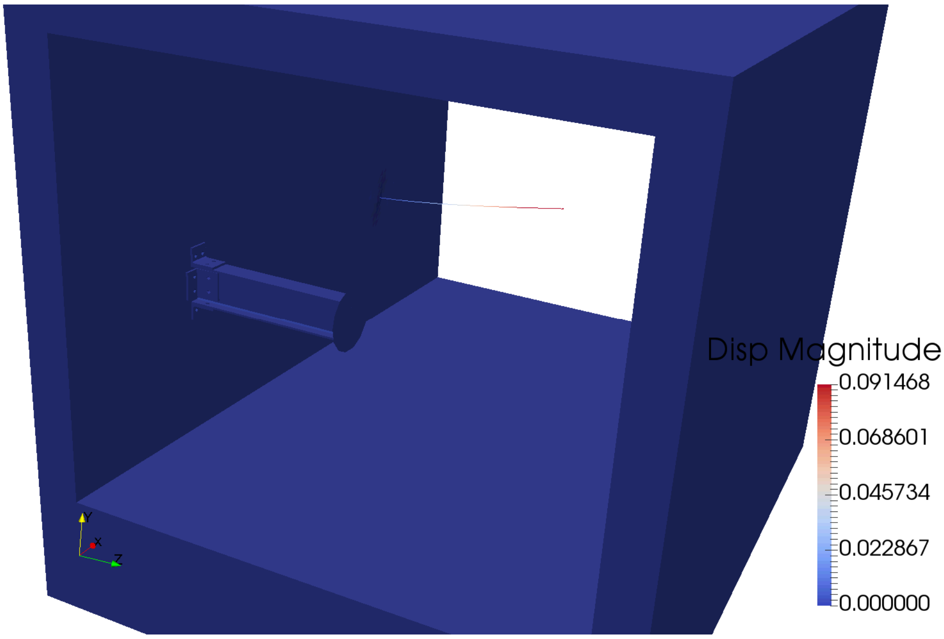

Figure 14: Mode 2 (13.48 Hz)

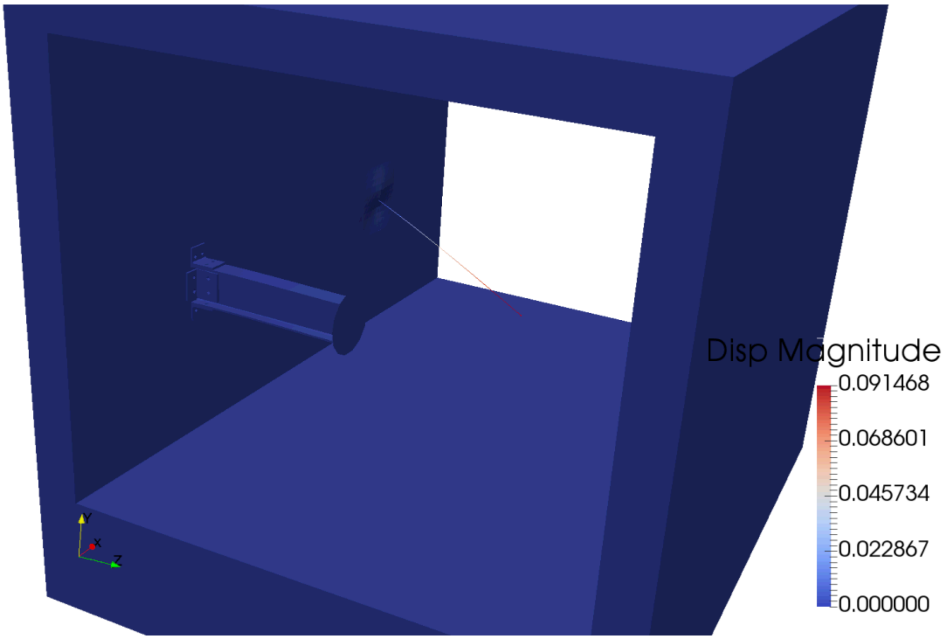

Figure 15: Mode 3 (20.96 Hz)

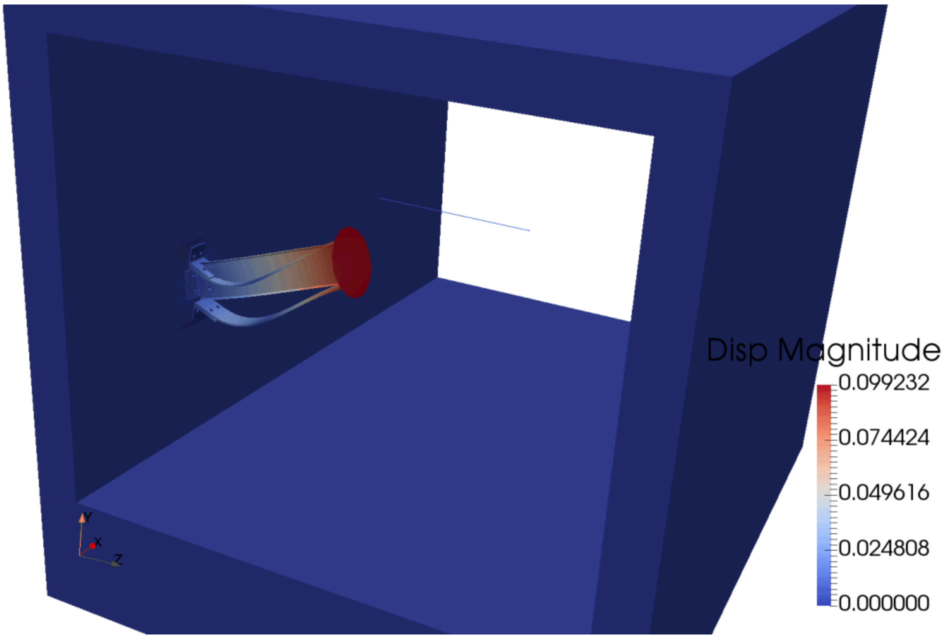

Figure 16: Mode 4 (22.34 Hz)

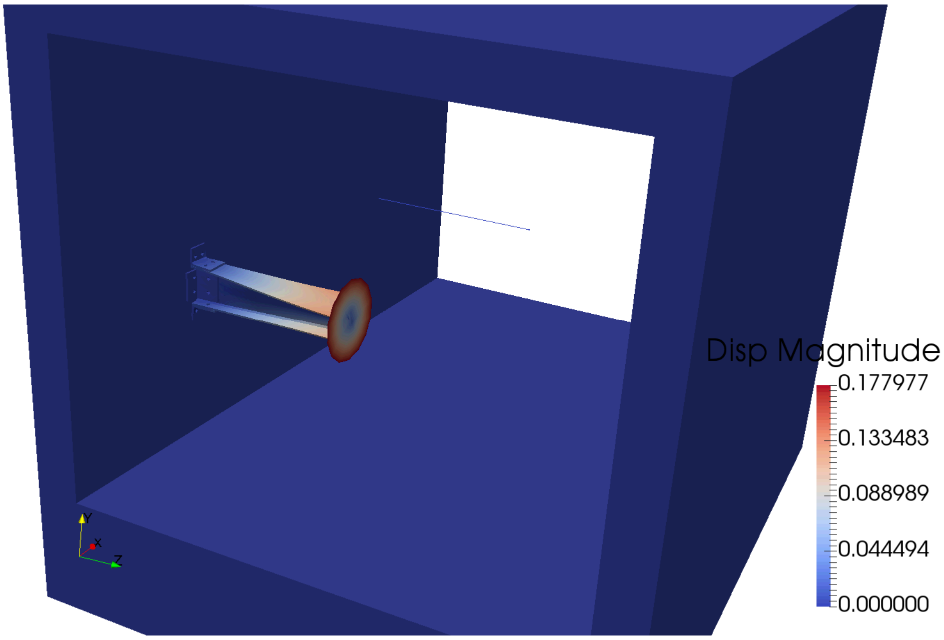

Figure 17: Mode 5 (31.77 Hz)

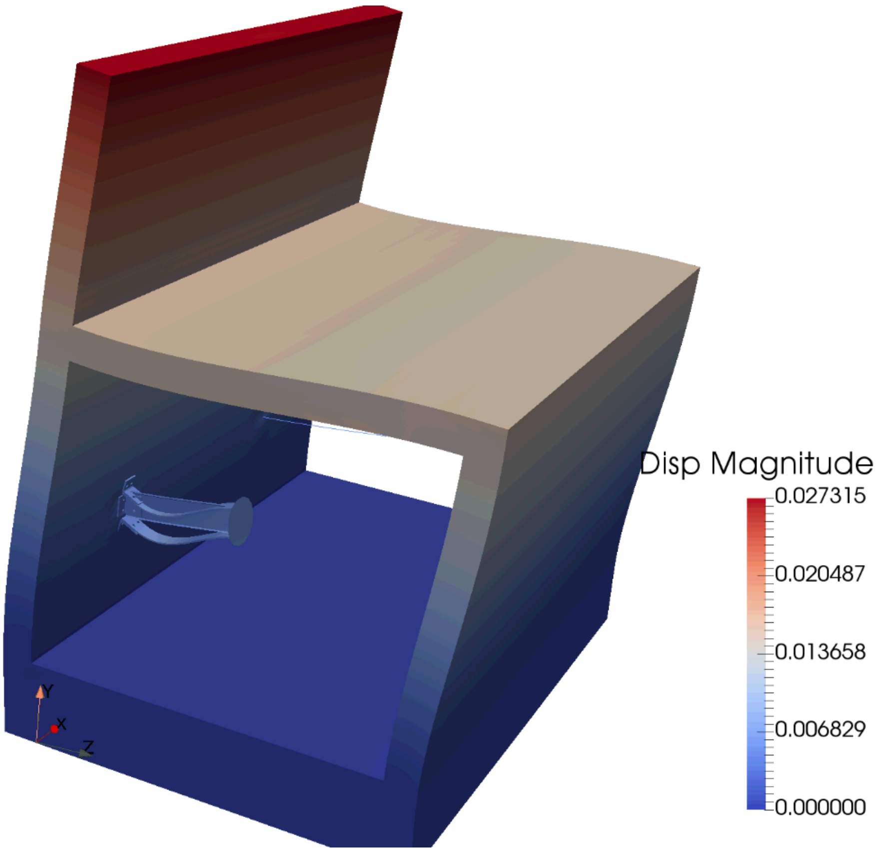

Figure 18: Mode 6 (37.52 Hz)

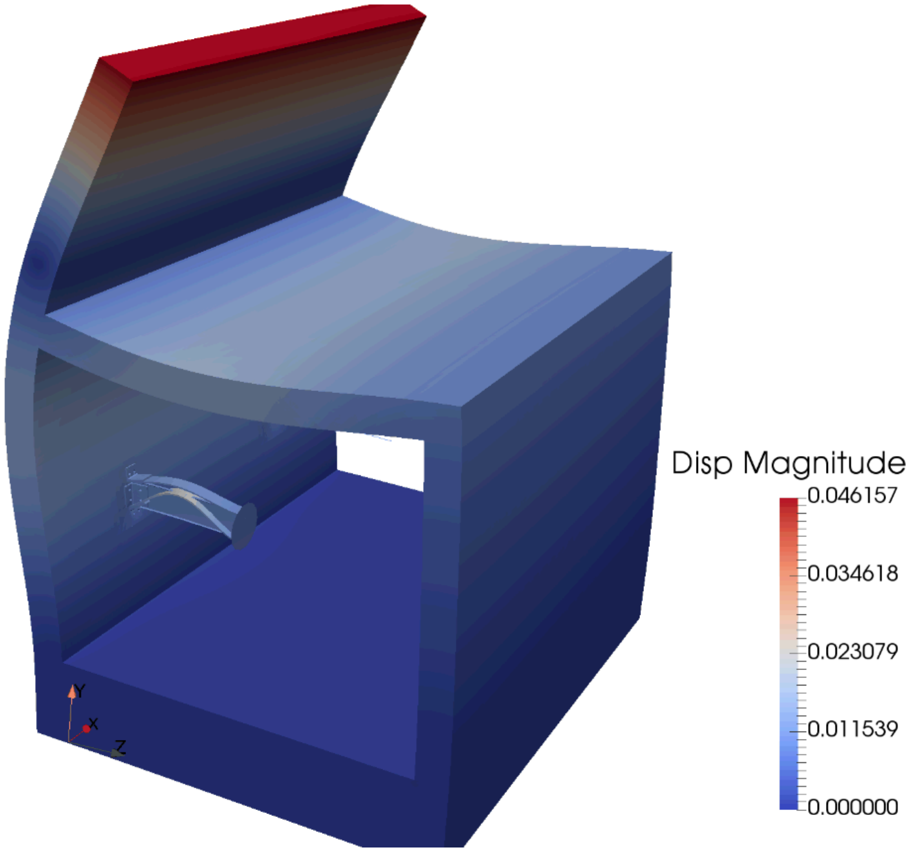

Figure 19: Mode 7 (82.06 Hz)

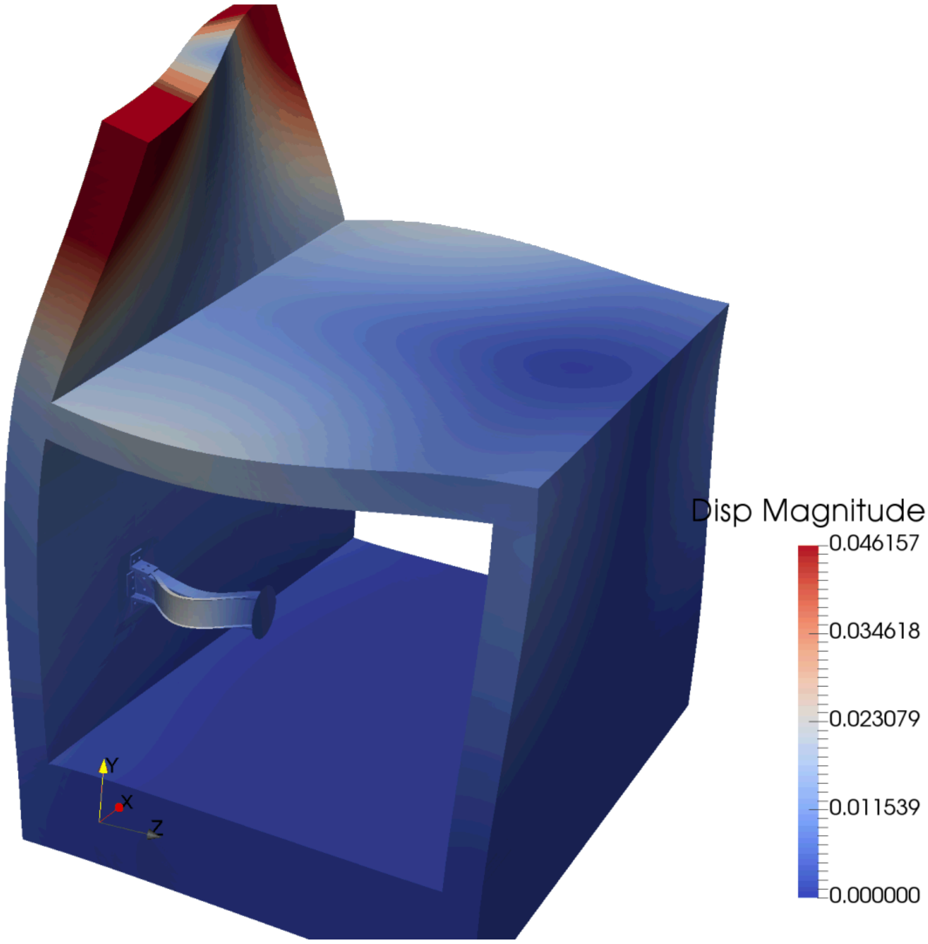

Figure 20: Mode 8 (82.06 Hz)

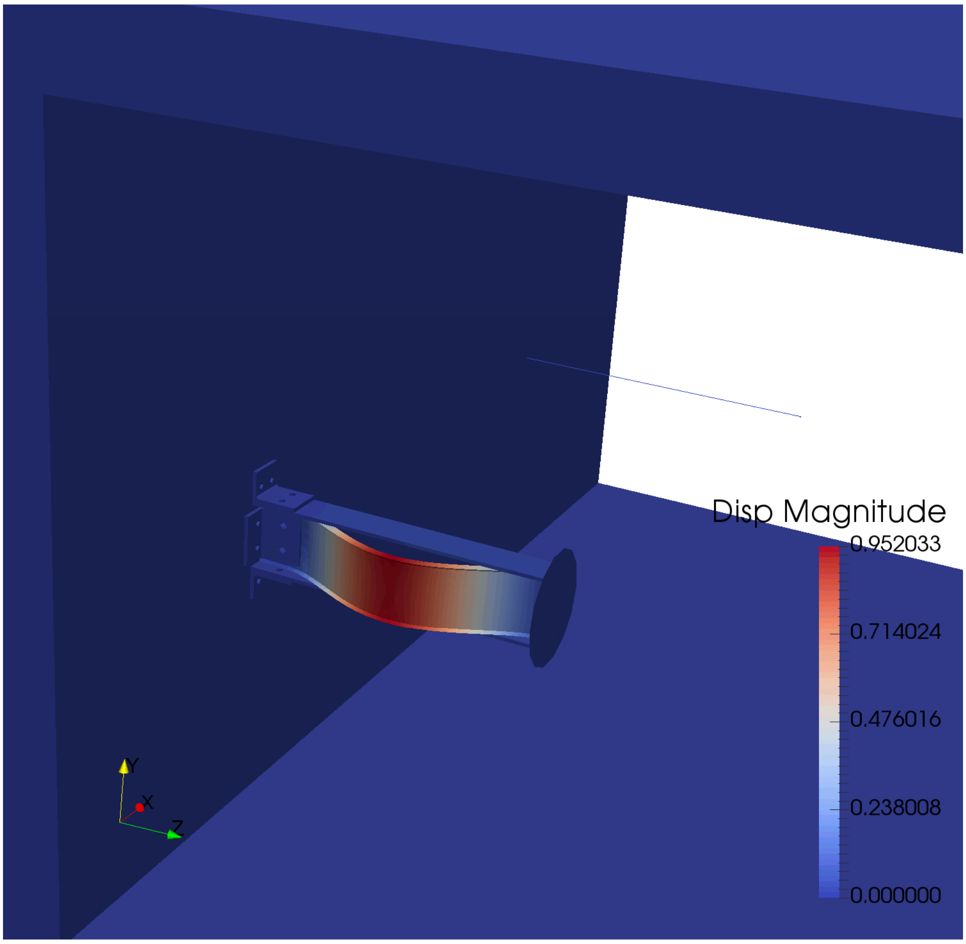

Figure 21: Mode 9 (104.24 Hz)

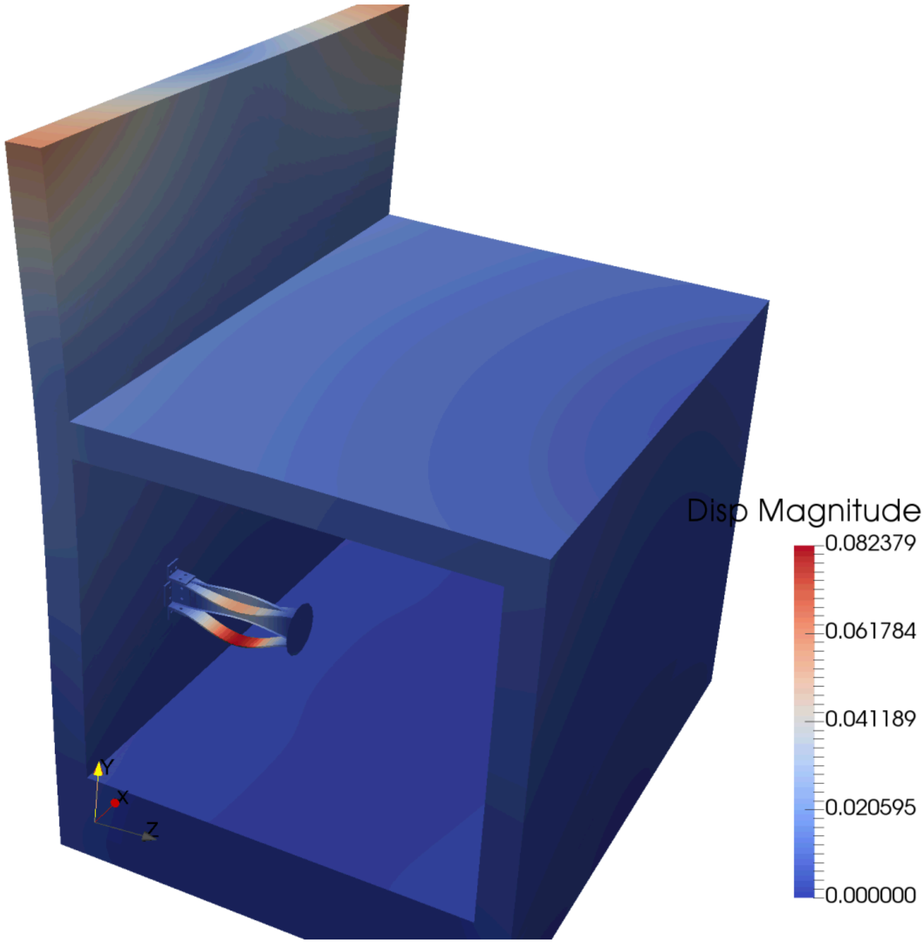

Figure 22: Mode 10 (112.27 Hz)

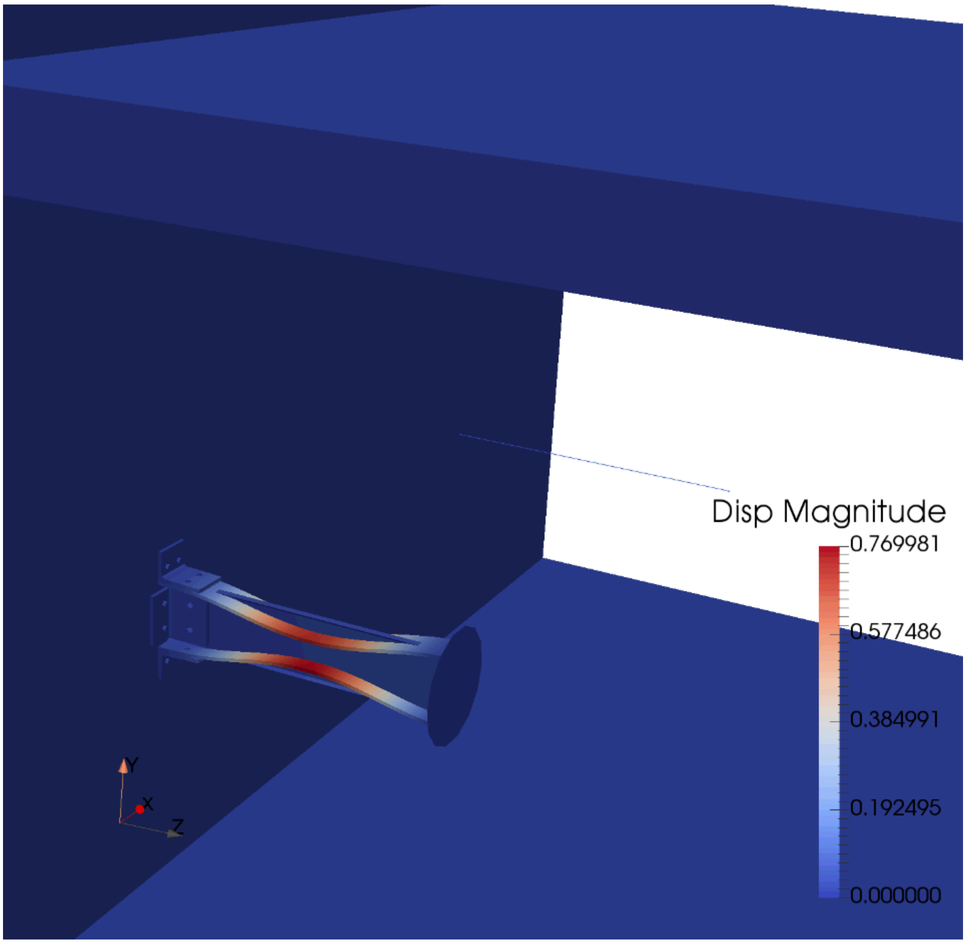

Figure 23: Mode 11 (116.33 Hz)

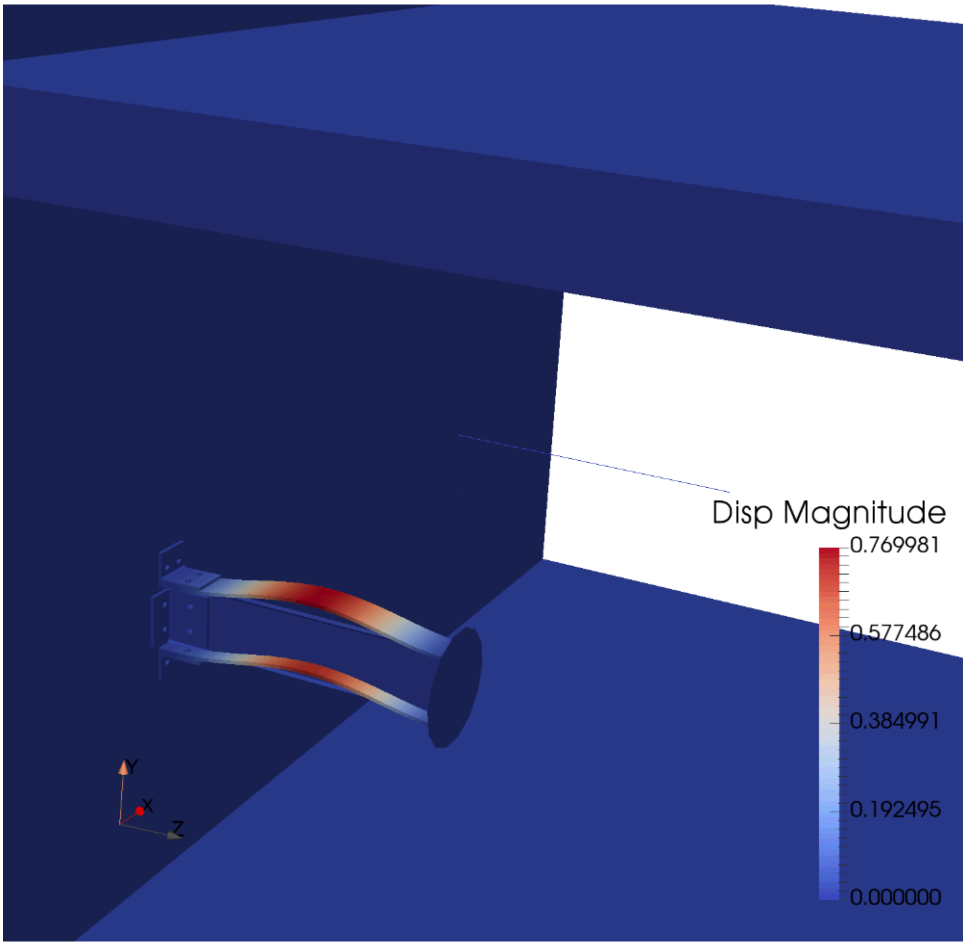

Figure 24: Mode 12 (115.89 Hz)

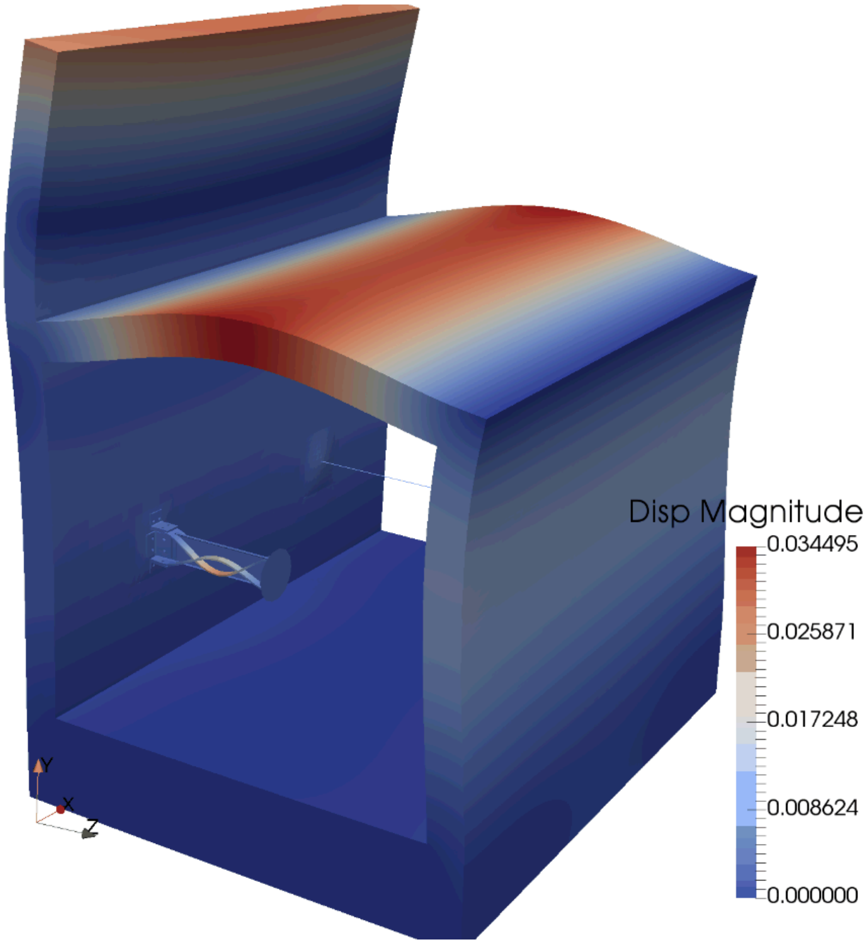

Figure 25: Mode 13 (128.06 Hz)

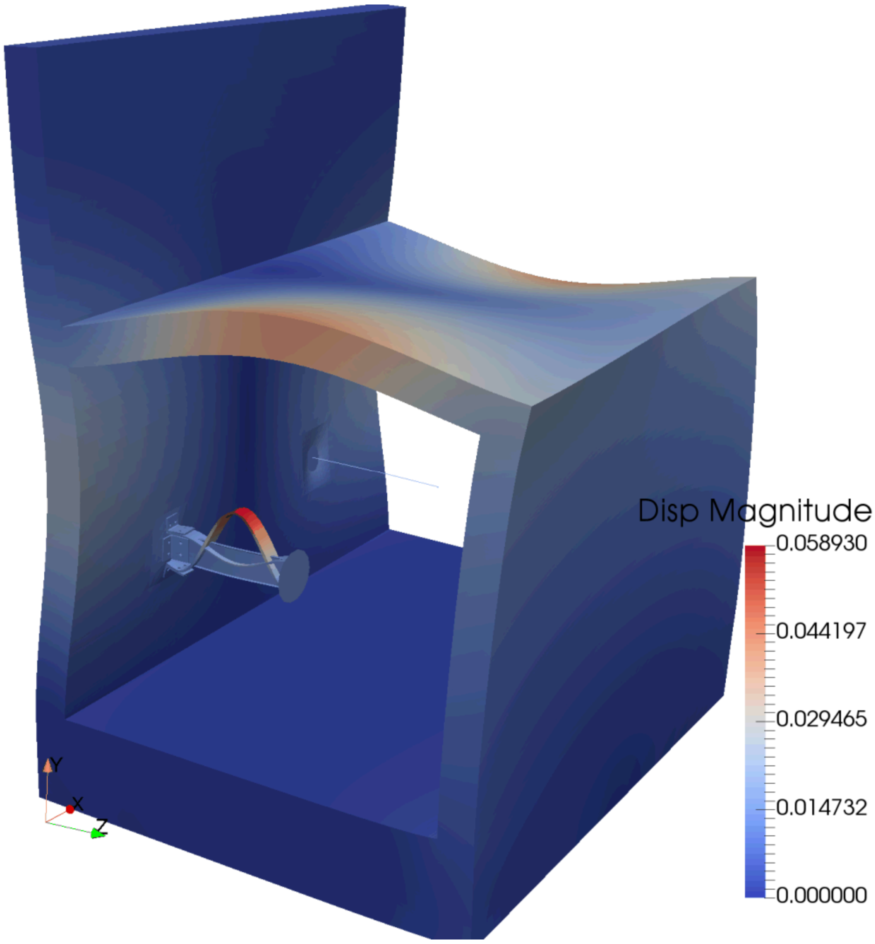

Figure 26: Mode 14 (133.0 Hz)

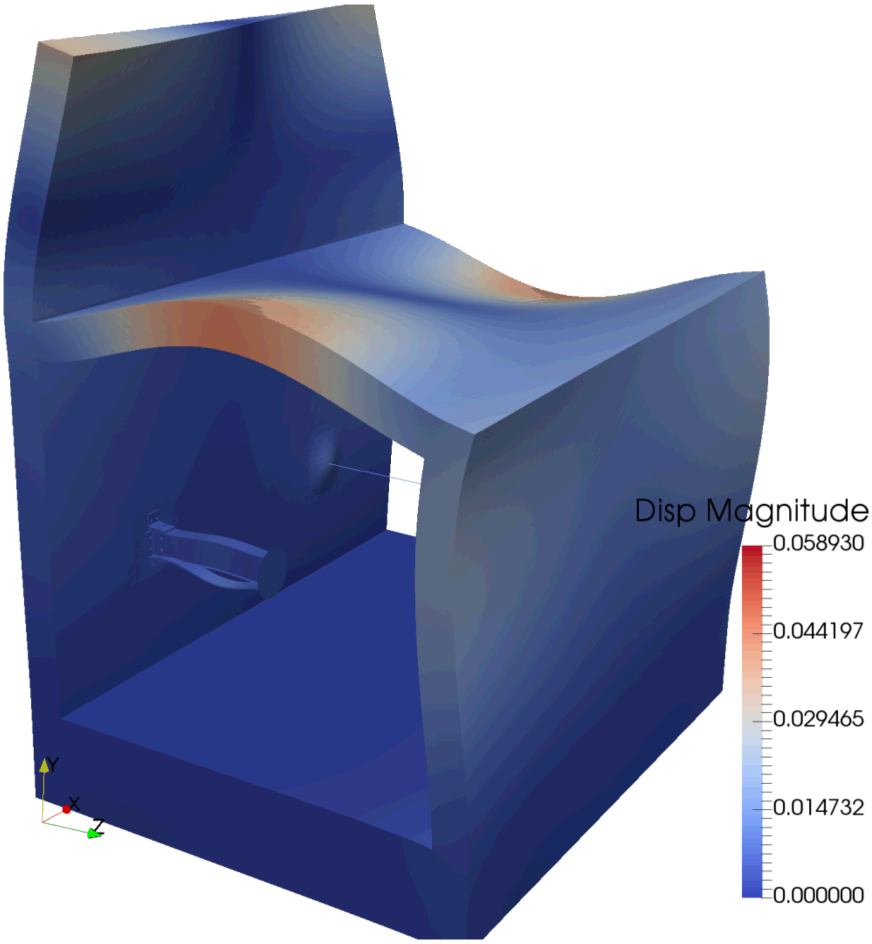

Figure 27: Mode 15 (164.37 Hz)

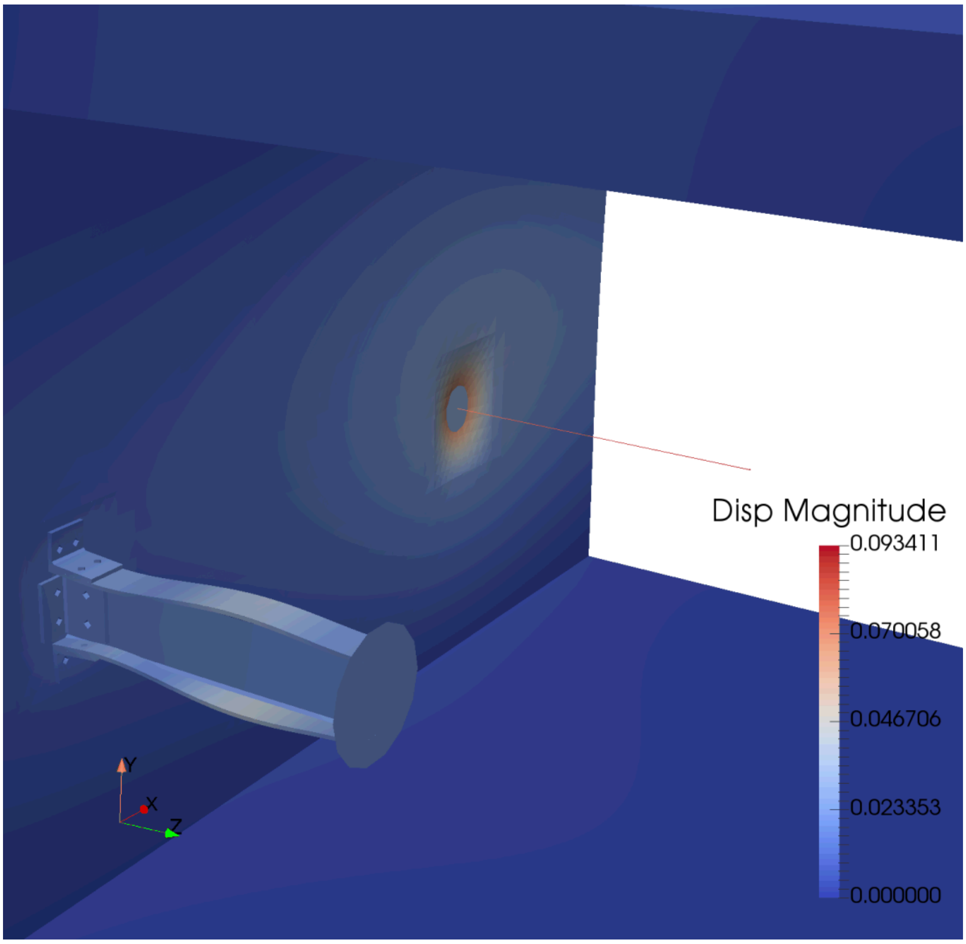

Figure 28: Mode 16 (170.9 Hz)

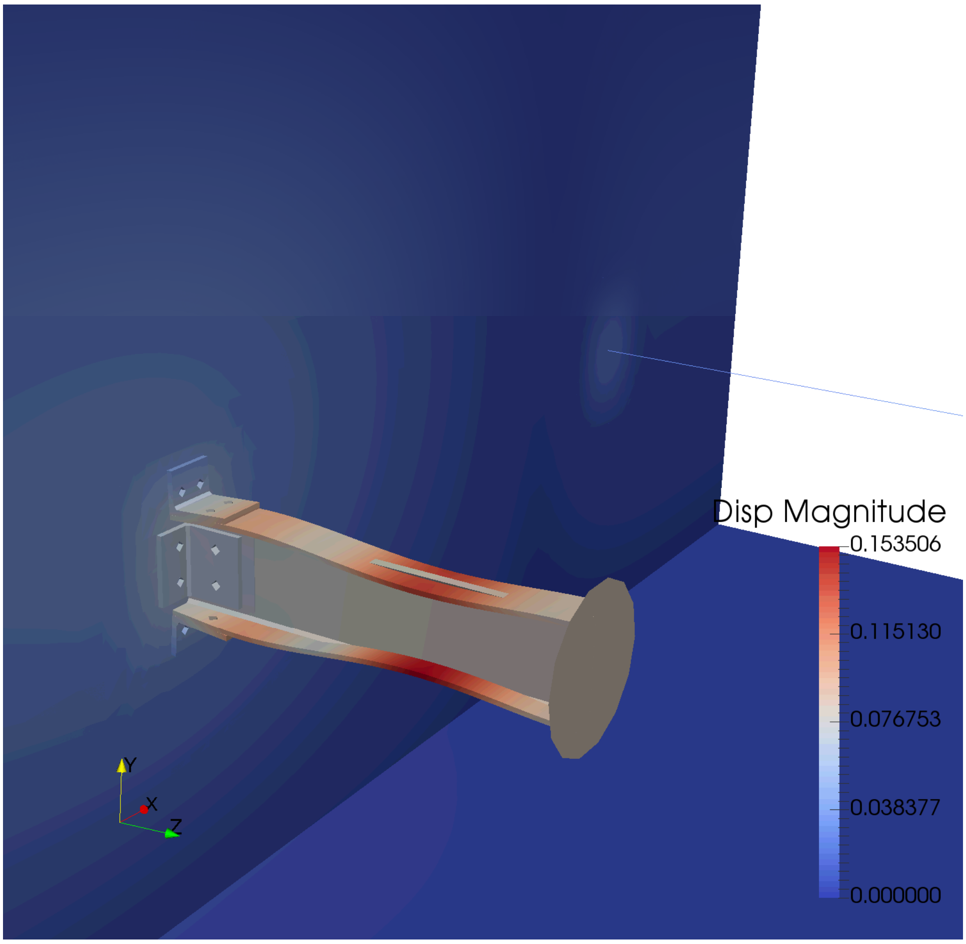

Figure 29: Mode 17 (183.7 Hz)

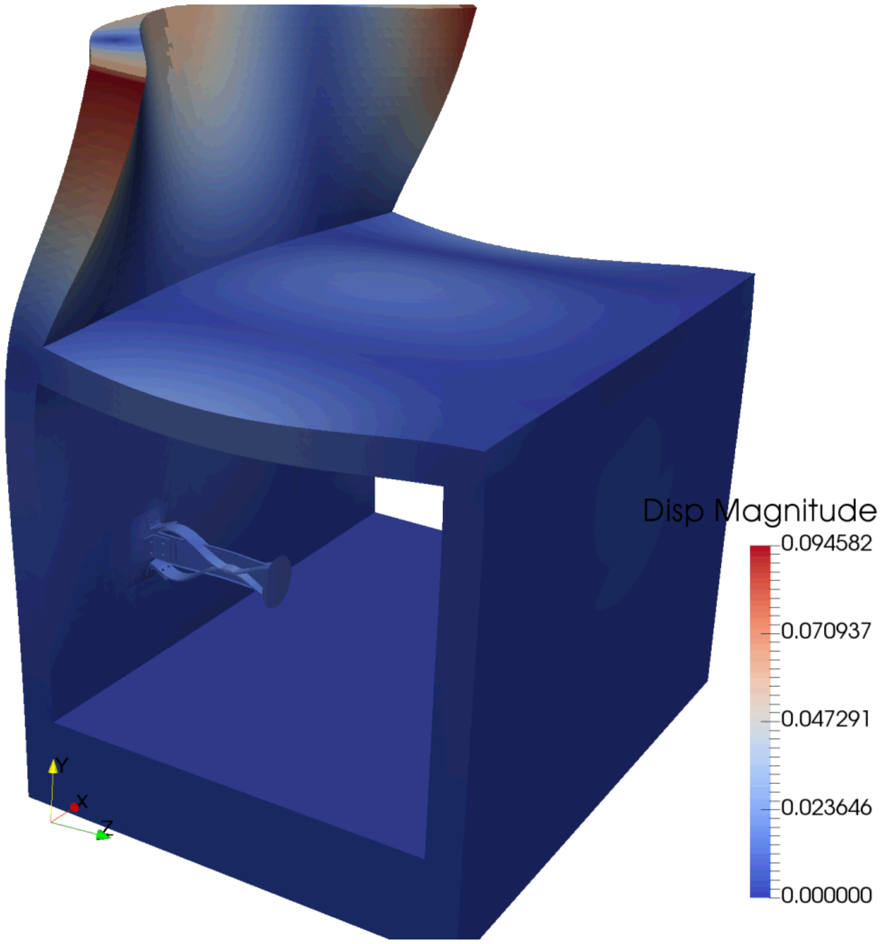

Figure 30: Mode 18 (185.3 Hz)

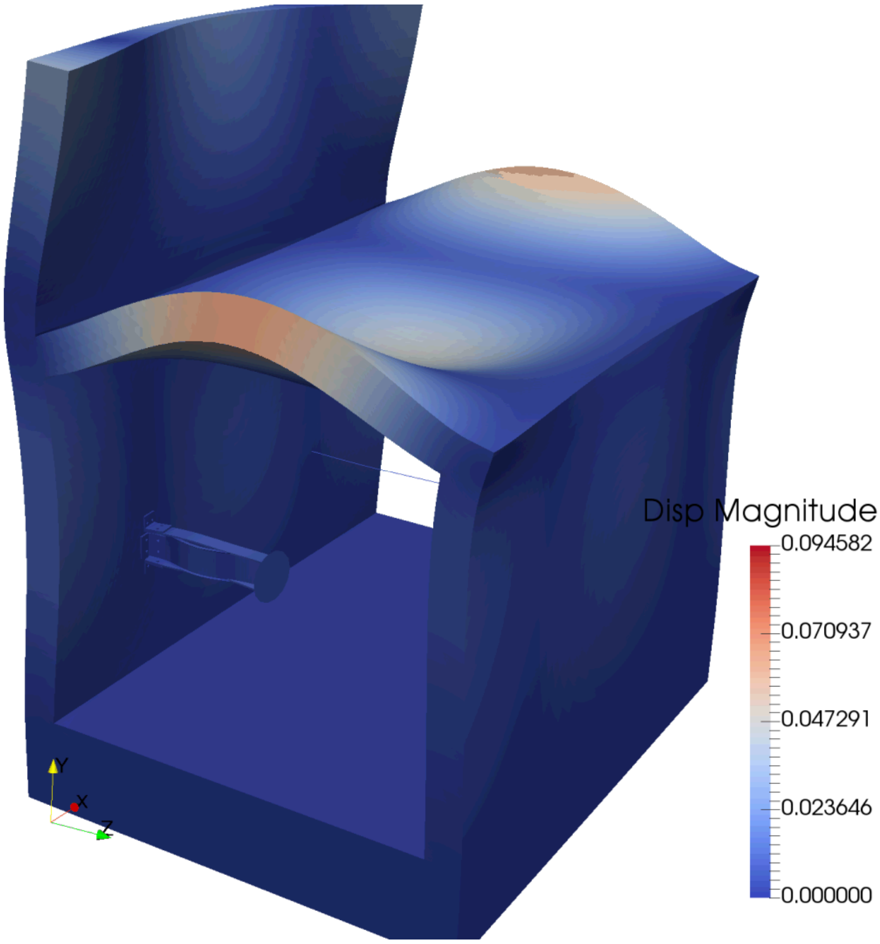

Figure 31: Mode 19 (223.8 Hz)

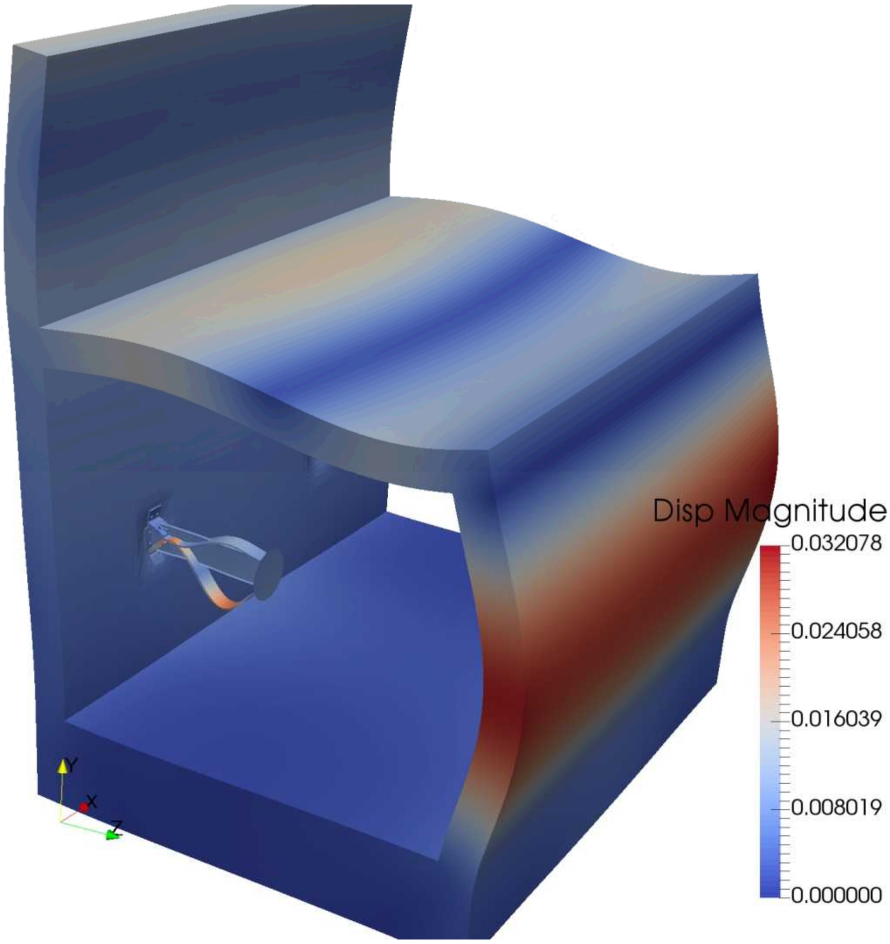

Figure 32: Mode 20 (226.8 Hz)

3. IRIS III results : 1st impact at velocity Va = 90 m/s

3.1 Missile results

3.1.1 Crushing results

The results of the missile crushing from the first 90 m/s simulation are shown below in Table 4. These values were obtained using analyst judgement to determine the transition from crushed to uncrushed. The visual output of the crushed missile is shown in Figure 33.

Table 4: Missile Crushing Results, 90 m/s

Original length (including hemispherical head)	2125 mm
Total length after crush	1549 mm
Crushed length H_T	1221 mm
Non-crushed length L_T	328 mm

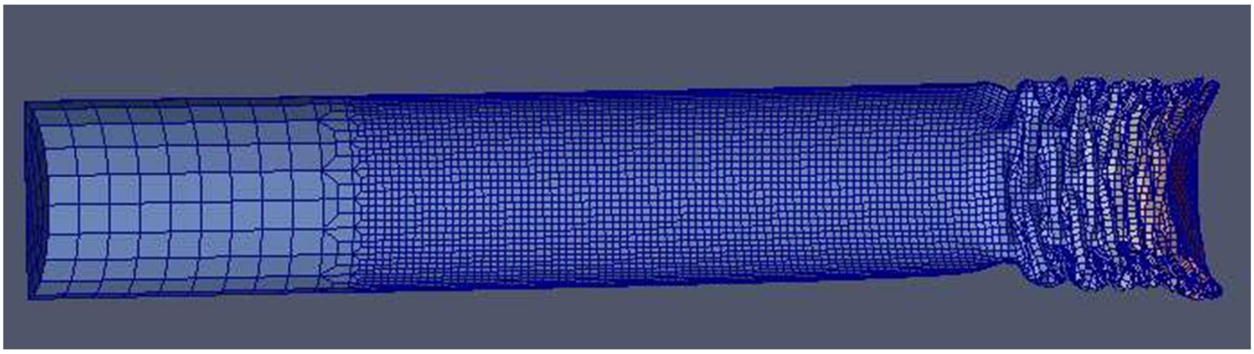

Figure 33: Crushed Missile from the First 90 m/s Impact Simulation

3.1.2 Time histories (Displacement, Velocity, Acceleration)

The time history plots pertaining to the missile behavior are shown below in Figure 34 through Figure 36.

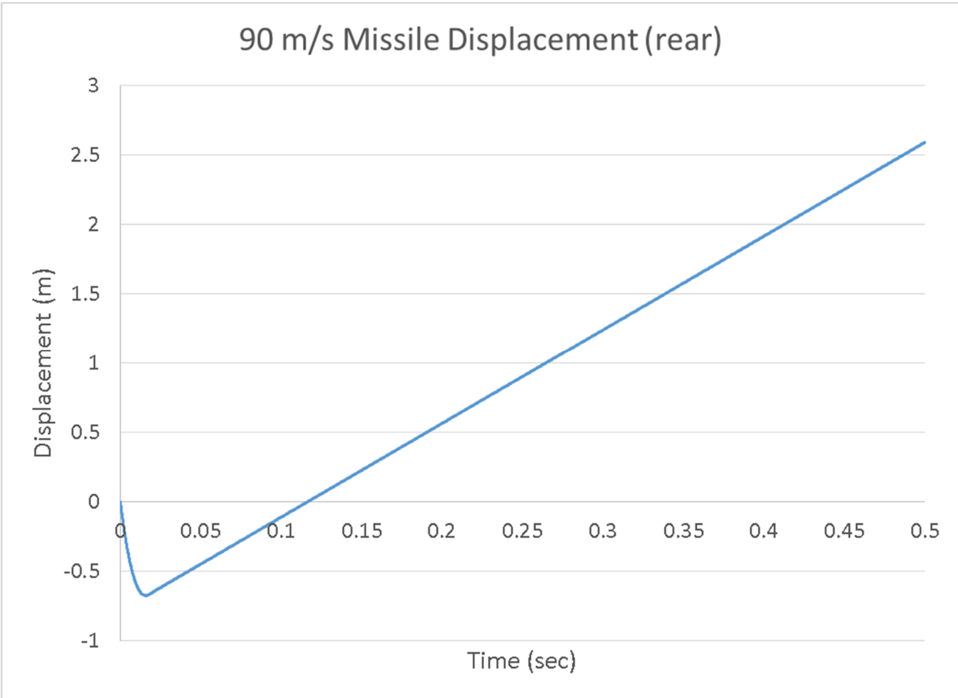

Figure 34: Displacement of the rear end of the 90 m/s missile

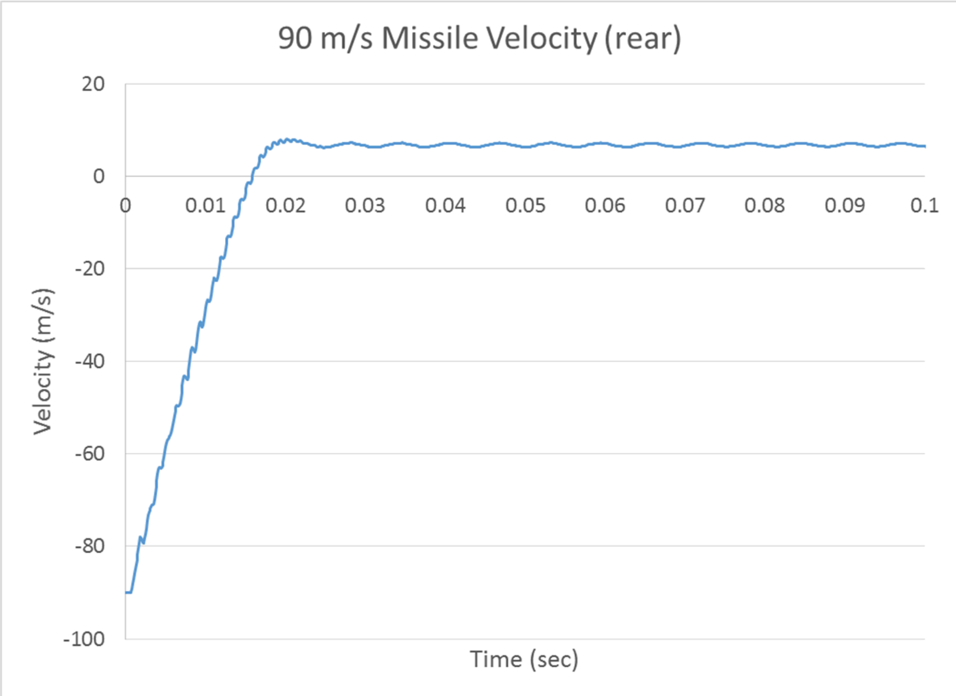

Figure 35: Velocity of the rear end of the 90 m/s missile

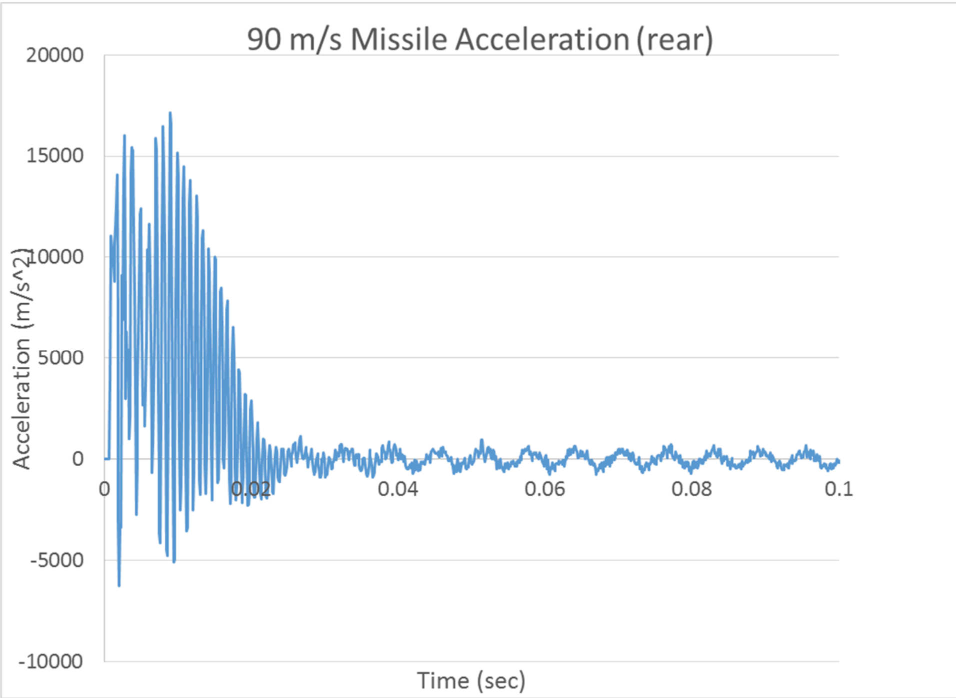

Figure 36: Acceleration of the rear of the 90 m/s missile

3.1.1 Contact force time history and impulse

The contact force imparted by the missile with respect to time is shown below in Figure 37 while the total impulse versus time is shown in Figure 38.

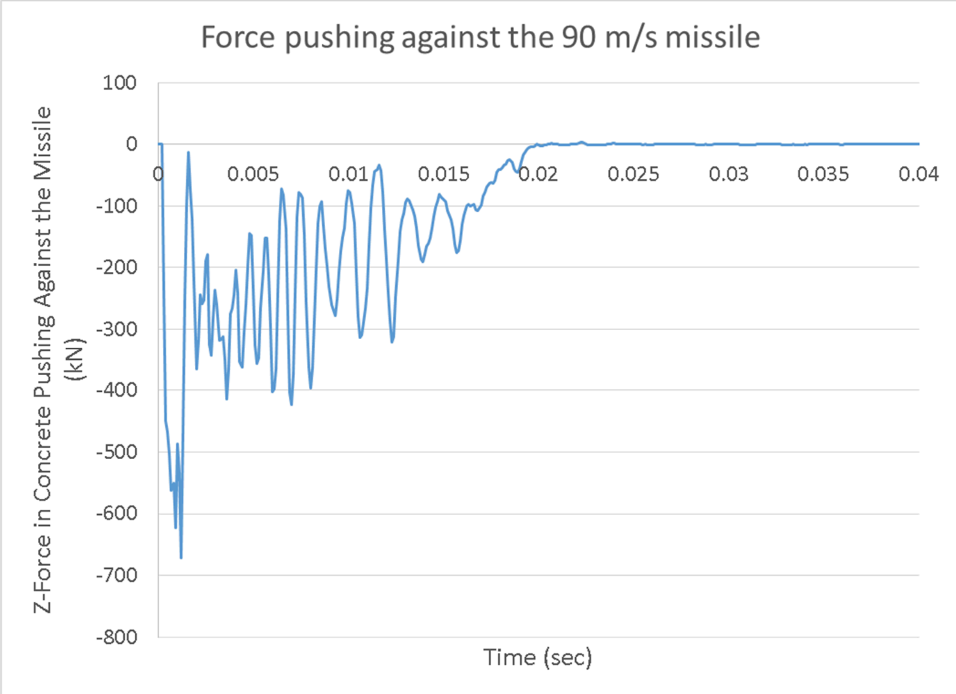

Figure 37: Force pushing against the 90 m/s missile

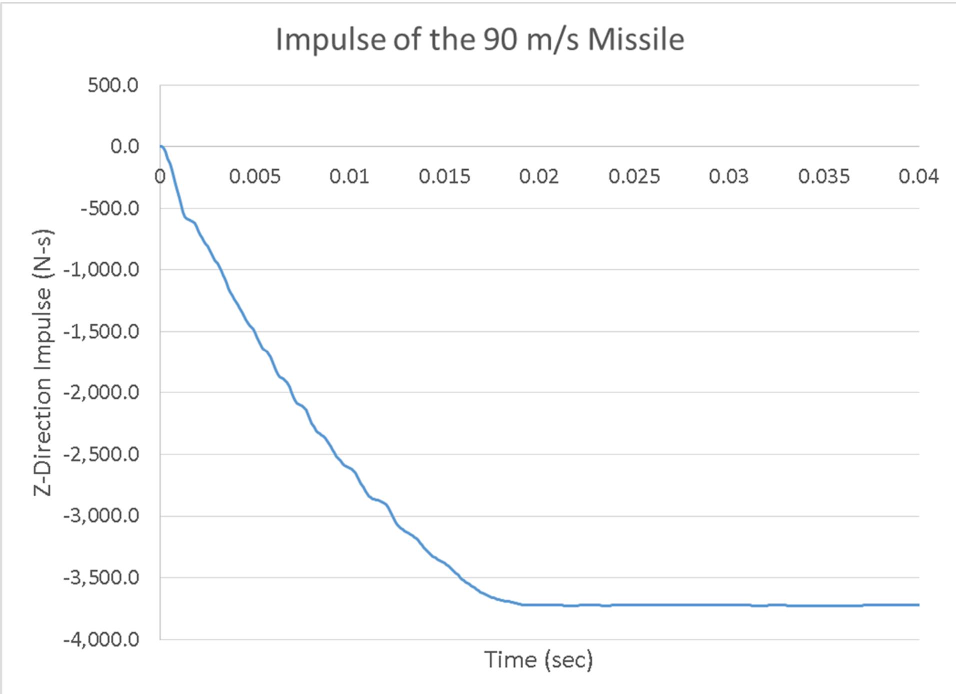

Figure 38: Impulse of the 90 m/s missile

3.2 Mock-up results

3.2.1 Global results

Calculation results from the first 90 m/s impact showing concrete damage are represented in Figure 39 through Figure 44. Note that the support pedestals have been removed from the visualization (though they were included in the simulation) to increase visibility to the concrete. Damage is plotted in these figures with damage = 1.0 representing fractured concrete.

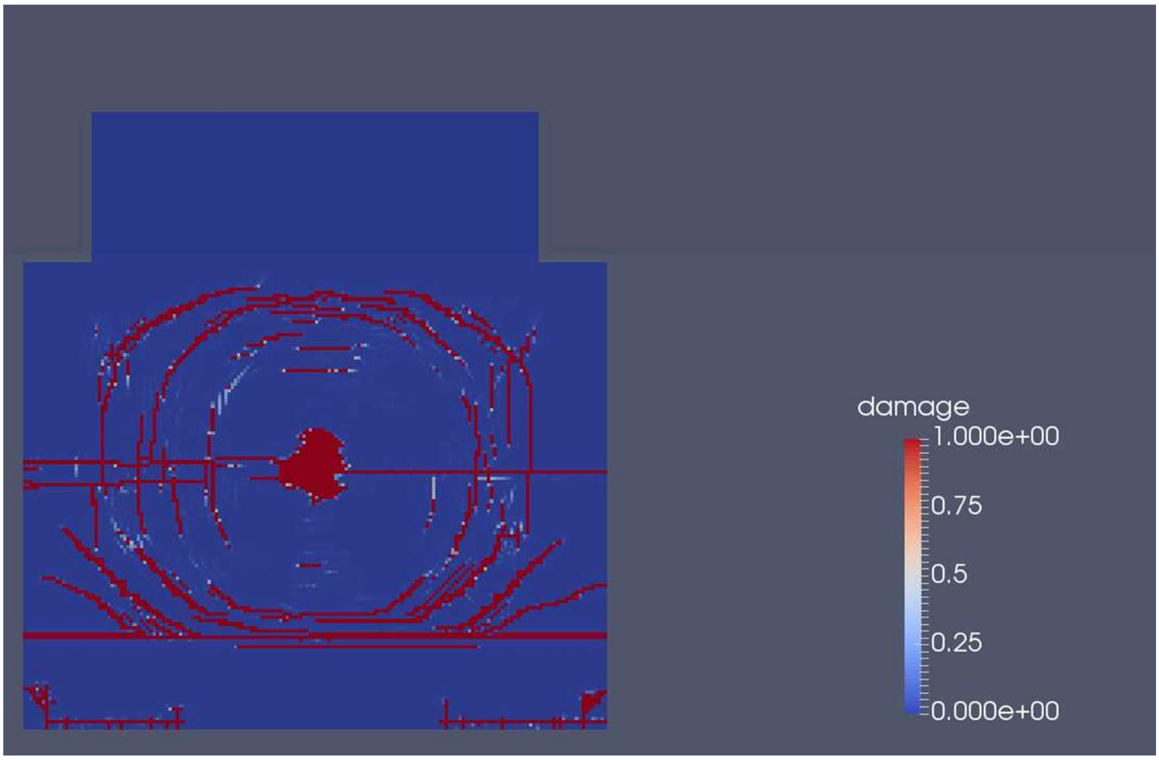

Figure 39: Damage on the front face of the mock-up from the 90 m/s missile

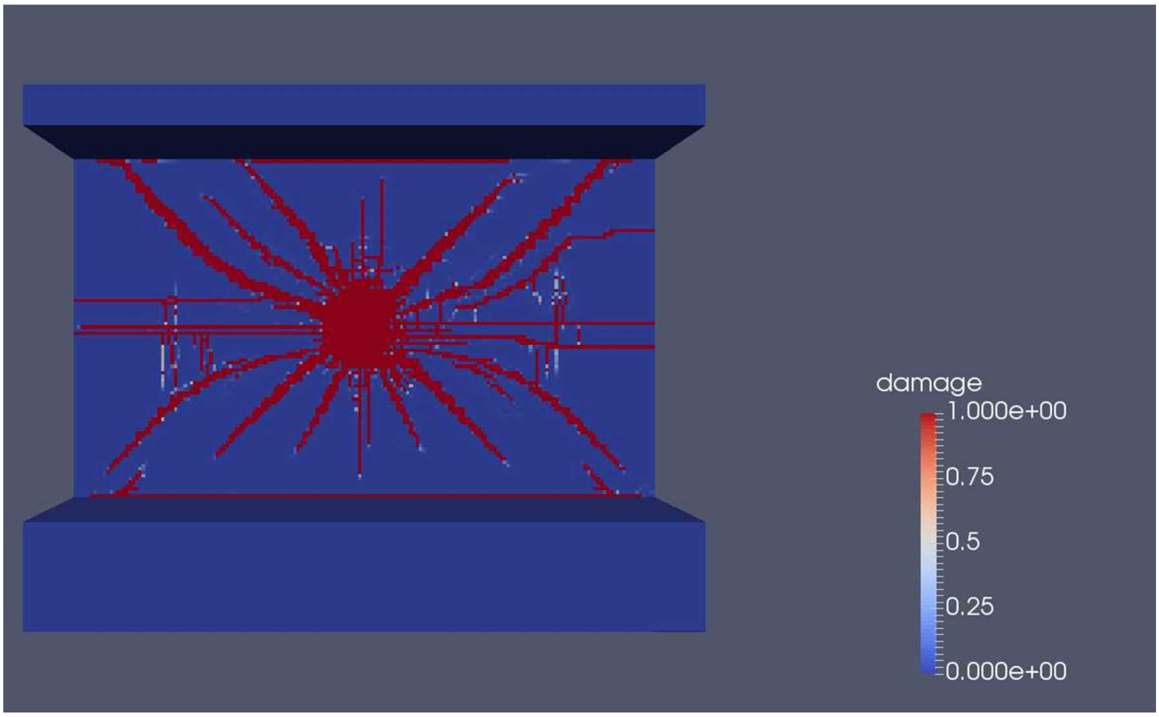

Figure 40: Damage on the back of the front face of the mock-up from the 90 m/s missile

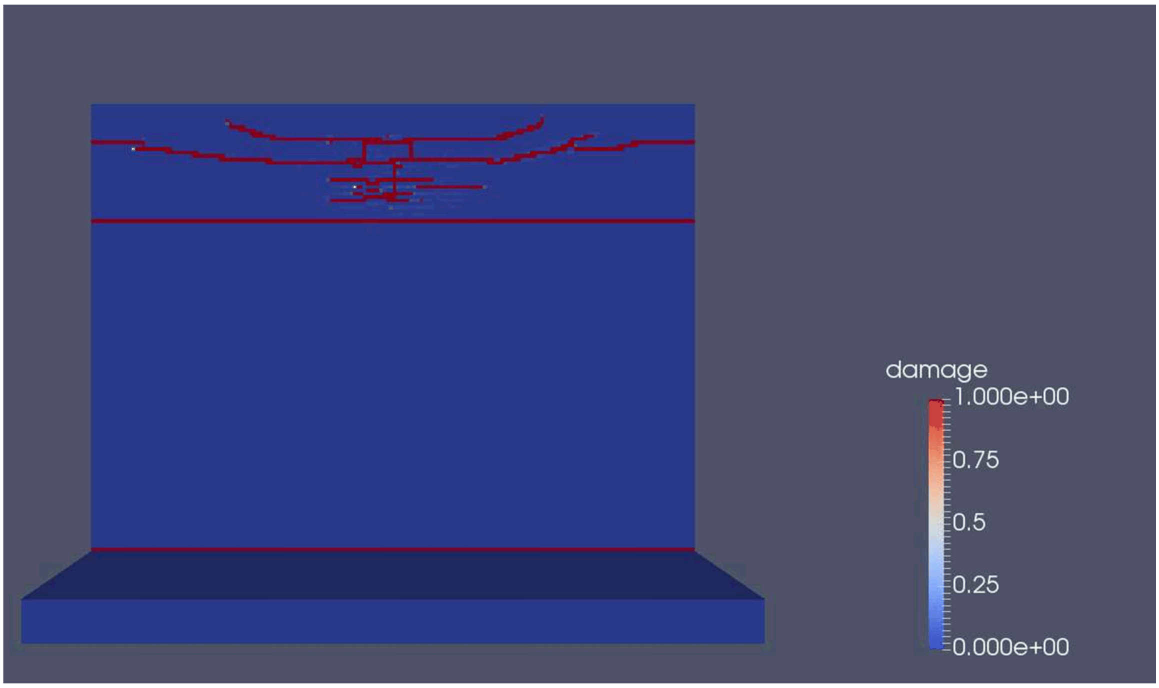

Figure 41: Damage on the top face of the mock-up from the 90 m/s missile

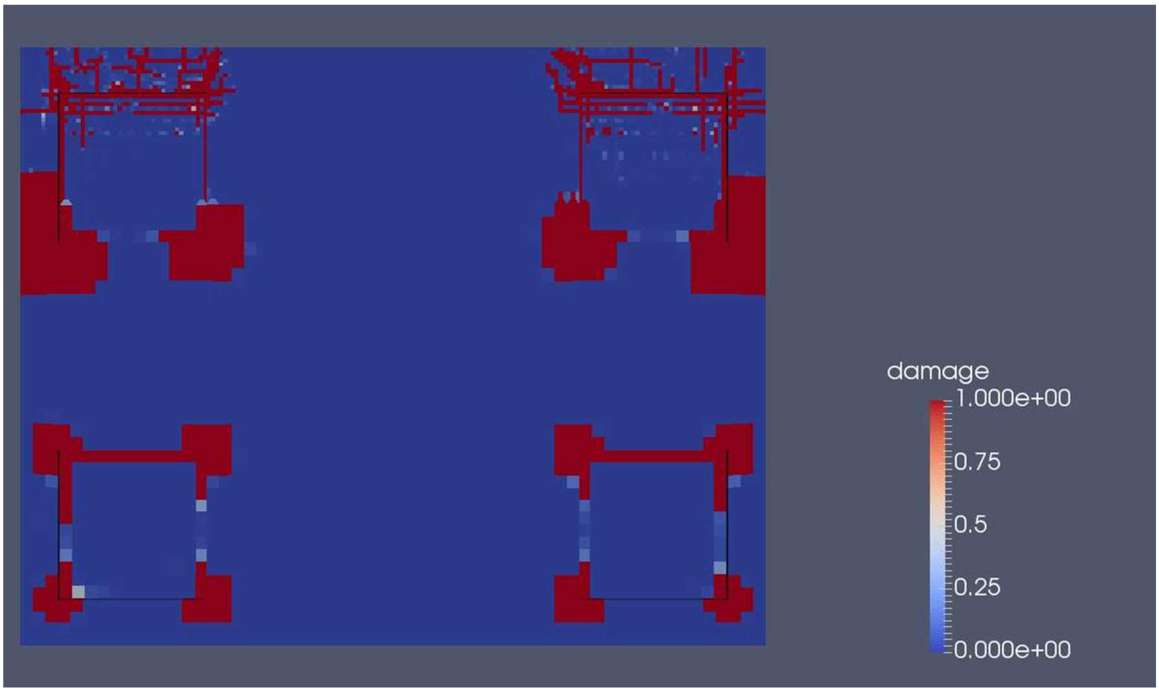

Figure 42: Damage on the bottom face of the mock-up from the 90 m/s missile

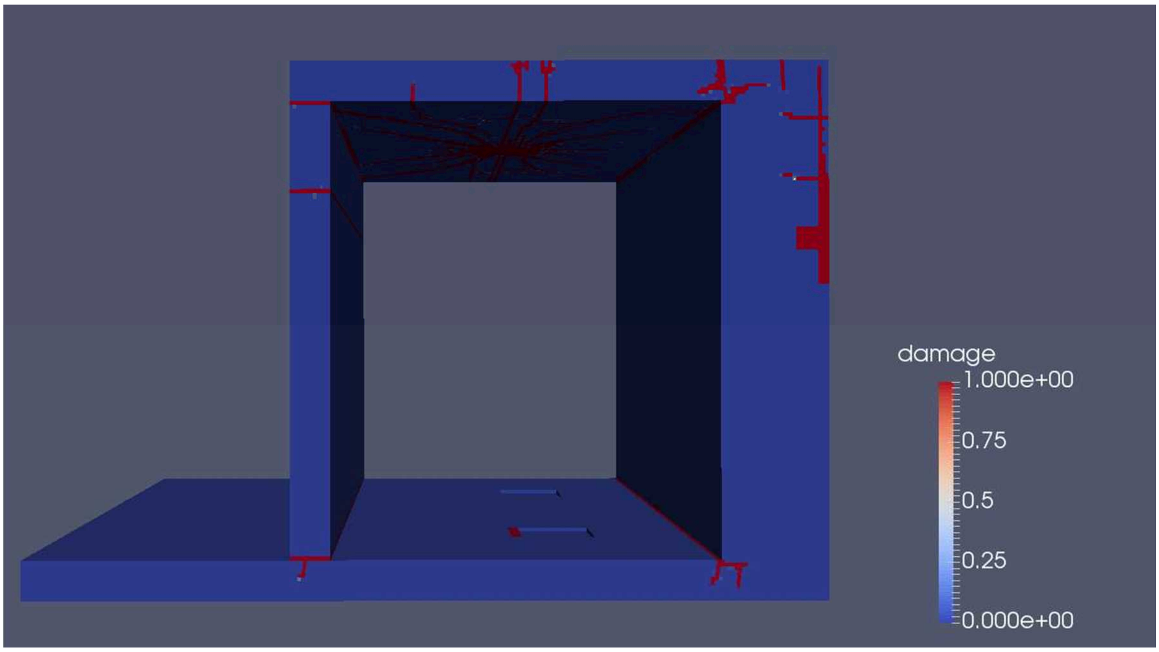

Figure 43: Damage on the side face of the mock-up from the 90 m/s missile

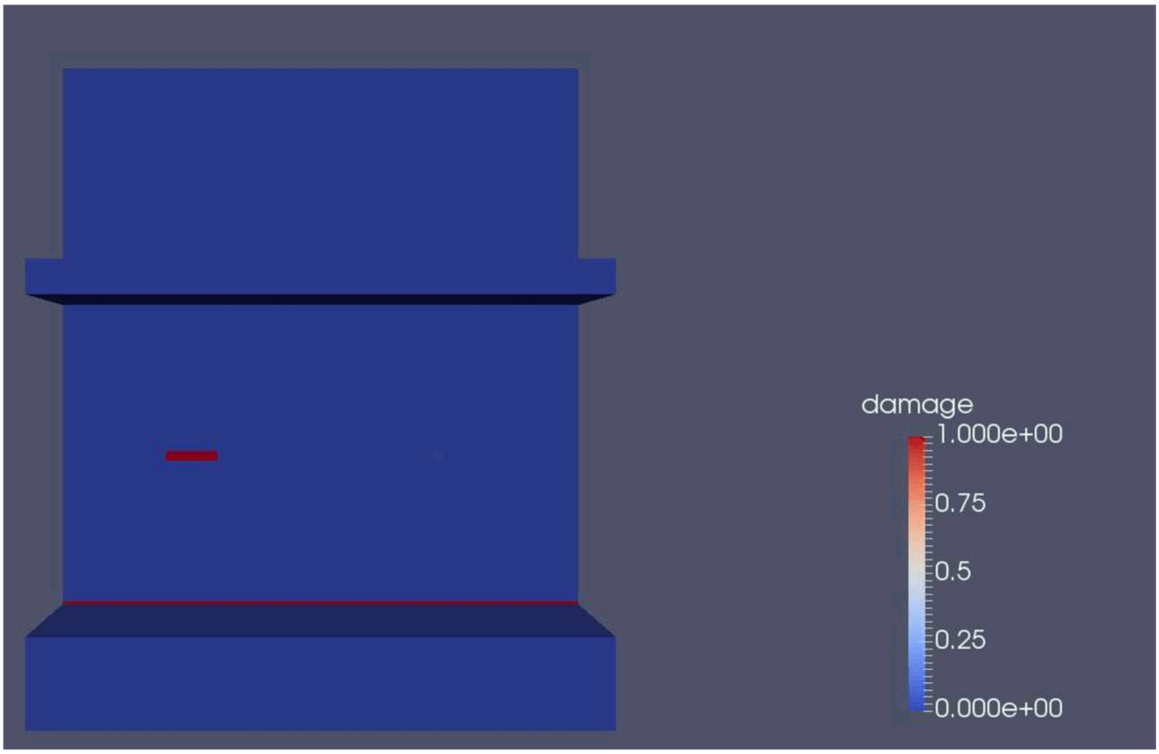

Figure 44: Damage on the front face of the back wall of the mock-up from the 90 m/s missile

The final displacements in the concrete are shown in Figure 45 and Figure 46.

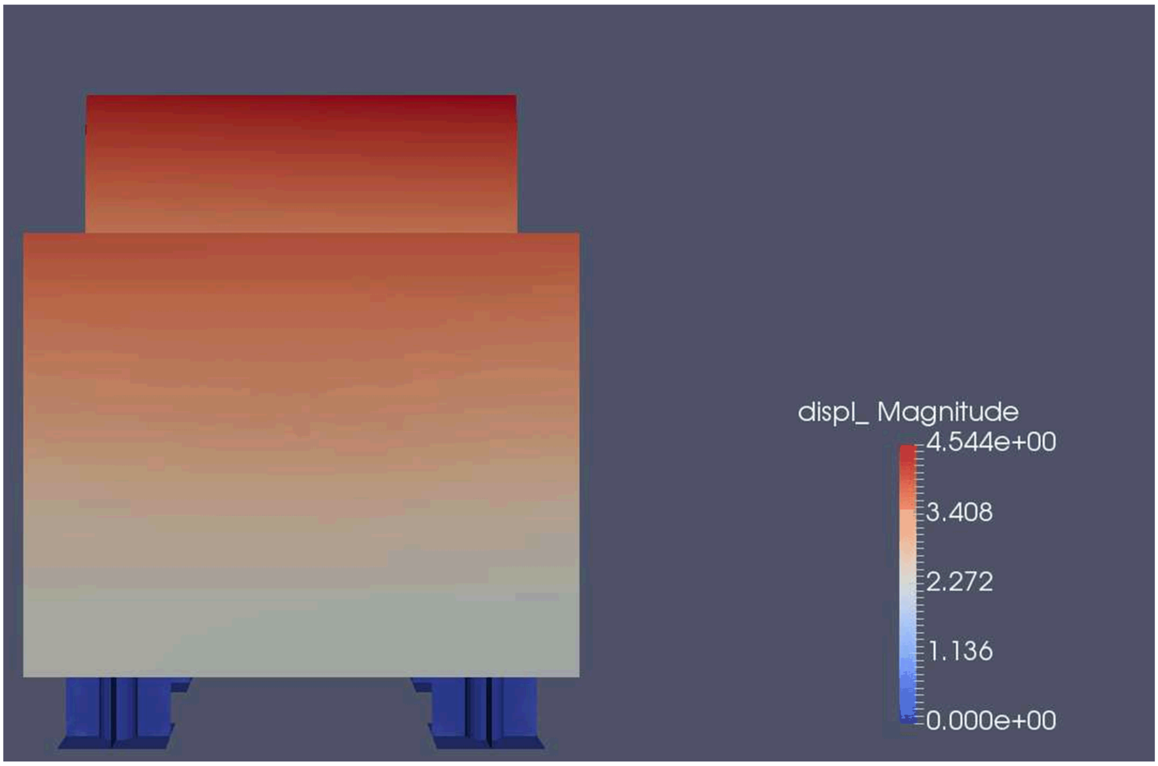

Figure 45: Front view of the final displacements of the mock-up (mm)

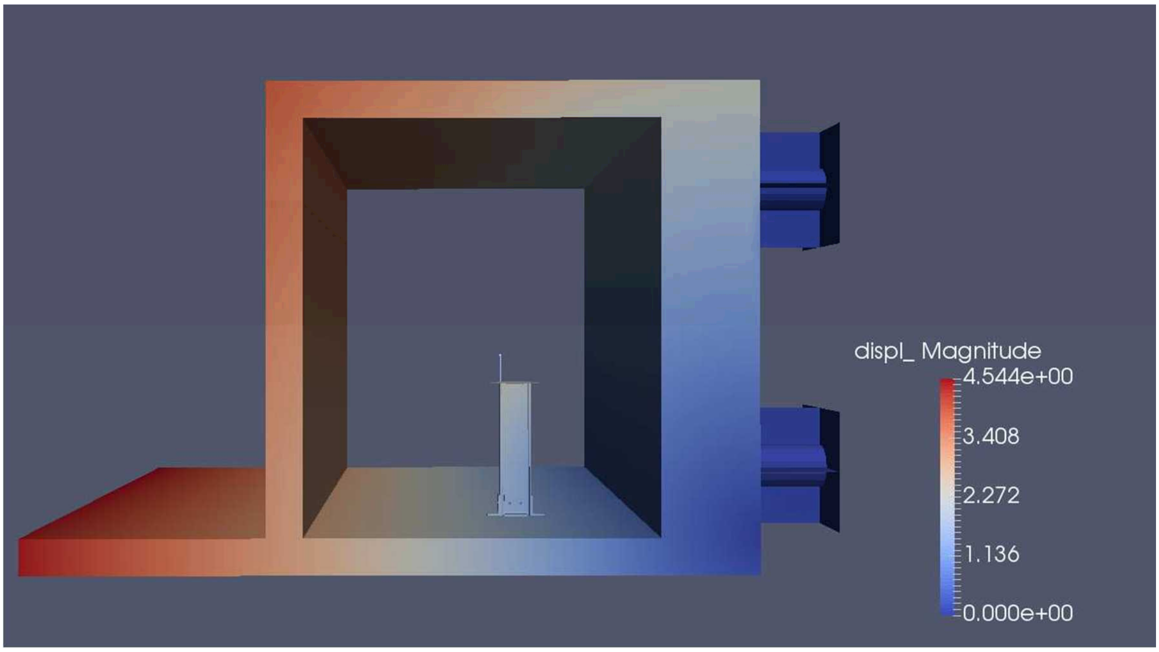

Figure 46: Side view of the final displacements of the mock-up (mm)

3.2.2 Concrete strains (at sensors locations)

The concrete strains corresponding to the requested output locations are presented in Table 5.

Table 5: Concrete Strains at Selected Output Locations, Va=90 m/s

Sensor	Peak Displacement (mm)	Final Displacement (mm)	Sensor	Peak Displacement (mm)	Final Displacement (mm)
D01	-7.07	-2.15	D6V	2.65	-0.11
D02	-6.76	-1.91	D7	-17.7	-4.44
D03	-8.58	-2.55	D7L	-17.1	-4.44
D1	-9.83	-2.88	D8HX	-0.08	0.01
D2	4.44	1.28	D8V	6.57	2.01
D3	-10.6	-3.08	D8HZ	-2.06	-0.61
D3L	-10.6	-3.08	D9	-4.61	-1.44
D4H	-2.18	-0.62	D9L	-4.63	-1.44
D4V	6.59	-1.98	D9W	-4.63	-1.41
D5	3.19	0.97	D10	3.63	1.45
D6H	-1.01	-0.28	D10W	6.54	-0.80

3.2.3 Rebars strains (at sensors locations)

The rebar strain values at the selected output locations are presented in Table 6.

Table 6: Rebar Strains at Selected Output Locations, Va=90 m/s

Sensor	Peak Strain (με)	Final Strain (με)	Sensor	Peak Strain (με)	Final Strain (με)
G0H	686	1.04	G3V	302	51.0
G0V	1251	41.3	G4V	851	114
G1V	619	26.5	G5V	153	-0.45
G2V	-247	21.6	G6V	146	1.04

3.2.4 Reaction forces at supports locations

The reaction forces at the supports are summarized in Table 7.

Table 7: Reaction Forces, Va=90 m/s

Support Location	Peak Force (kN)	Final Force (kN)
Front left	281	24.5
Front right	289	18.6
Rear left	297	27.7
Rear right	320	5.8

In order to reduce the high-frequency noise believed to be associated with numerical effects, the data was filtered using a 4th order low pass Butterworth filter with a cutoff frequency of 1000 Hz. The reaction force vs time responses for the four supports are shown in Figure 47 through Figure 50.

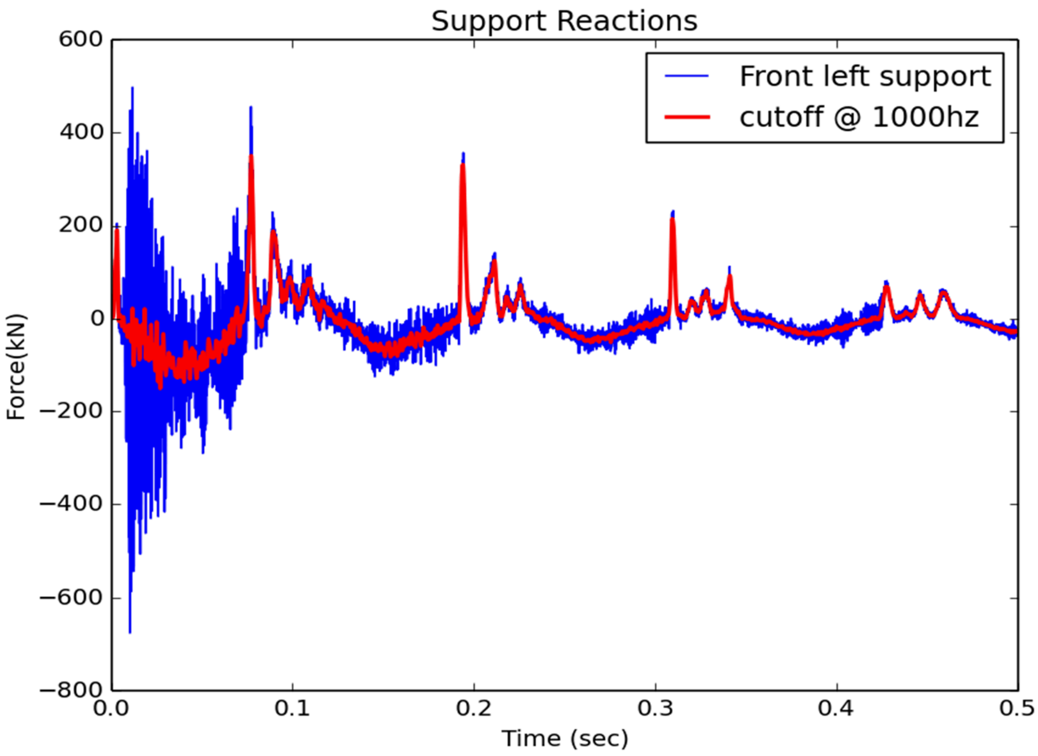

Figure 47: Front left support reaction force vs time

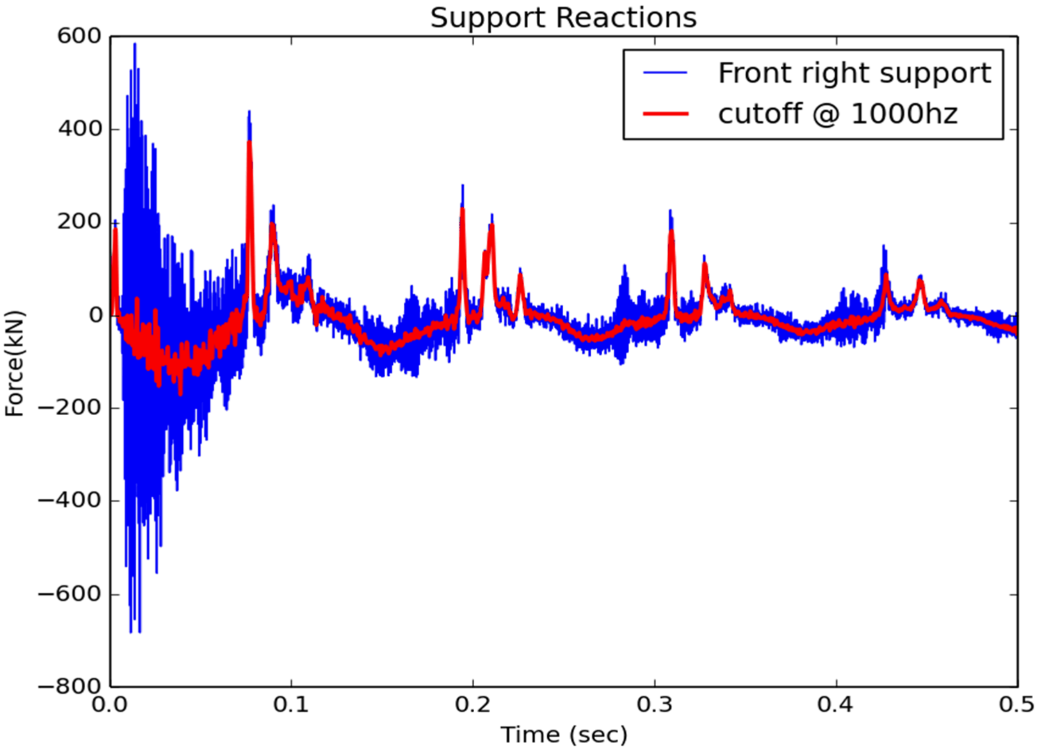

Figure 48: Front right support reaction force vs time

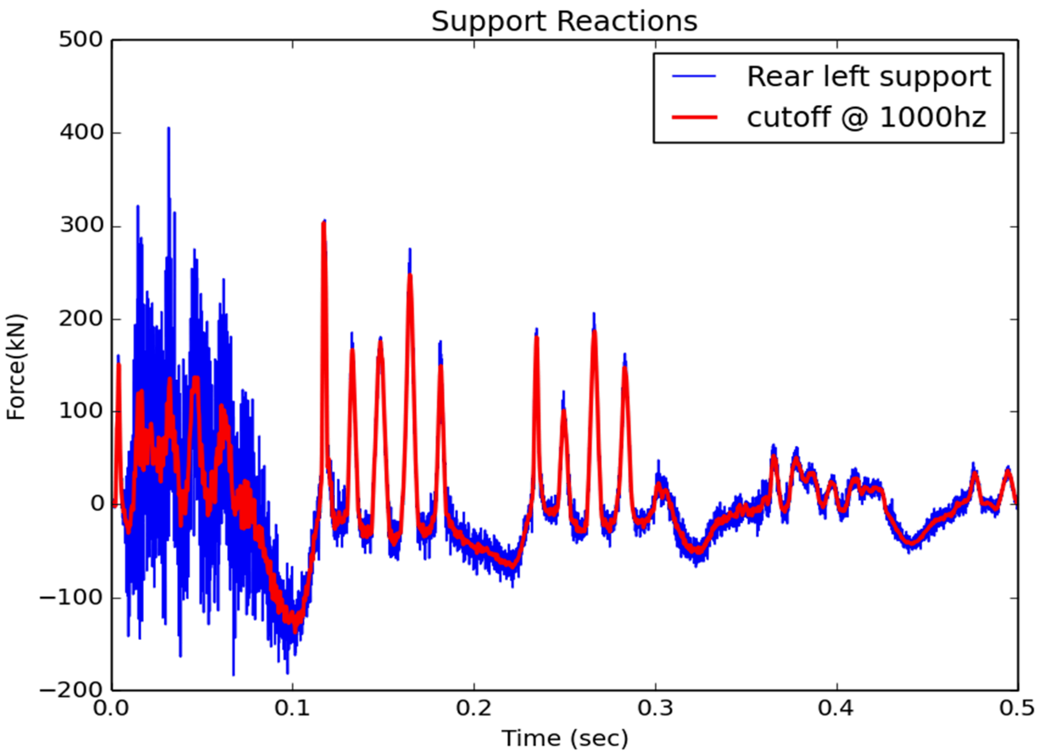

Figure 49: Rear left support reaction force vs time

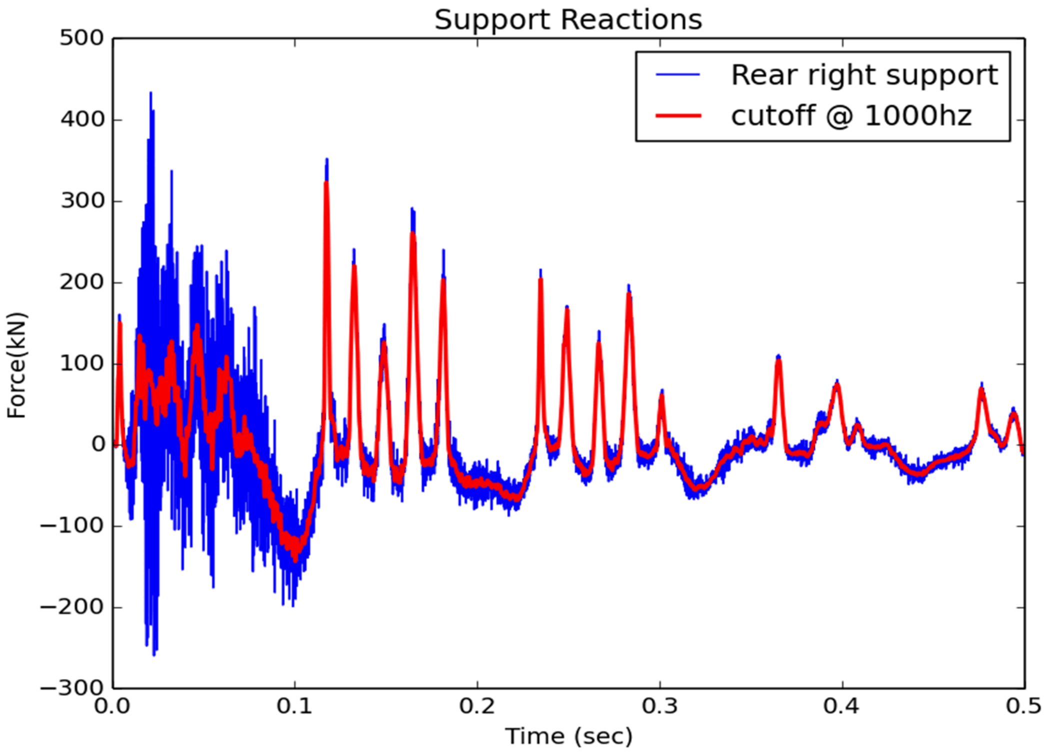

Figure 50: Rear right support reaction force vs time

3.2.5 Time histories (Displacements, Accelerations at sensors locations)

3.2.5.1 Displacements

The displacement versus time response for the selected locations from the first 90 m/s impact are presented in Figure 51 through Figure 54.

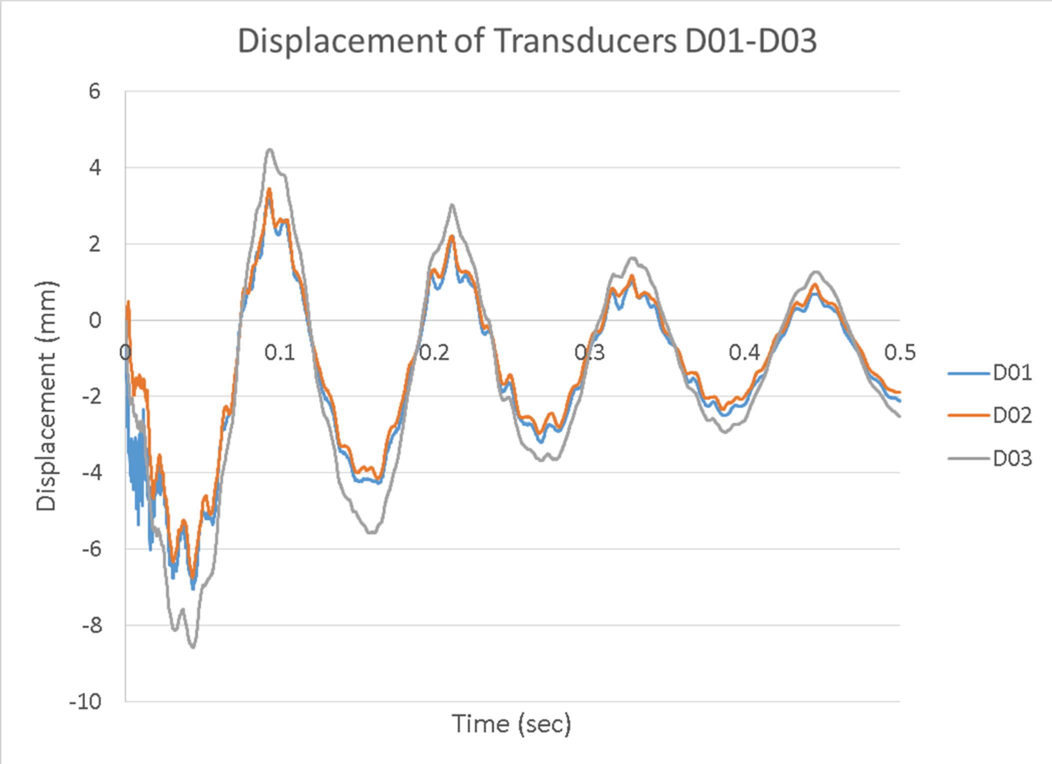

Figure 51: Displacements of transducers D01-D03 (mm)

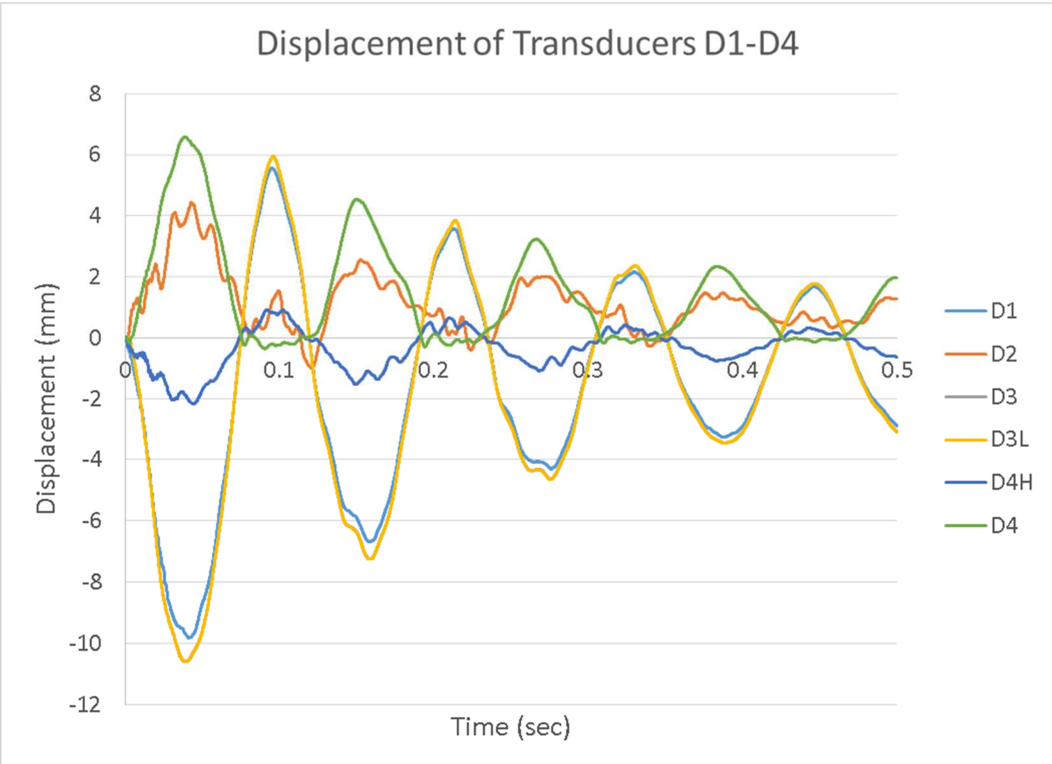

Figure 52: Displacements of transducers D1-D4 (mm)

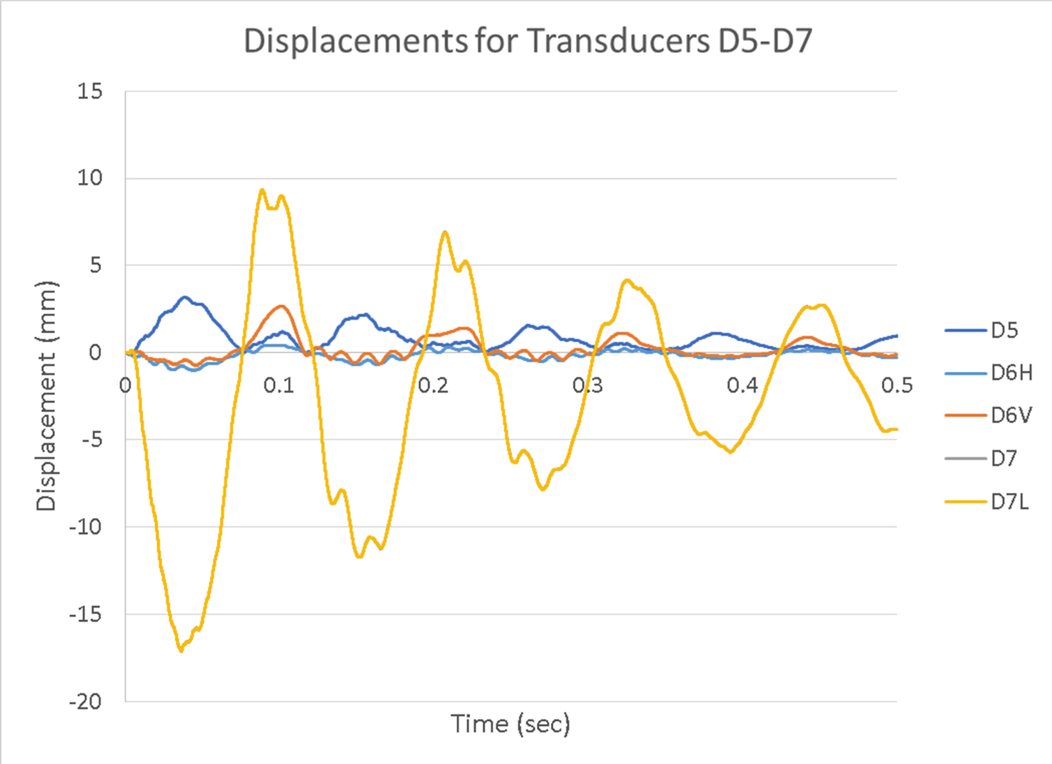

Figure 53: Displacements of transducers D5-D7 (mm)

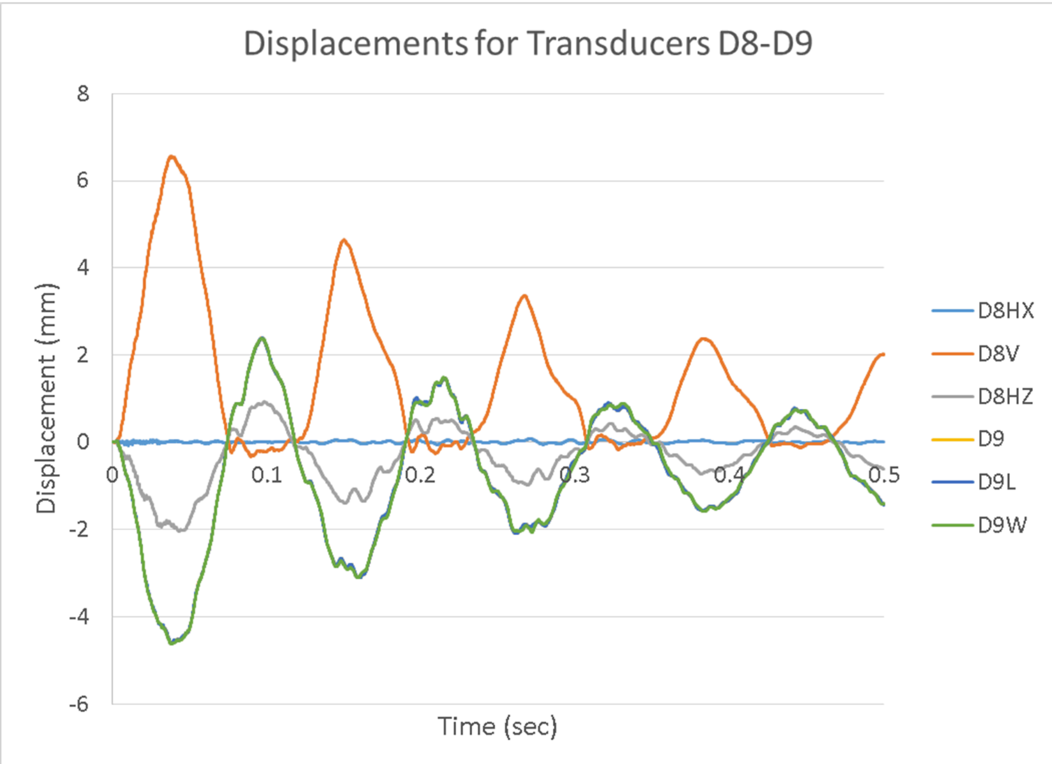

Figure 54: Displacements of transducers D8-D9 (mm)

3.2.5.2 Accelerations

Similar to the reaction forces above, the acceleration data was filtered to reduce high-frequency data. Figure 55 through Figure 69 show the acceleration versus time response at the selected output locations.

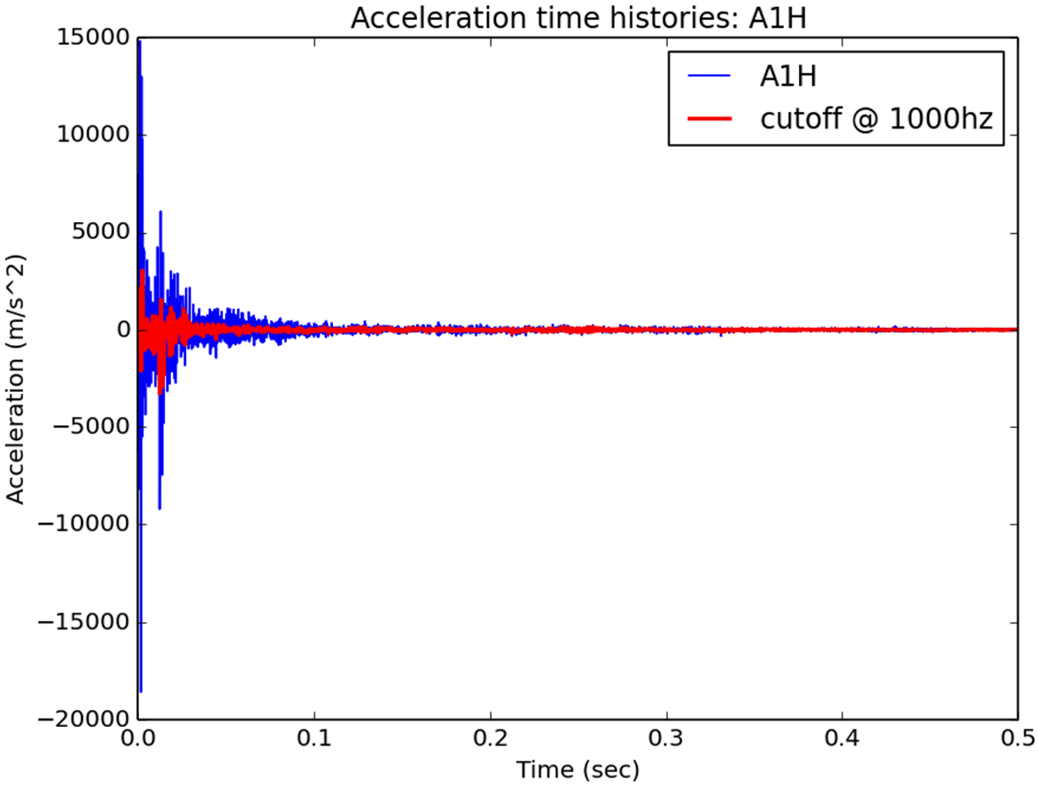

Figure 55: Acceleration versus time for A1H

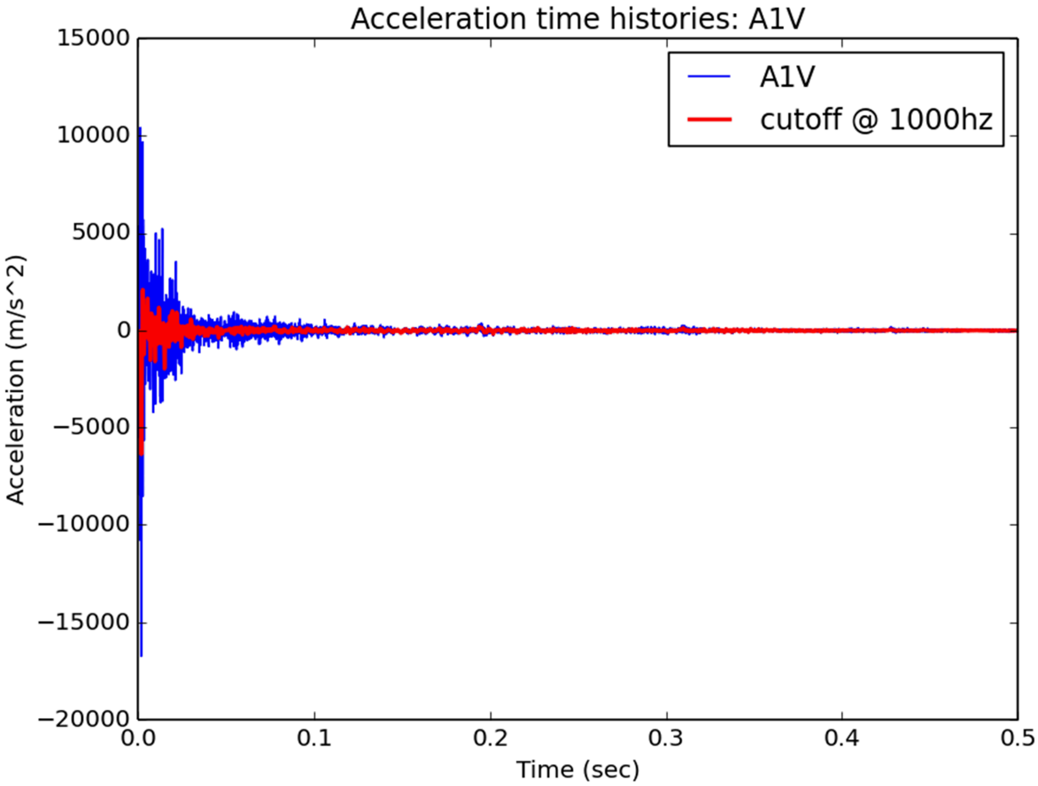

Figure 56: Acceleration versus time for A1V

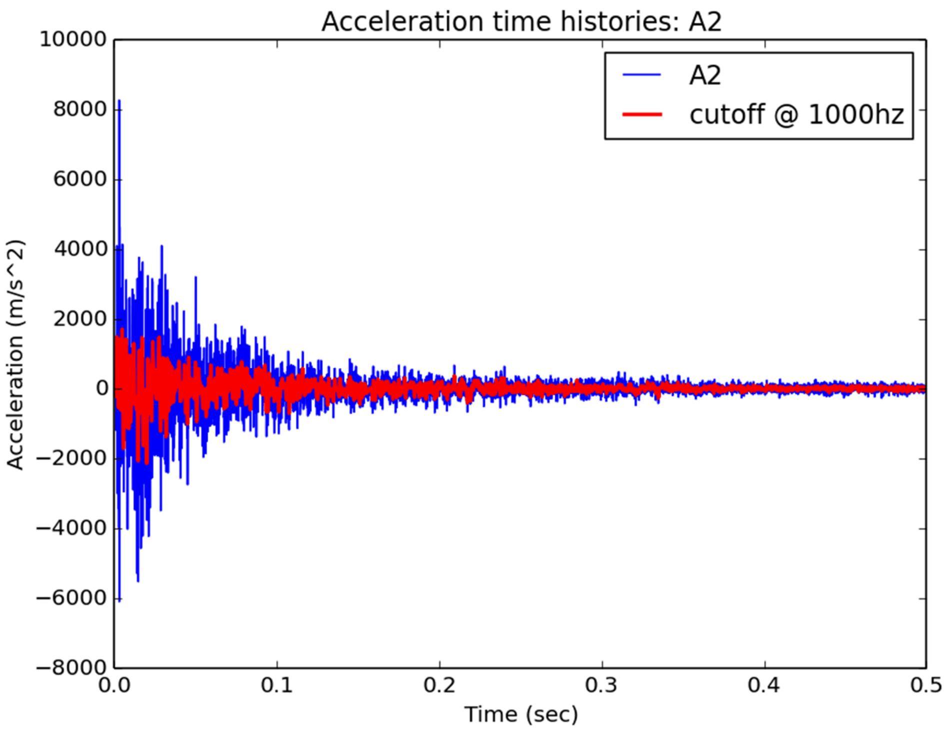

Figure 57: Acceleration versus time for A2

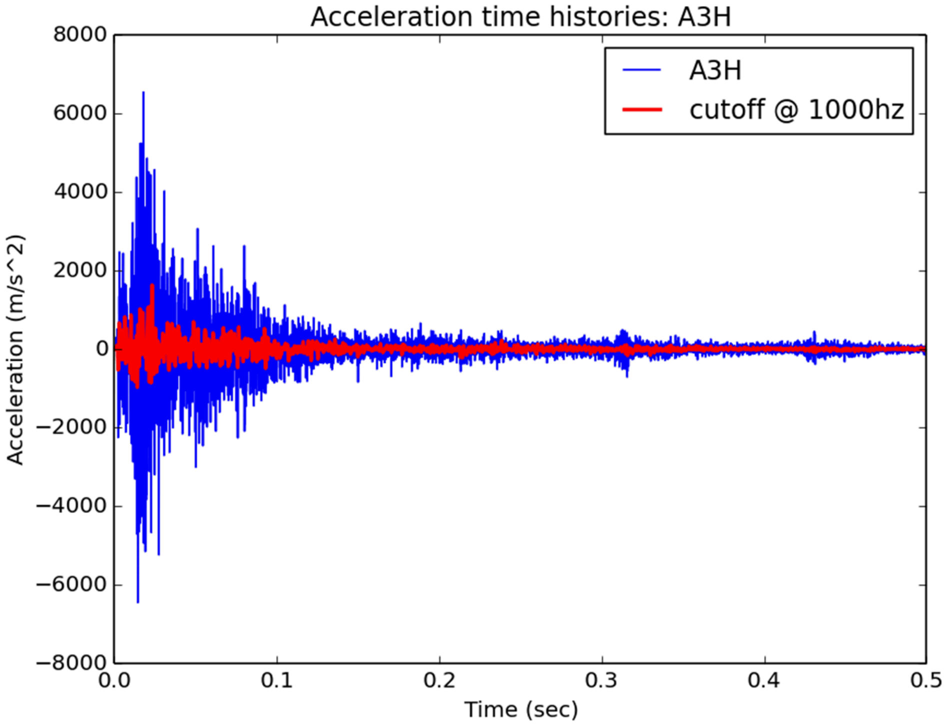

Figure 58: Acceleration versus time for A3H

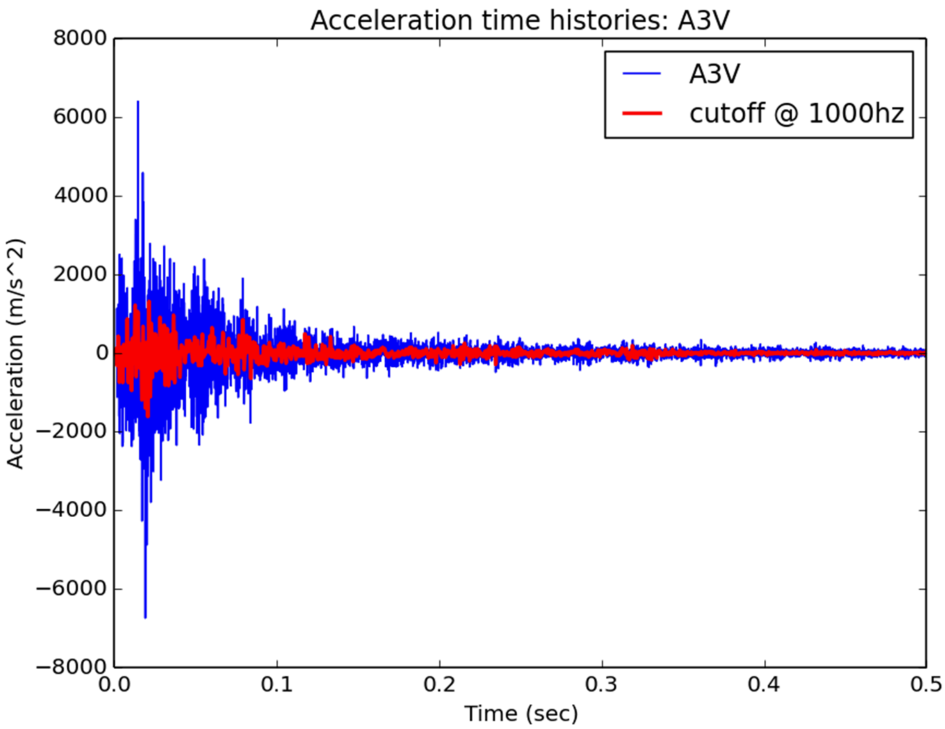

Figure 59: Acceleration versus time for A3V

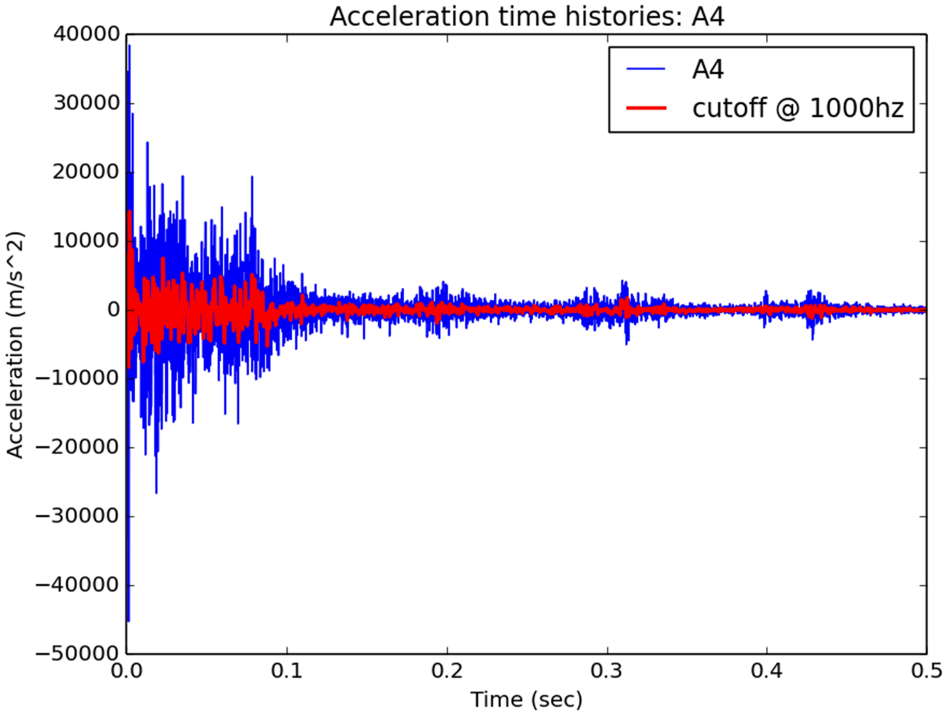

Figure 60: Acceleration versus time for A4

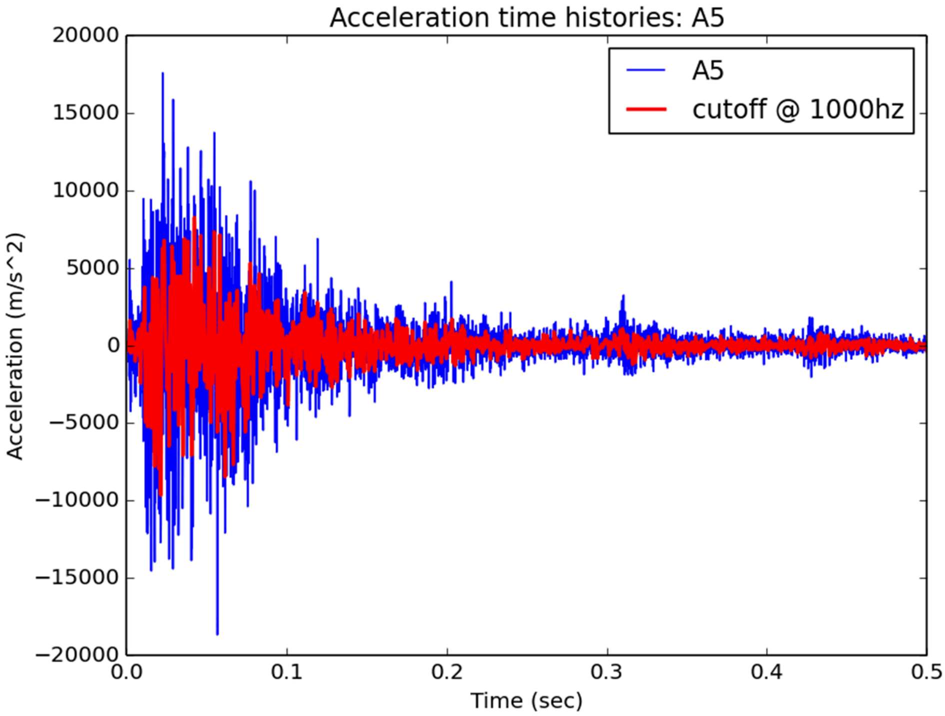

Figure 61: Acceleration versus time for A5

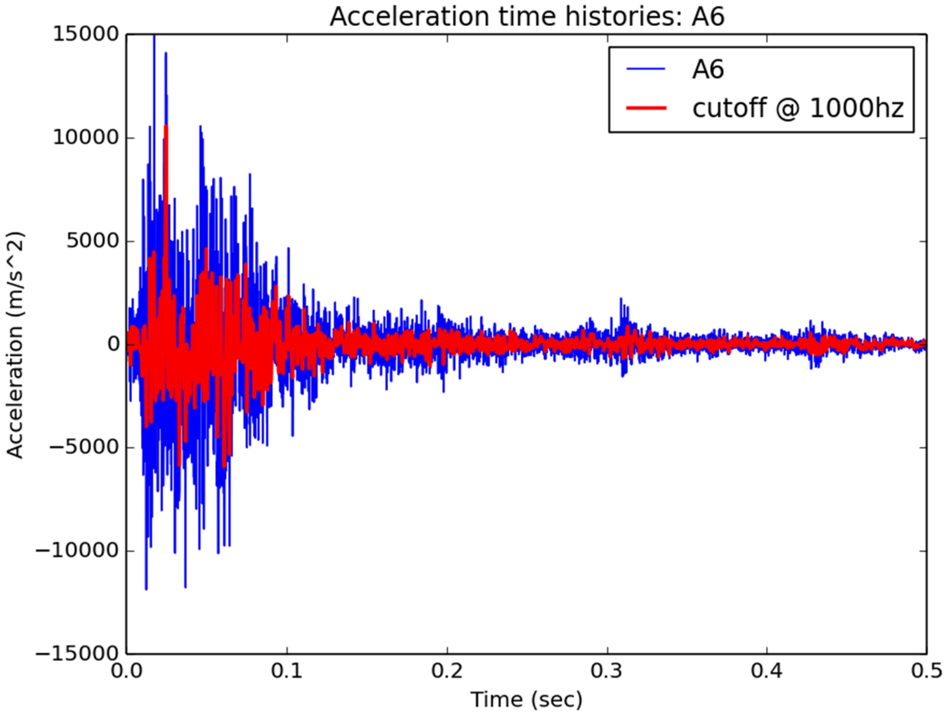

Figure 62: Acceleration versus time for A6

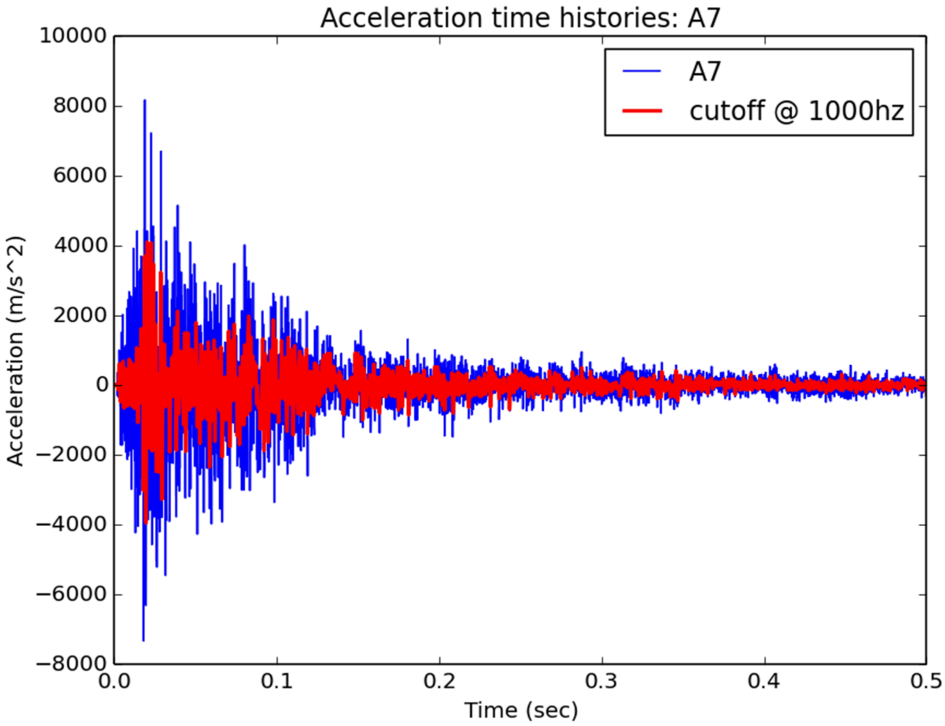

Figure 63: Acceleration versus time for A7

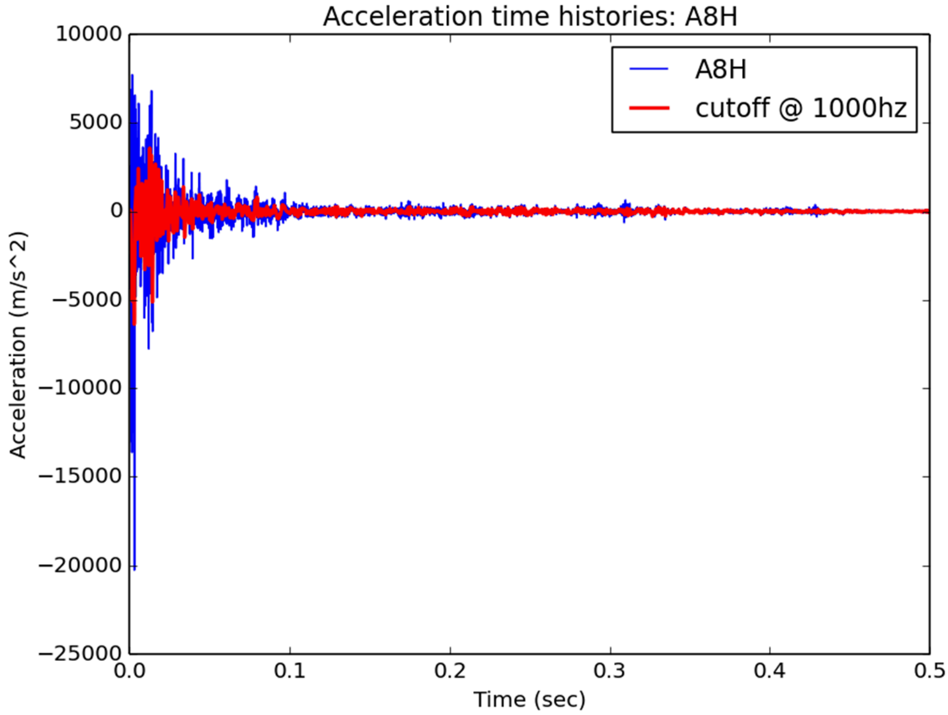

Figure 64: Acceleration versus time for A8H

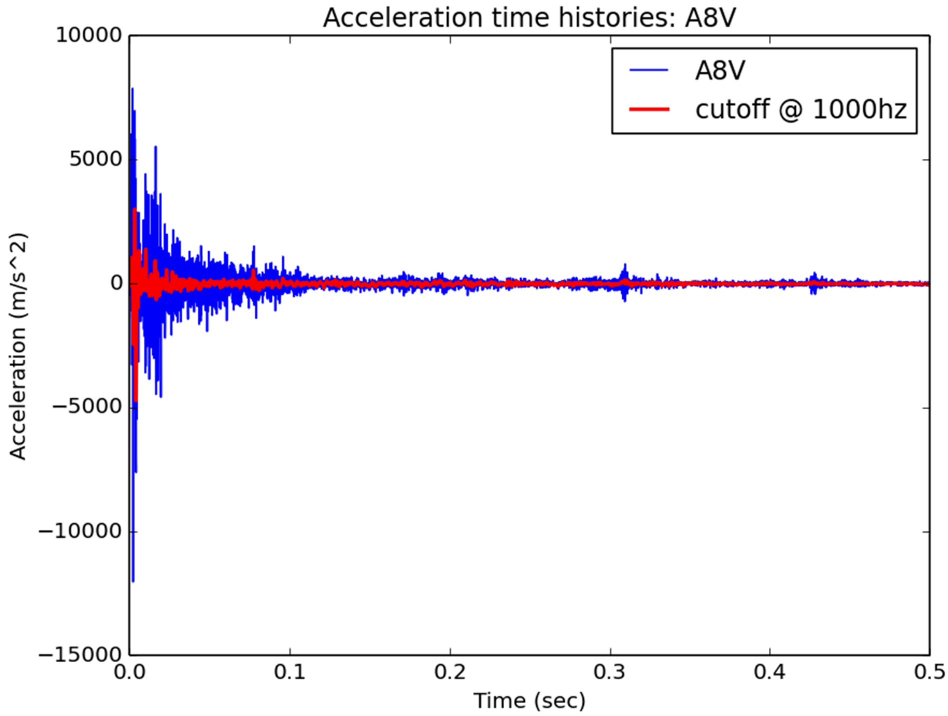

Figure 65: Acceleration versus time for A8V

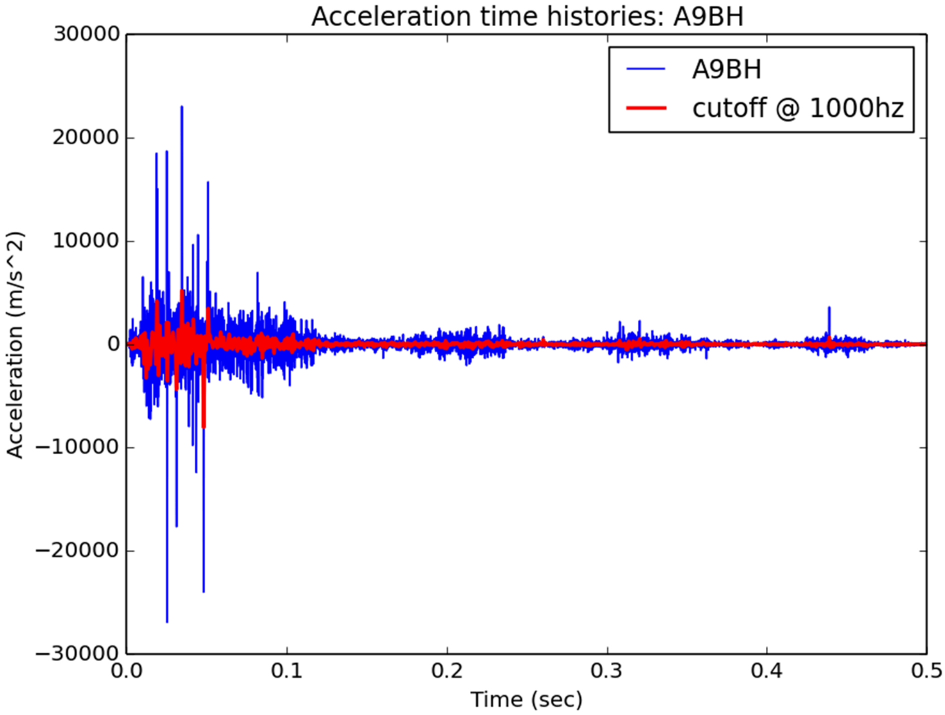

Figure 66: Acceleration versus time for A9H

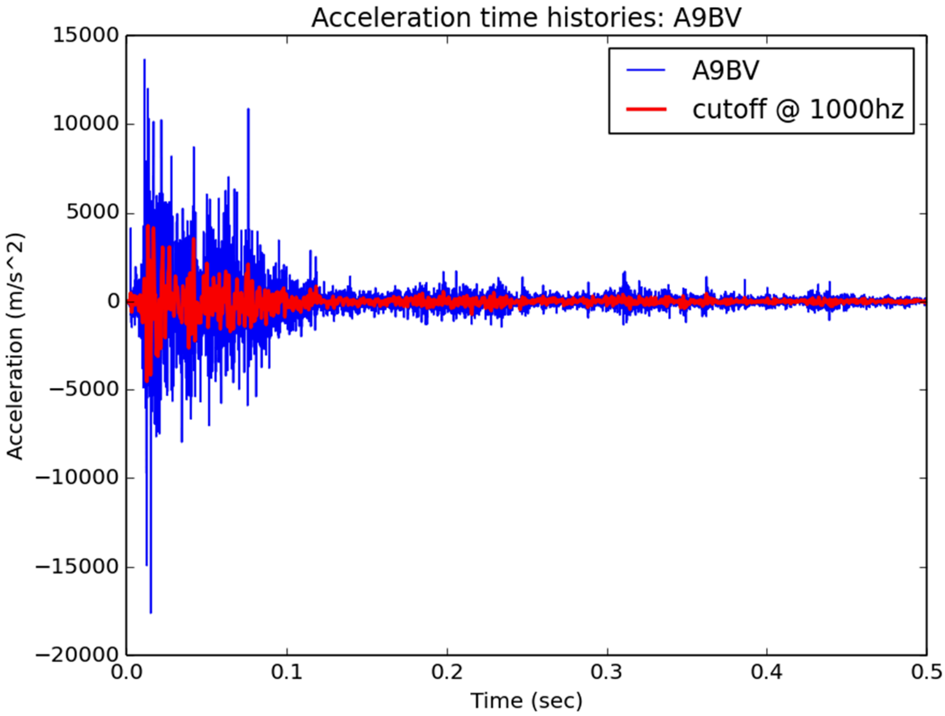

Figure 67: Acceleration versus time for A9V

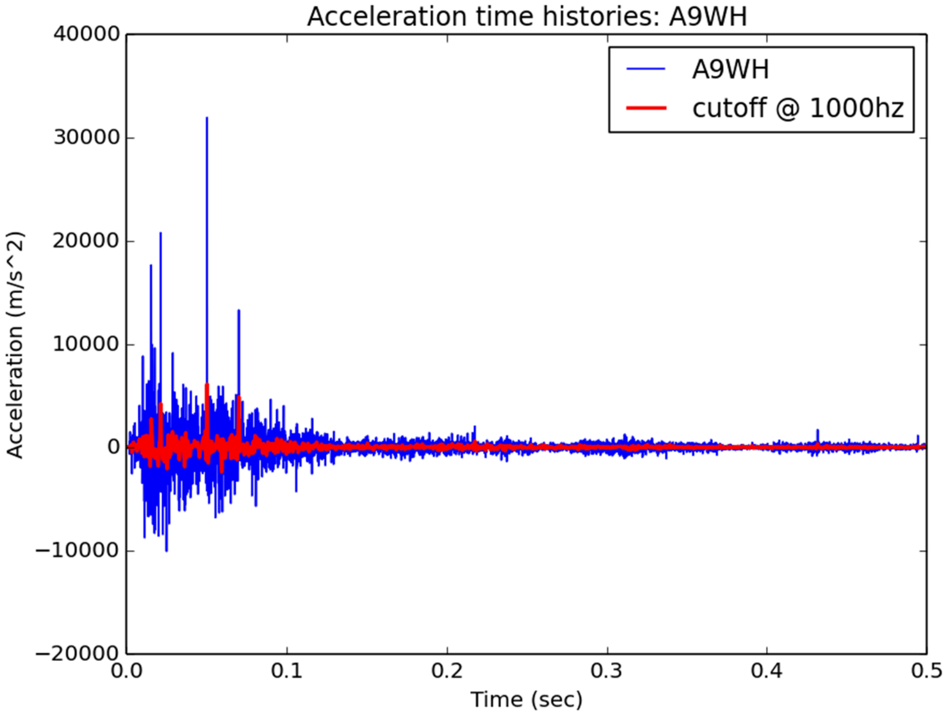

Figure 68: Acceleration versus time for A9WH

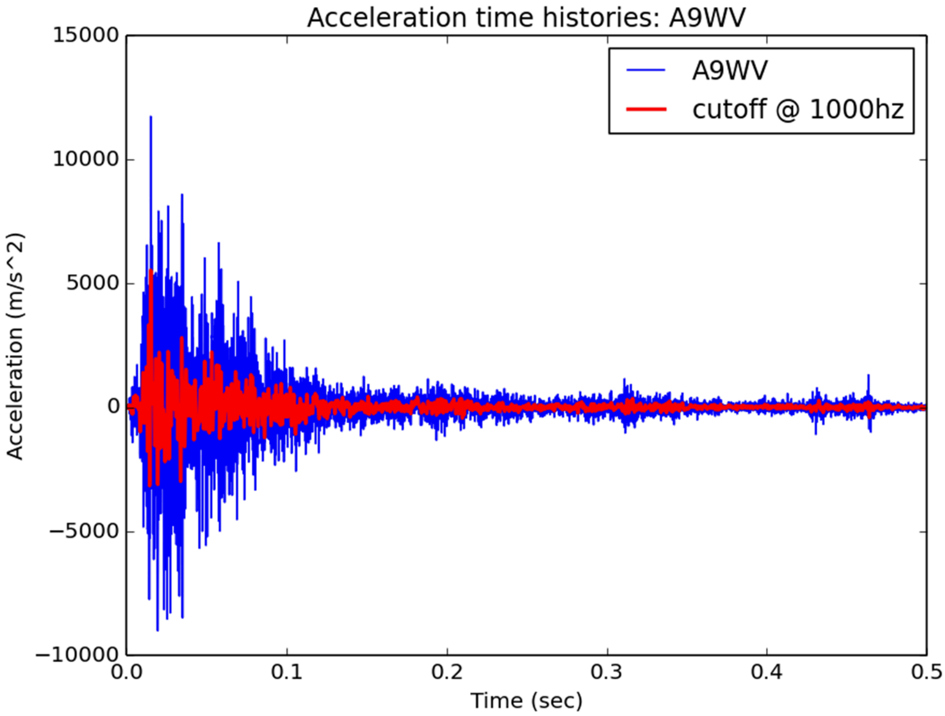

Figure 69: Acceleration versus time for A9WV

3.2.6 Response spectra at 5 % damping

No damping was implemented in this simulation.

3.2.7 Acceleration frequency content analysis (FFT, Power Spectral Density, …)

To assess the acceleration frequency content, Fast Fourier Transform analysis was performed on the filtered acceleration versus time data for the selected output locations and presented in section 3.2.5.2. These results are presented in Figure 70 through Figure 84.

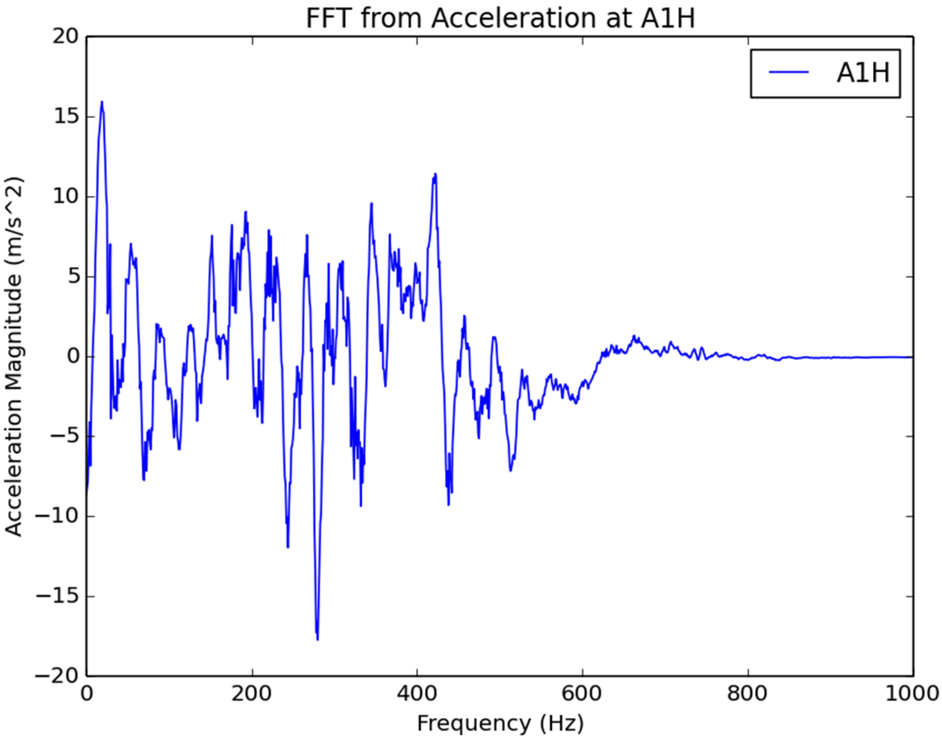

Figure 70: Acceleration Fast Fourier Transform for A1H

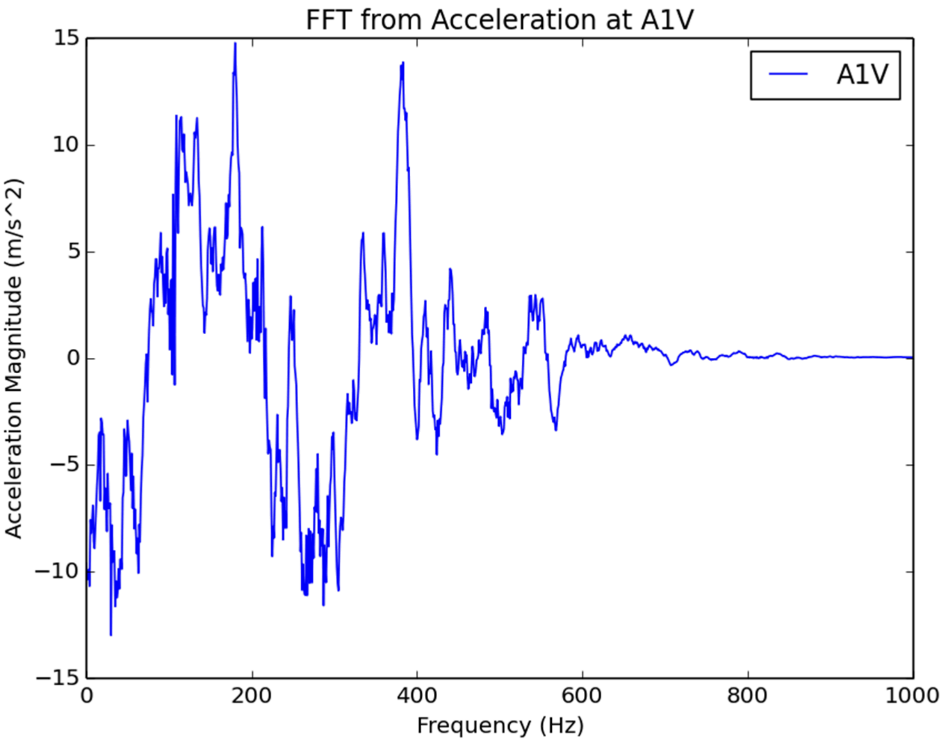

Figure 71: Acceleration Fast Fourier Transform for A1V

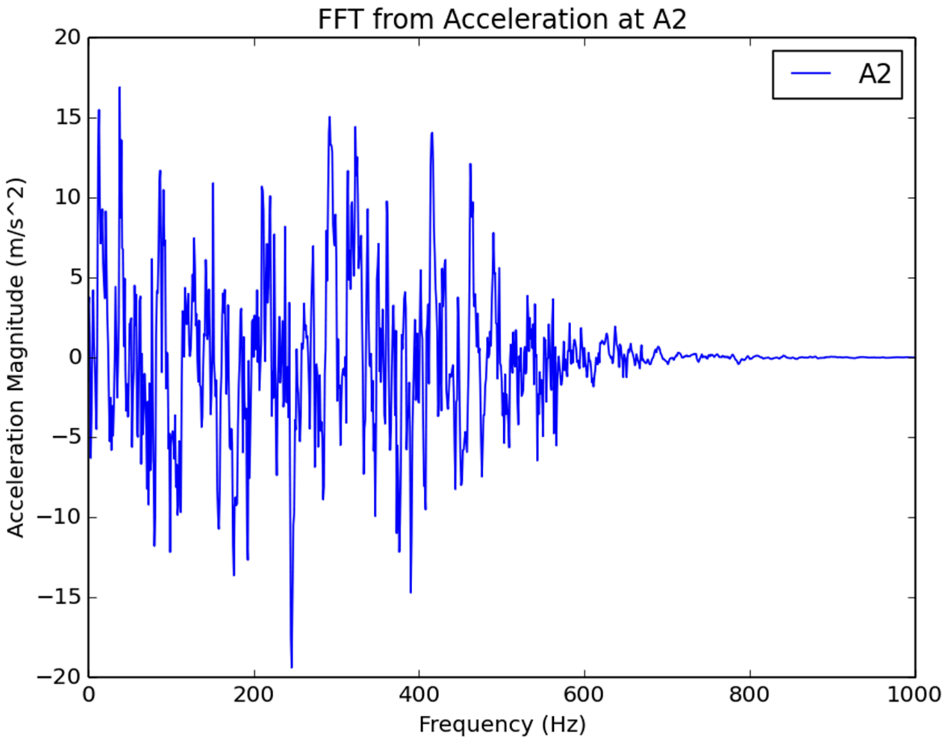

Figure 72: Acceleration Fast Fourier Transform for A2

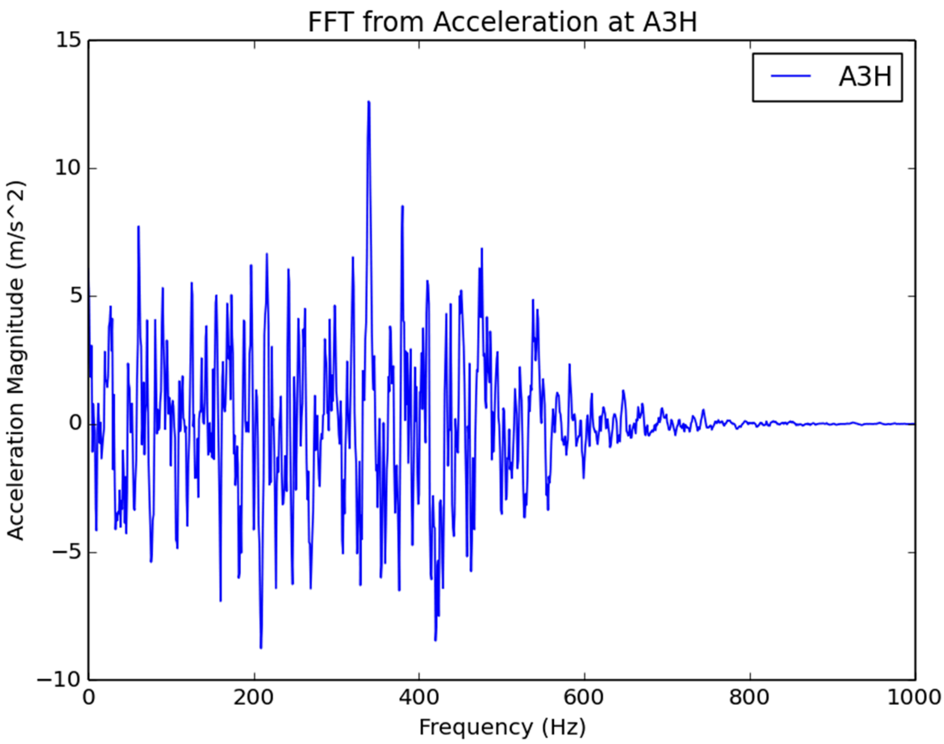

Figure 73: Acceleration Fast Fourier Transform for A3H

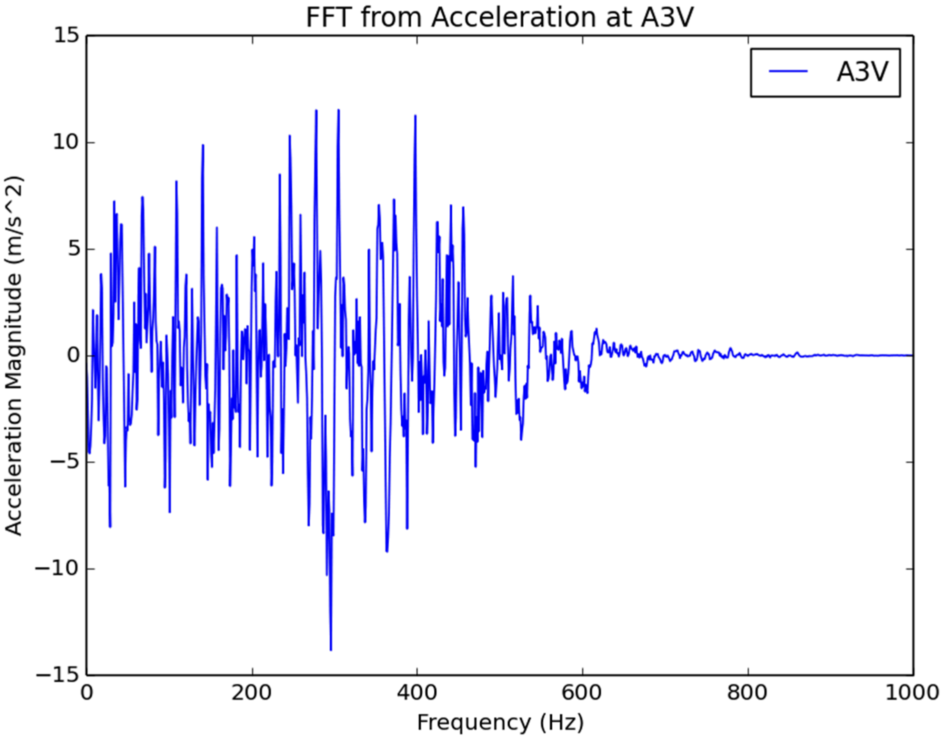

Figure 74: Acceleration Fast Fourier Transform for A3V

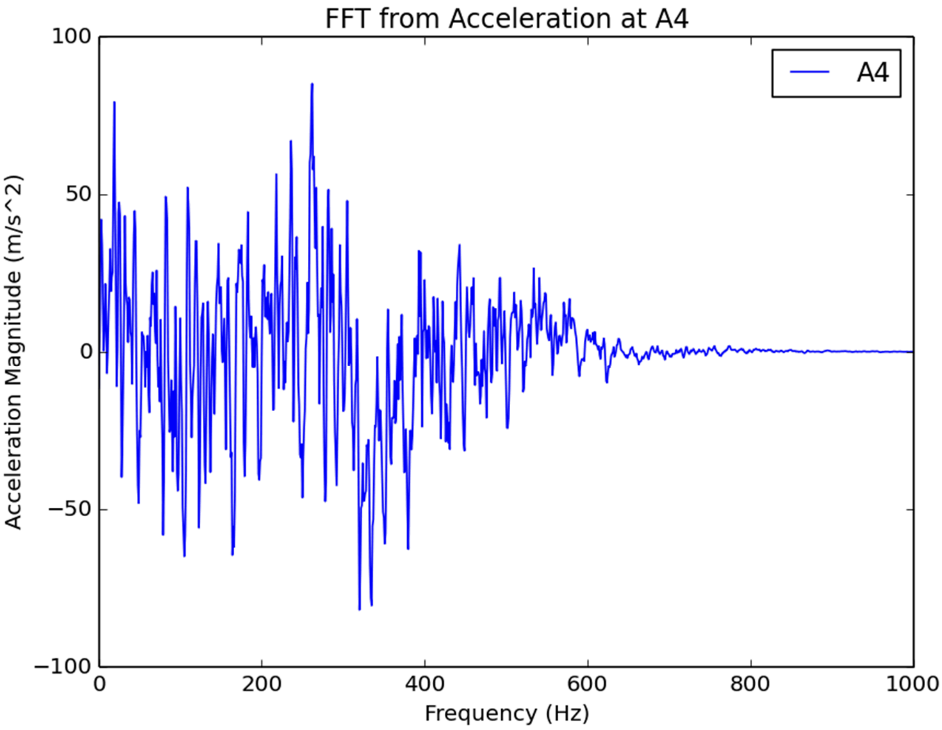

Figure 75: Acceleration Fast Fourier Transform for A4

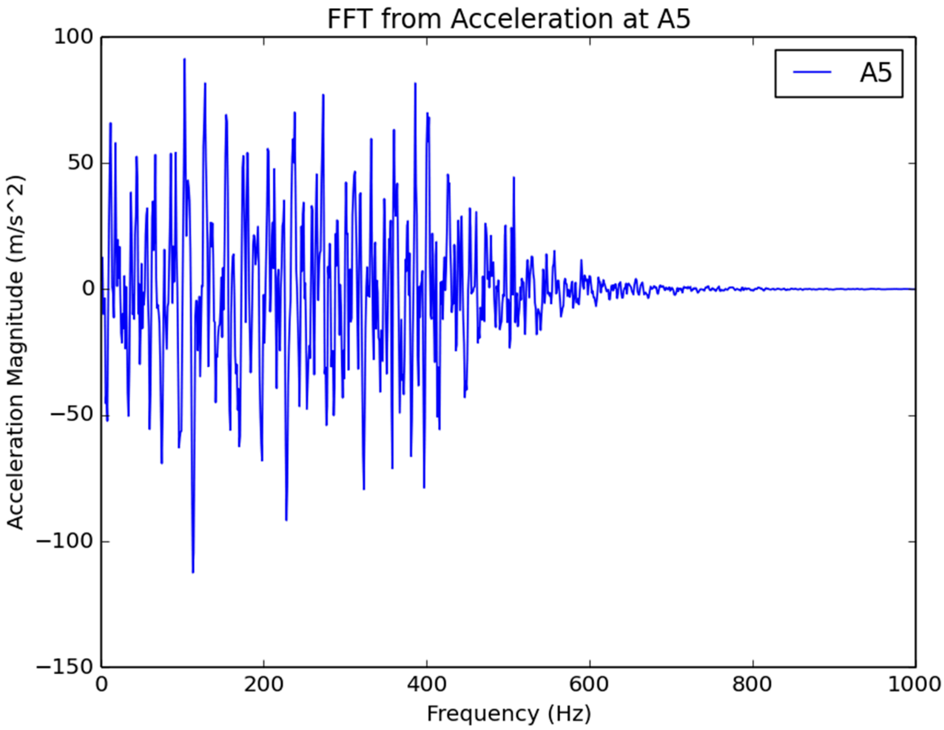

Figure 76: Acceleration Fast Fourier Transform for A5

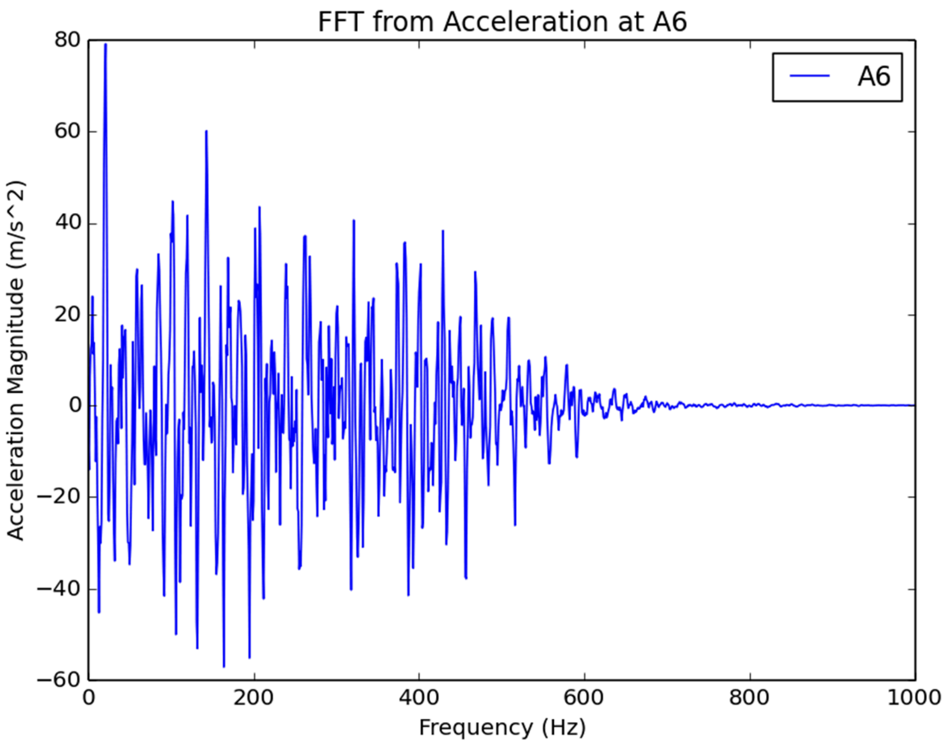

Figure 77: Acceleration Fast Fourier Transform for A6

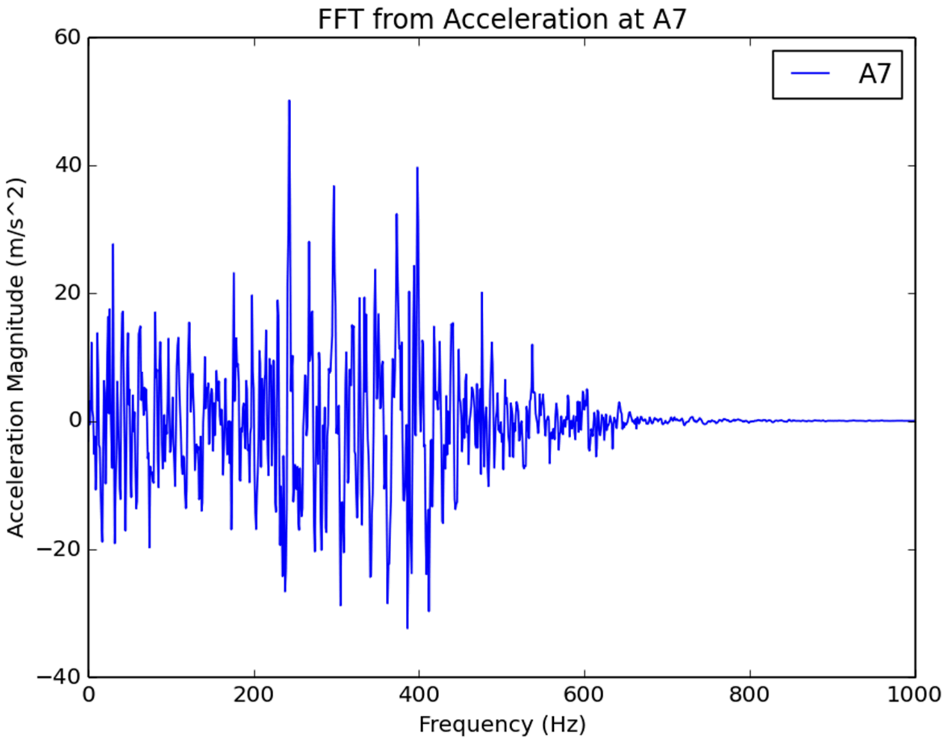

Figure 78: Acceleration Fast Fourier Transform for A7

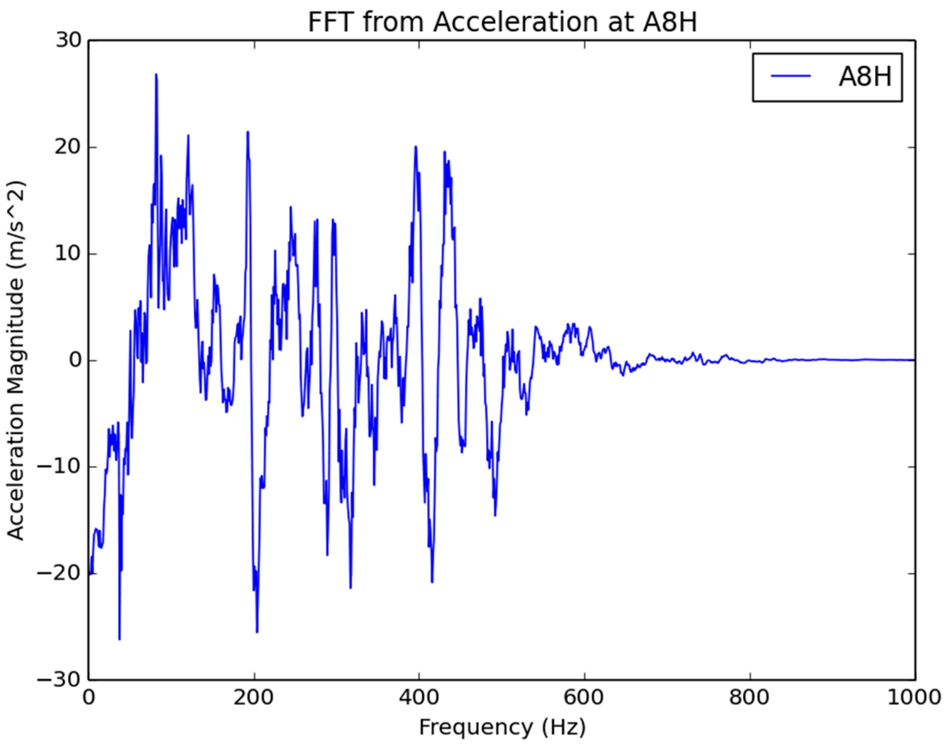

Figure 79: Acceleration Fast Fourier Transform for A8H

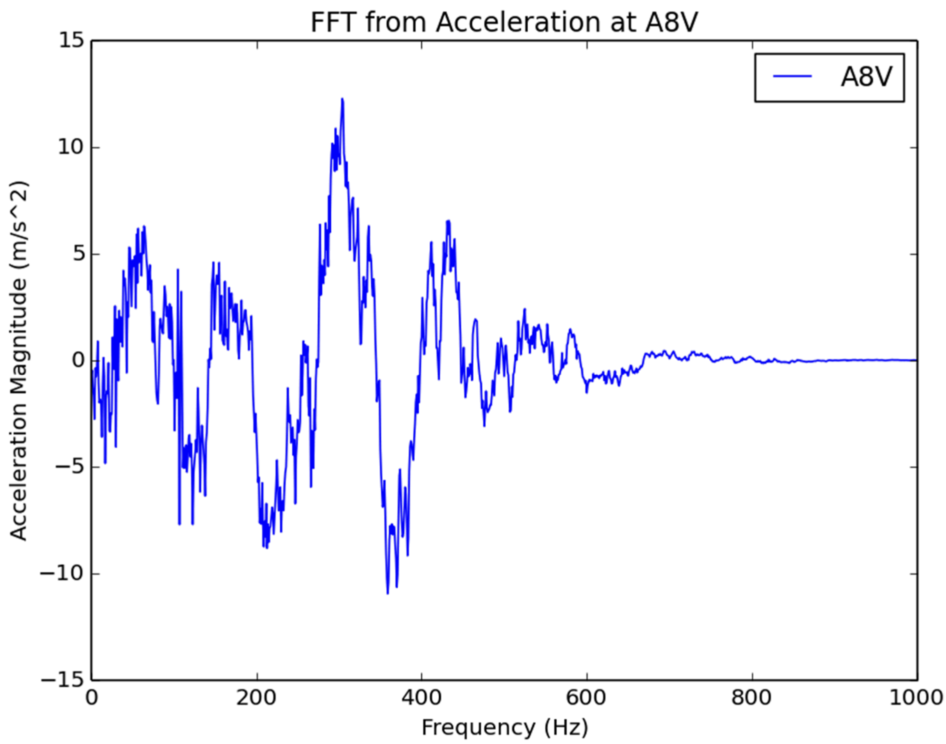

Figure 80: Acceleration Fast Fourier Transform for A8V

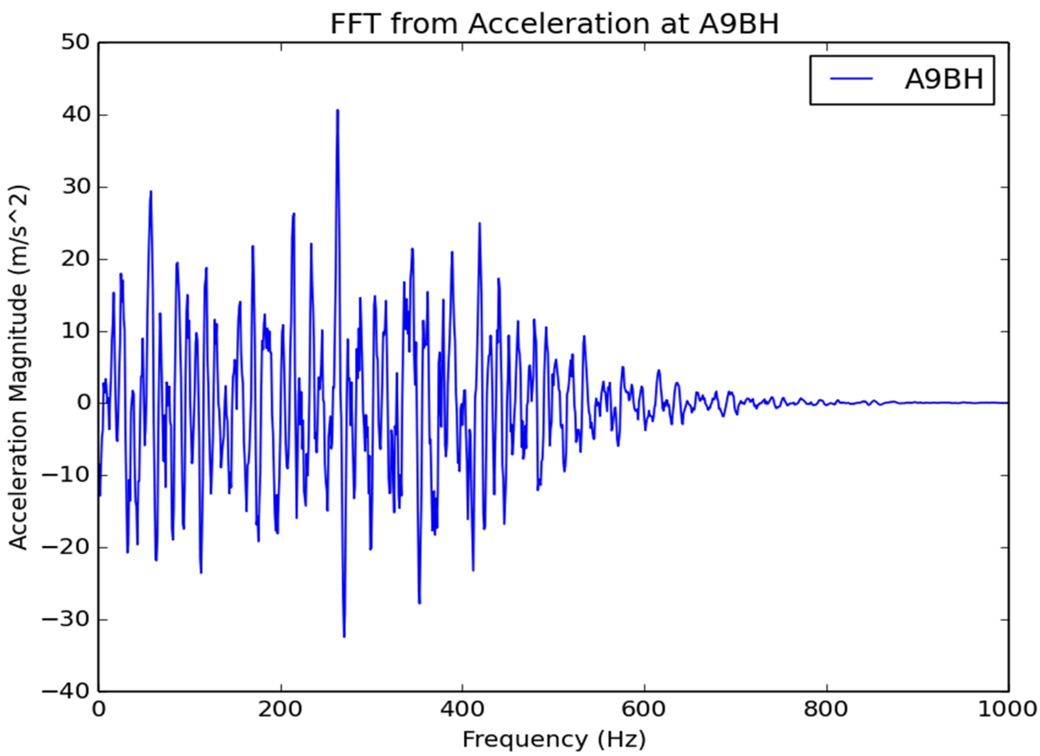

Figure 81: Acceleration Fast Fourier Transform for A9BH

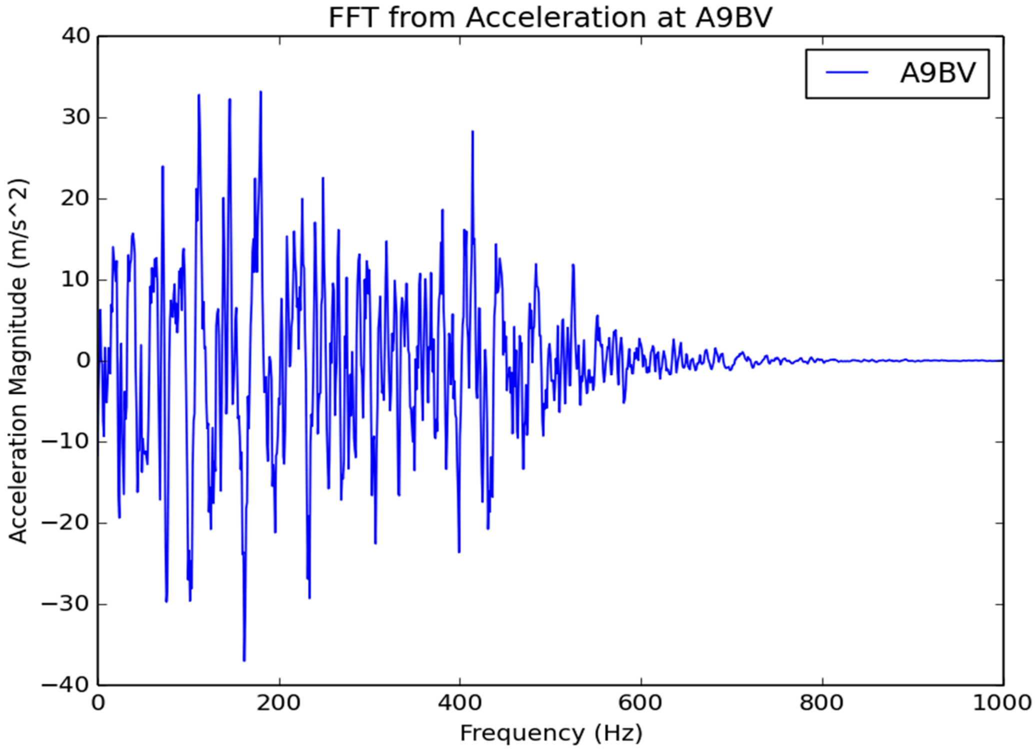

Figure 82: Acceleration Fast Fourier Transform for A9BV

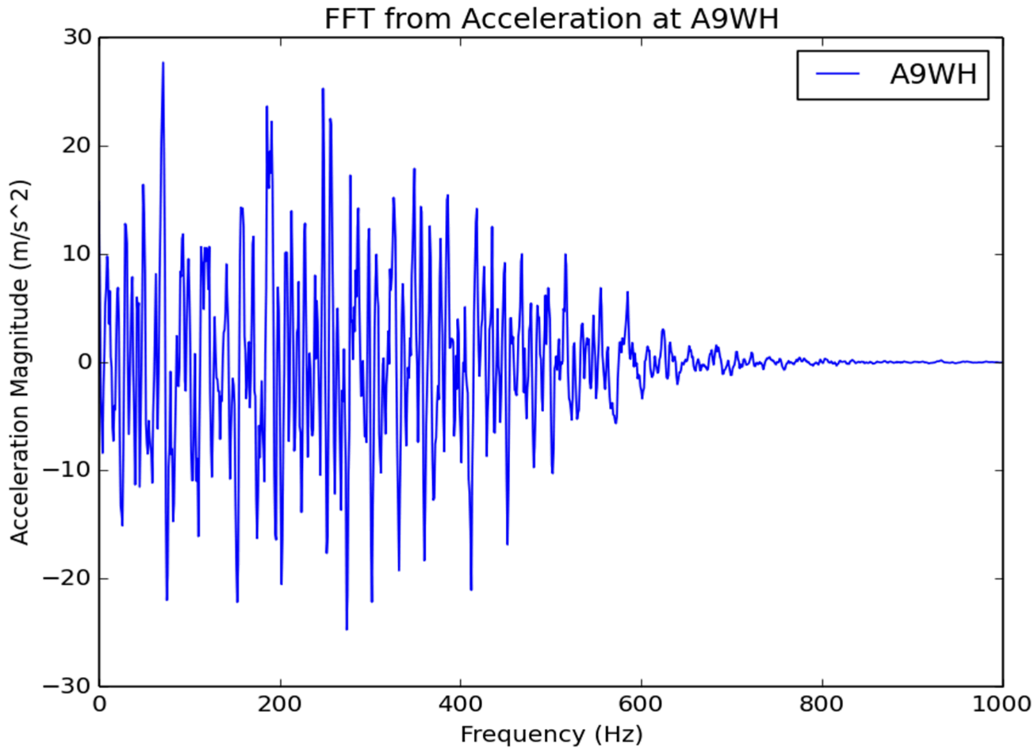

Figure 83: Acceleration Fast Fourier Transform for A9WH

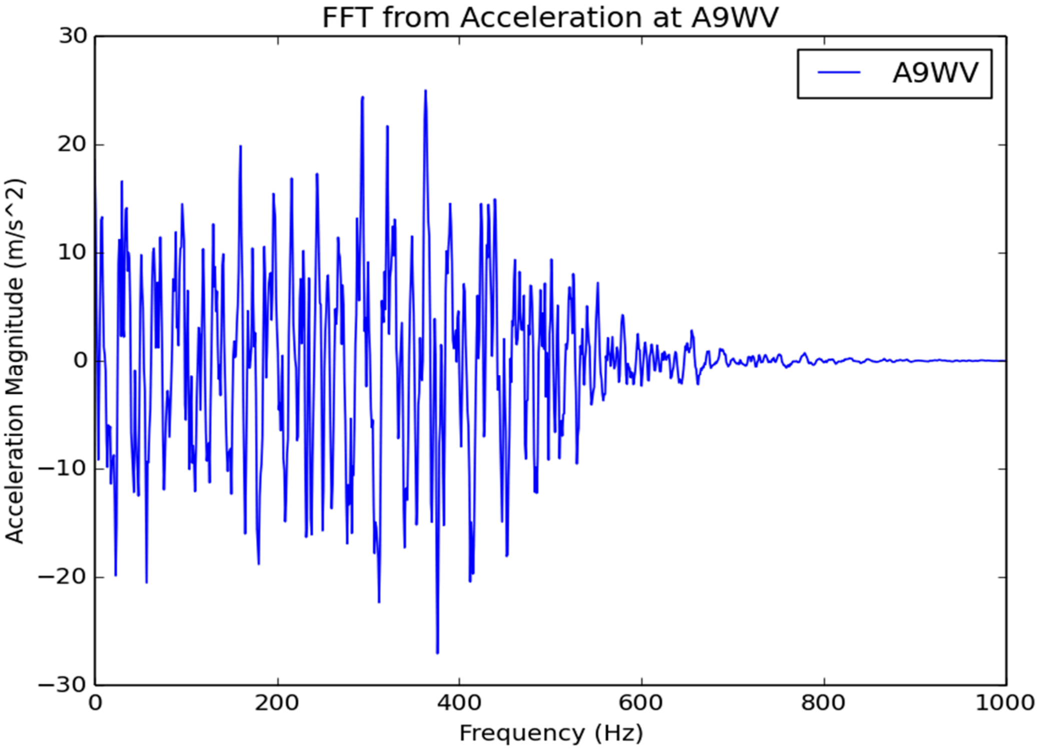

Figure 84: Acceleration Fast Fourier Transform for A9WV

3.3 Pseudo-equipments results

3.3.1 Time histories

3.3.1.1 Displacements

The displacement versus time response for the bolted and welded beams in the model is presented in Figure 85. The 'D10' data corresponds to the bolted beam while the 'D10W' response corresponds to the welded beam.

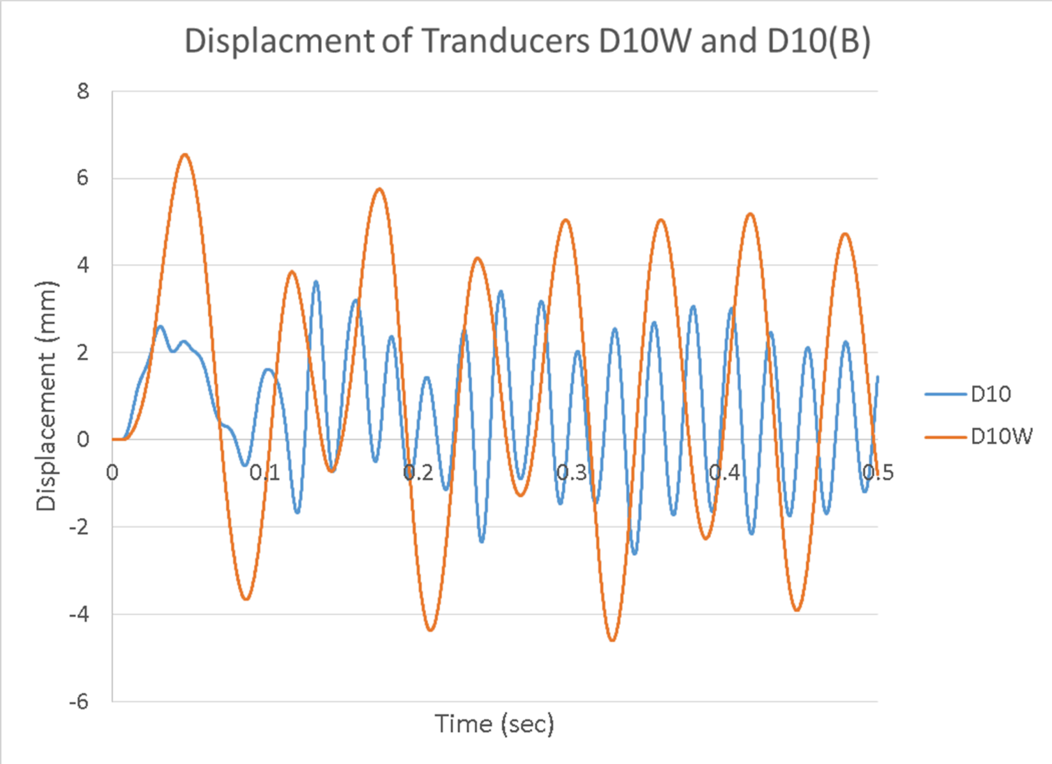

Figure 85: Time displacement history for D10 and D10W

3.3.1.2 Accelerations

Similar to above, the acceleration vs time data was filtered using a Butterworth 4th order low pass filter with a cutoff at 1000 Hz. The filtered and raw data from the simulations for the bolted and welded beams are presented in Figure 86 through Figure 89.

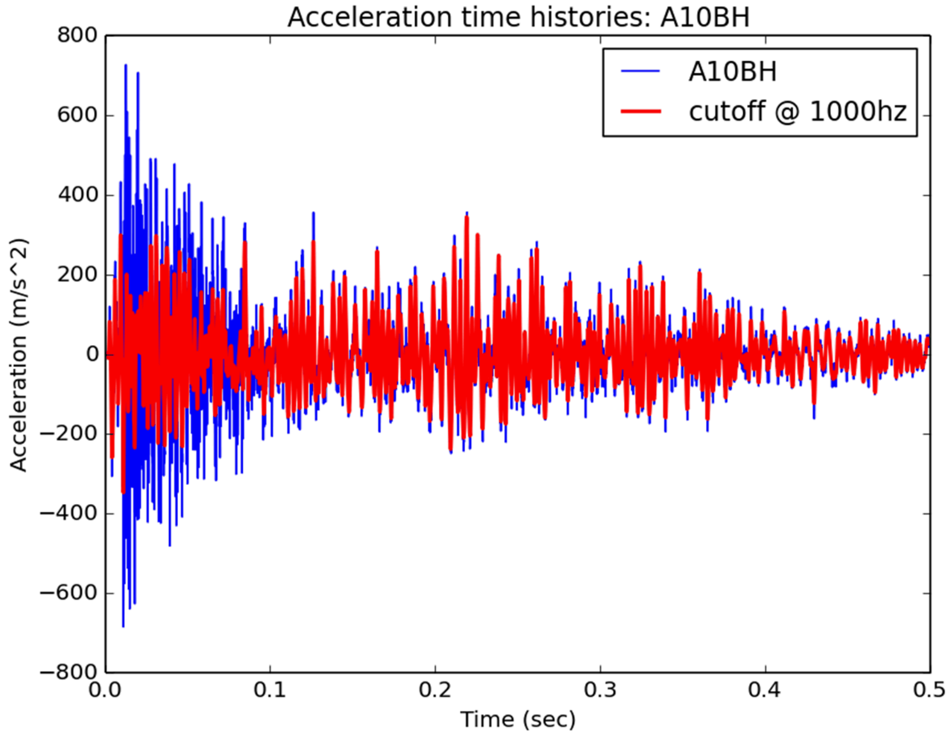

Figure 86: Acceleration versus time for A10BH

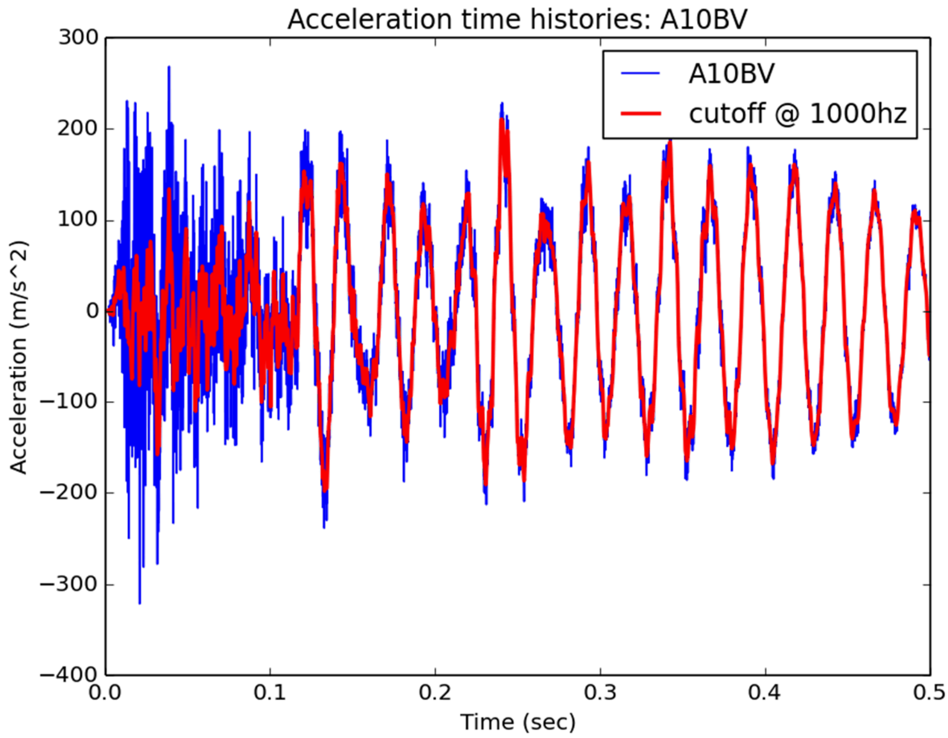

Figure 87: Acceleration versus time for A10BV

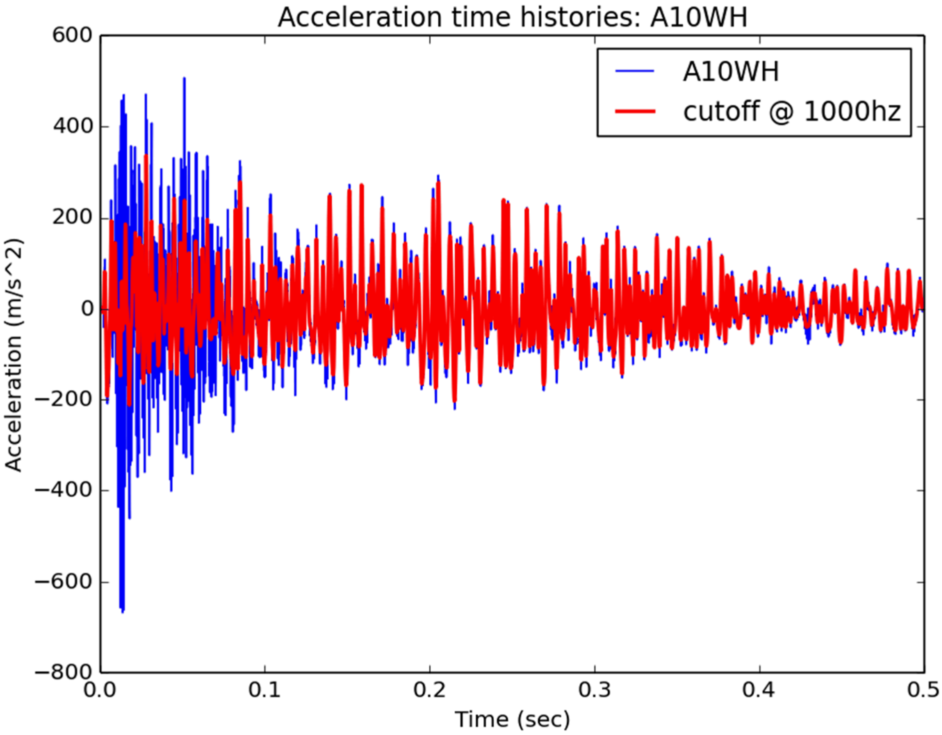

Figure 88: Acceleration versus time for A10WH

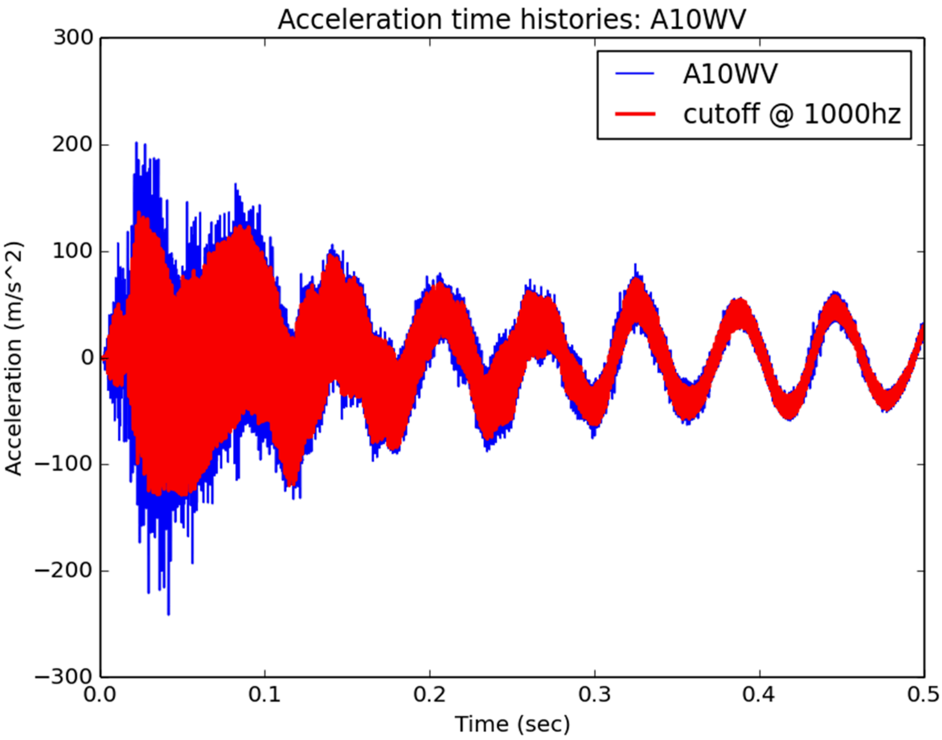

Figure 89: Acceleration versus time for A10WV

3.3.2 Acceleration frequency content analysis

Fast Fourier Transform results from the filtered acceleration data for the bolted and welded beams are shown in Figure 90 through Figure 93.

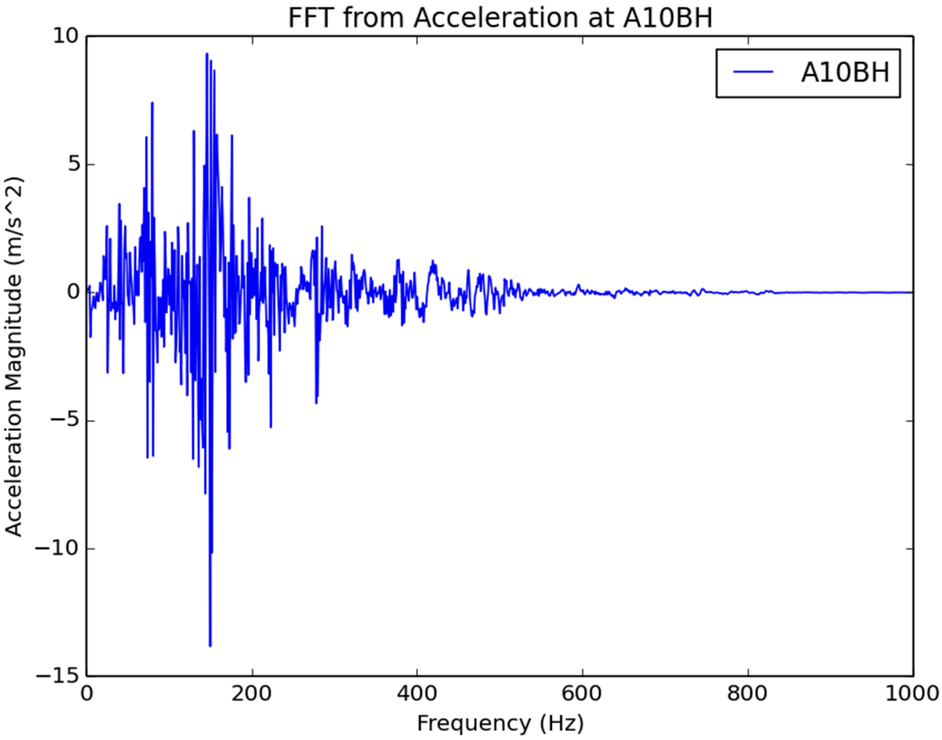

Figure 90: Acceleration Fast Fourier Transform for A10BH

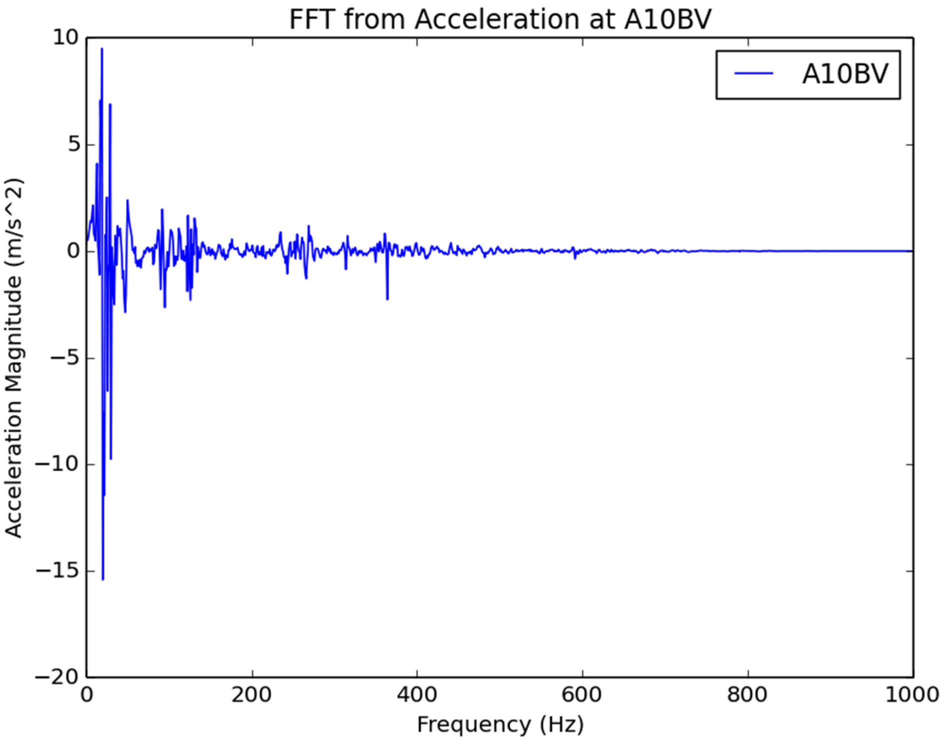

Figure 91: Acceleration Fast Fourier Transform for A10BV

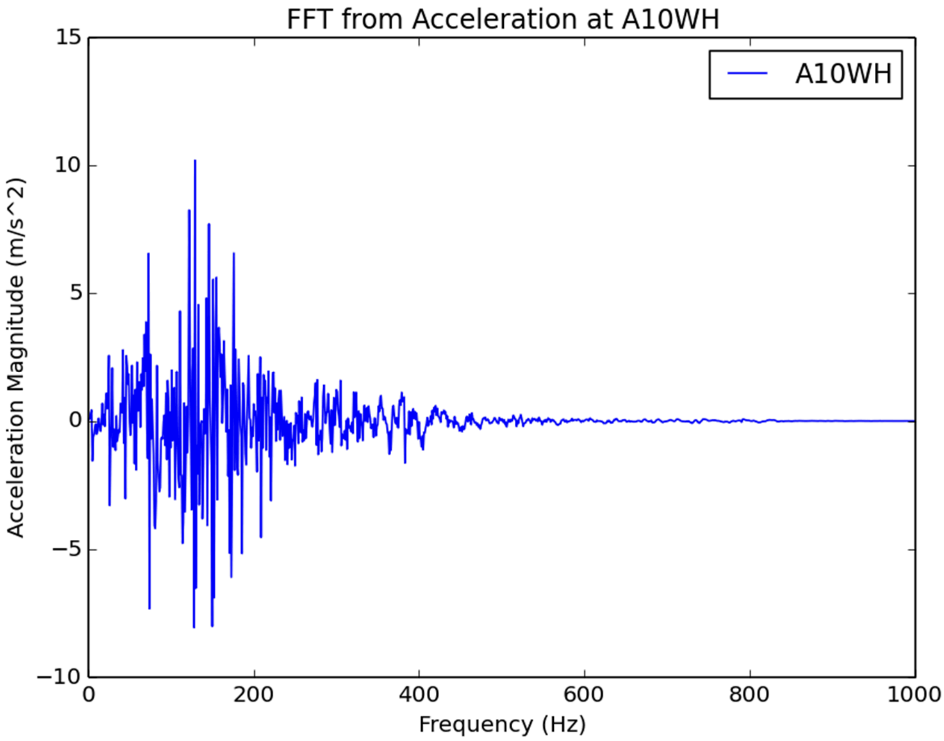

Figure 92: Acceleration Fast Fourier Transform for A10WH

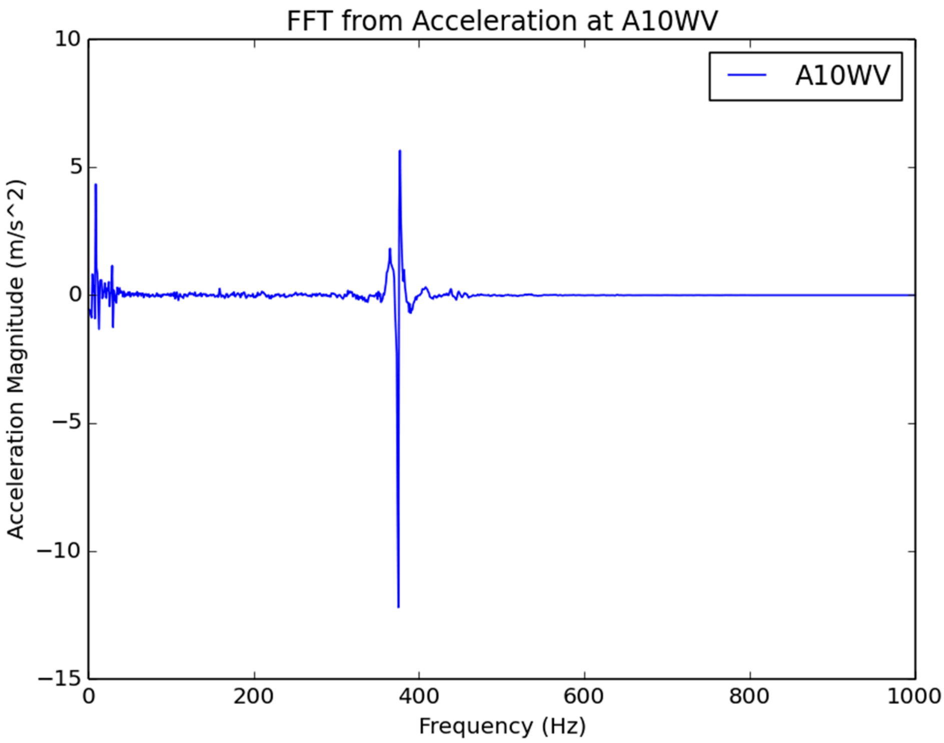

Figure 93: Acceleration Fast Fourier Transform for A10WV

3.4 IRIS III Va test conclusions

The missile did not penetrate the concrete. Damage accrued primarily on the front face and at corners in the concrete, including any corners where a steel plate was attached. There was a vast difference in behavior between the two pseudo-equipments in both oscillation frequency and amplitude; this could be due to the fact that the I-beam with a welded connection was 100 mm longer than the I-beam with a bolted connection, and the pseudo-equipment masses were both the same.

4. IRIS III results : 2nd impact at velocity Vb = 90 m/s

The second 90 m/s impact simulation was nearly identical to the first Va 90 m/s simulation. The difference between the Va and Vb simulations is that the missile in the Vb simulation impacted the concrete with a 1 mm eccentricity in the x-z plane.

4.1 Missile results

4.1.1 Crushing results (crushing length, …)

The missile crush up results are shown below in Table 8 and Figure 94.

Table 8: Missile Crushing Results, 90 m/s

Original length (including hemispherical head)	2125 mm
Total length after crush	1553 mm
Crushed length H_T	1263 mm
Non-crushed length L_T	290 mm

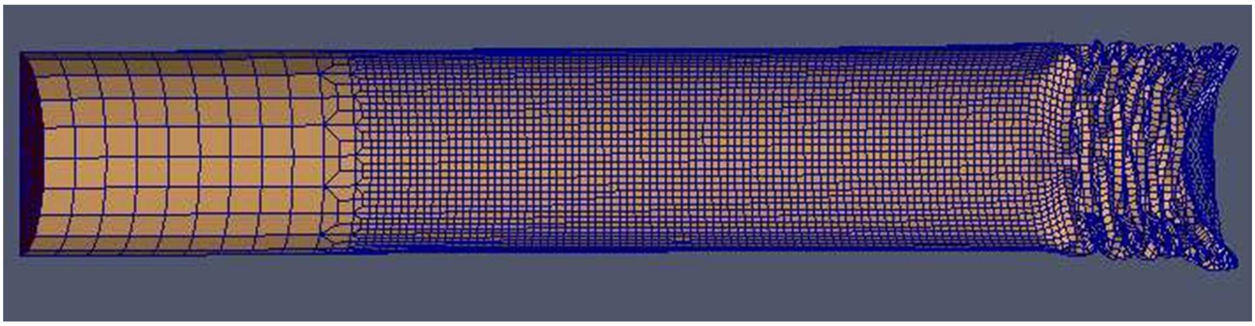

Figure 94: 90 m/s eccentric missile at t_{imp}

4.1.2 Time histories (Displacement, Velocity, Acceleration)

The time history plots pertaining to the missile behavior are shown below in Figure 95 through Figure 97.

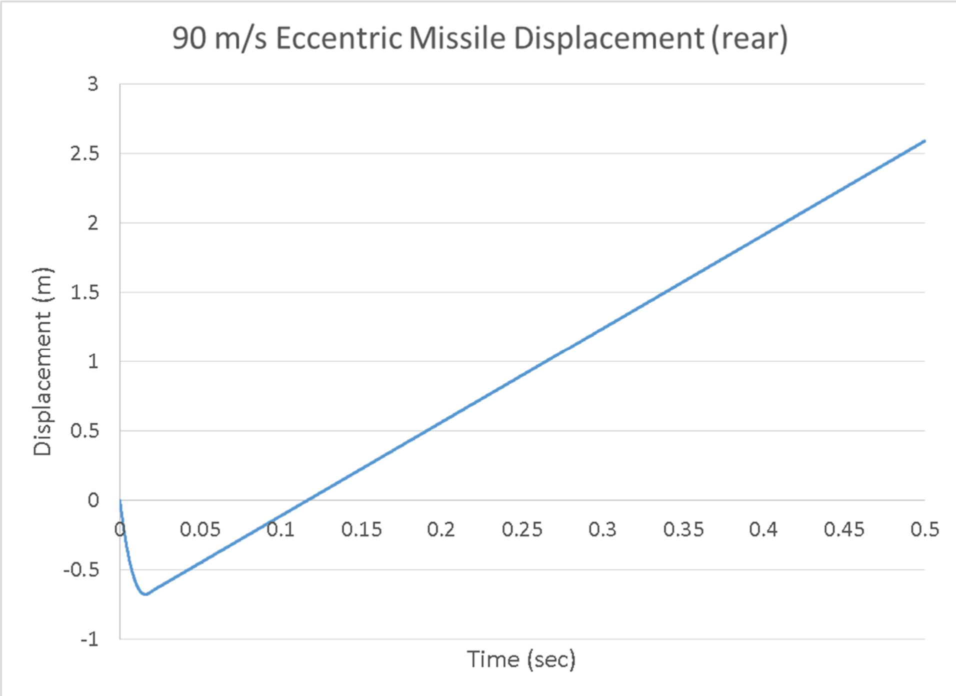

Figure 95: Displacement of the rear end of the 90 m/s eccentric missile

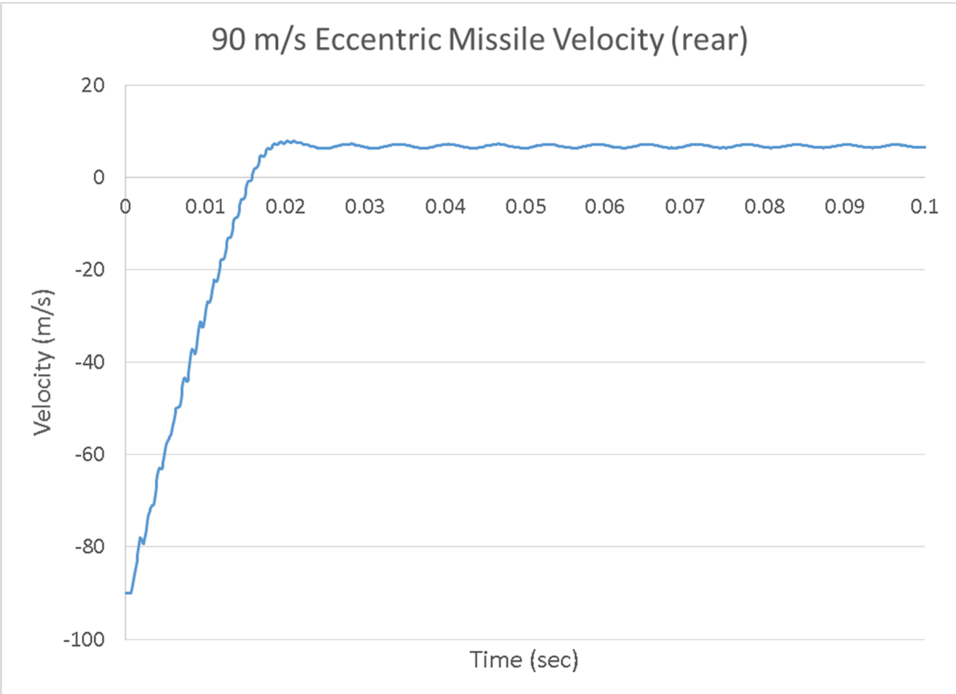

Figure 96: Velocity of the rear end of the 90 m/s eccentric missile

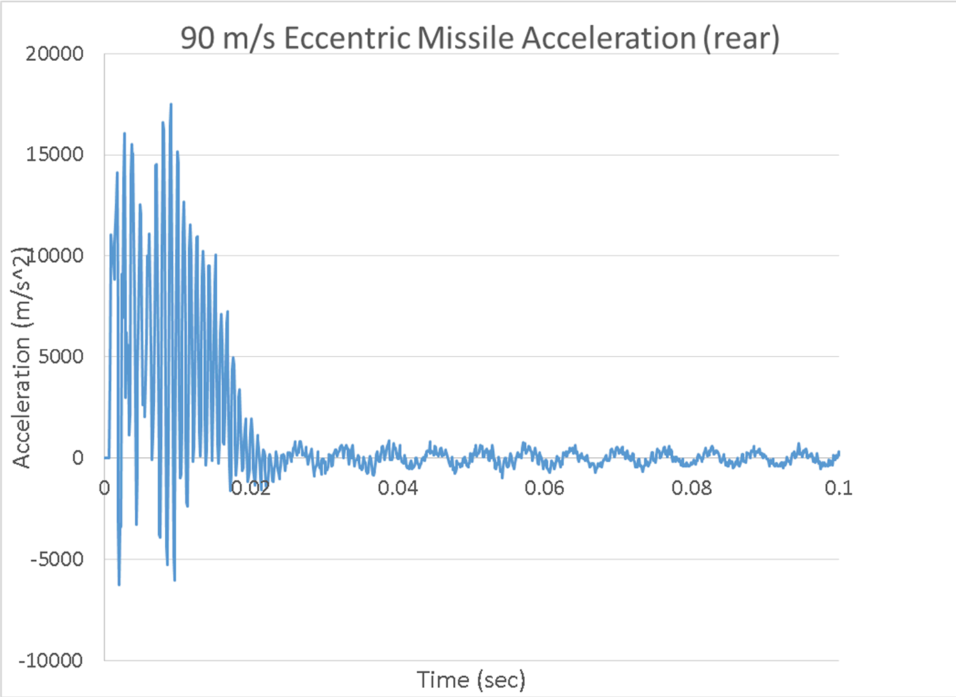

Figure 97: Acceleration of the rear end of the 90 m/s eccentric missile

4.1.3 Contact force time history and impulse

The contact force versus time and impulse versus time plots are shown in Figure 98 and Figure 99

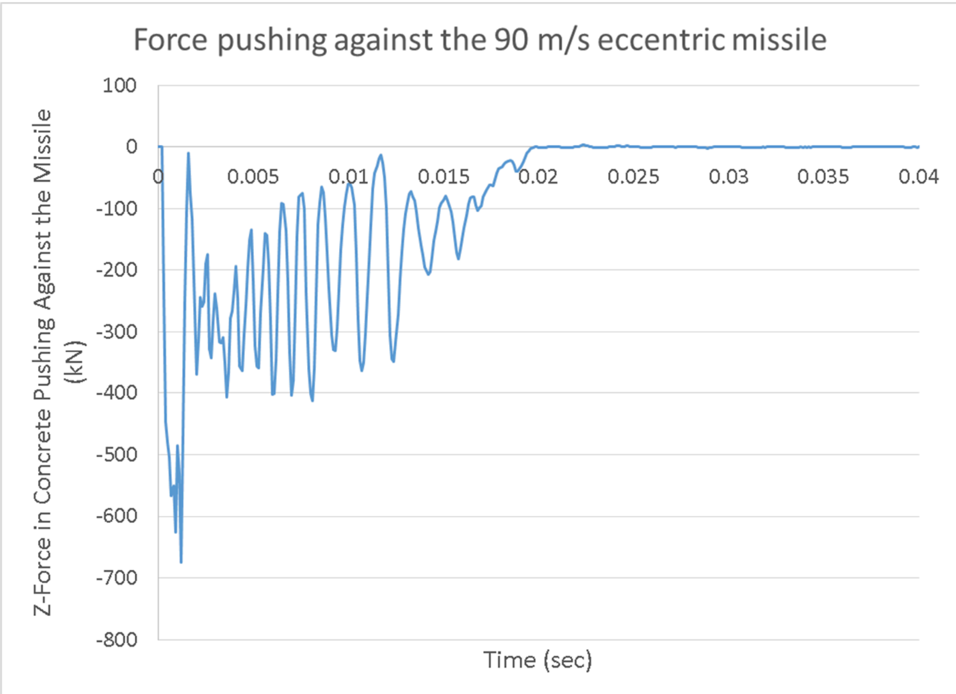

Figure 98: Force pushing against the 90 m/s eccentric missile

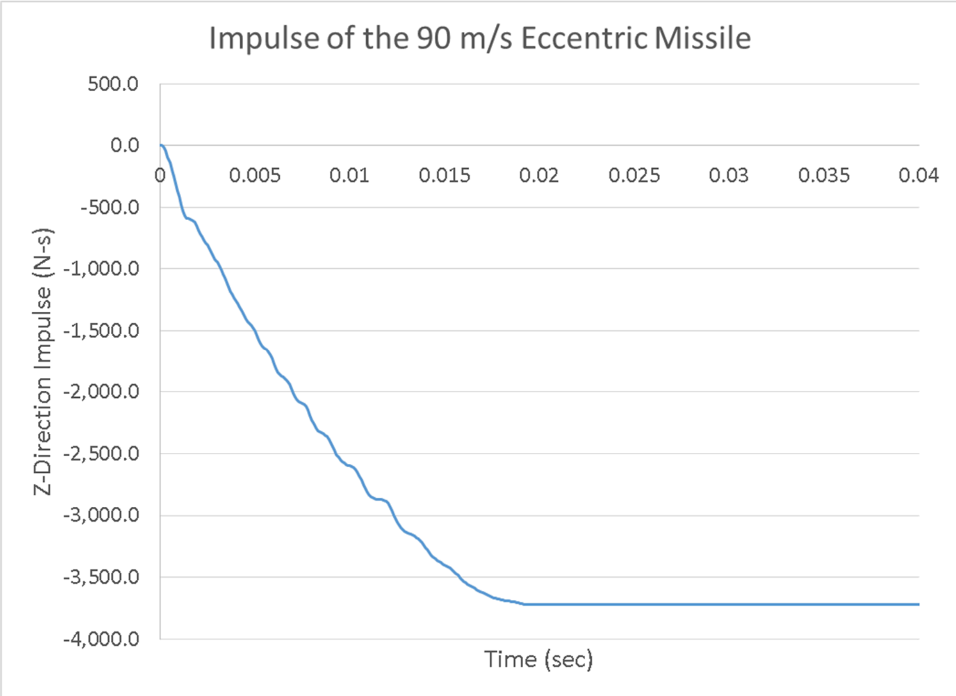

Figure 99: Impulse of the 90 m/s eccentric missile

4.2 Mock-up results

4.2.1 Global results

Calculation results from the first 90 m/s impact showing concrete damage are represented in Figure 100 through Figure 105. Note that the support pedestals have been removed from the visualization (though they were included in the simulation) to increase visibility to the concrete. Damage is plotted in these figures with damage = 1.0 representing fractured concrete.

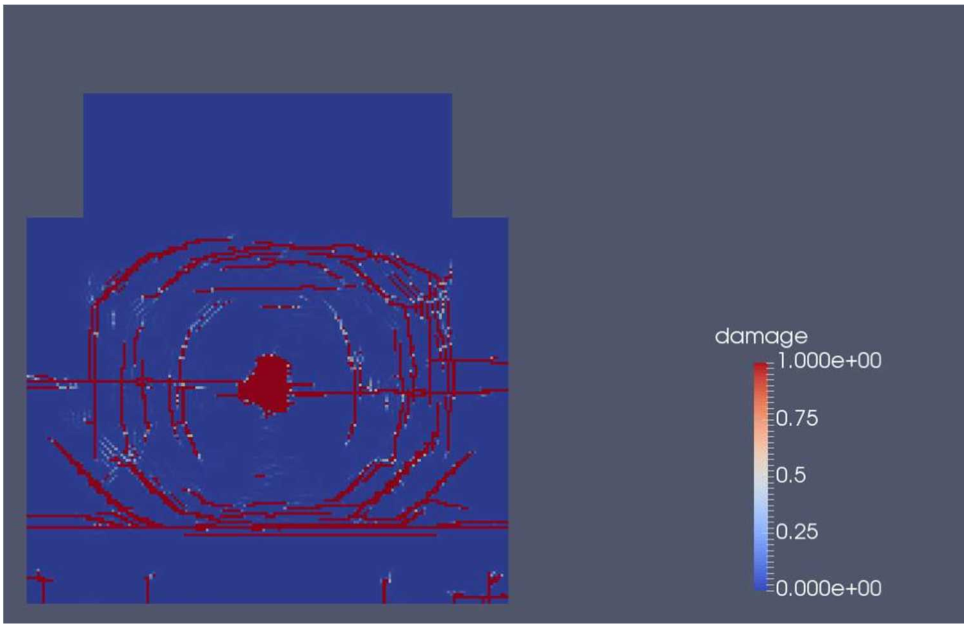

Figure 100: Damage on the front face of the mock-up from the 90 m/s eccentric missile

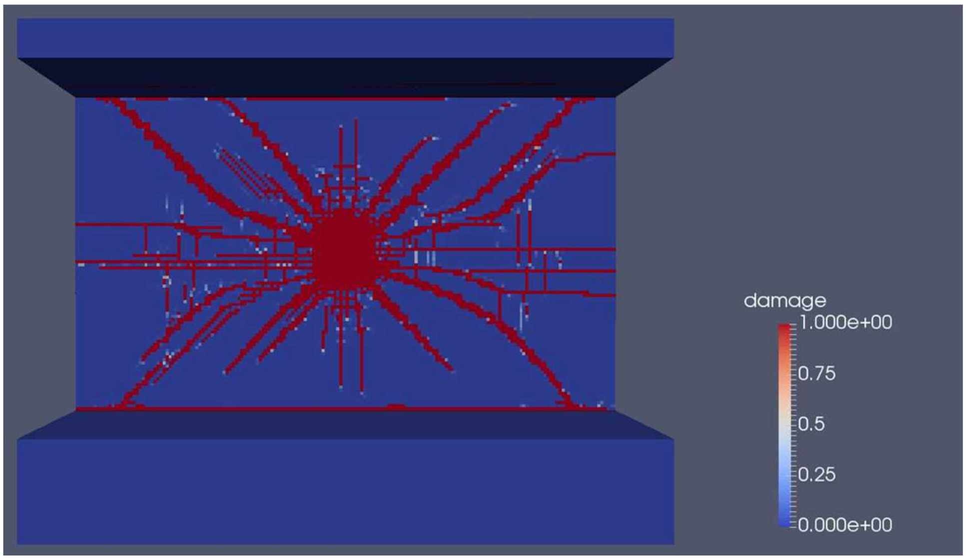

Figure 101: Damage on the back of the front face of the mock-up from the 90 m/s eccentric missile

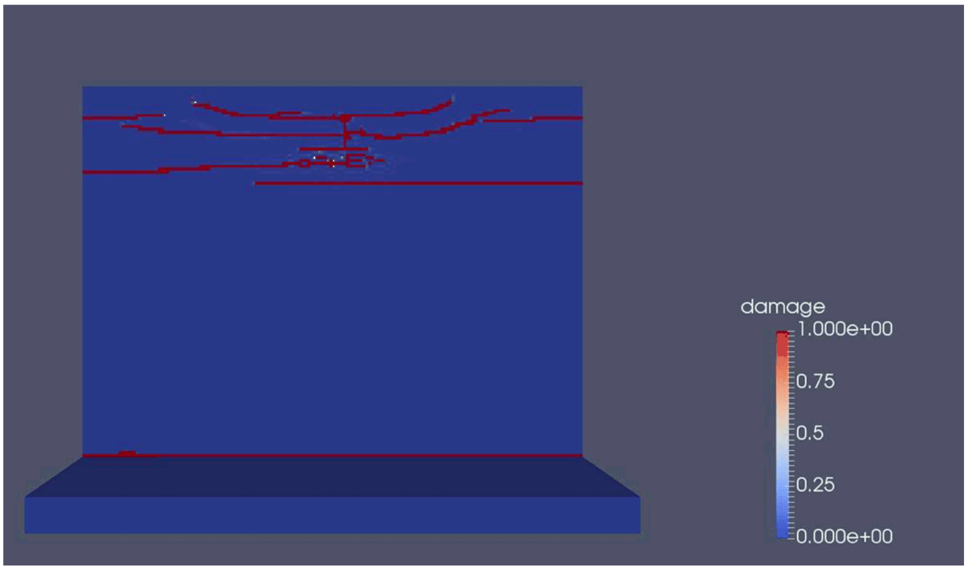

Figure 102: Damage on the top faces of the mock-up from the 90 m/s eccentric missile

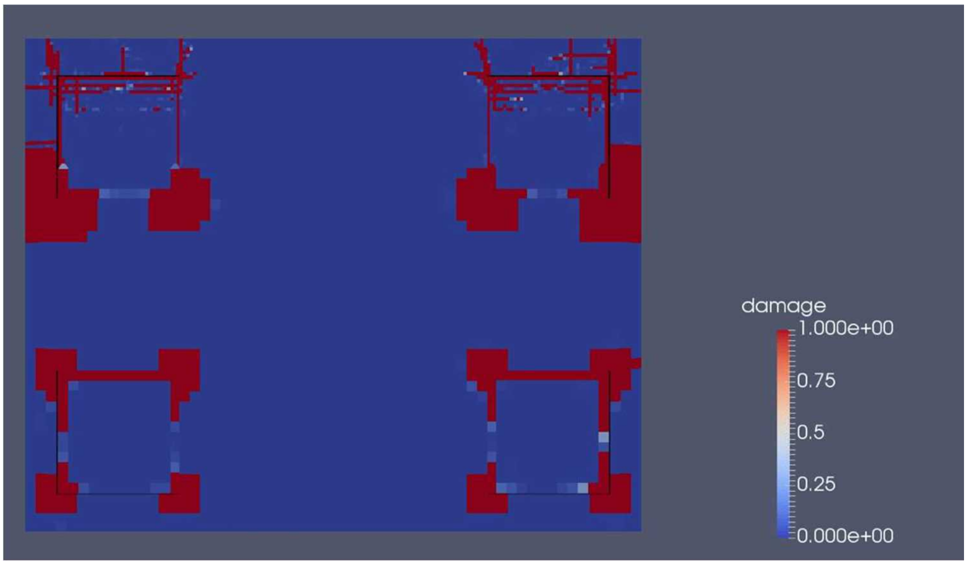

Figure 103: Damage on the bottom face of the mock-up from the 90 m/s eccentric missile

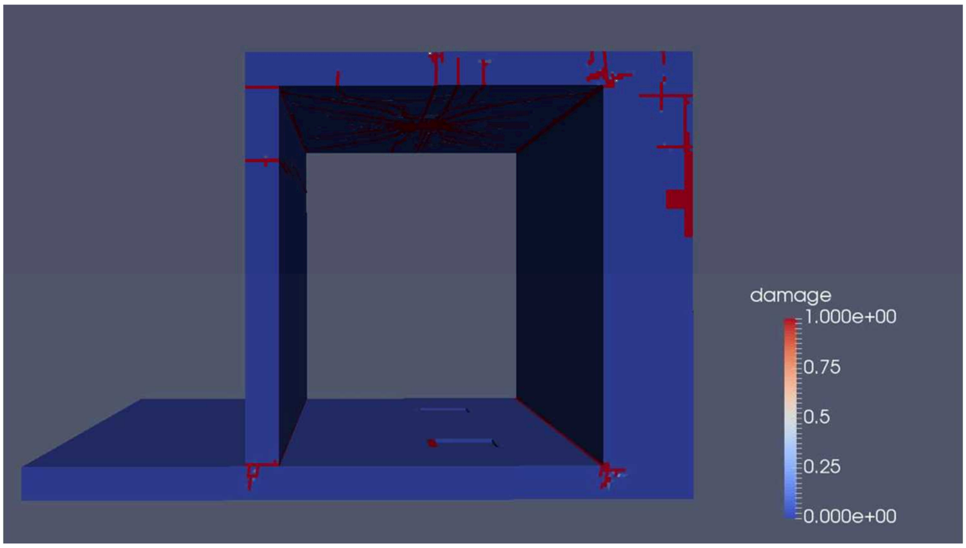

Figure 104: Damage on the side face of the mock-up from the 90 m/s eccentric missile

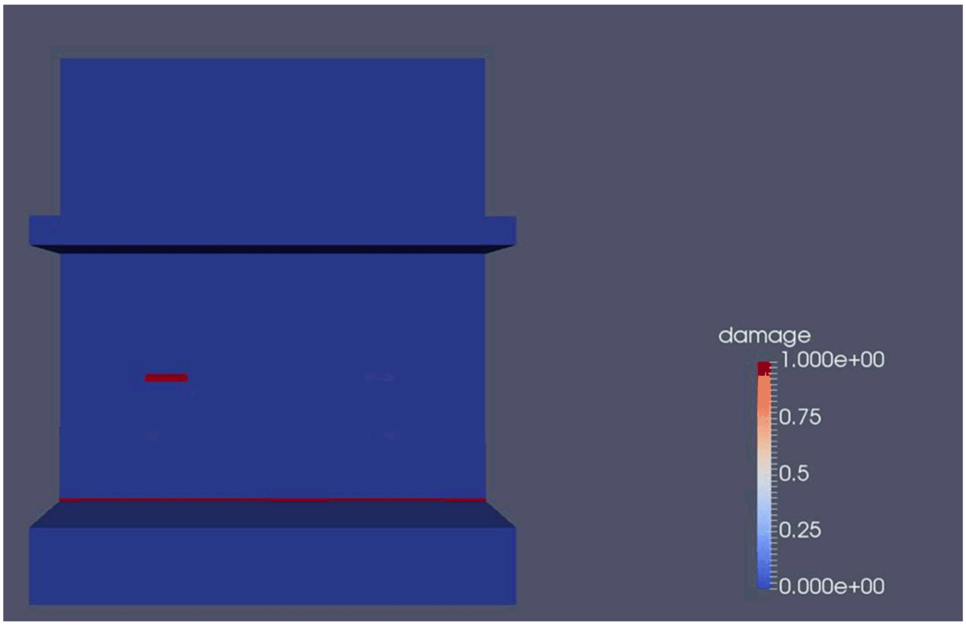

Figure 105: Damage on the front face of the back wall of the mock-up from the 90 m/s eccentric missile

The final displacements in the concrete are shown in Figure 106 and Figure 107.

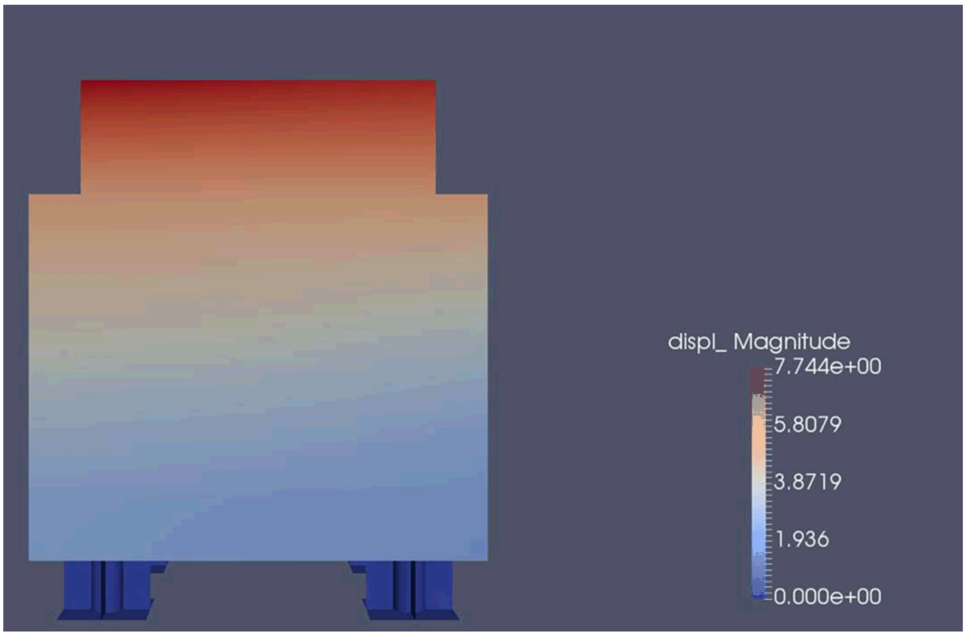

Figure 106: Front view of the final displacements of the mock-up from the 90 m/s eccentric missile (mm)

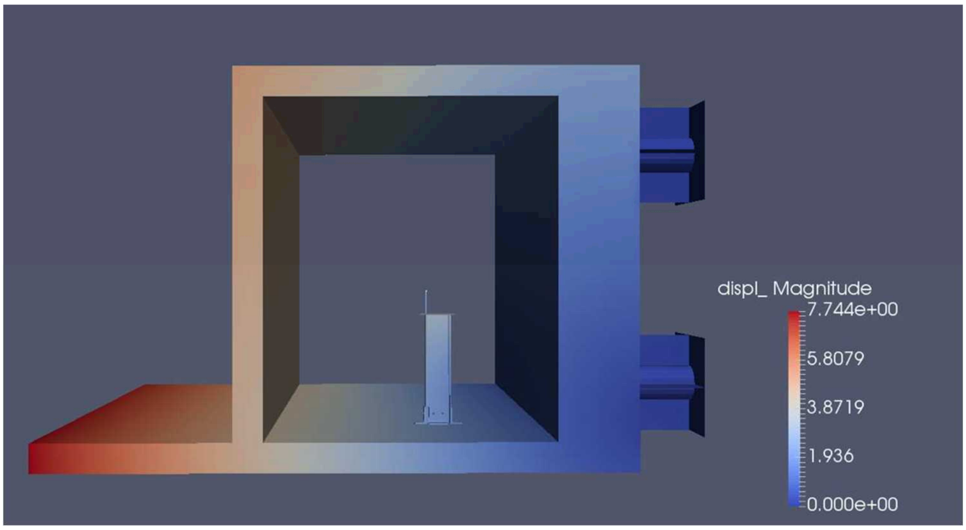

Figure 107: Side view of the final displacements of the mock-up from the 90 m/s eccentric missile (mm)

4.2.2 Concrete strains (at sensors locations)

The concrete strain values corresponding to the requested output locations are presented in Table 9.

Table 9: Concrete Strains at Selected Output Locations

Sensor	Peak Displacement (mm)	Final Displacement (mm)	Sensor	Peak Displacement (mm)	Final Displacement (mm)
D01	-6.94	-2.65	D6V	2.95	-0.25
D02	-6.94	-2.74	D7	-17.0	-7.43
D03	-8.75	-3.48	D7L	-17.0	-7.41
D1	-9.91	-4.13	D8HX	-0.21	-.06
D2	4.01	1.13	D8V	6.67	2.08
D3	-10.7	-4.50	D8HZ	-2.12	-0.77
D3L	-10.7	-4.51	D9	-4.77	-1.84
D4H	-2.24	-0.70	D9L	-4.77	-1.84
D4V	6.72	1.97	D9W	-4.78	-1.79
D5	3.22	0.89	D10	4.71	1.91
D6H	-1.01	-0.32	D10W	6.63	-1.93

4.2.3 Rebars strains

The rebar strain values corresponding to the requested output locations are presented in Table 10

Table 10: Rebar Strains at Selected Output Locations

Sensor	Peak Strain (με)	Final Strain (με)	Sensor	Peak Strain (με)	Final Strain (με)
G0H	750	-0.9	G3V	337	38.5
G0V	1265	-10.8	G4V	861	162
G1V	674	-25.7	G5V	248	80.1
G2V	-250	42.6	G6V	156	-23.6

4.2.4 Reaction forces at supports locations

The reaction forces at the supports are summarized in Table 11.

Table 11: Reaction Forces

Support Location	Peak Force (kN)	Final Force (kN)
Front left	293	67
Front right	321	41.2
Rear left	-319	-11.7
Rear right	300	43.0

As noted previously, to reduce the high-frequency noise believed to be associated with numerical effects, the reaction force versus time data was filtered using a 4th order low pass Butterworth filter with a cutoff frequency of 1000 Hz. The reaction force vs time responses for the four supports are shown in Figure 108 through Figure 111.

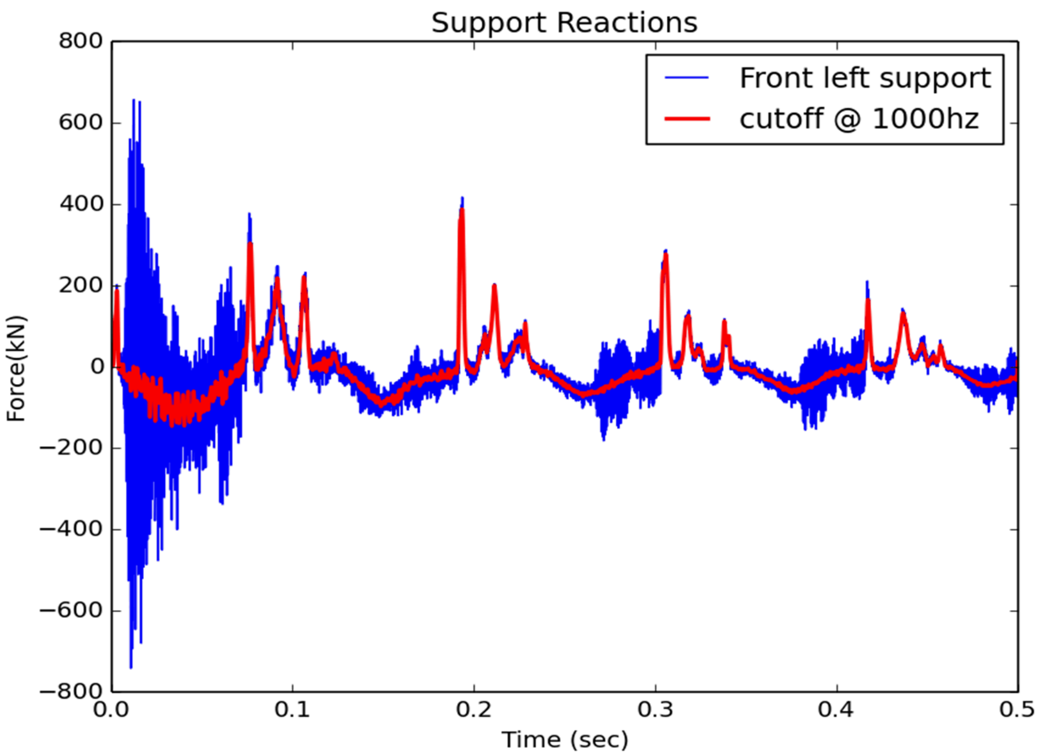

Figure 108: Front left support reaction force vs time

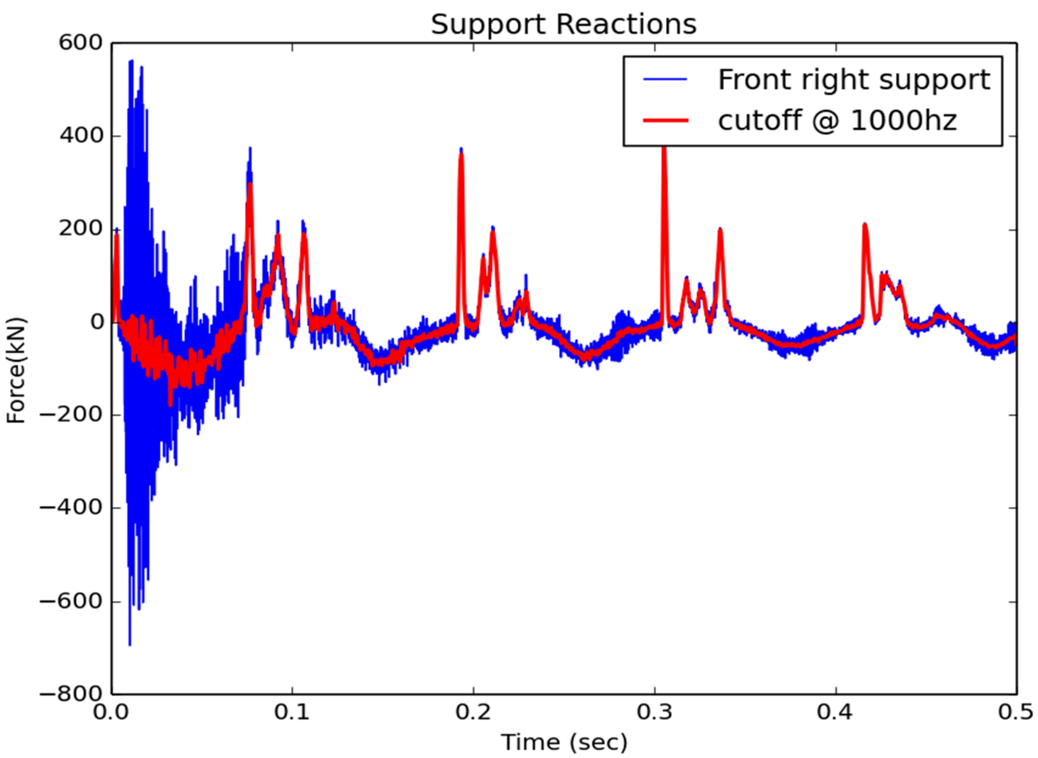

Figure 109: Front right support reaction force vs time

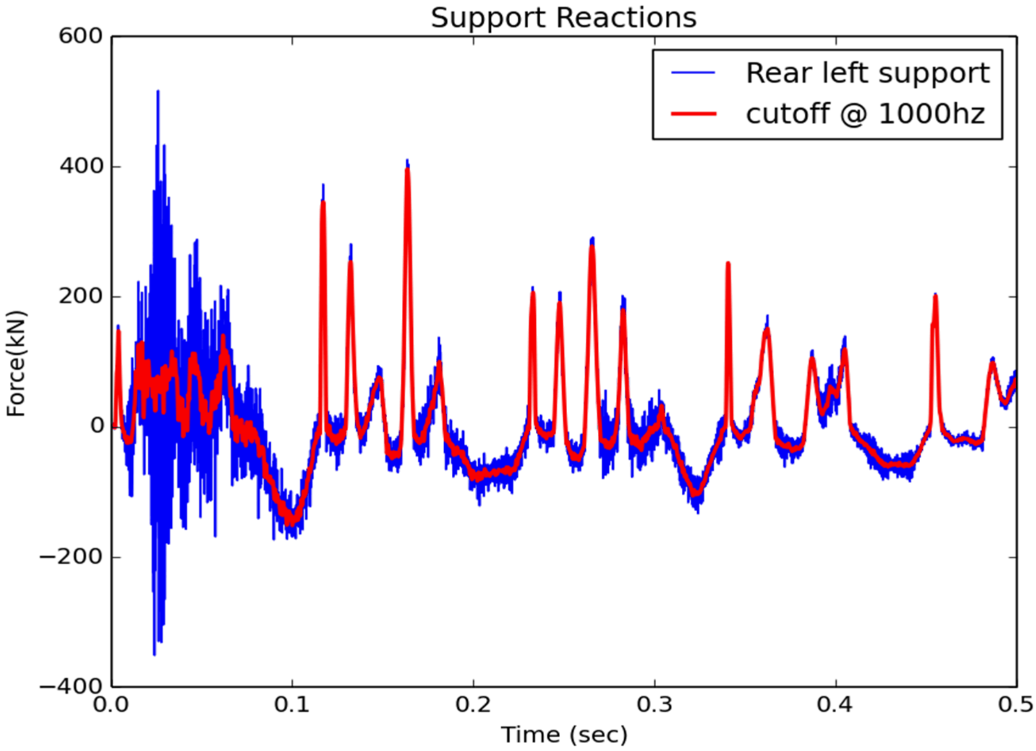

Figure 110: Rear left support reaction force vs time

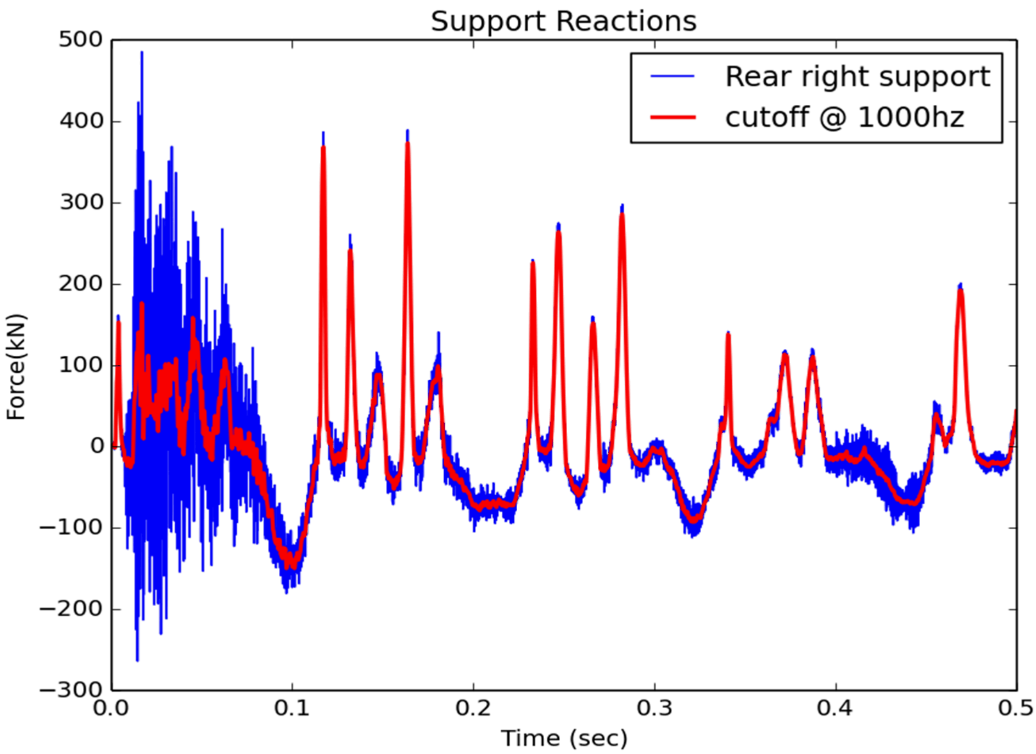

Figure 111: Rear right support reaction force vs time

4.2.5 Time histories (Displacements, Accelerations at sensors locations)

4.2.5.1 Displacements

The displacement versus time response for the selected output locations from the second 90 m/s impact simulation are presented in Figure 112 through Figure 115.

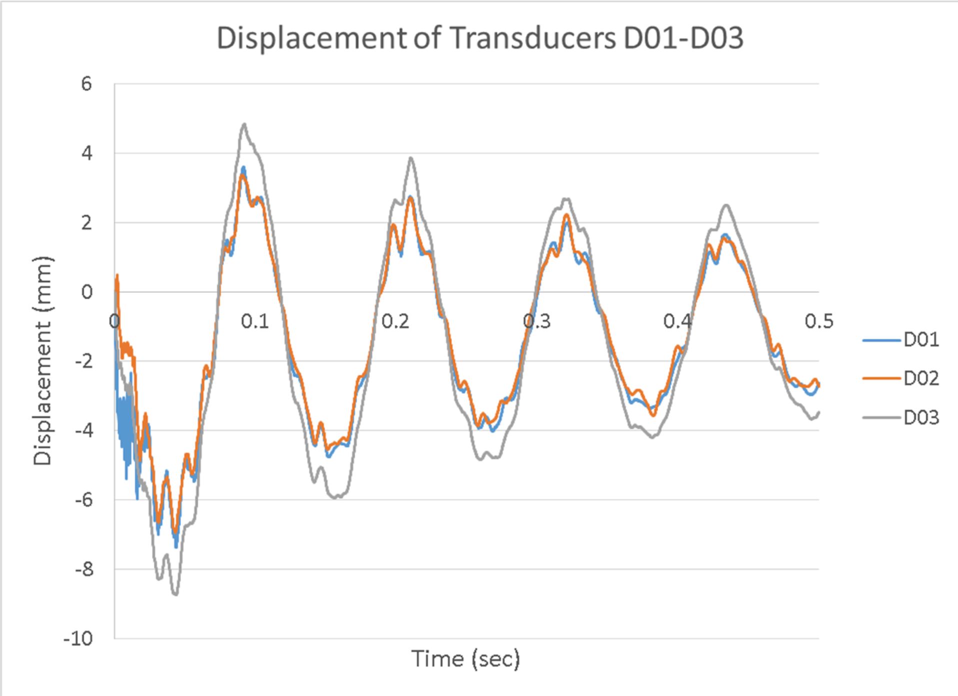

Figure 112: Displacements of transducers D01-D03 (mm)

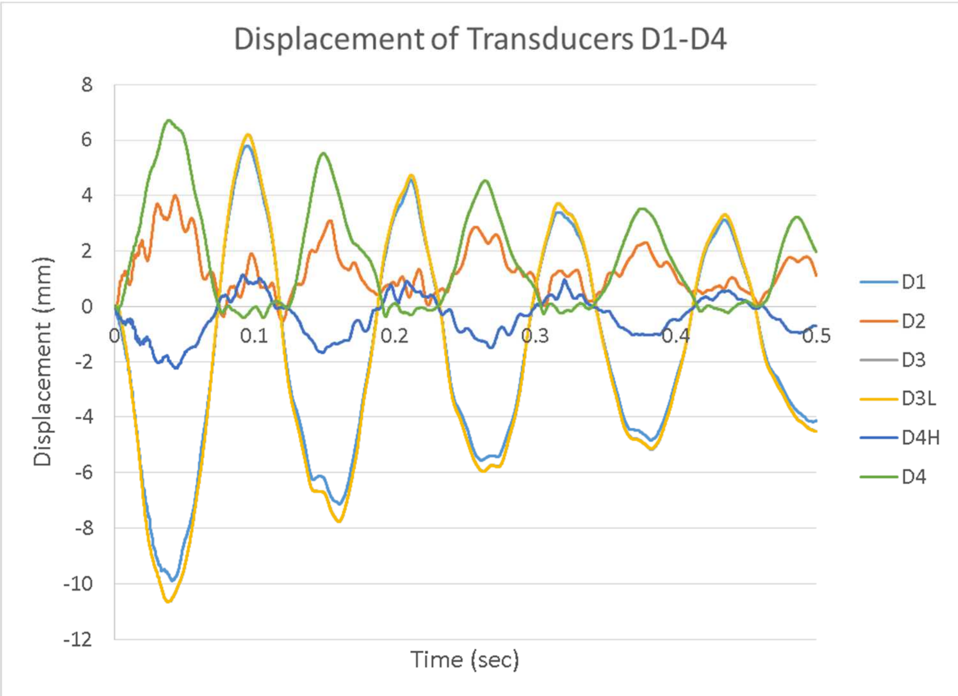

Figure 113: Displacements of transducers D1-D4 (mm)

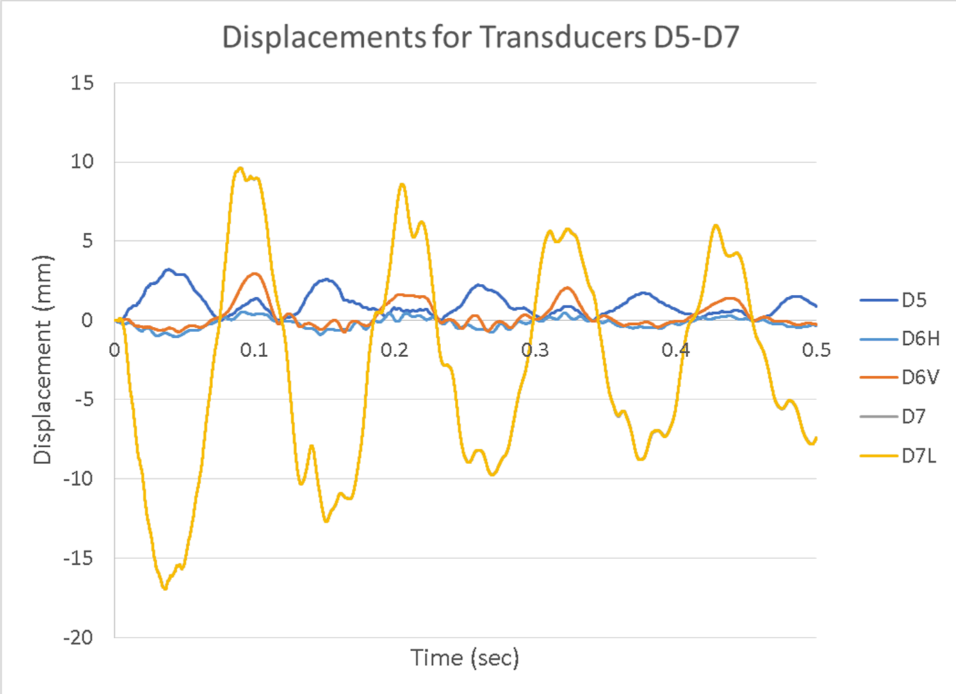

Figure 114: Displacements of transducers D5-D7 (mm)

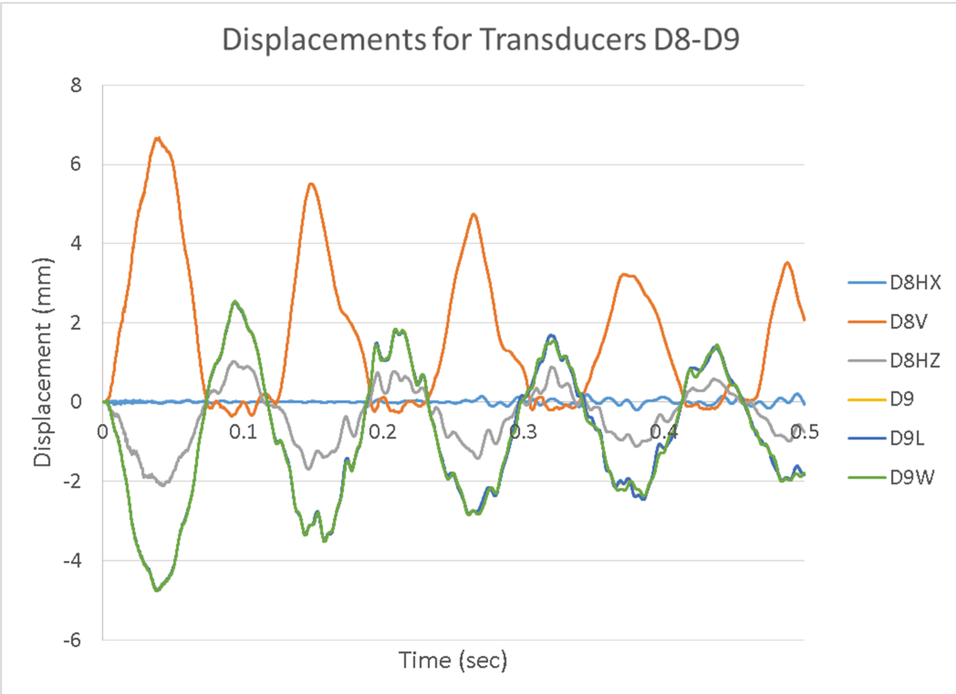

Figure 115: Displacements of transducers D8-D9 (mm)

4.2.5.2 Accelerations

The filtered acceleration versus time response for the selected output locaitons are presented in Figure 116 through Figure 130.

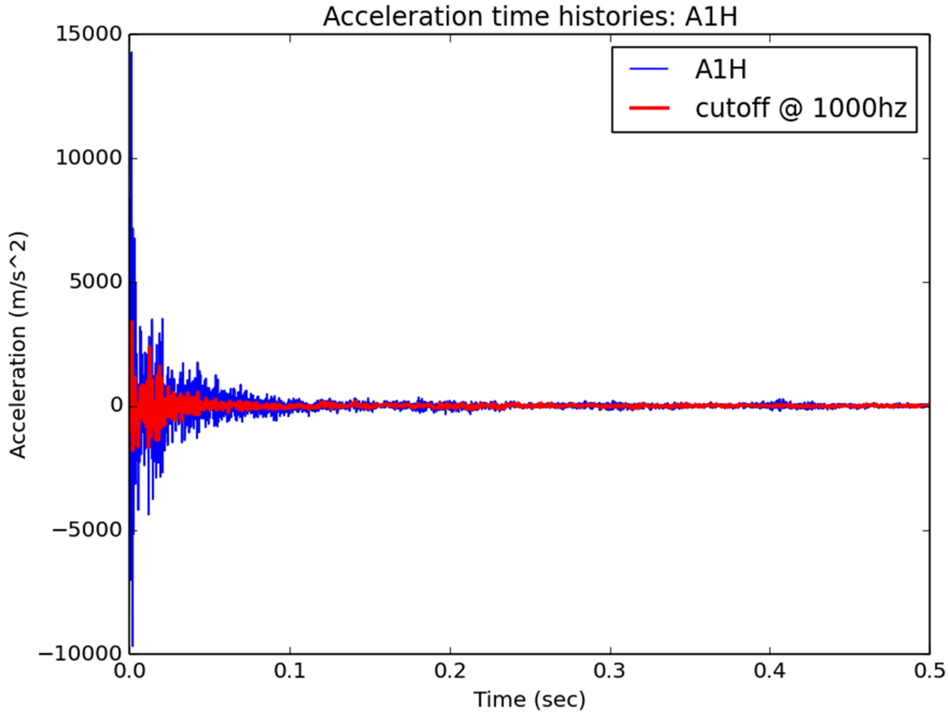

Figure 116: Acceleration versus time for A1H

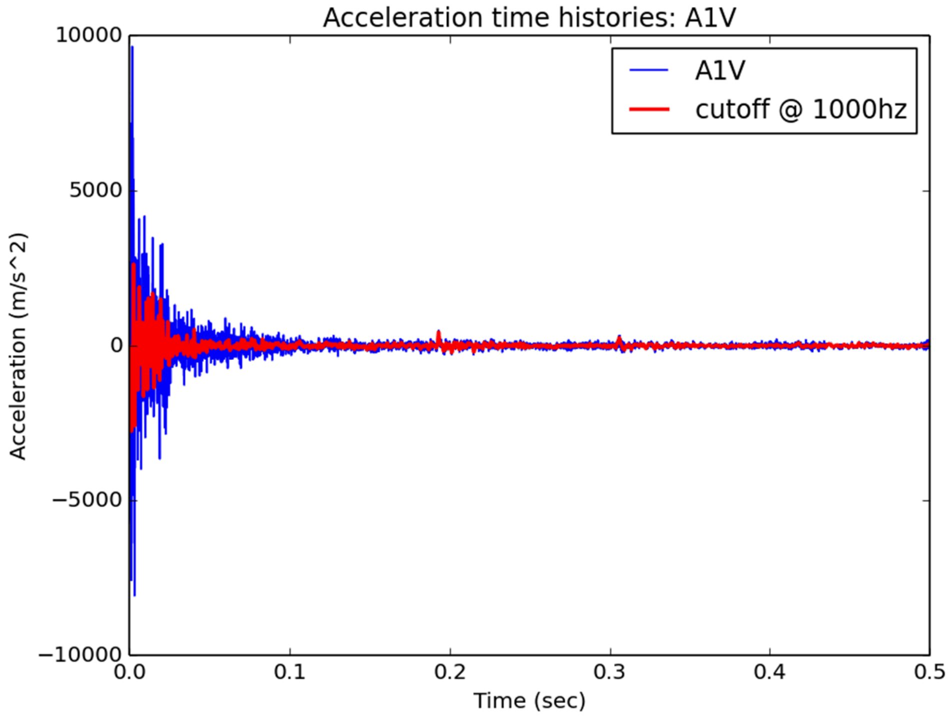

Figure 117: Acceleration versus time for A1V

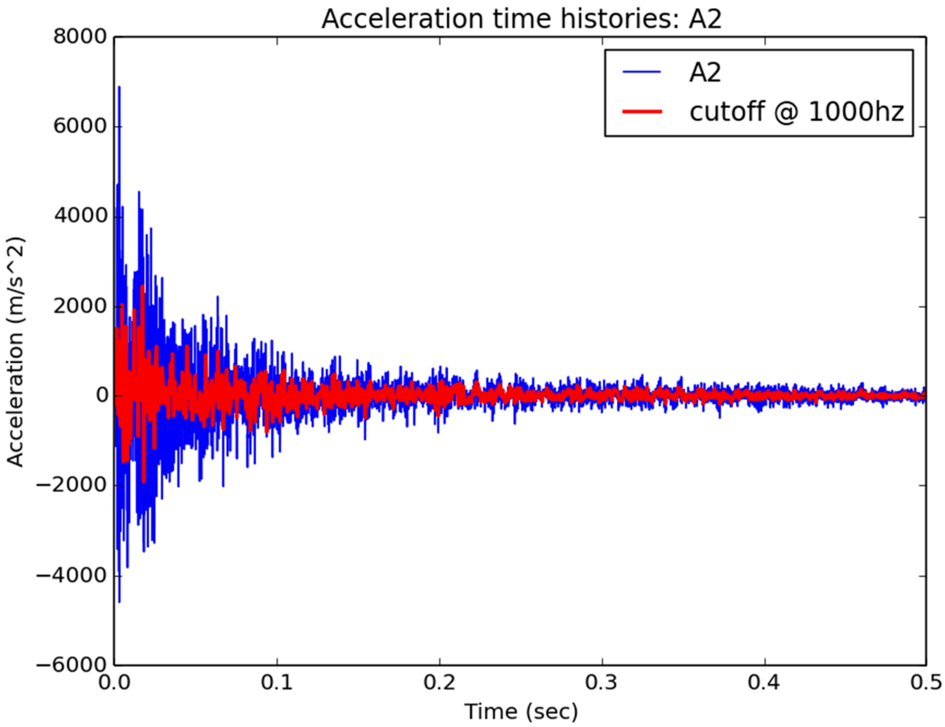

Figure 118: Acceleration versus time for A2

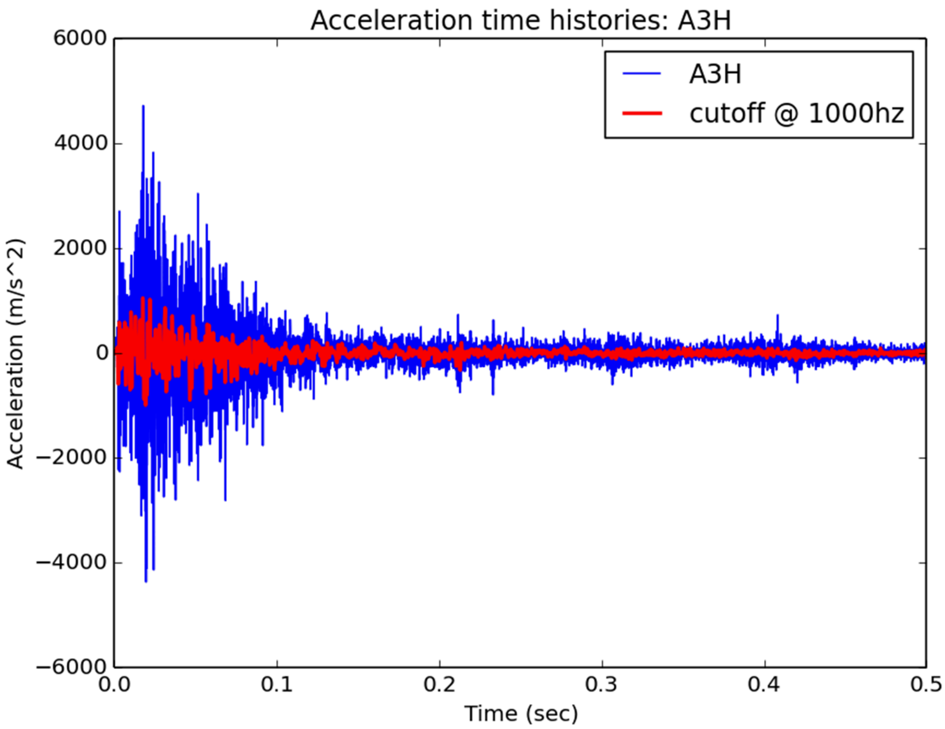

Figure 119: Acceleration versus time for A3H

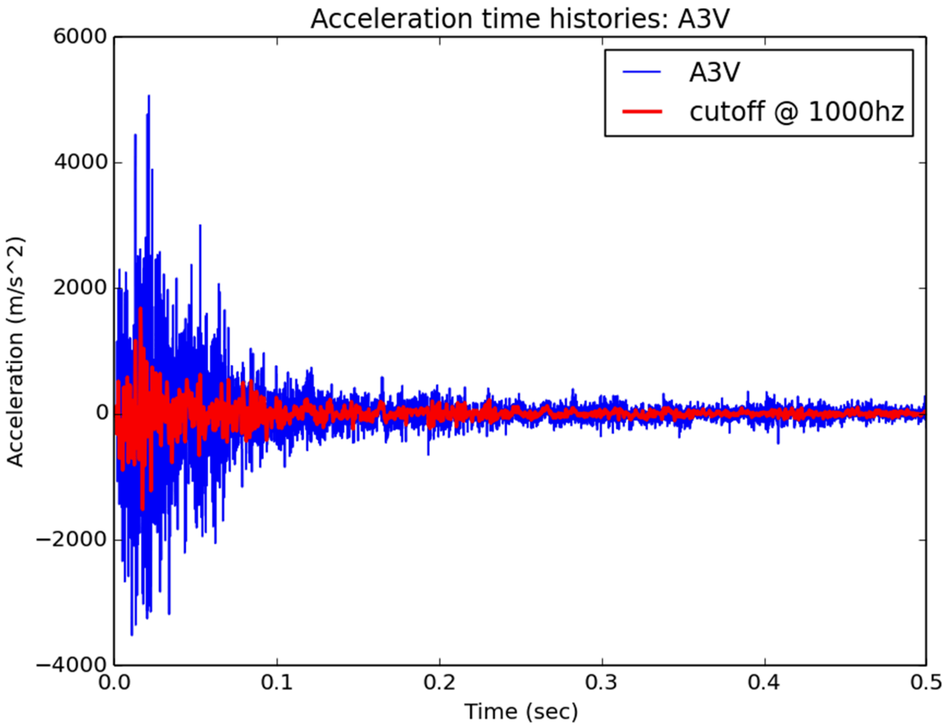

Figure 120: Acceleration versus time for A3V

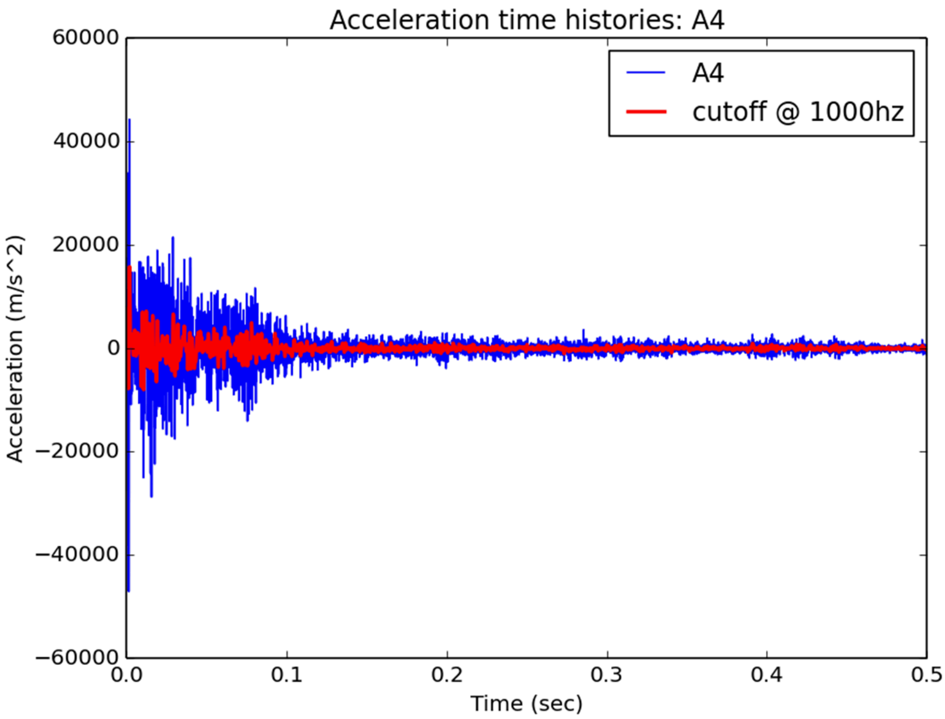

Figure 121: Acceleration versus time for A4

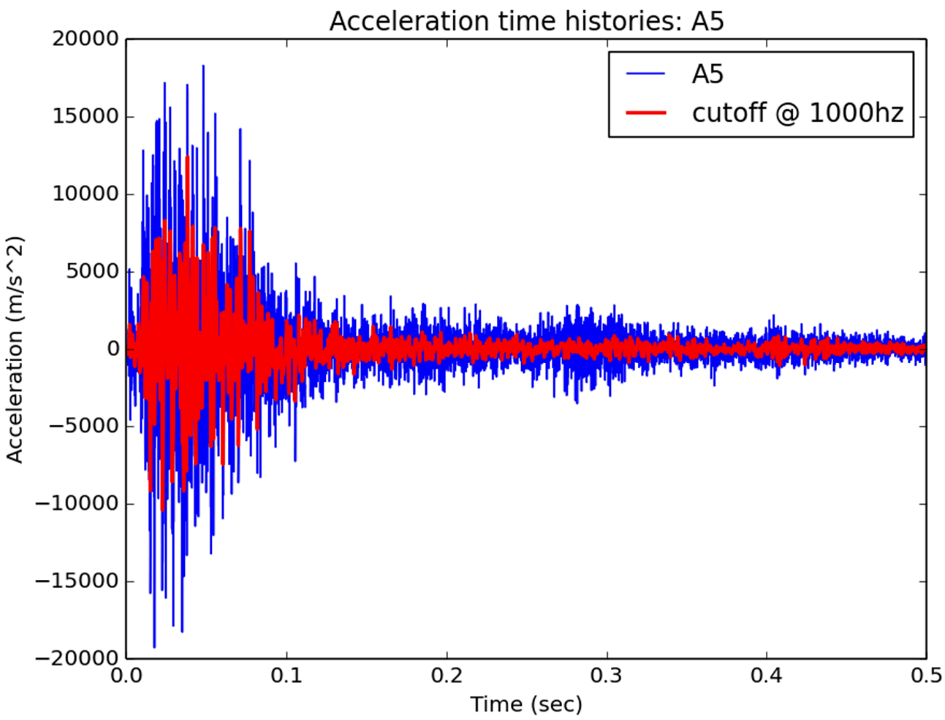

Figure 122: Acceleration versus time for A5

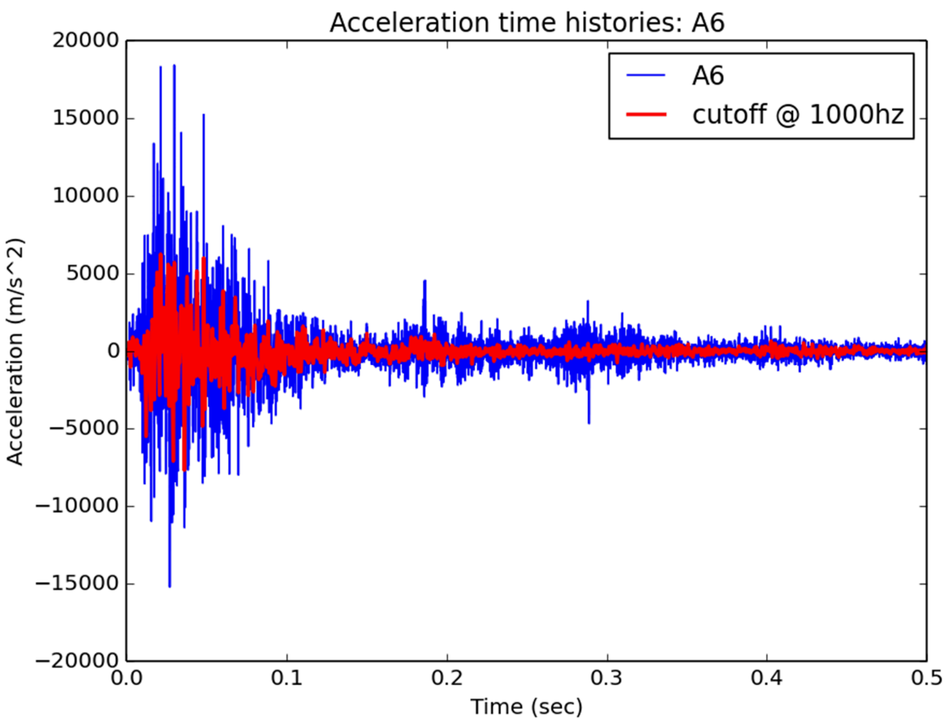

Figure 123: Acceleration versus time for A6

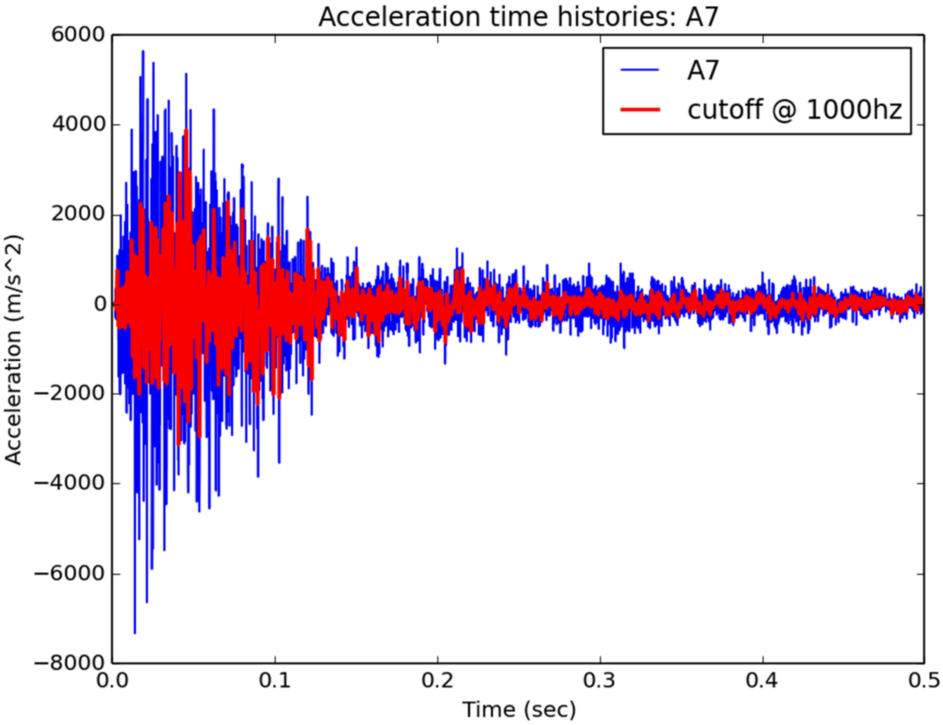

Figure 124: Acceleration versus time for A7

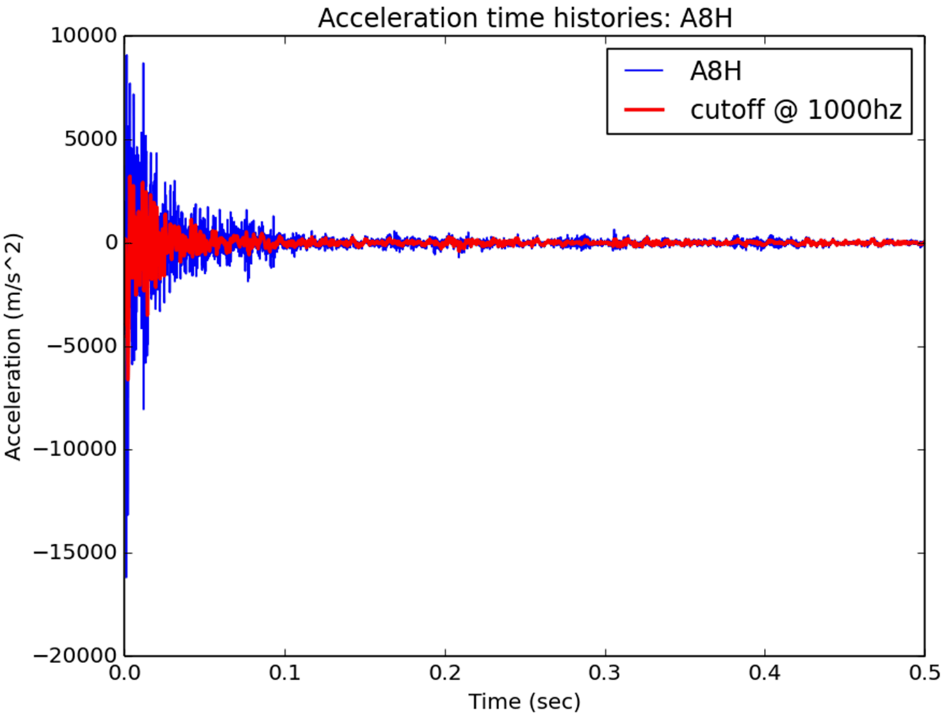

Figure 125: Acceleration versus time for A8H

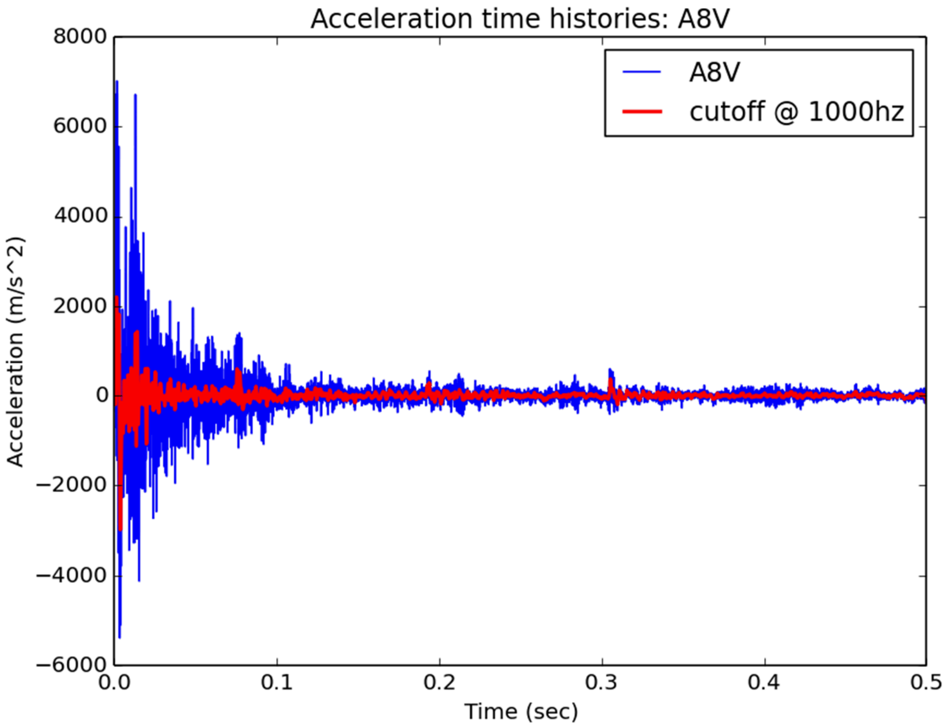

Figure 126: Acceleration versus time for A8V

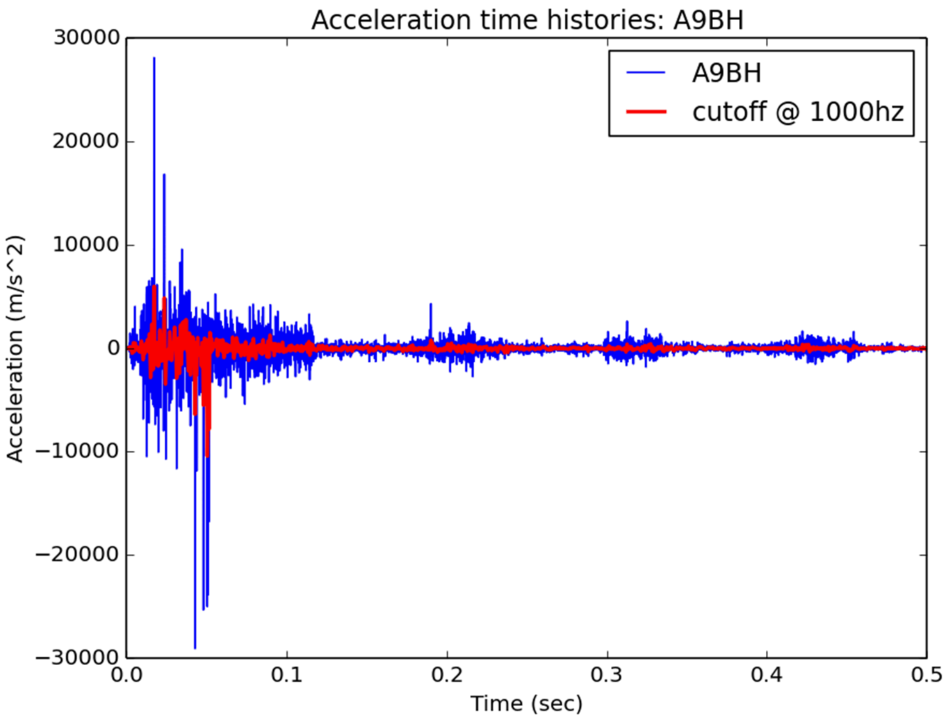

Figure 127: Acceleration versus time for A9BH

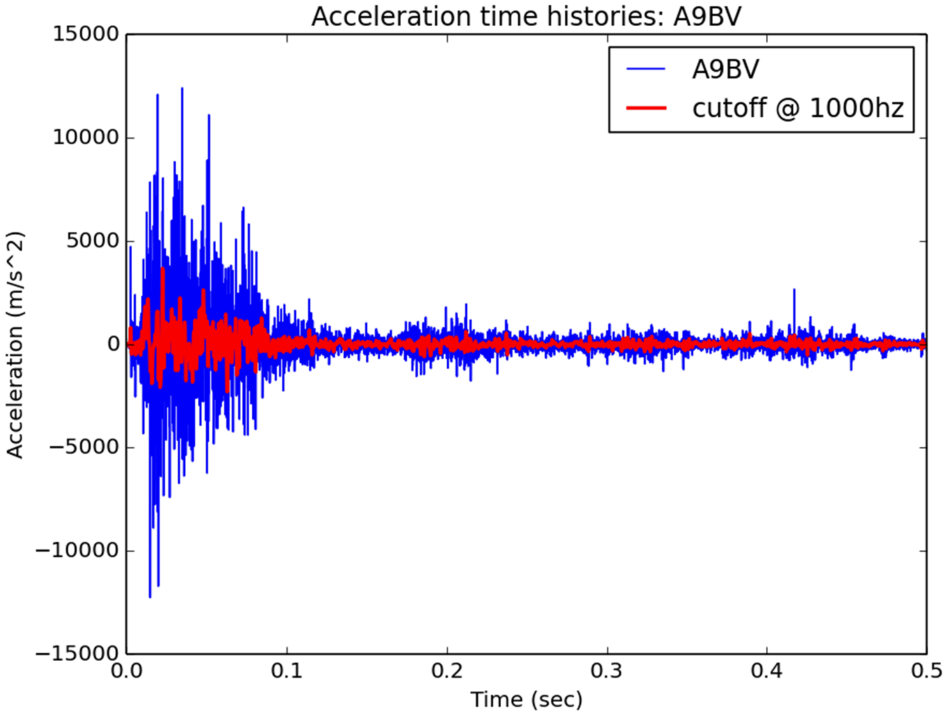

Figure 128: Acceleration versus time for A9BV

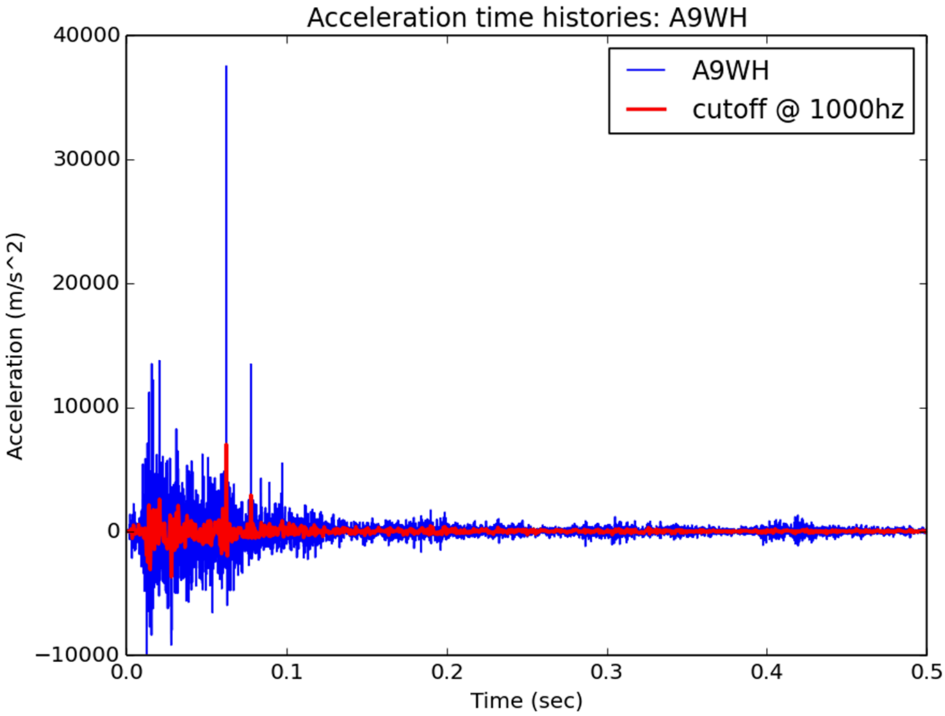

Figure 129: Acceleration versus time for A9WH

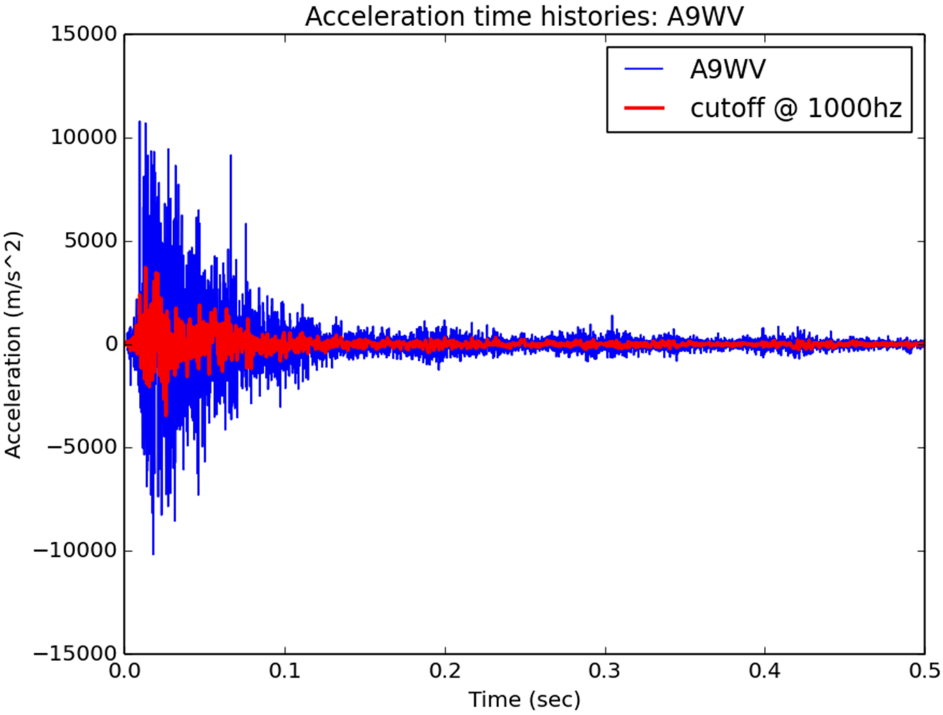

Figure 130: Acceleration versus time for A9WV

4.2.6 Response spectra at 5 % damping

No damping was implemented in this simulation.

4.2.7 Acceleration frequency content analysis (FFT, Power Spectral Density, …)

Fast Fourier Transform analysis was performed on the filtered acceleration versus time data for the second impact and these results are presented in Figure 131 through Figure 145.

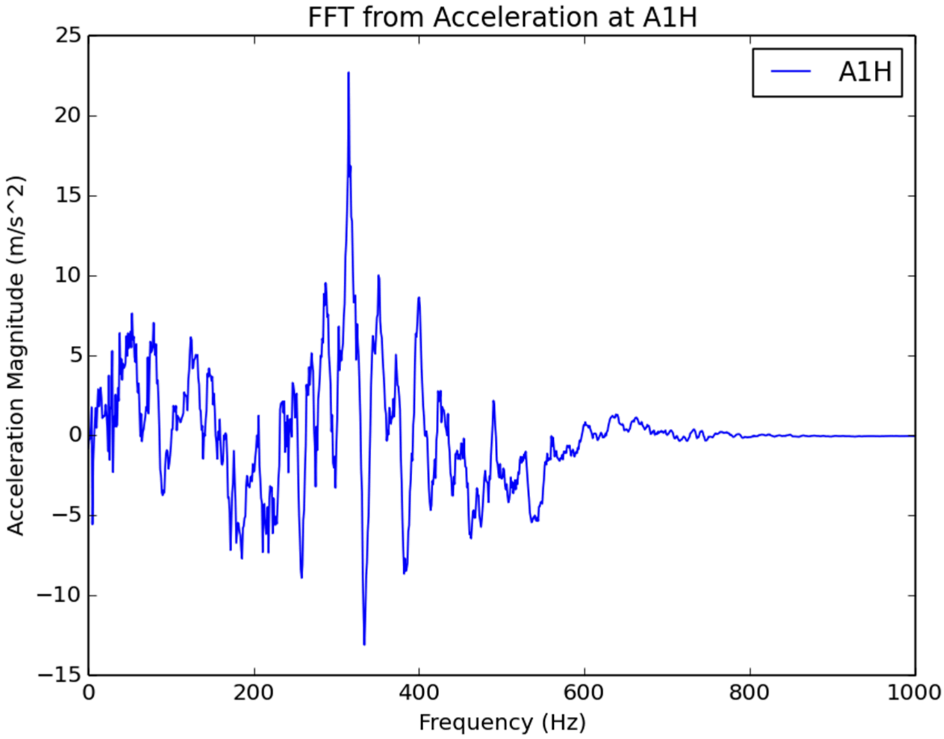

Figure 131: Acceleration Fast Fourier Transform for A1H

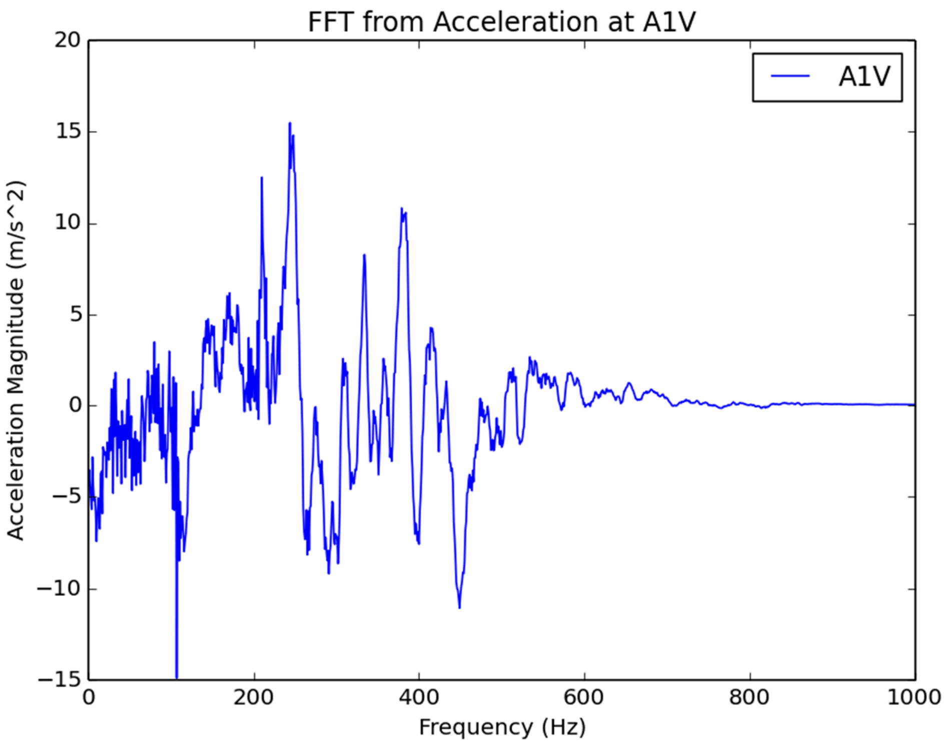

Figure 132: Acceleration Fast Fourier Transform for A1V

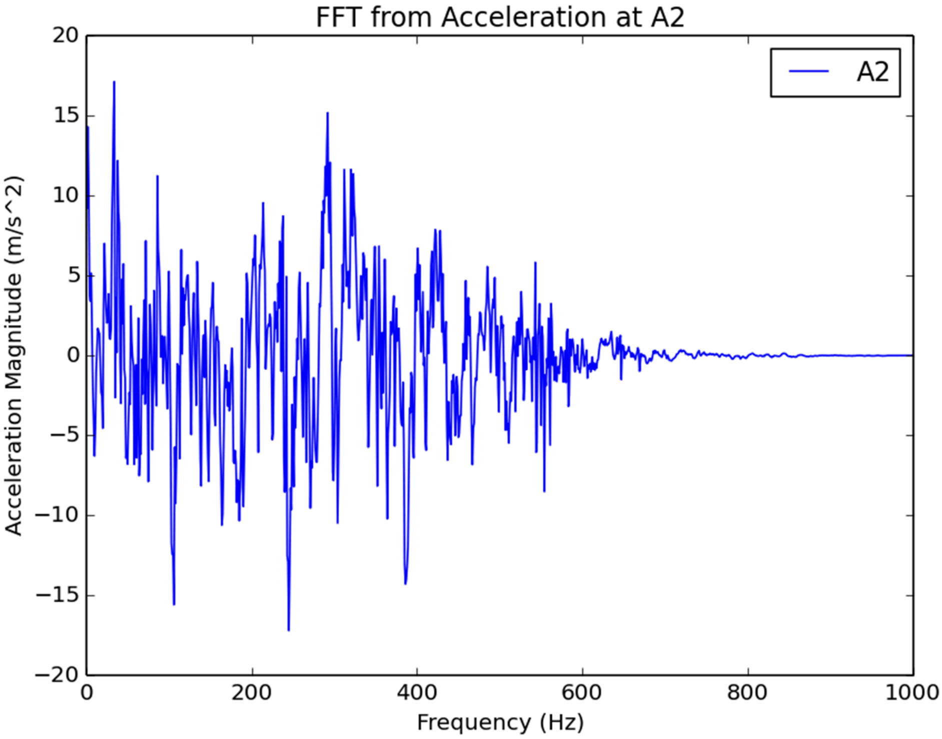

Figure 133:Acceleration Fast Fourier Transform for A2

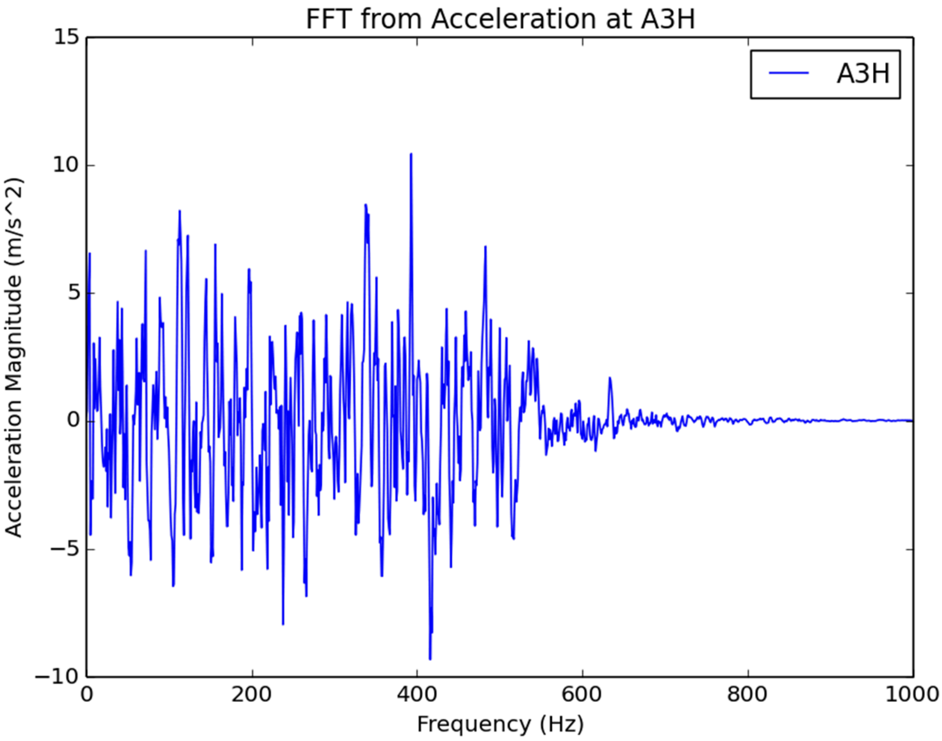

Figure 134: Acceleration Fast Fourier Transform for A3H

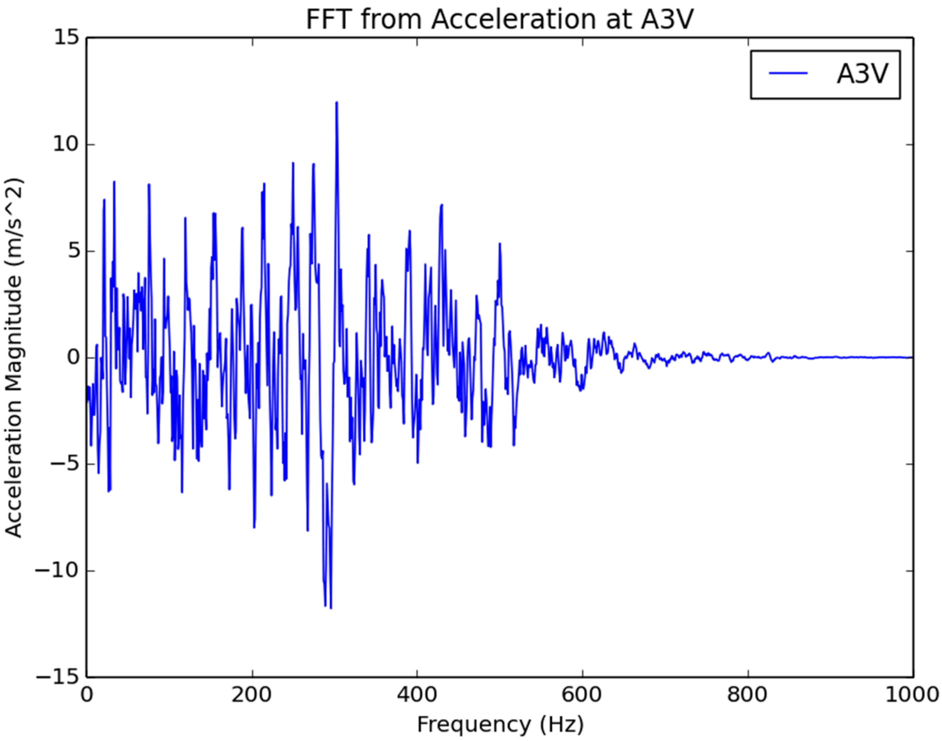

Figure 135: Acceleration Fast Fourier Transform for A3V

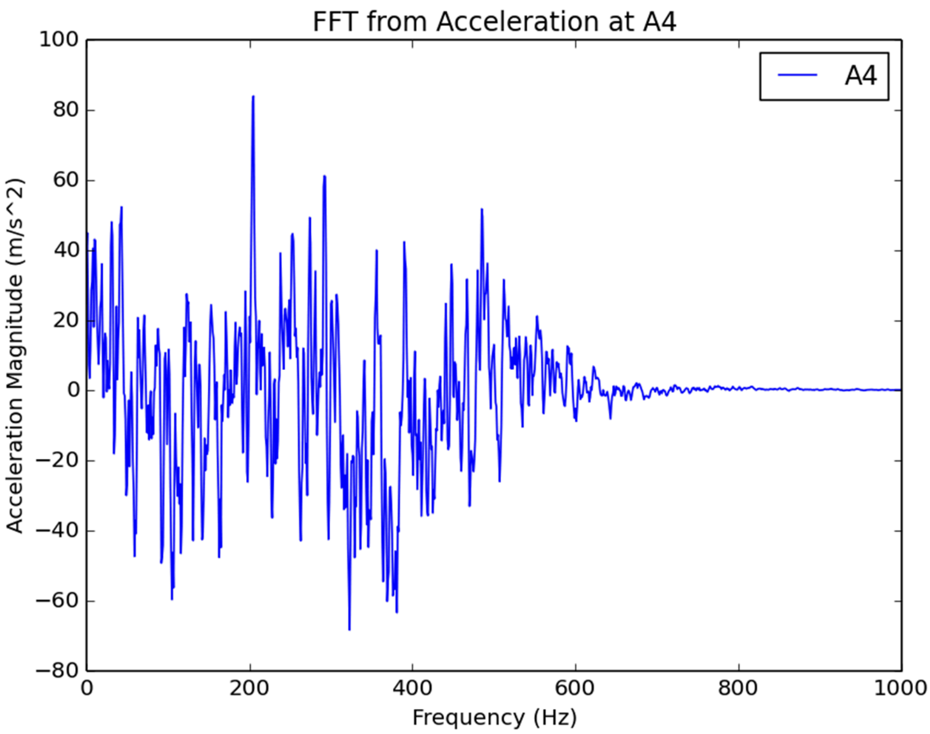

Figure 136: Acceleration Fast Fourier Transform for A4

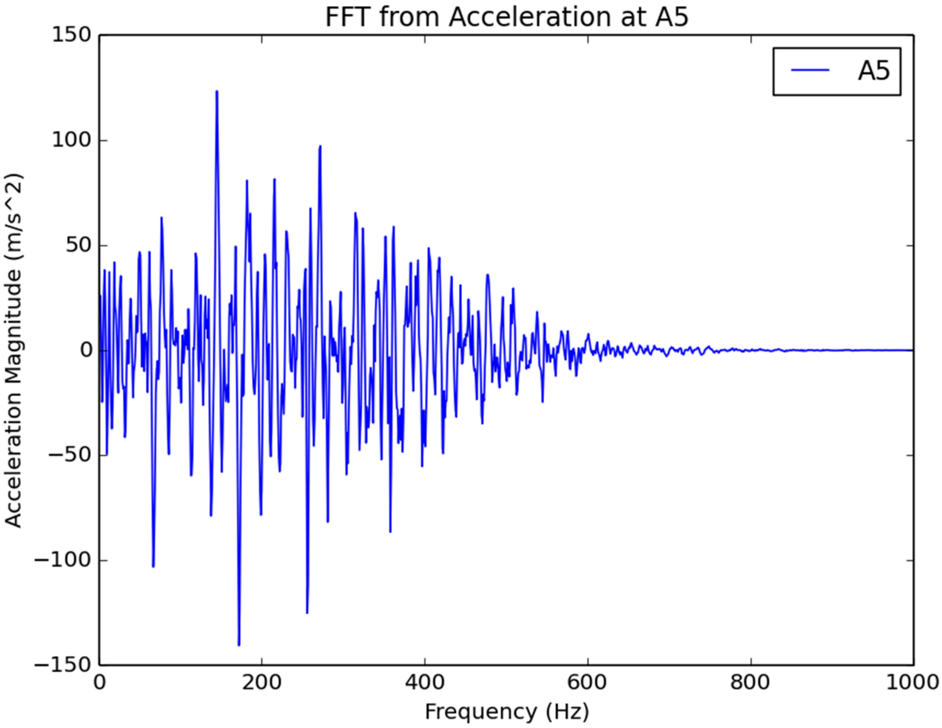

Figure 137: Acceleration Fast Fourier Transform for A5

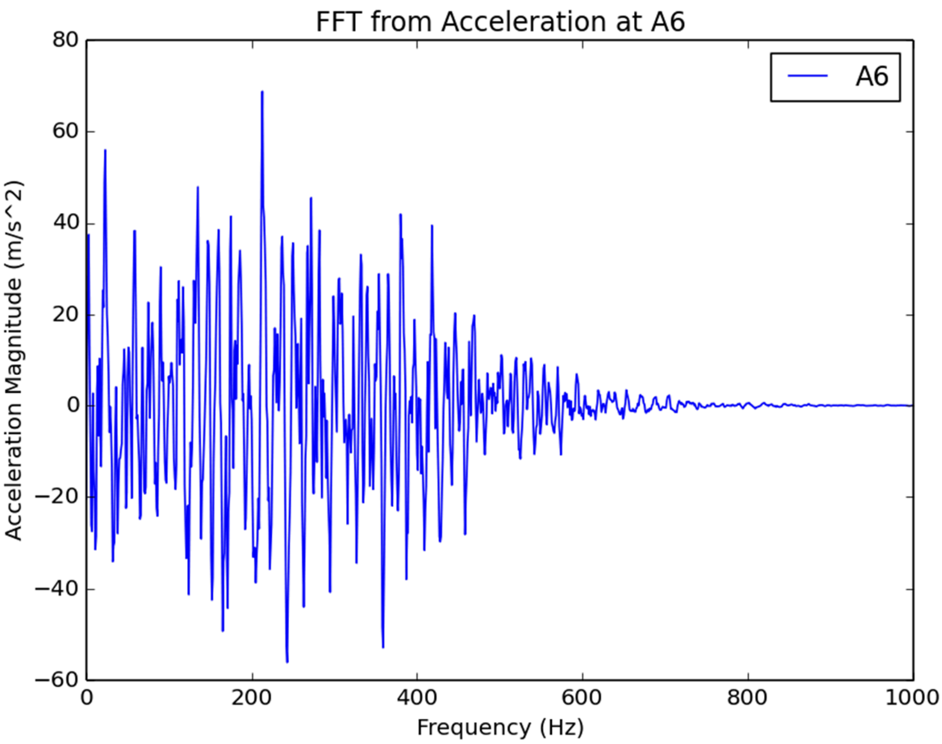

Figure 138: Acceleration Fast Fourier Transform for A6

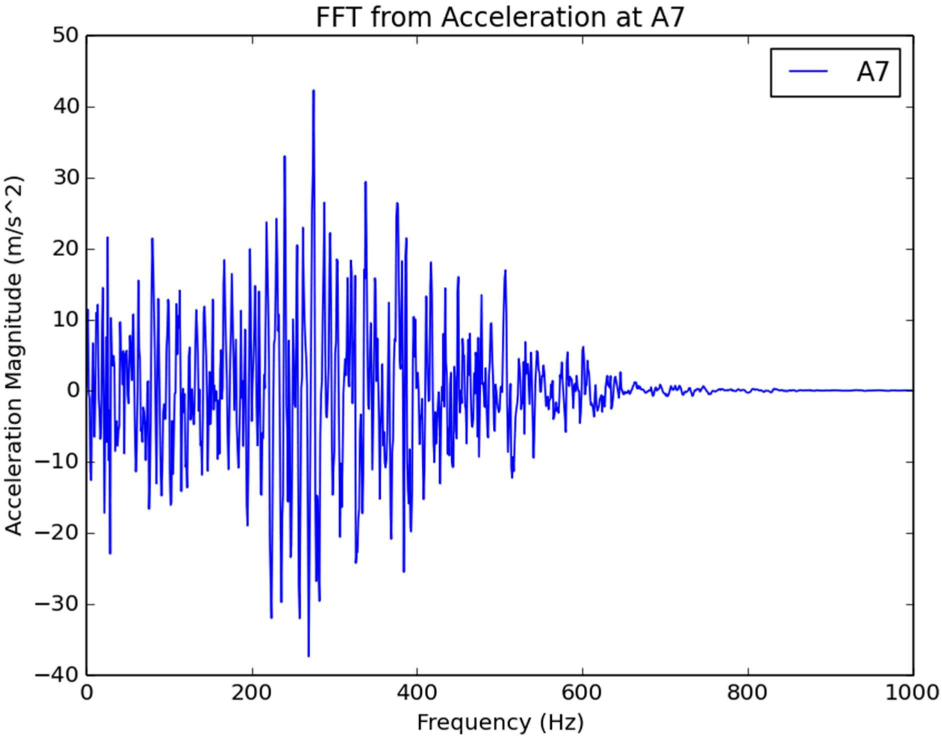

Figure 139: Acceleration Fast Fourier Transform for A7

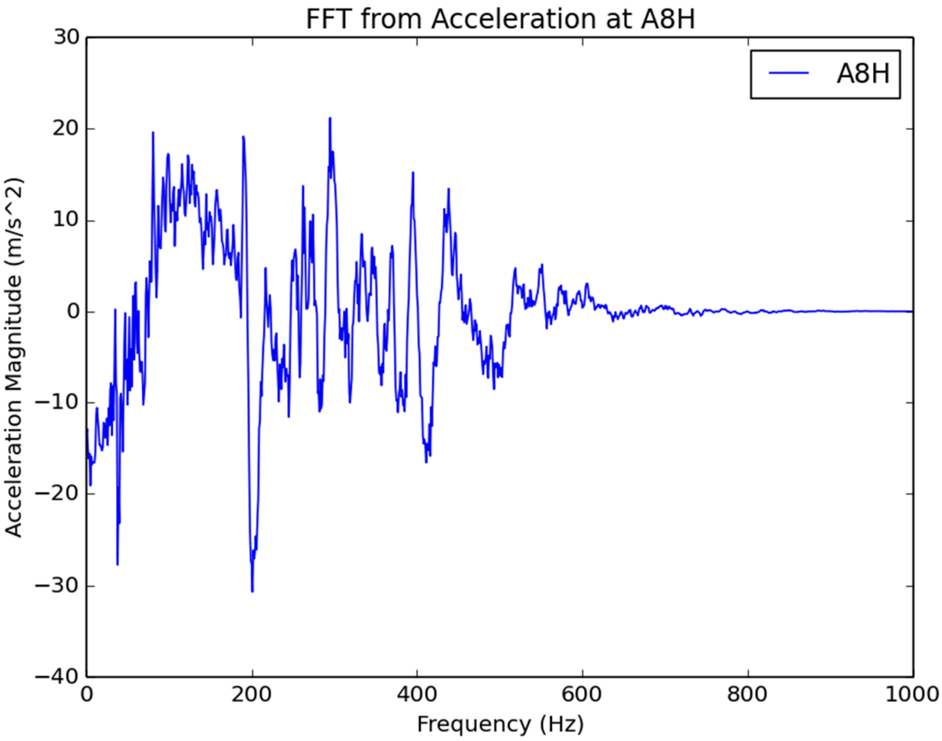

Figure 140: Acceleration Fast Fourier Transform for A8H

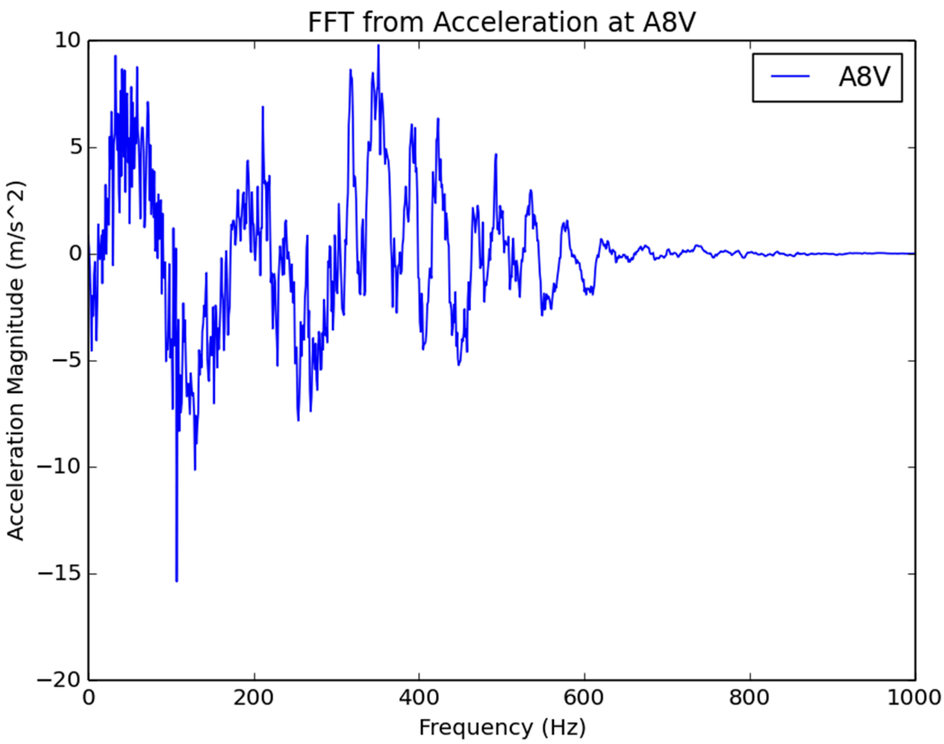

Figure 141: Acceleration Fast Fourier Transform for A8V

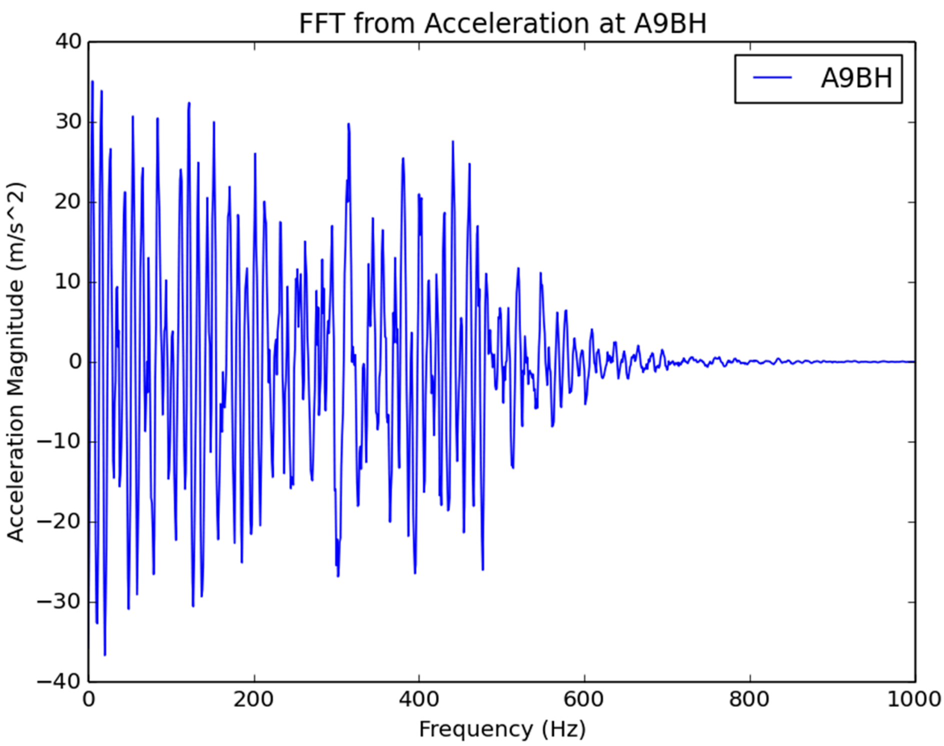

Figure 142: Acceleration Fast Fourier Transform for A9BH

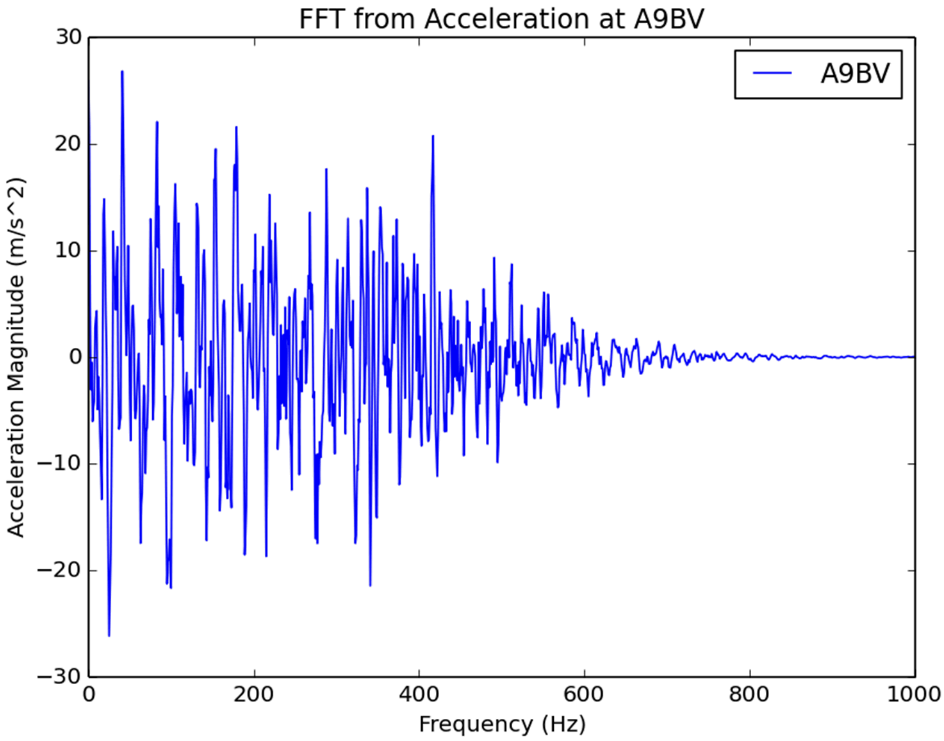

Figure 143: Acceleration Fast Fourier Transform for A9BV

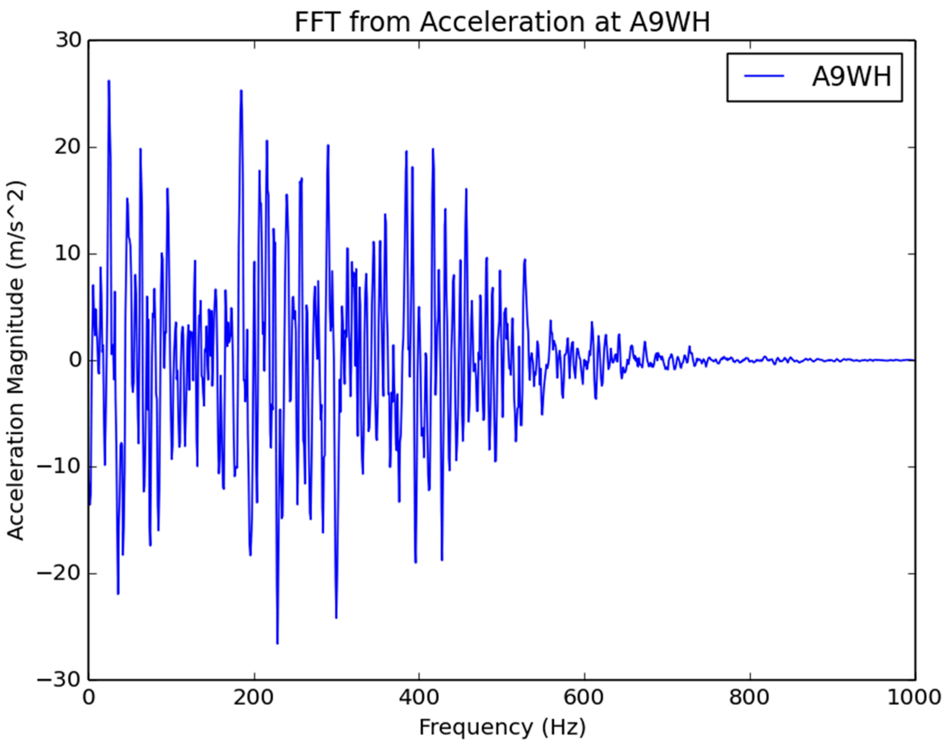

Figure 144: Acceleration Fast Fourier Transform for A9WH

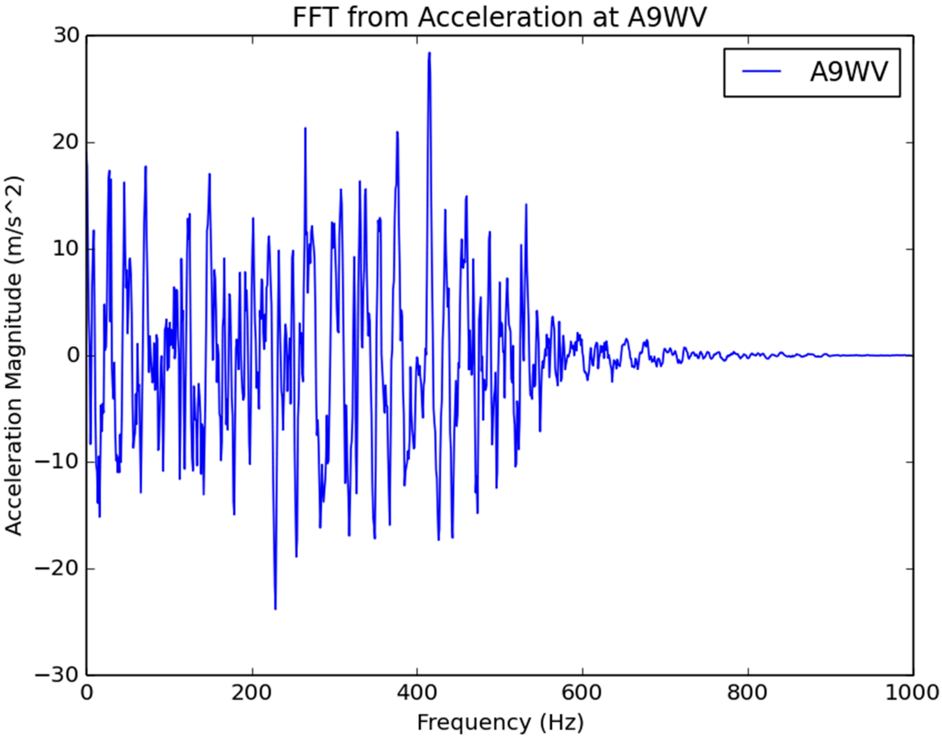

Figure 145: Acceleration Fast Fourier Transform for A9WV

4.3 Pseudo-equipments results

4.3.1 Time histories

4.3.1.1 Displacements

The displacement versus time response for the two beams (welded and bolted) are shown in Figure 146.

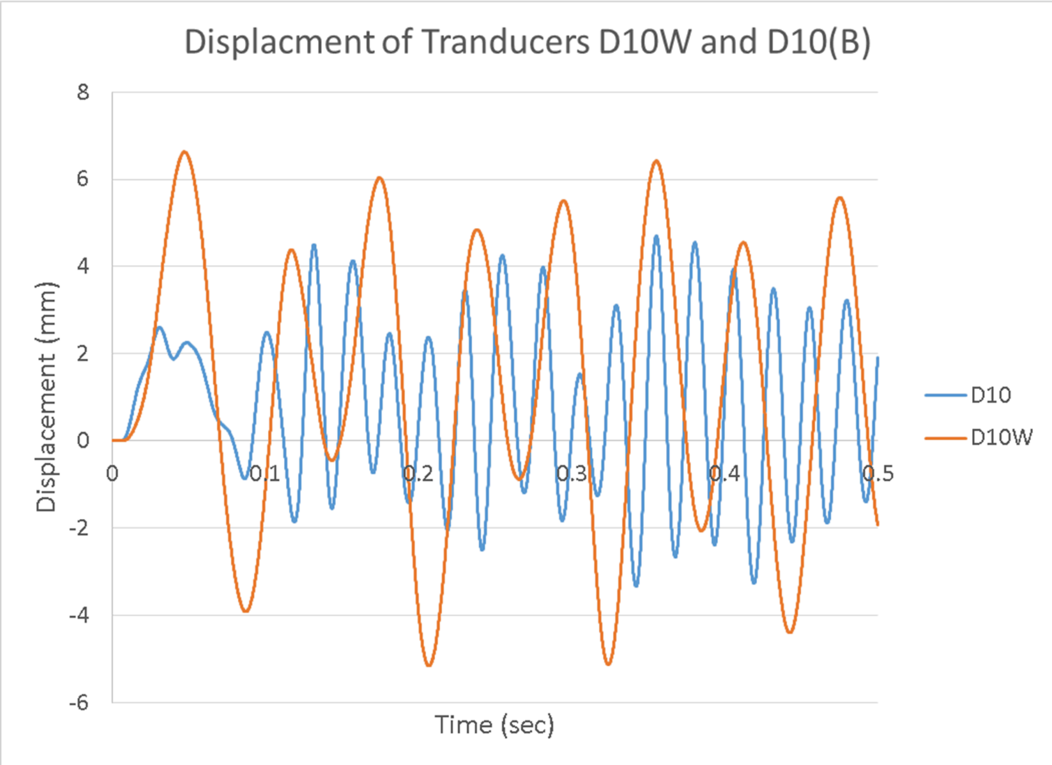

Figure 146: Time displacement history for D10 and D10W

4.3.1.2 Accelerations

The filtered acceleration versus time response from the simulation for the two beams in the horizontal and vertical planes is presented in Figure 147 through Figure 150.

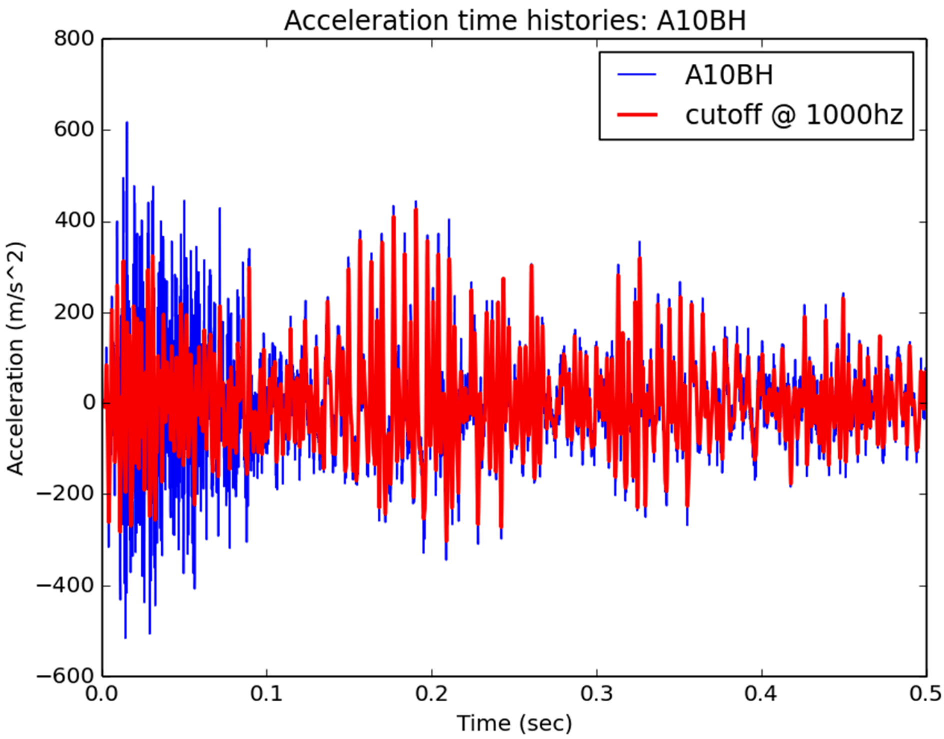

Figure 147: Acceleration versus time for A10H

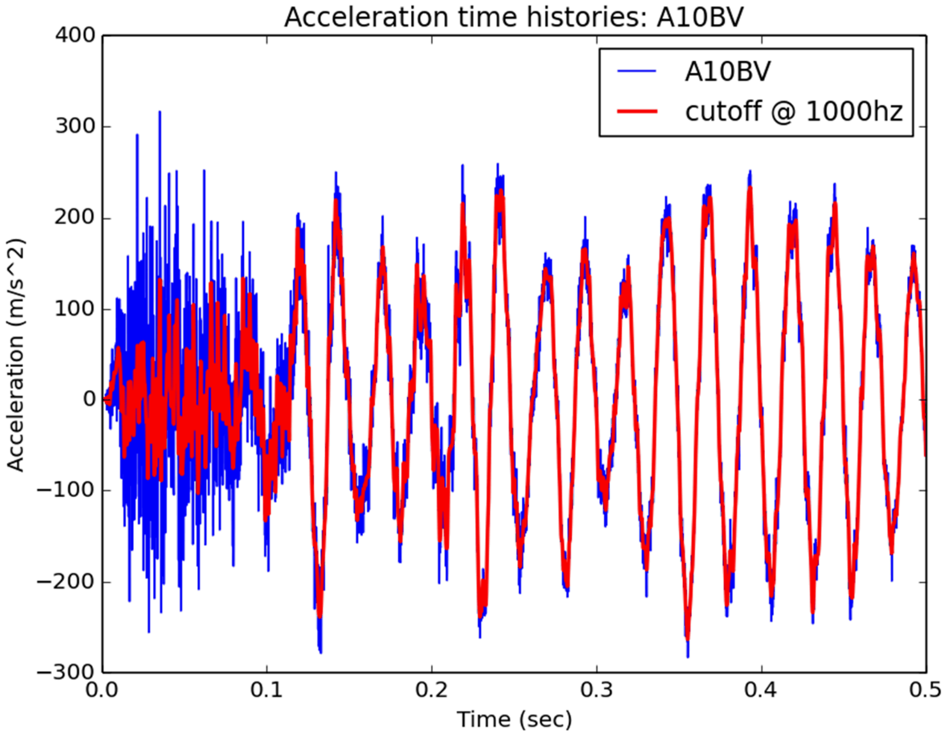

Figure 148: Acceleration versus time for A10V

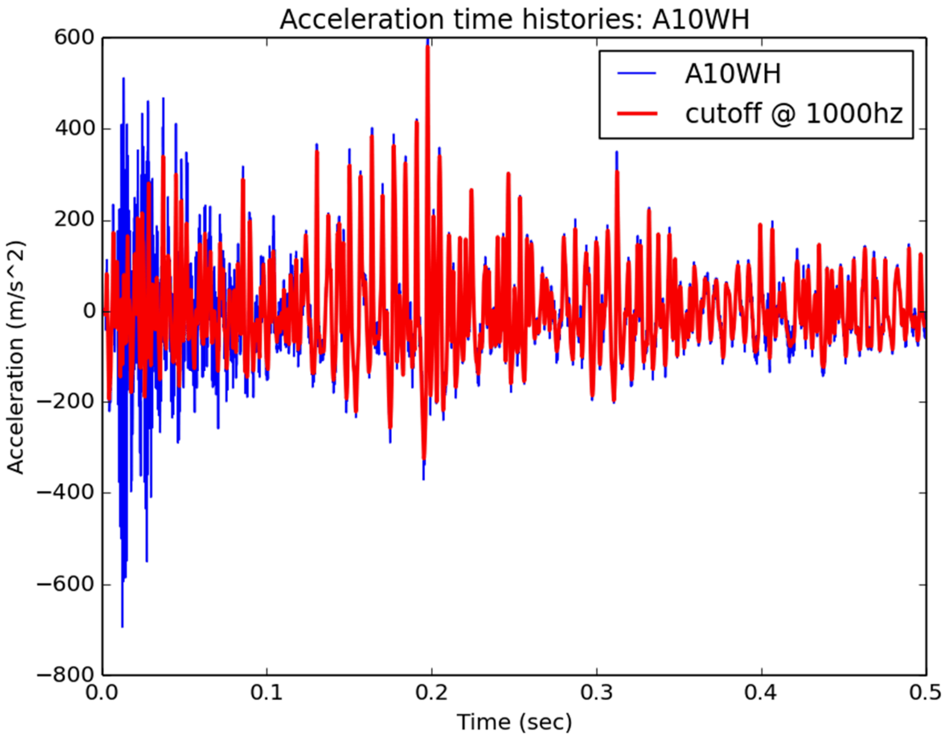

Figure 149: Acceleration versus time for A10WH

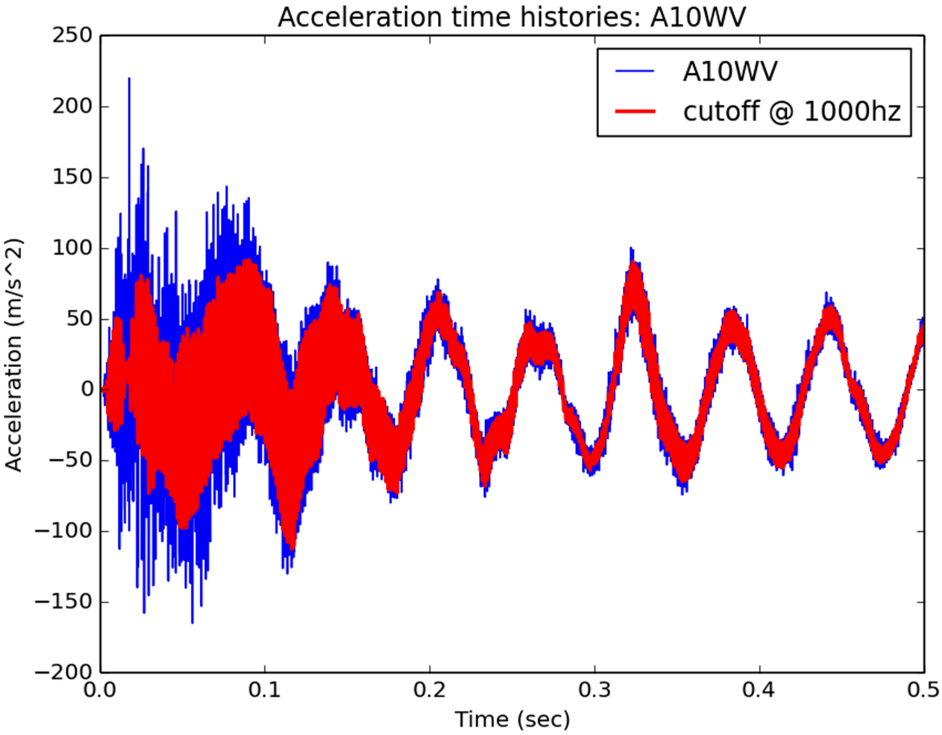

Figure 150: Acceleration versus time for A10WV

4.3.2 Acceleration frequency content analysis

Fast Fourier Transform analysis of the filtered acceleration versus time response for the second 90 m/s impact for the welded and bolted beams were performed and these results are shown in Figure 151 through Figure 154.

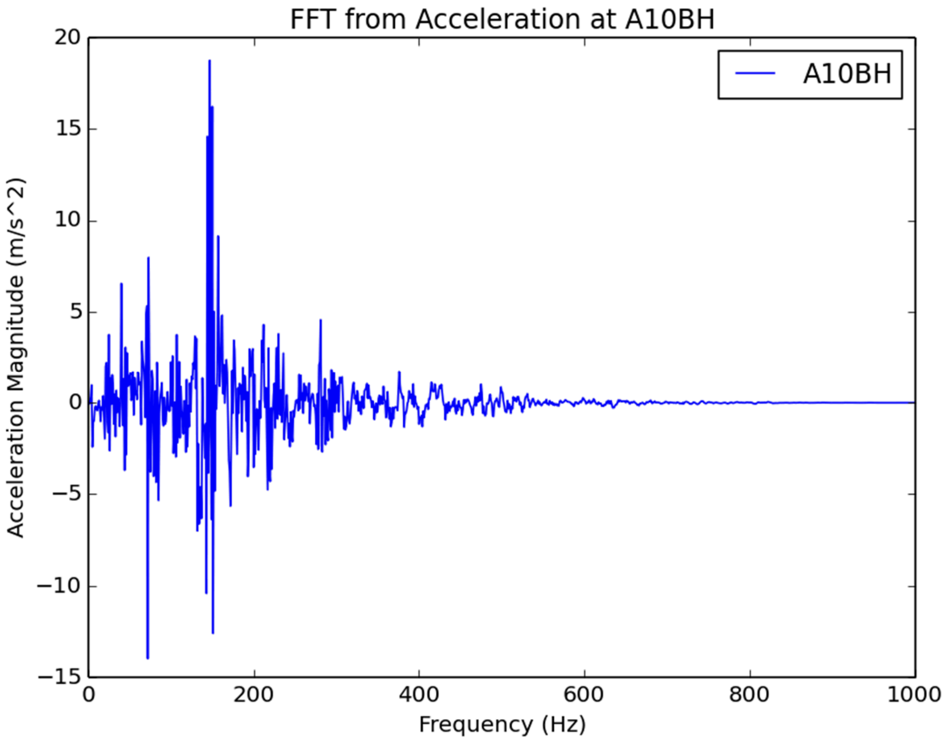

Figure 151: Acceleration Fast Fourier Transform for A10BH

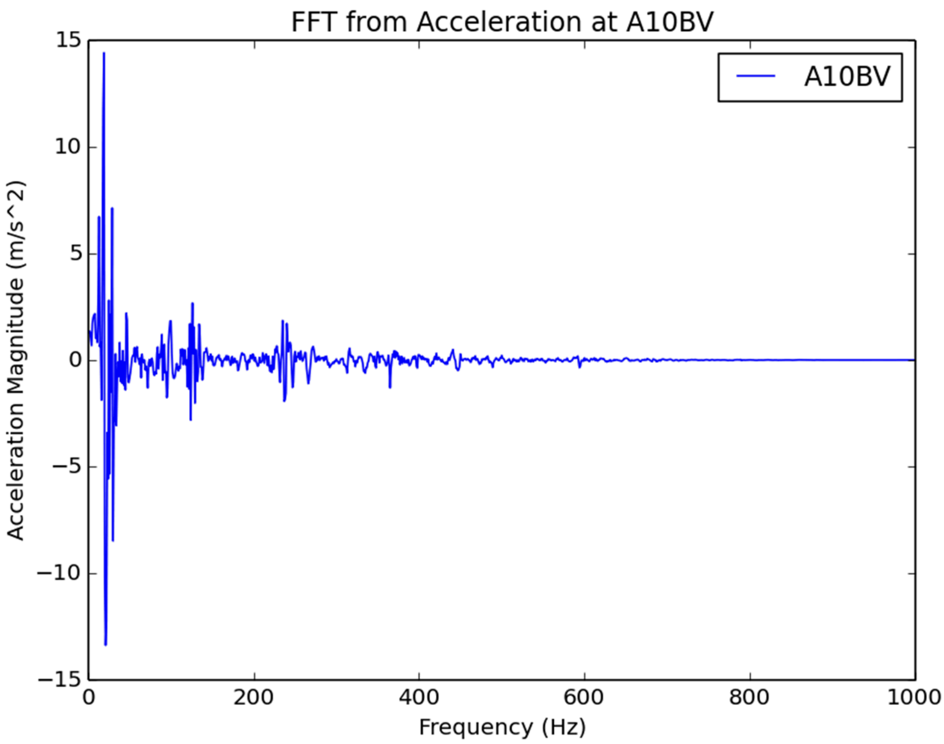

Figure 152: Acceleration Fast Fourier Transform for A10BV

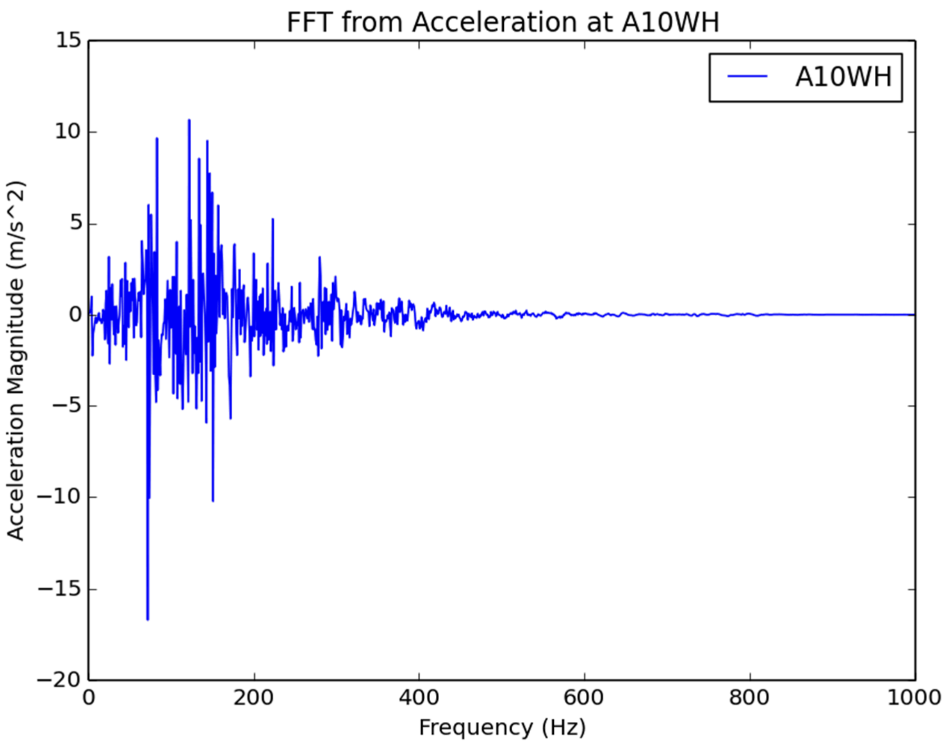

Figure 153: Acceleration Fast Fourier Transform for A10WH

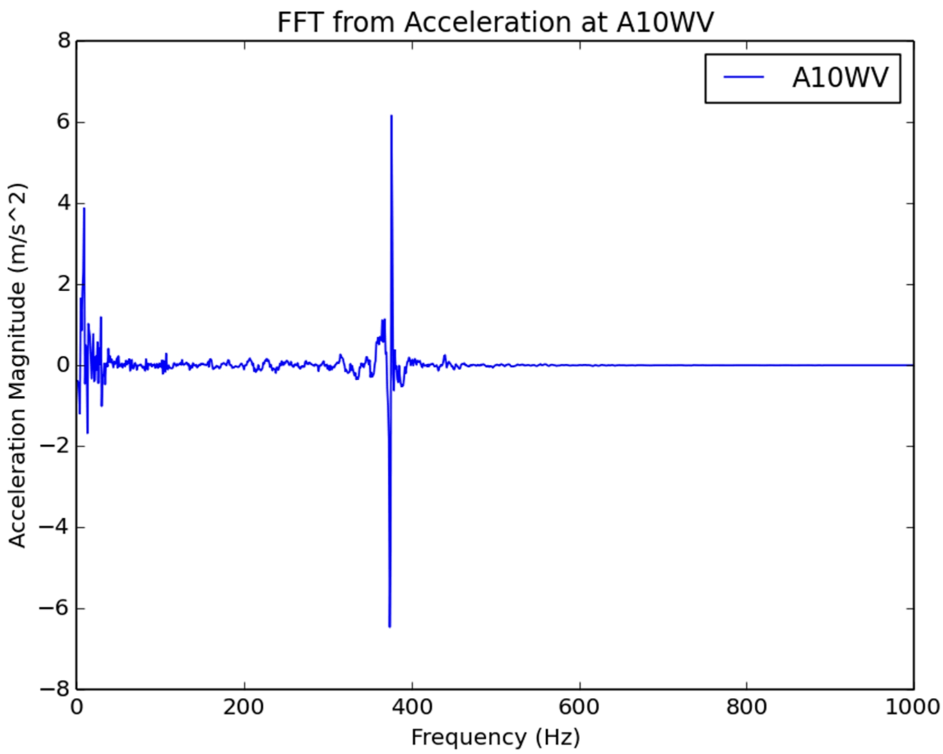

Figure 154: Acceleration Fast Fourier Transform for A10WV

4.4 IRIS III Vb test conclusions

This simulation performed much the same as the V_a simulation. The missile did not penetrate the concrete. Damage accrued primarily on the front face and at corners in the concrete, including any corners where a steel plate was attached. There was a vast difference in behavior between the two pseudo-equipments in both oscillation frequency and amplitude; this could be due to the fact that the I-beam with a welded connection was 100 mm longer than the I-beam with a bolted connection, and the pseudo-equipment masses were both the same. The V_a and V_b simulations did vary slightly in the degree of x-displacement as shown in D8HX in Figure 54 and Figure 115. D8HX in shows almost no displacement for the first 90 m/s simulation, while D8HX in begins to show x-direction oscillations towards the end of the simulation for the second, eccentric 90 m/s simulation, suggesting that any eccentricity will have significant impact on the mock-up only after the initial damage from the missile is already done.

5. IRIS III results : 1st impact at velocity Vc = 170 m/s

5.1 Missile results

This section is not requested for « OPTION 1 : Equivalent force » missile modeling.

5.1.1 Crushing results (crushing length, …)

The missile crushing results are shown in Table 12 and Figure 155.

Table 12: Missile Crushing Results, 170 m/s

Original length (including hemispherical head)	2525 mm
Total length after crush	879 mm
Crushed length H_T	380 mm
Non-crushed length L_T	499 mm

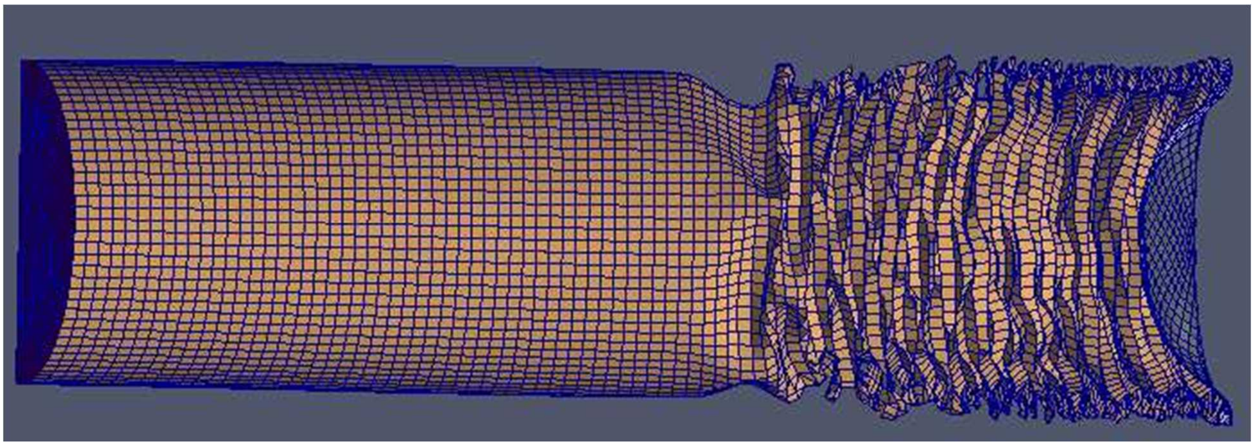

Figure 155: 170 m/s missile at t_{imp}

5.1.2 Time histories (Displacement, Velocity, Acceleration)

The displacement, velocity, and acceleration versus time response of the 170 m/s missile impact are presented in Figure 156 through Figure 158.

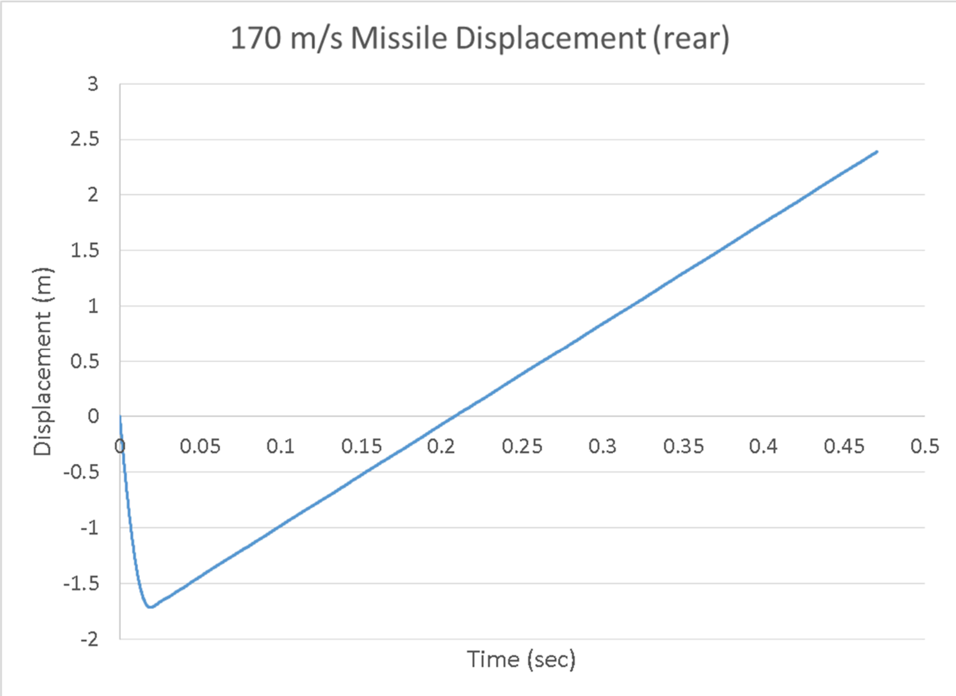

Figure 156: Displacement of the rear end of the 170 m/s missile

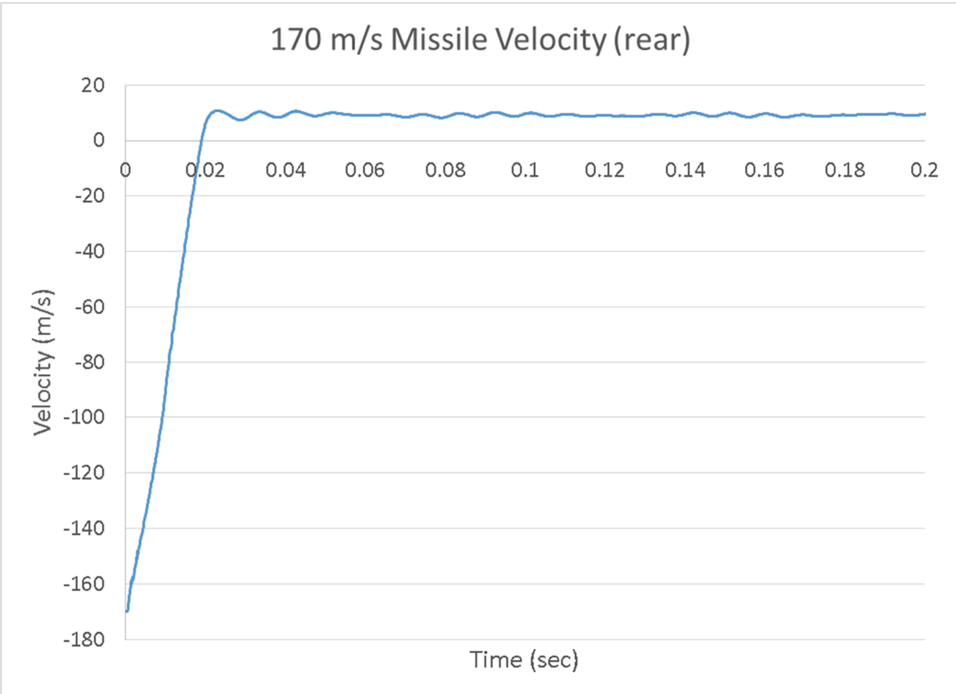

Figure 157: Velocity of the rear end of the 170 m/s missile

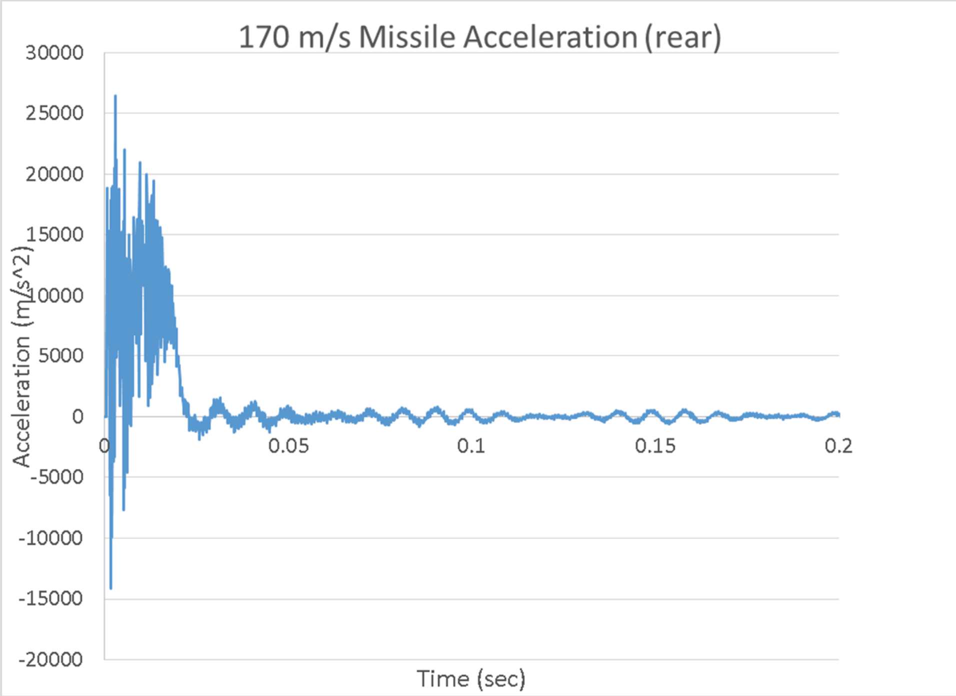

Figure 158: Acceleration of the rear end of the 170 m/s missile

5.1.3 Contact force time history and impulse

The contact force versus time and impulse versus time response of the missile in the 170 m/s impact are shown in Figure 159 and Figure 160.

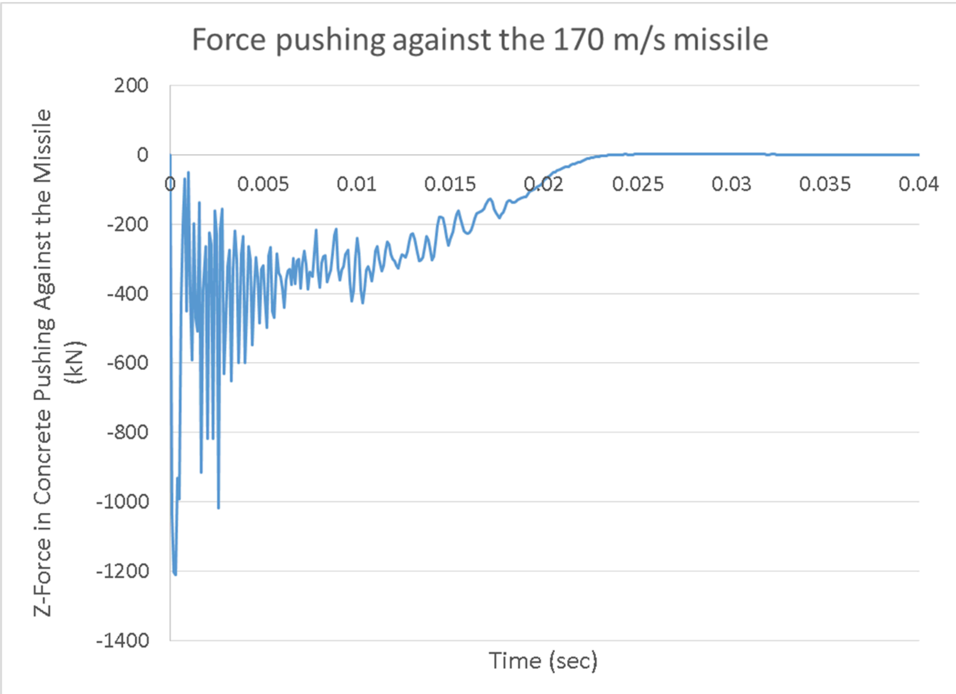

Figure 159: Force pushing against the 170 m/s missile

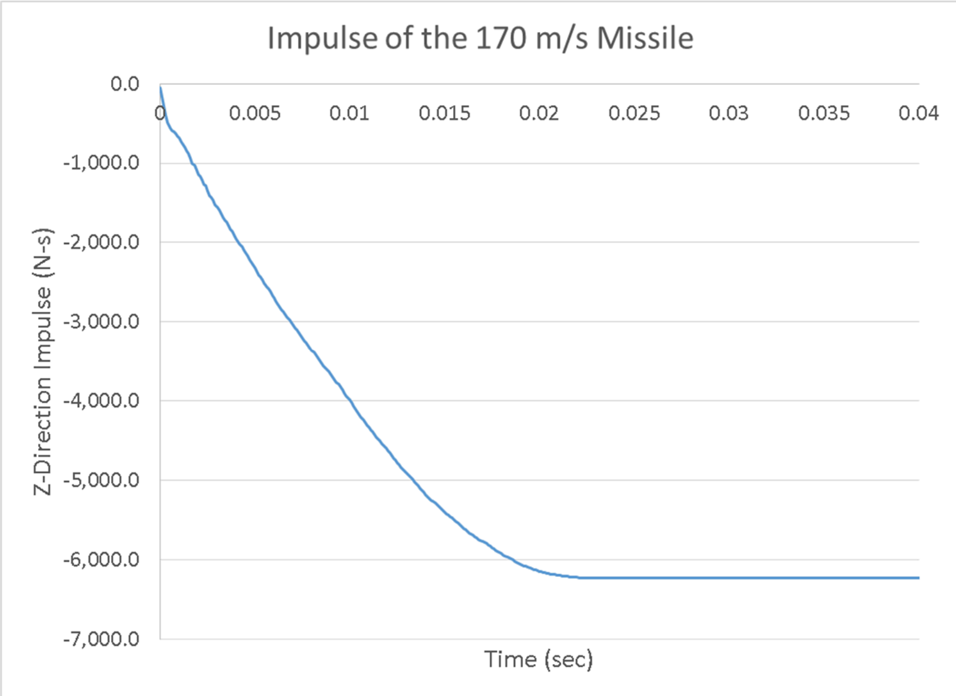

Figure 160: Impulse of the 170 m/s missile

5.2 Mock-up results

5.2.1 Global results

The damage to the concrete structure is shown in Figure 161 through Figure 166. Note that the support pedestals have been removed from the visualization (though they were included in the simulation) to increase visibility to the concrete. Damage is plotted in these figures with damage = 1.0 representing fractured concrete.

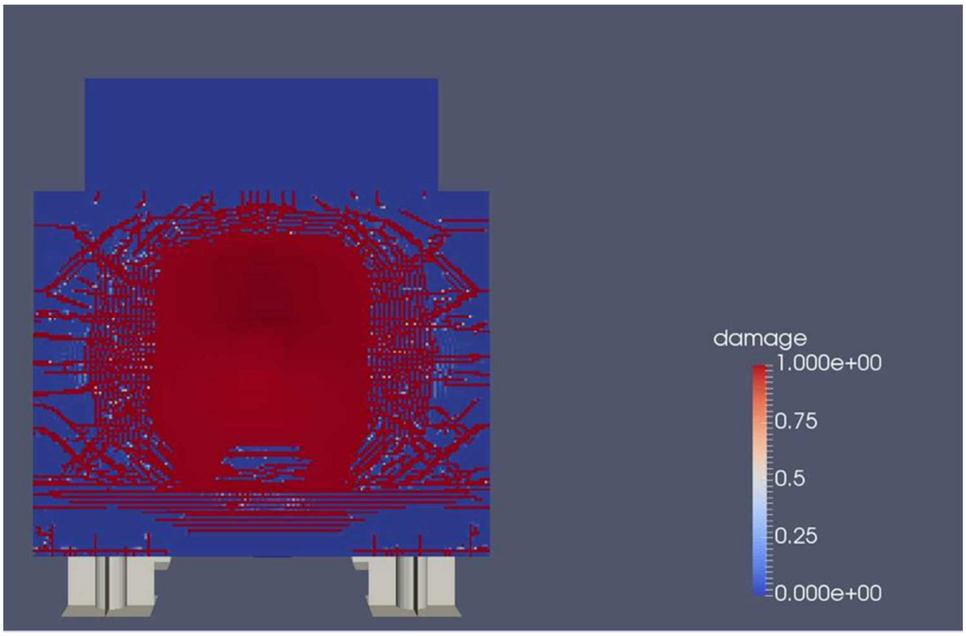

Figure 161: Damage on the front face of the mock-up from the 170 m/s missile

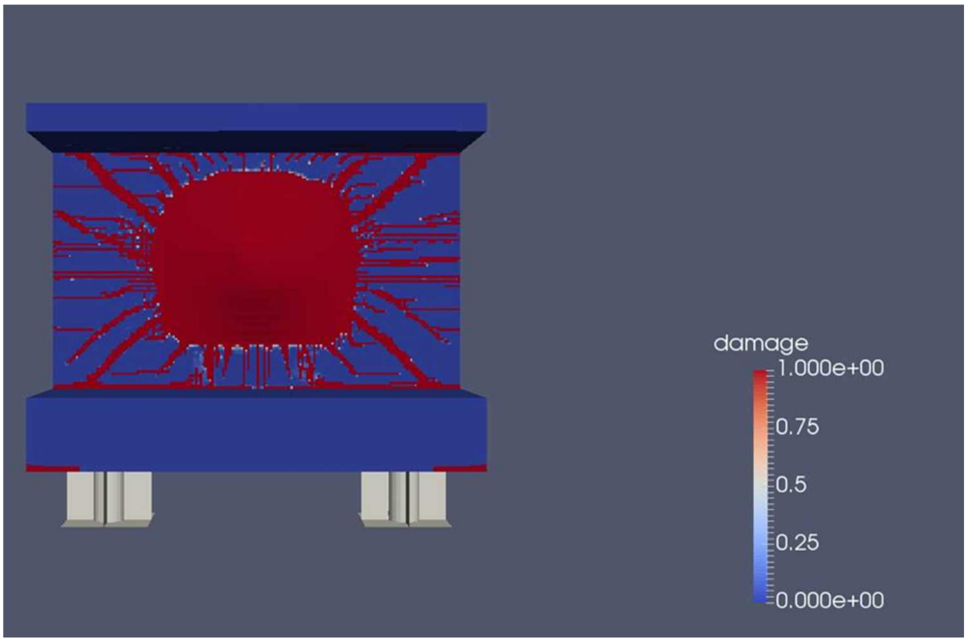

Figure 162: Damage on the back of the front face of the mock-up from the 170 m/s missile

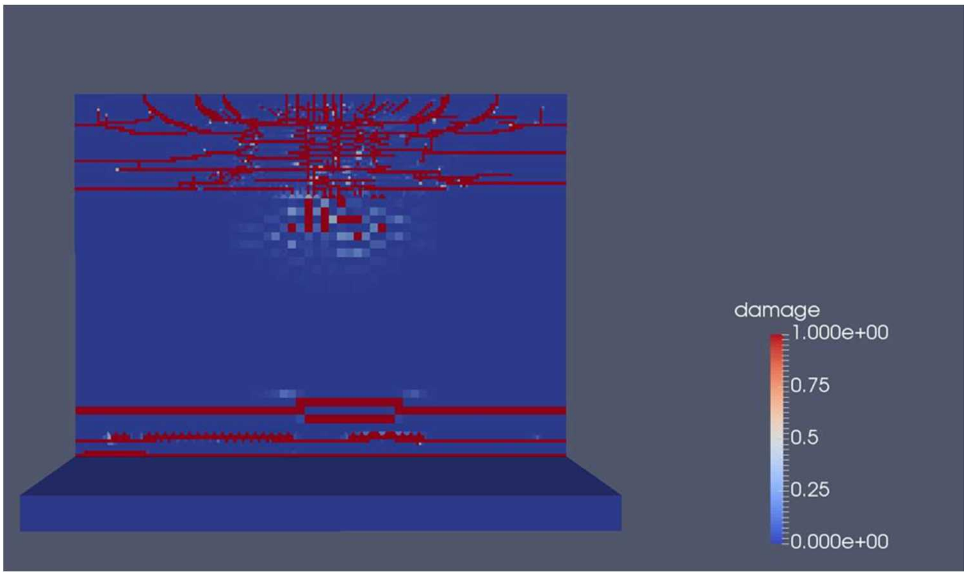

Figure 163: Damage on the top faces of the mock-up from the 170 m/s missile

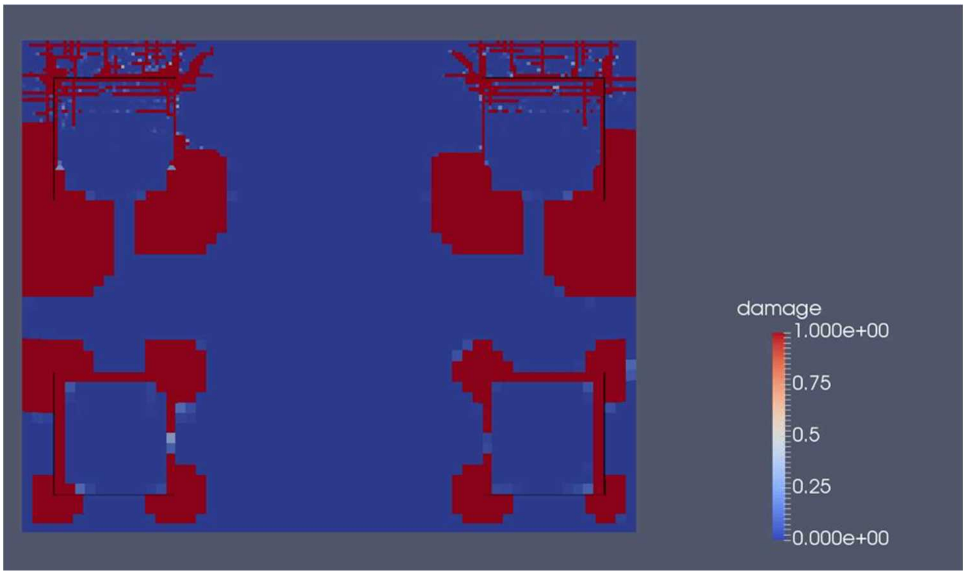

Figure 164: Damage on the bottom face of the mock-up from the 170 m/s missile

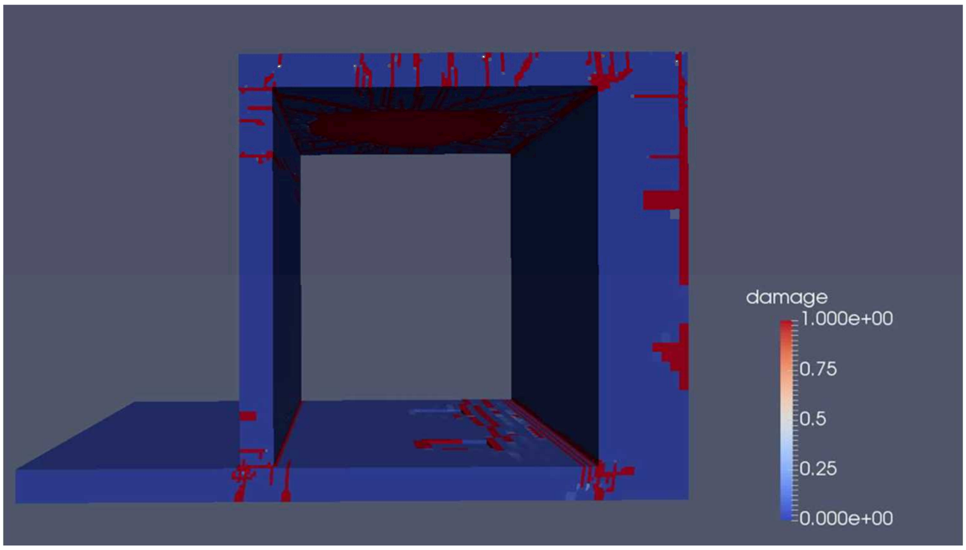

Figure 165: Damage on the side face of the mock-up from the 170 m/s missile

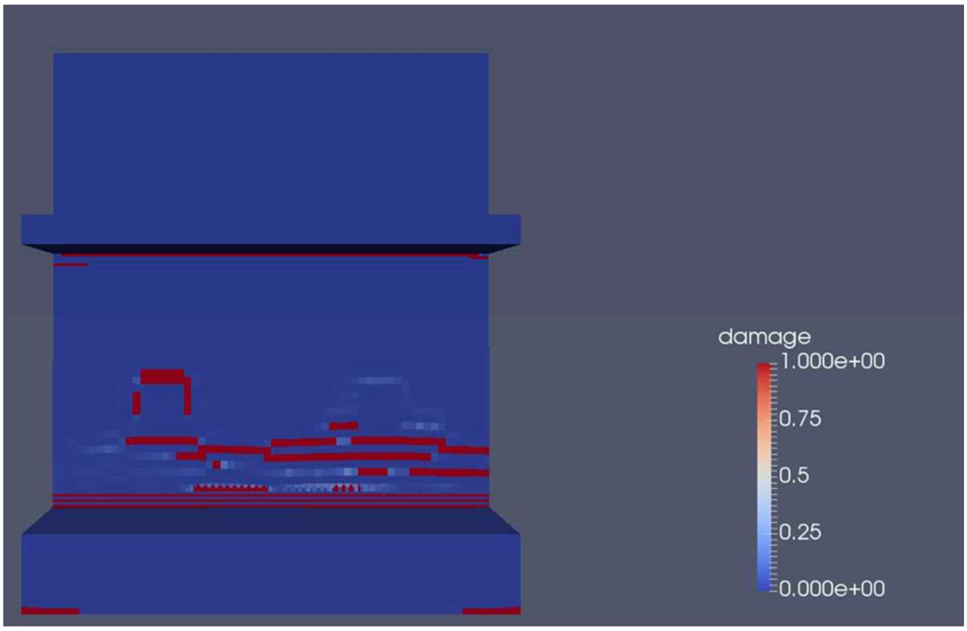

Figure 166: Damage on the front face of the back wall of the mock-up from the 170 m/s missile

The final displacement of the mockup is shown in Figure 167 and Figure 168.

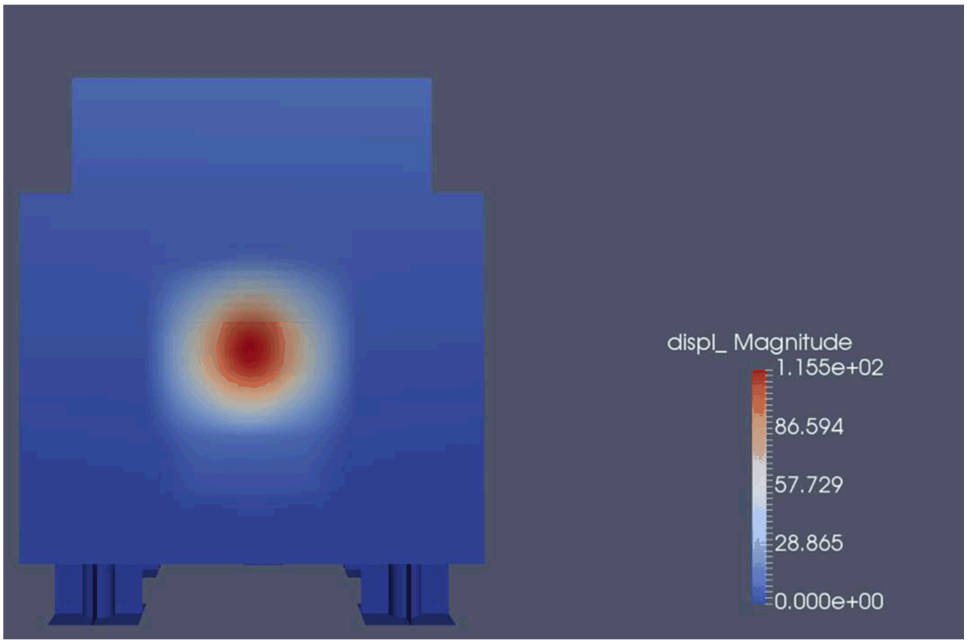

Figure 167: Front view of the final displacements of the mock-up from the 170 m/s missile (mm). The displacements are large in the center of the impact face due to missile penetration and excessive plastic rebar deformation

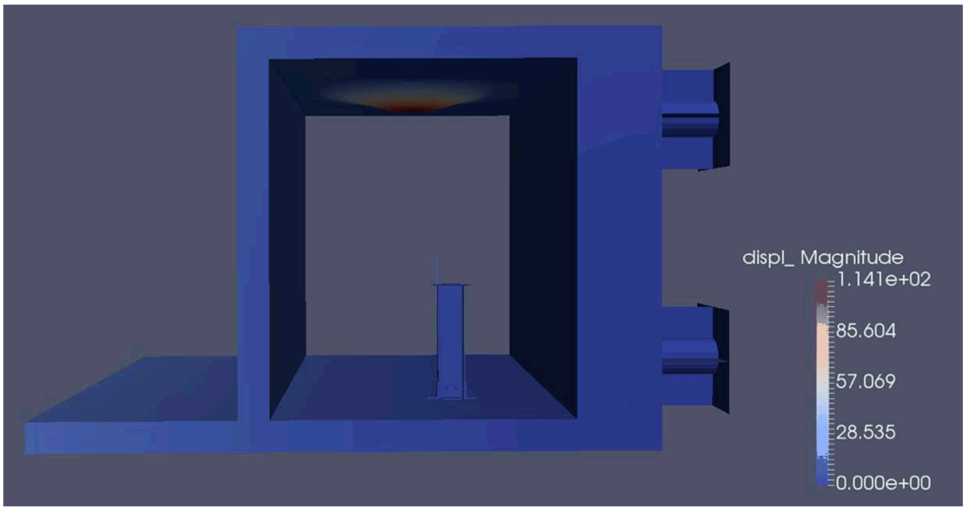

Figure 168: Side view of the final displacements of the mock-up from the 170 m/s missile (mm). The displacements are large in the center of the impact face due to missile penetration and excessive plastic rebar deformation

5.2.2 Concrete strains (at sensors locations)

The concrete strains at the selected output locations are shown in Table 13.

Table 13: Concrete Strains at Selected Output Locations

Sensor	Peak Displacement (mm)	Final Displacement (mm)	Sensor	Peak Displacement (mm)	Final Displacement (mm)
D01	-137	-115	D6V	4.53	-0.40
D02	-14.1	-5.59	D7	-35.8	-16.0
D03	-65.7	-52.9	D7L	-35.8	-16.0
D1	-21.5	-9.20	D8HX	.06	.02
D2	7.75	2.09	D8V	12.0	3.03
D3	-22.8	-9.58	D8HZ	-4.00	-1.10
D3L	-22.8	-9.59	D9	-9.92	-3.47
D4H	-5.99	-3.05	D9L	-9.90	-3.47
D4V	12.2	2.95	D9W	-9.95	-3.49
D5	5.77	1.36	D10	7.05	1.89
D6H	-1.78	-0.42	D10W	14.1	4.73

5.2.3 Rebars strains (at sensors locations)

The rebar strains at the selected output locations are show Table 14.

Table 14: Rebar Strains at Selected Output Locations

Sensor	Peak Strain (με)	Final Strain (με)	Sensor	Peak Strain (με)	Final Strain (με)
G0H	-736	-64.8	G3V	464	-159
G0V	6889	4310	G4V	1498	507
G1V	1391	-5.29	G5V	651	171
G2V	787	25.9	G6V	421	5.93

5.2.4 Reaction forces at supports locations

The reaction forces at the supports are summarized in Table 15.

Table 15: Reaction Forces

Support Location	Peak Force (kN)	Final Force (kN)
Front left	345	116.0
Front right	312	49.0
Rear left	-337	105.2
Rear right	-412	97.4

As noted previously, to reduce the high-frequency noise believed to be associated with numerical effects, the reaction force versus time data was filtered using a 4th order low pass Butterworth filter with a cutoff frequency of 1000 Hz. The reaction force vs time responses for the four supports are shown in Figure 169 through Figure 172.

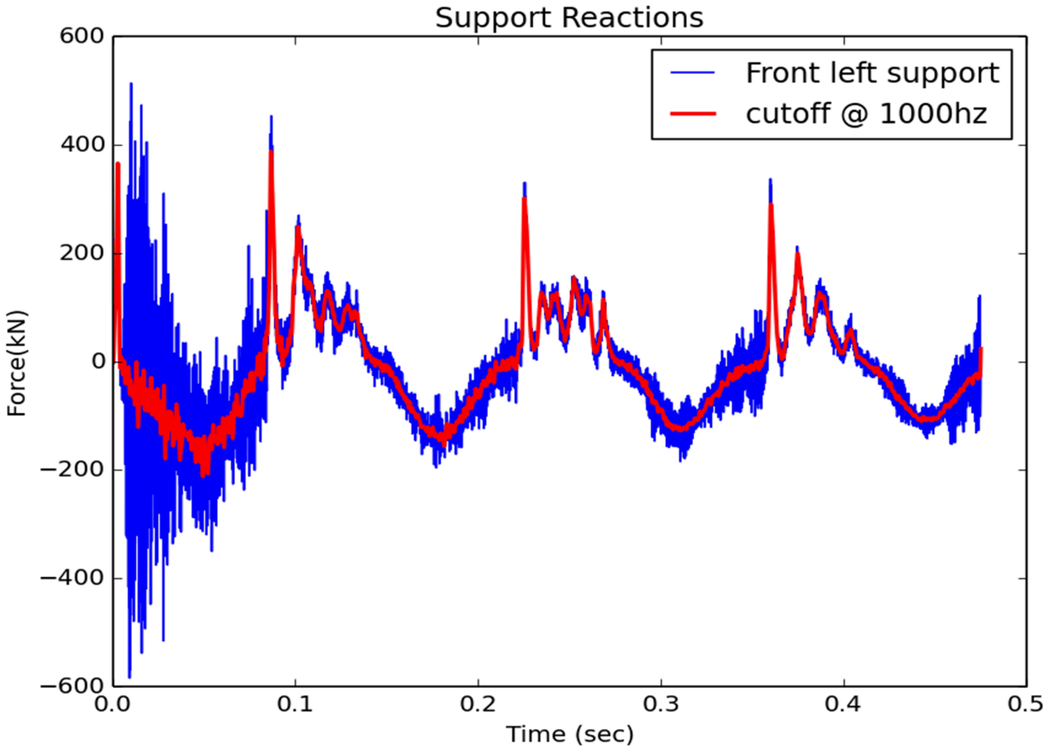

Figure 169: Front left support reaction force vs time

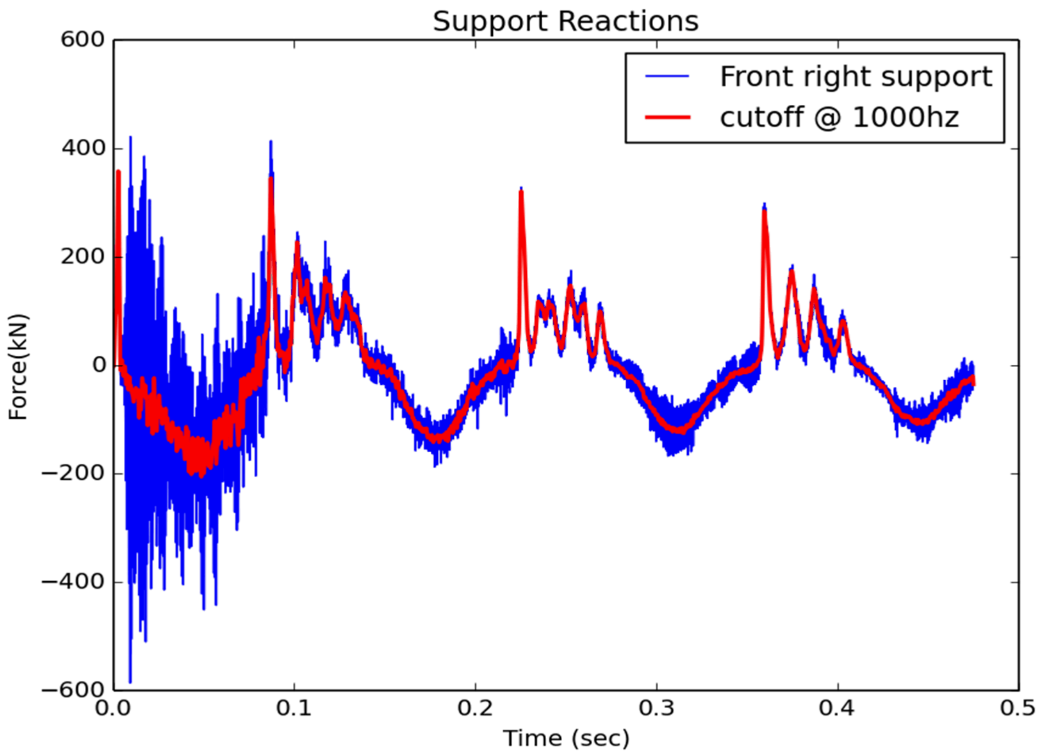

Figure 170: Front right support reaction force vs time

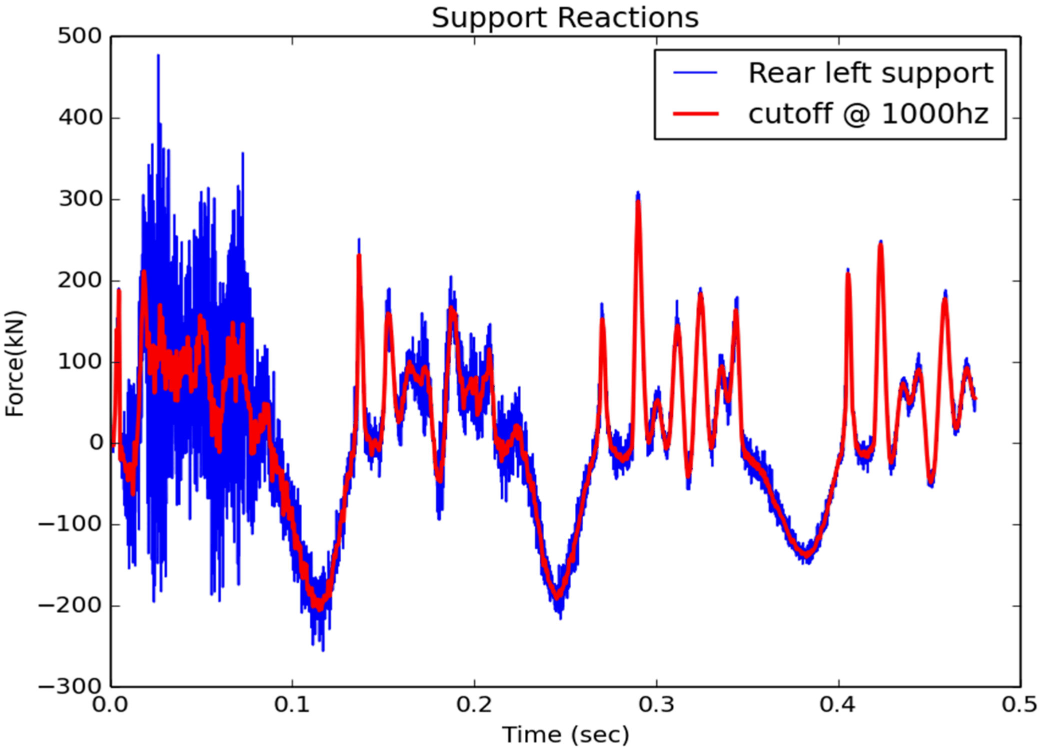

Figure 171: Rear left support reaction force vs time

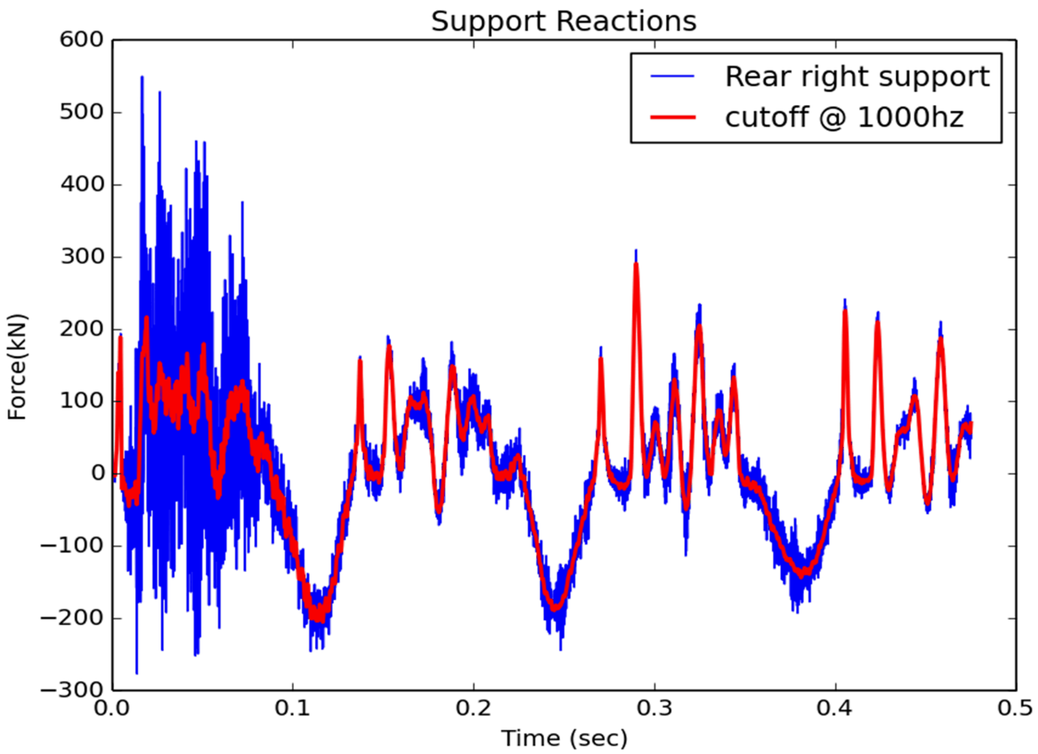

Figure 172: Rear right support reaction force vs time

5.2.5 Time histories (Displacements, Accelerations at sensors locations)

5.2.5.1 Displacements

The displacement versus time histories for the selected output locations are shown in Figure 173 through Figure 176.

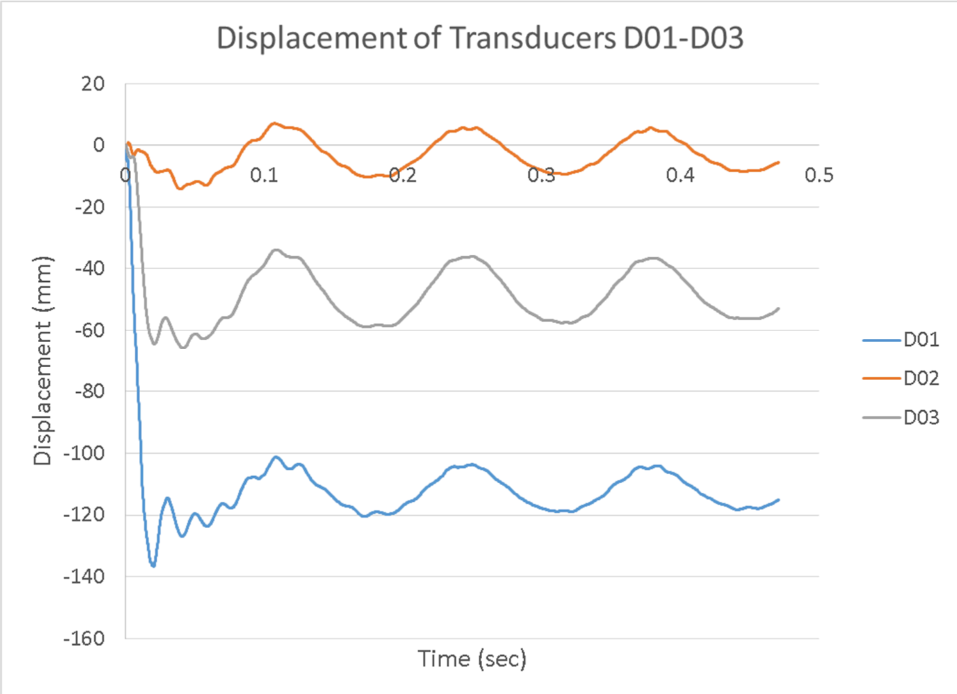

Figure 173: Displacements of transducers D01-D03 (mm)

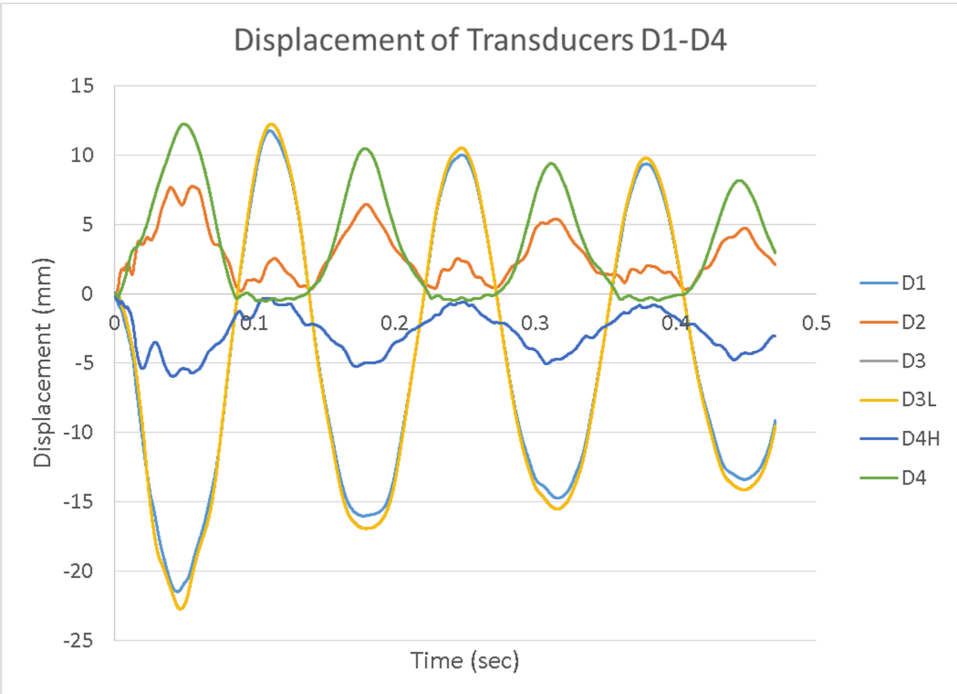

Figure 174: Displacements of transducers D1-D4 (mm)

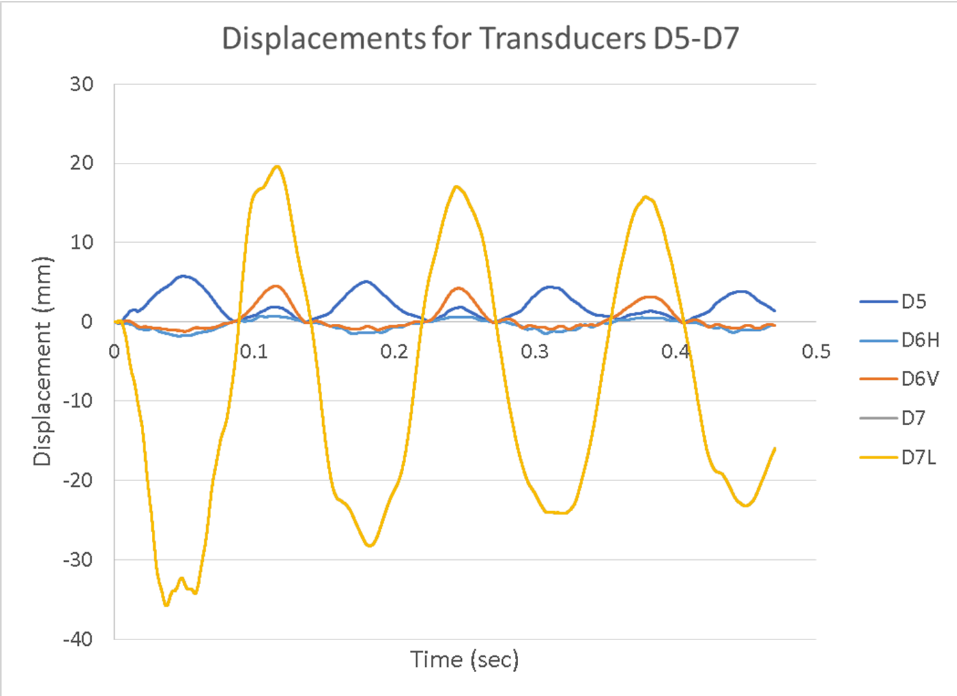

Figure 175: Displacements of transducers D5-D7 (mm)

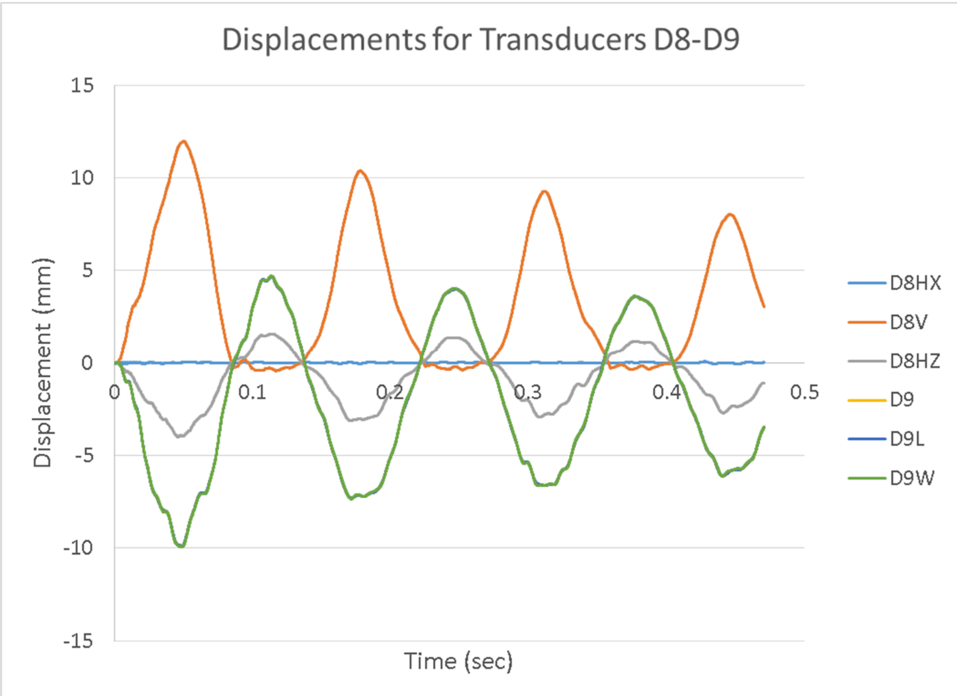

Figure 176: Displacements of transducers D8-D9 (mm)

5.2.5.2 Accelerations

As discussed previously, the acceleration versus time data was filtered using a Butterworth 4th order low pass filter with a cutoff at 100 Hz. The filtered acceleration versus time data is plotted in Figure 177 through Figure 191 for the selected output locations.

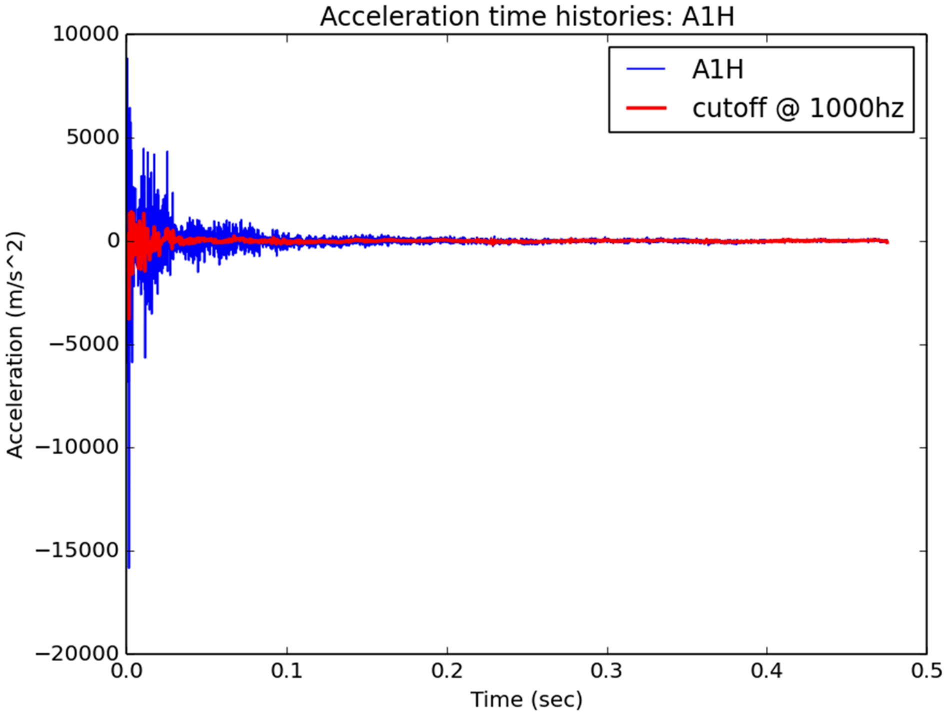

Figure 177: Acceleration versus time for A1H

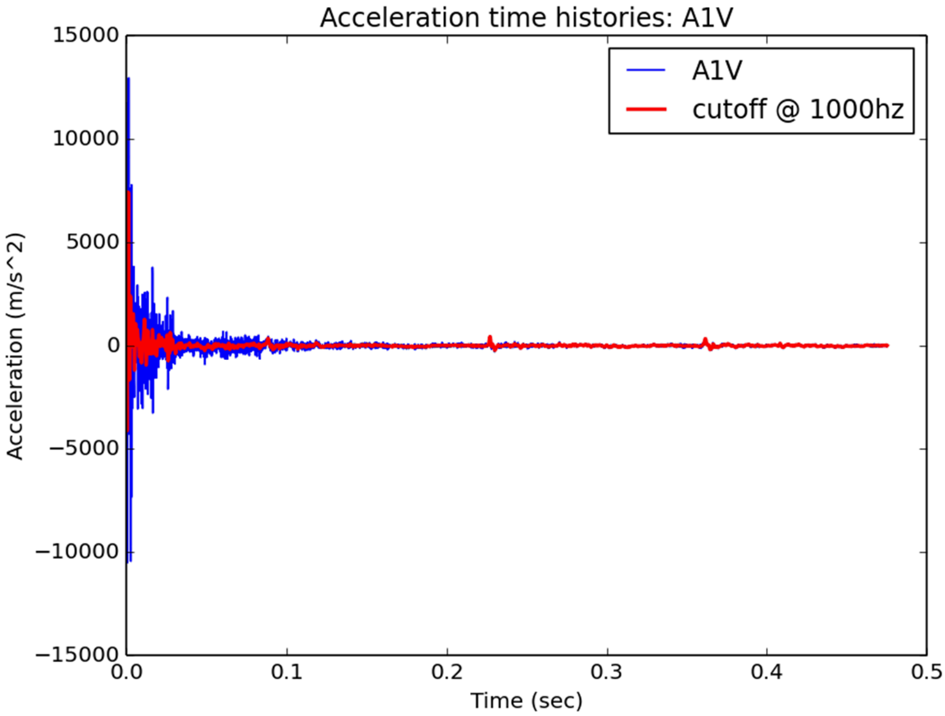

Figure 178: Acceleration versus time for A1V

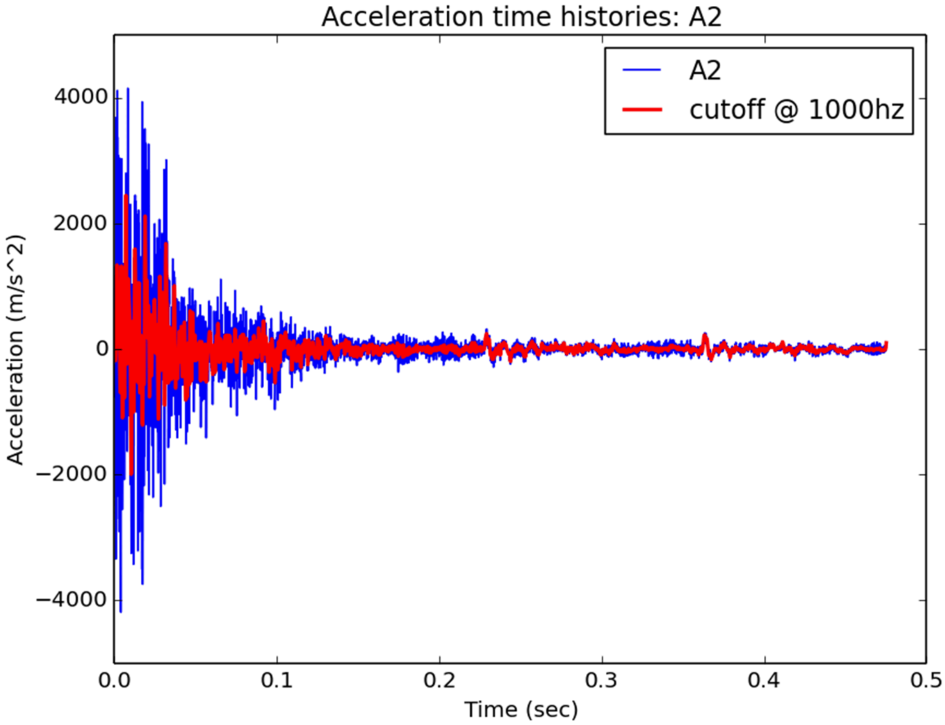

Figure 179: Acceleration versus time for A2

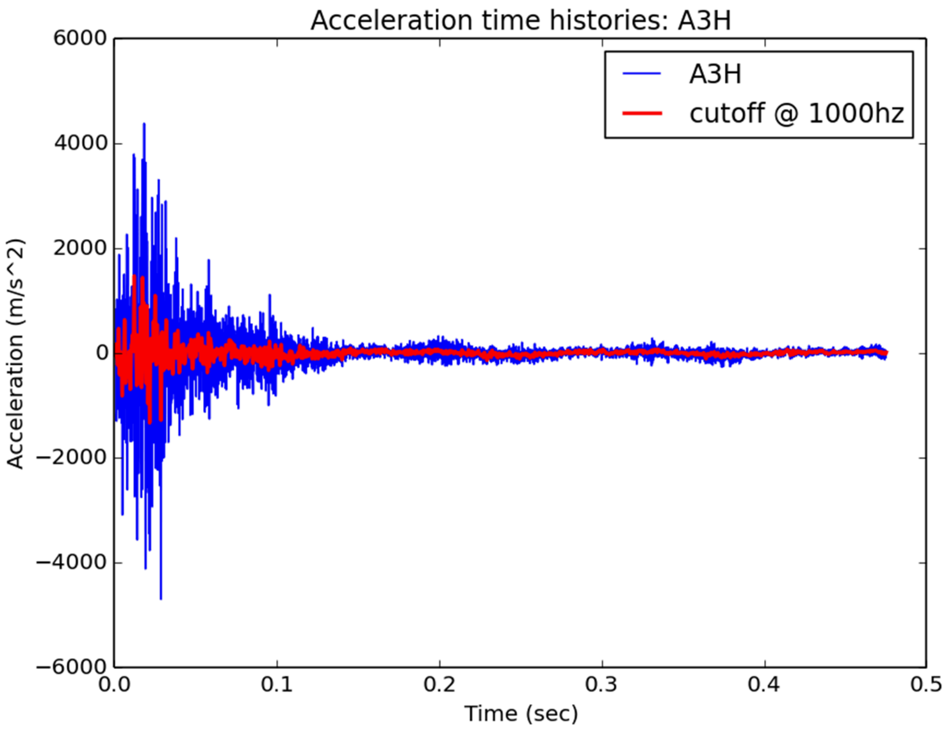

Figure 180: Acceleration versus time for A3H

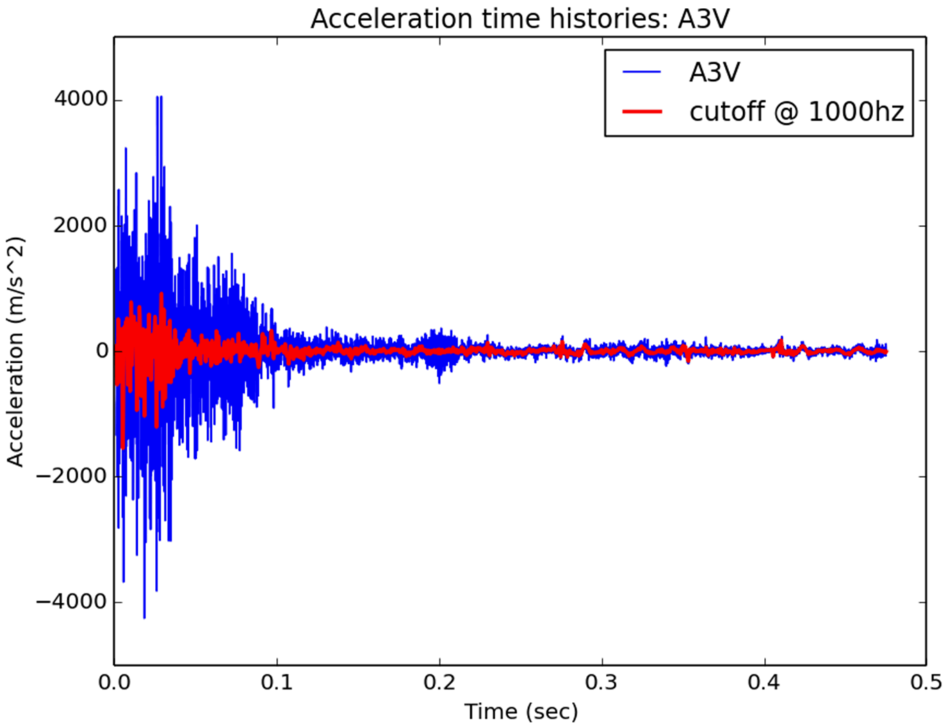

Figure 181: Acceleration versus time for A3V

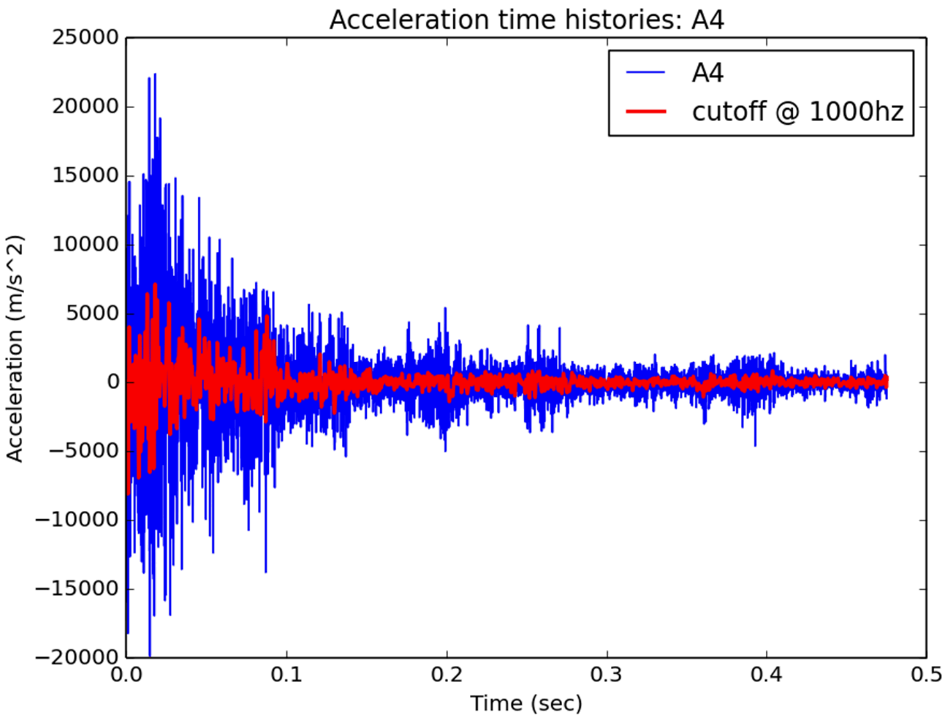

Figure 182: Acceleration versus time for A4

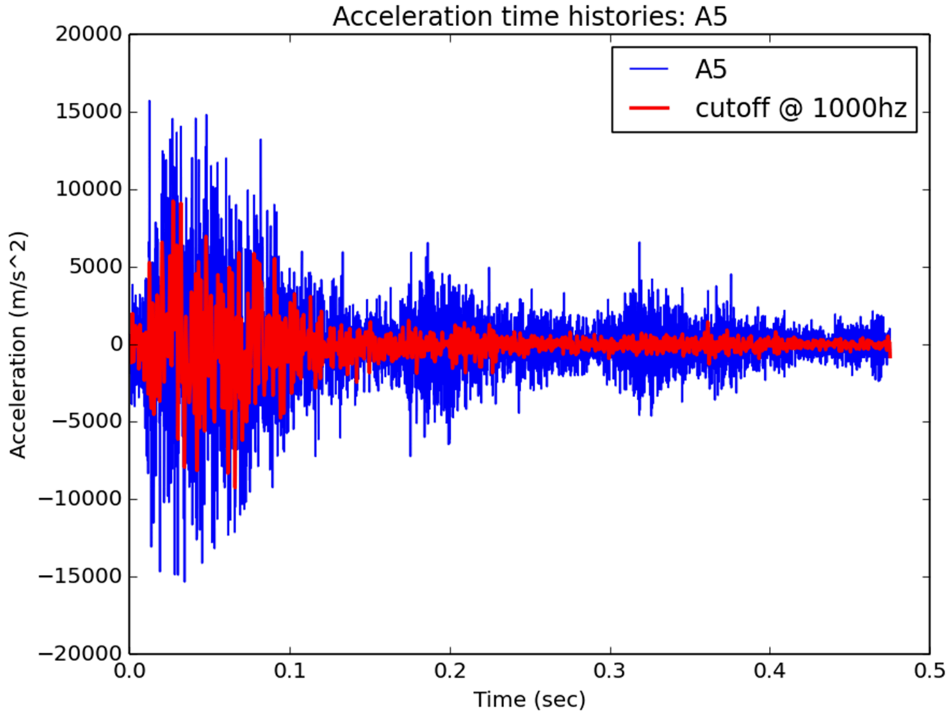

Figure 183: Acceleration versus time for A5

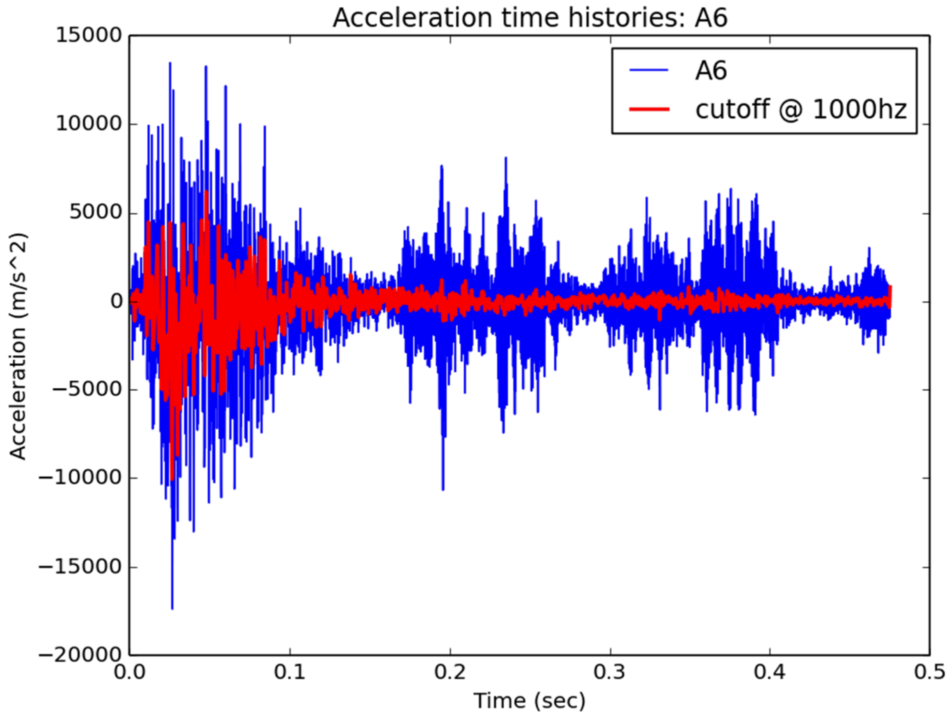

Figure 184: Acceleration versus time for A6

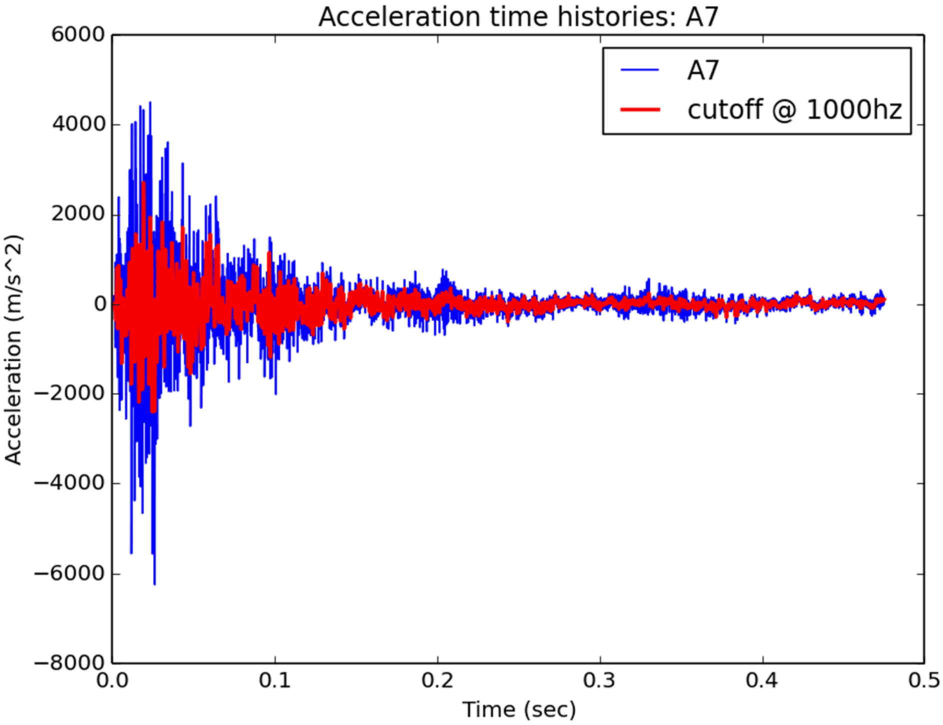

Figure 185: Acceleration versus time for A7

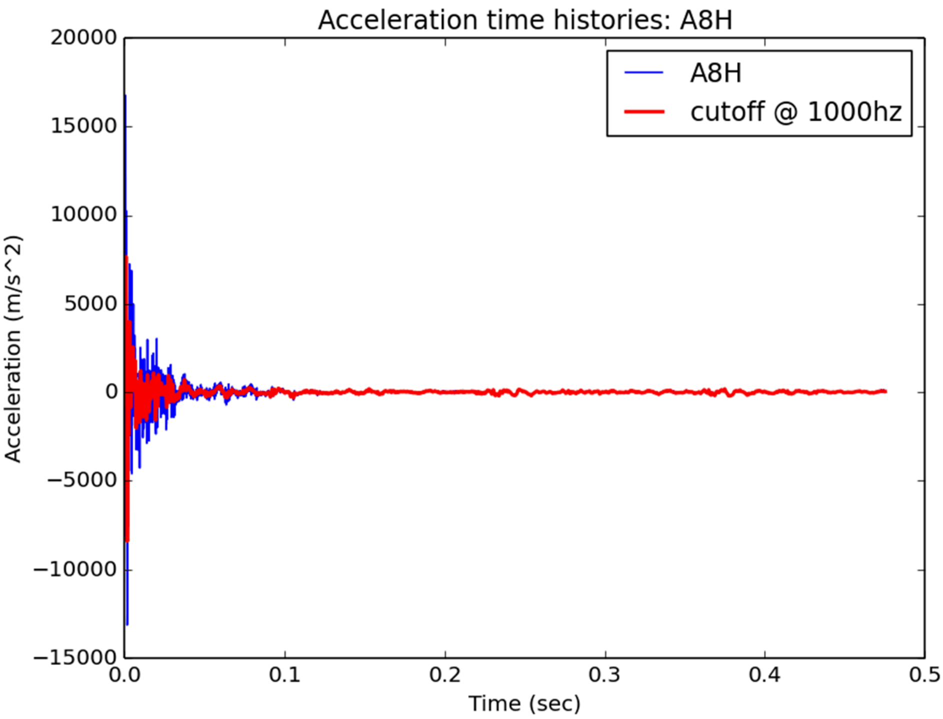

Figure 186: Acceleration versus time for A8H

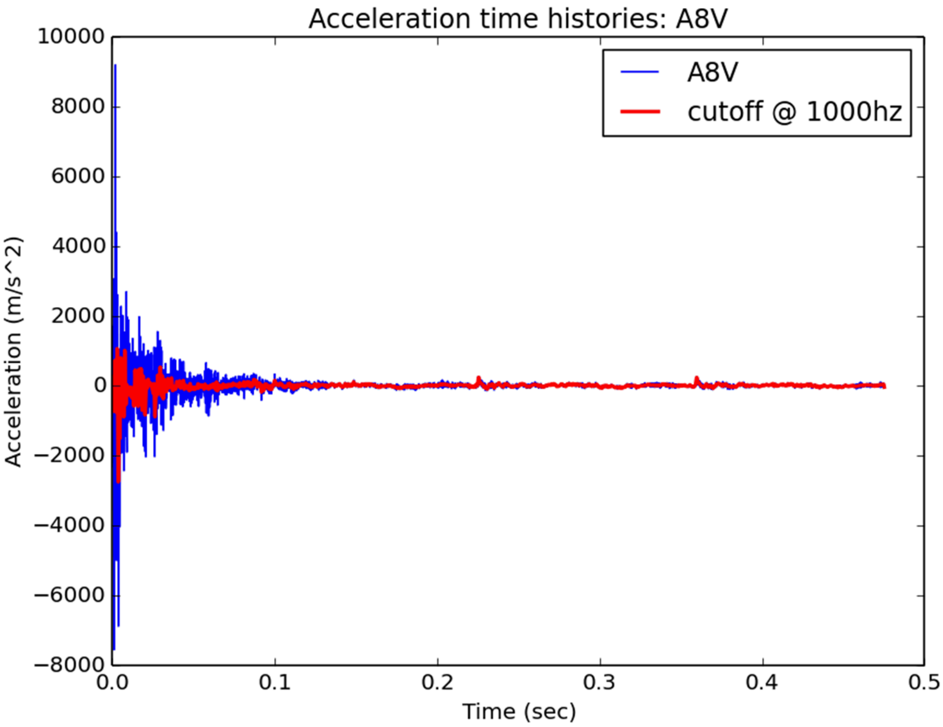

Figure 187: Acceleration versus time for A8V

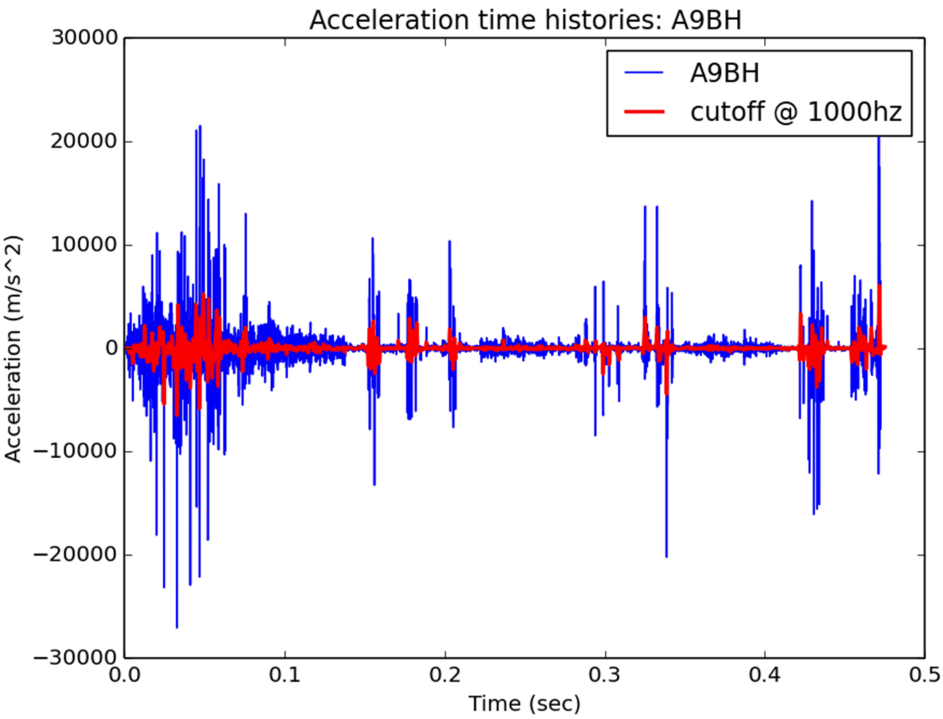

Figure 188: Acceleration versus time for A9BH

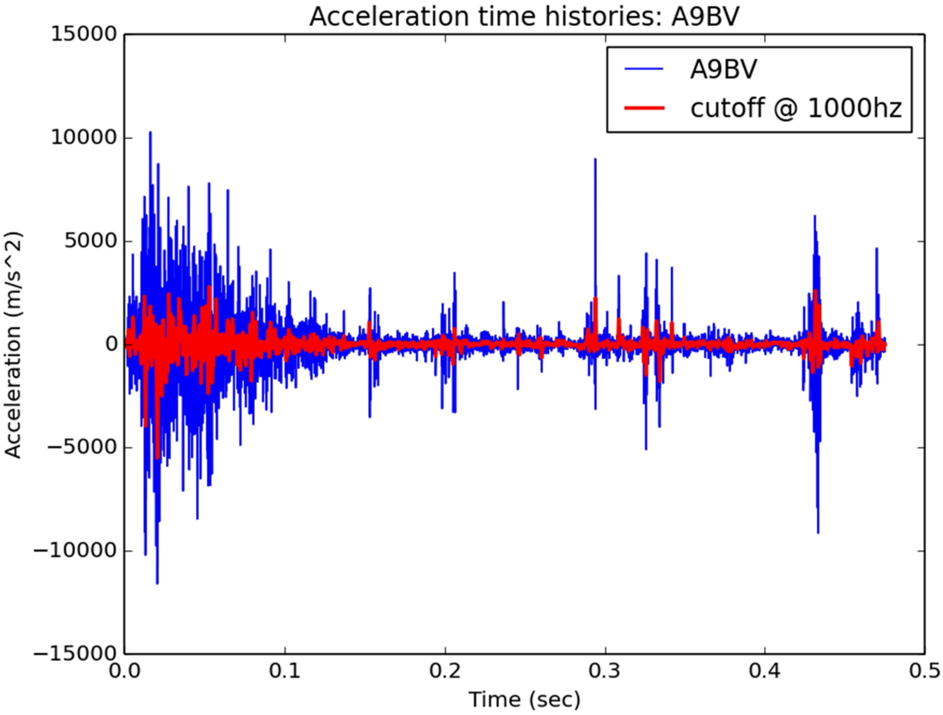

Figure 189: Acceleration versus time for A9BV

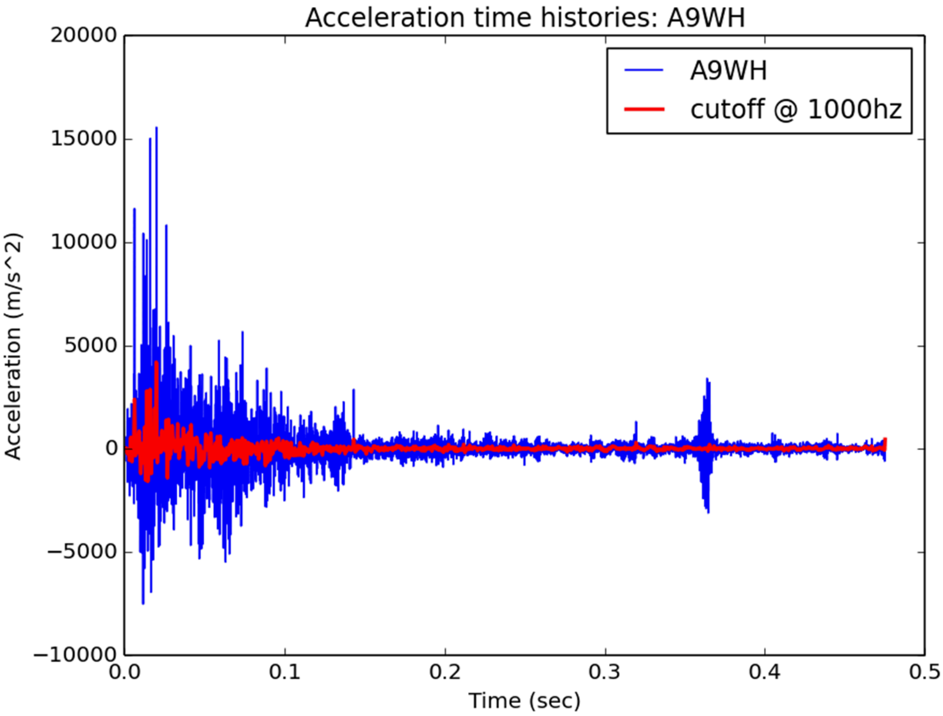

Figure 190: Acceleration versus time for A9WH

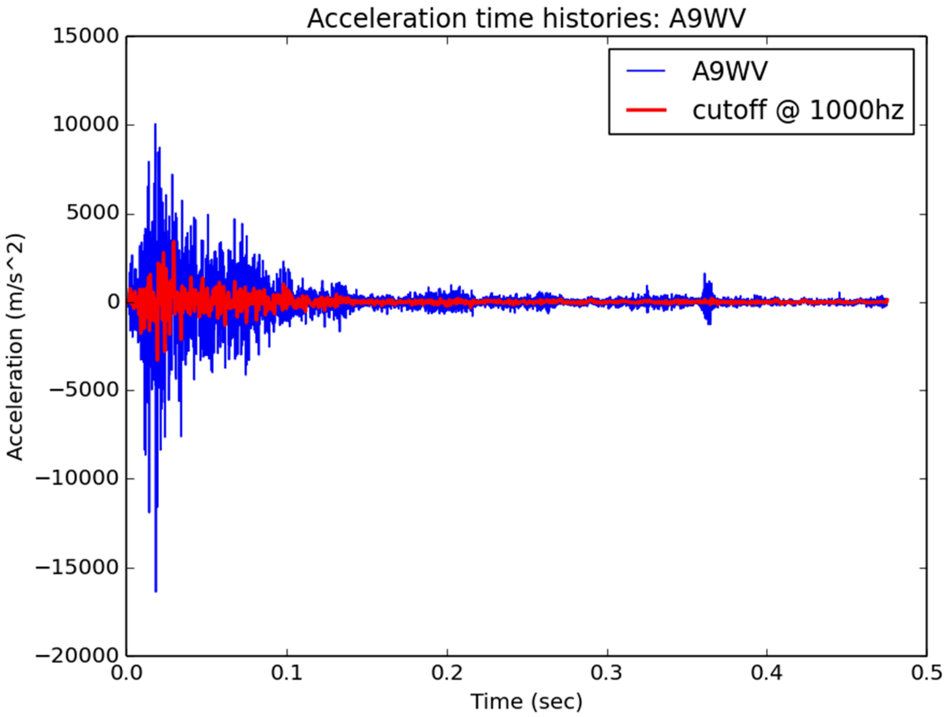

Figure 191: Acceleration versus time for A9WV

5.2.6 Response spectra at 5 % damping

No damping was implemented in this simulation.

5.2.7 Acceleration frequency content analysis (FFT, Power Spectral Density, …)

Fast Fourier Transform analysis results for the filtered acceleration versus time data for the selected output locations are shown in Figure 192 through Figure 206.

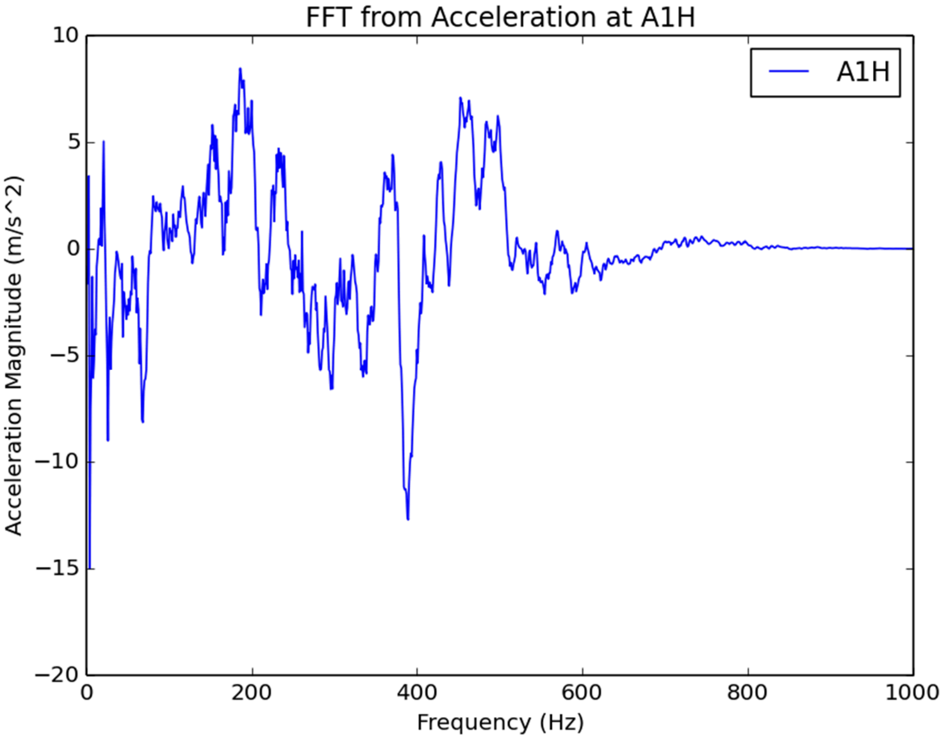

Figure 192: Acceleration Fast Fourier Transform for A1H

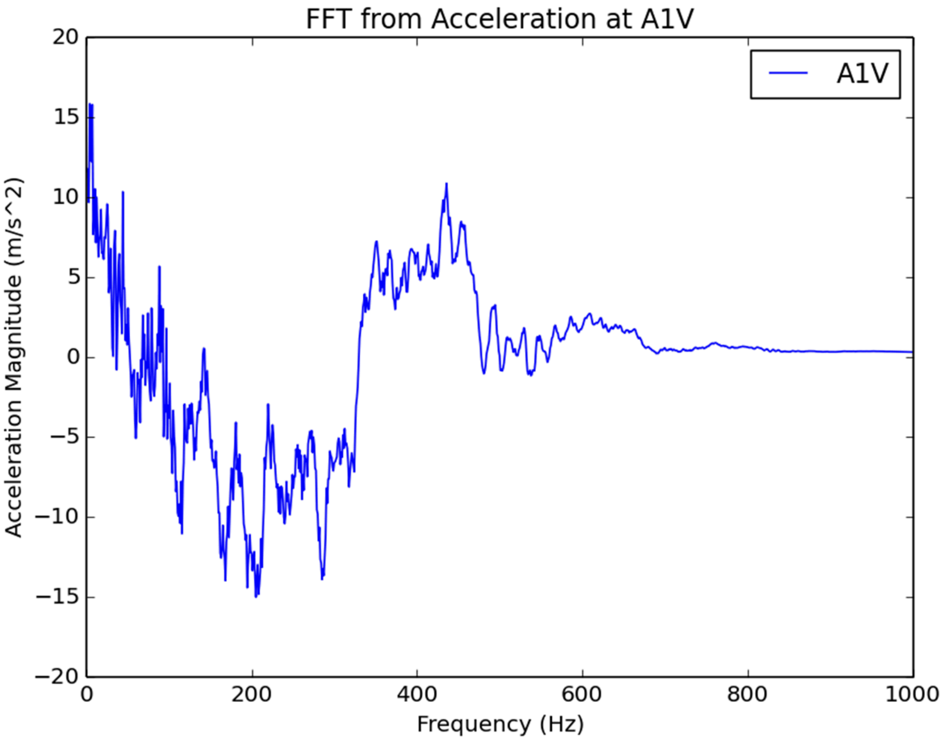

Figure 193: Acceleration Fast Fourier Transform for A1V

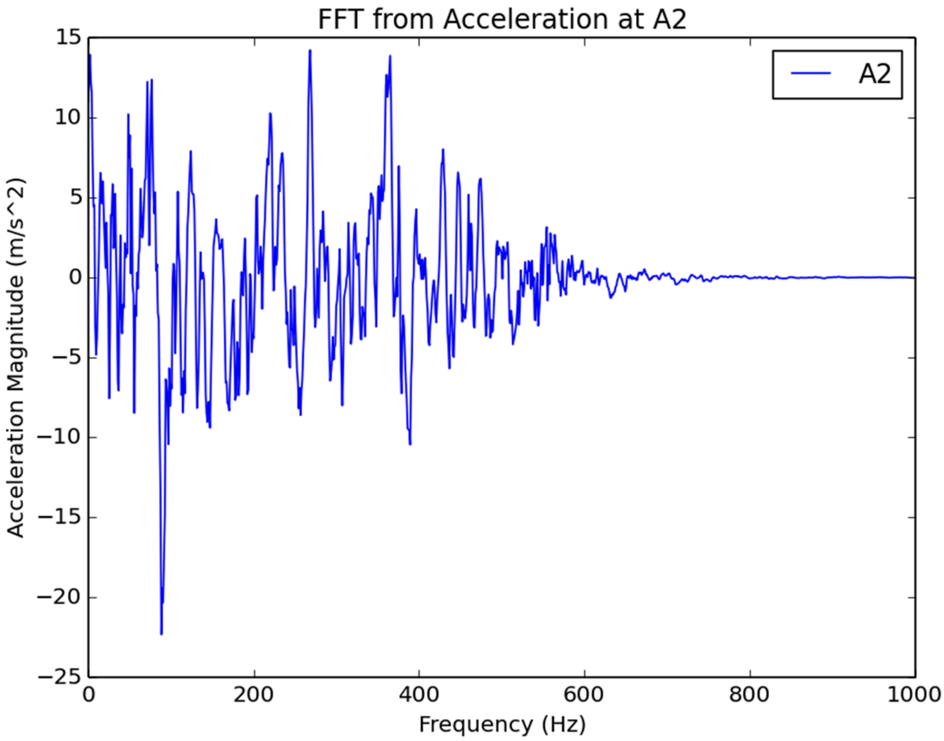

Figure 194: Acceleration Fast Fourier Transform for A2

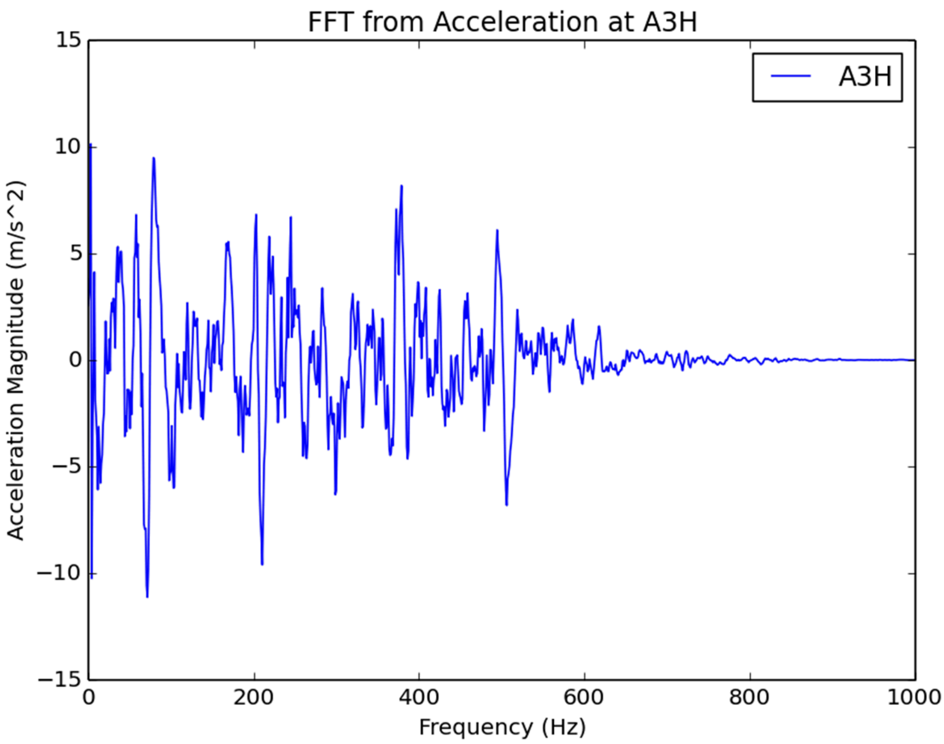

Figure 195: Acceleration Fast Fourier Transform for A3H

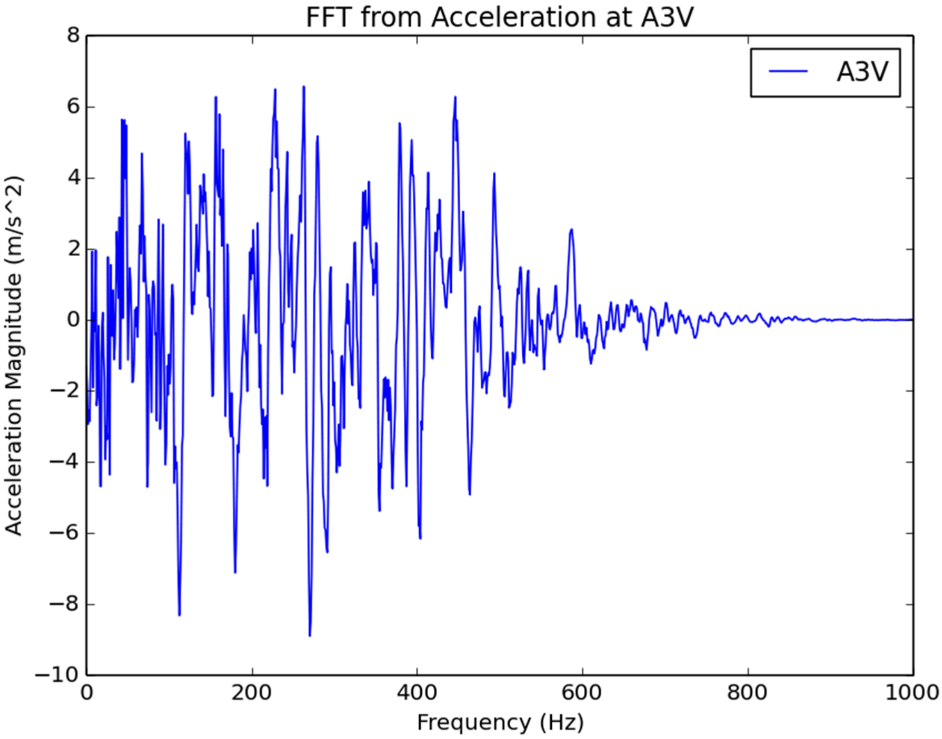

Figure 196: Acceleration Fast Fourier Transform for A3V

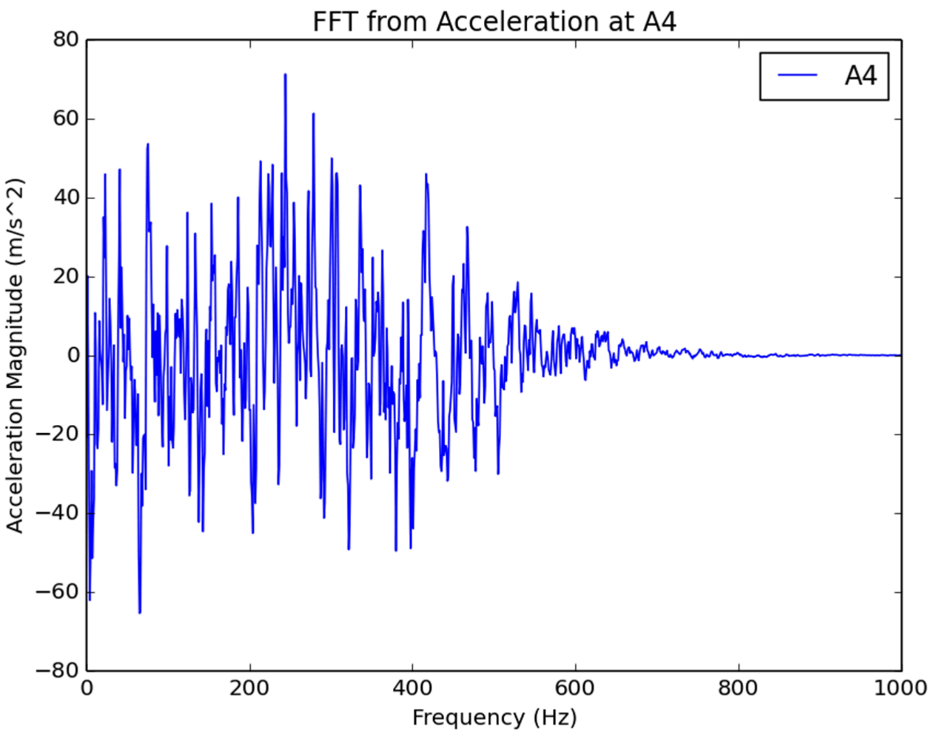

Figure 197: Acceleration Fast Fourier Transform for A4

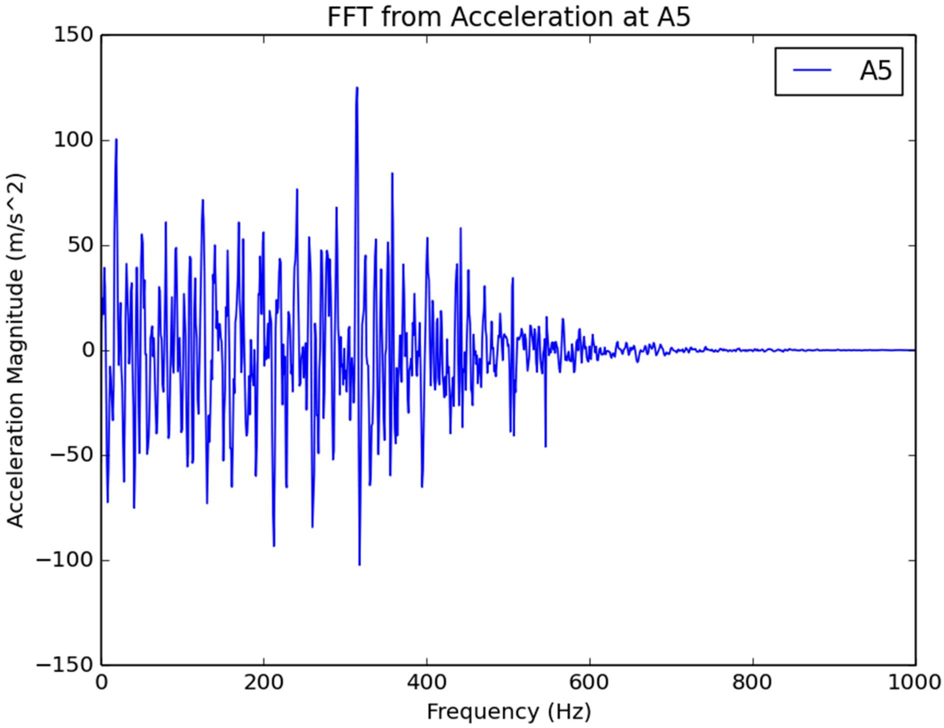

Figure 198: Acceleration Fast Fourier Transform for A5

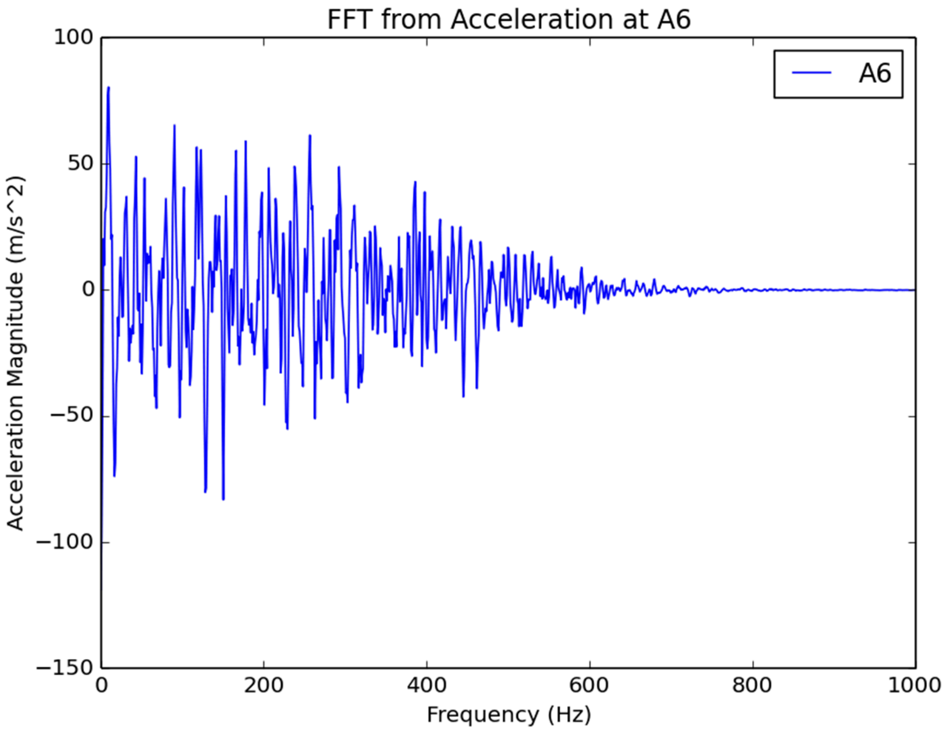

Figure 199: Acceleration Fast Fourier Transform for A6

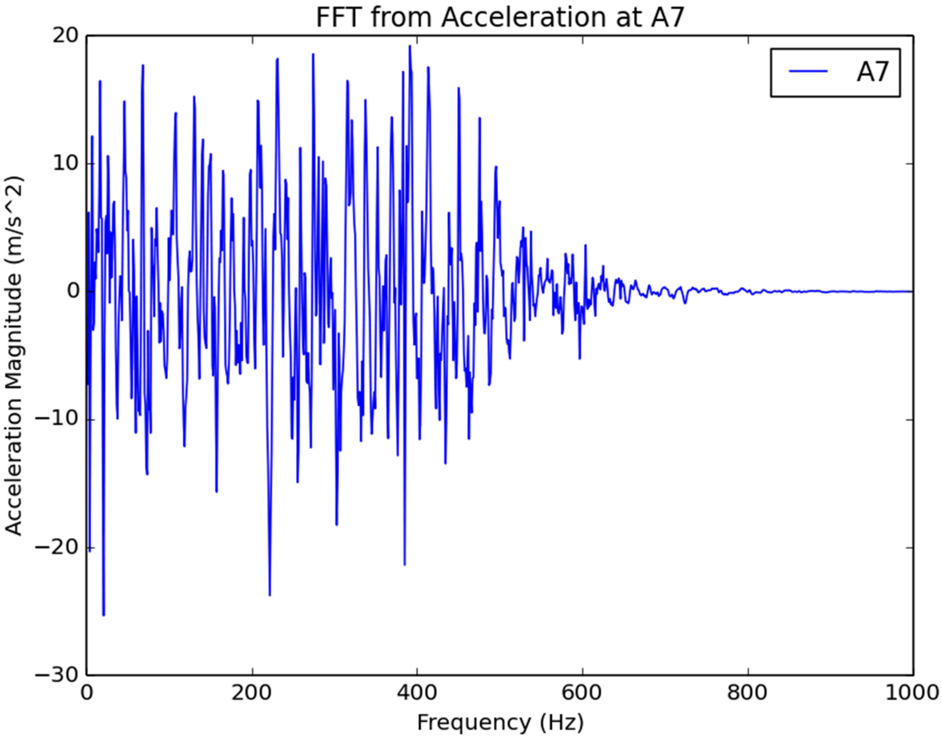

Figure 200: Acceleration Fast Fourier Transform for A7

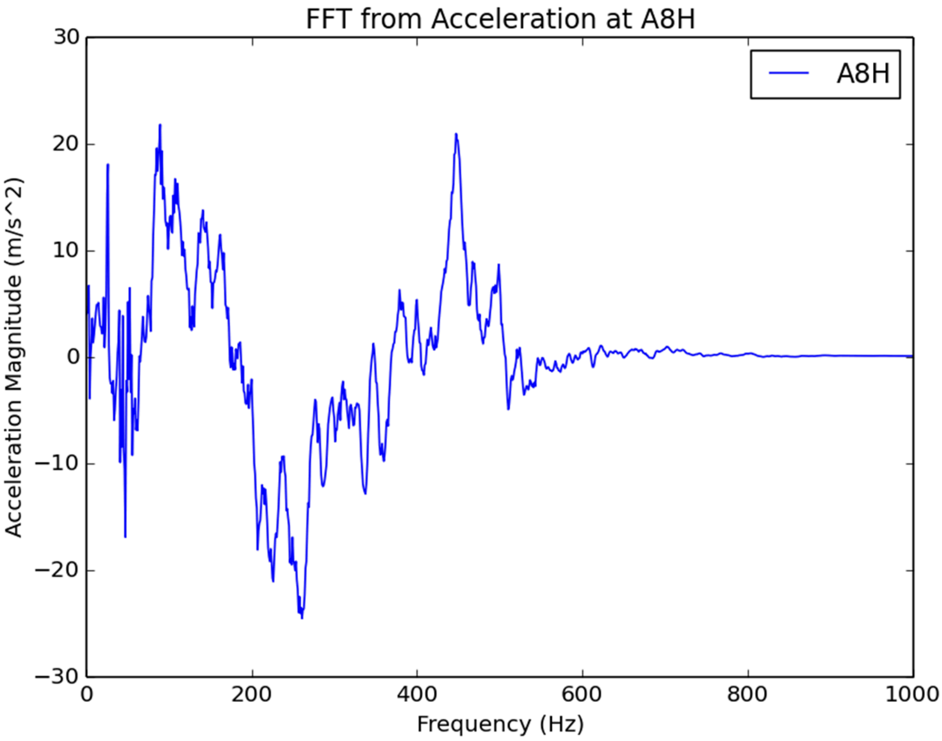

Figure 201: Acceleration Fast Fourier Transform for A8H

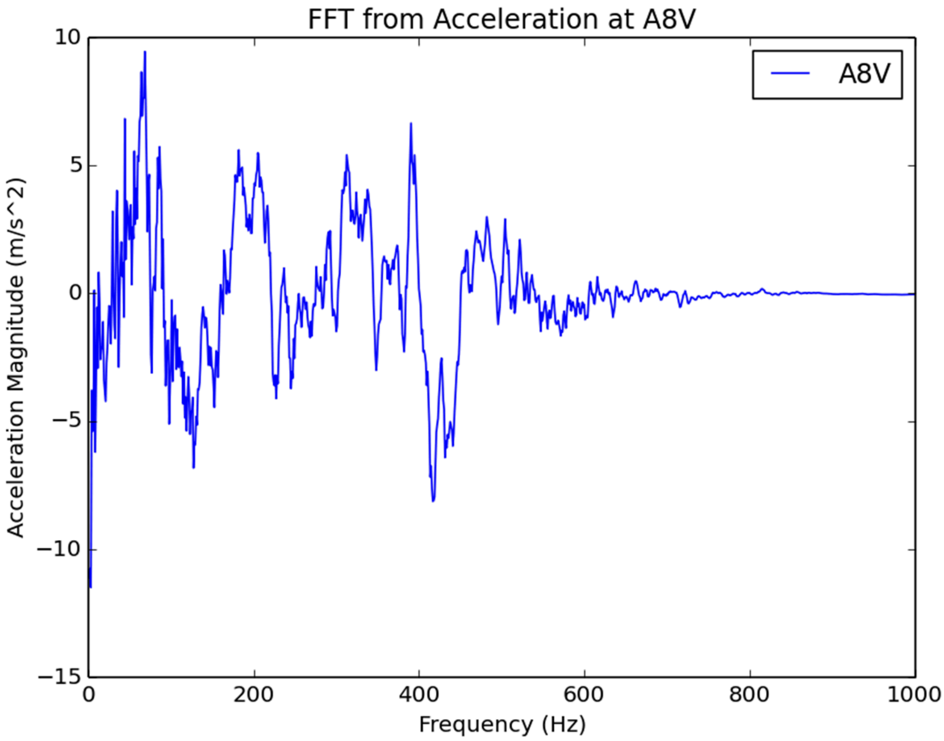

Figure 202: Acceleration Fast Fourier Transform for A8V

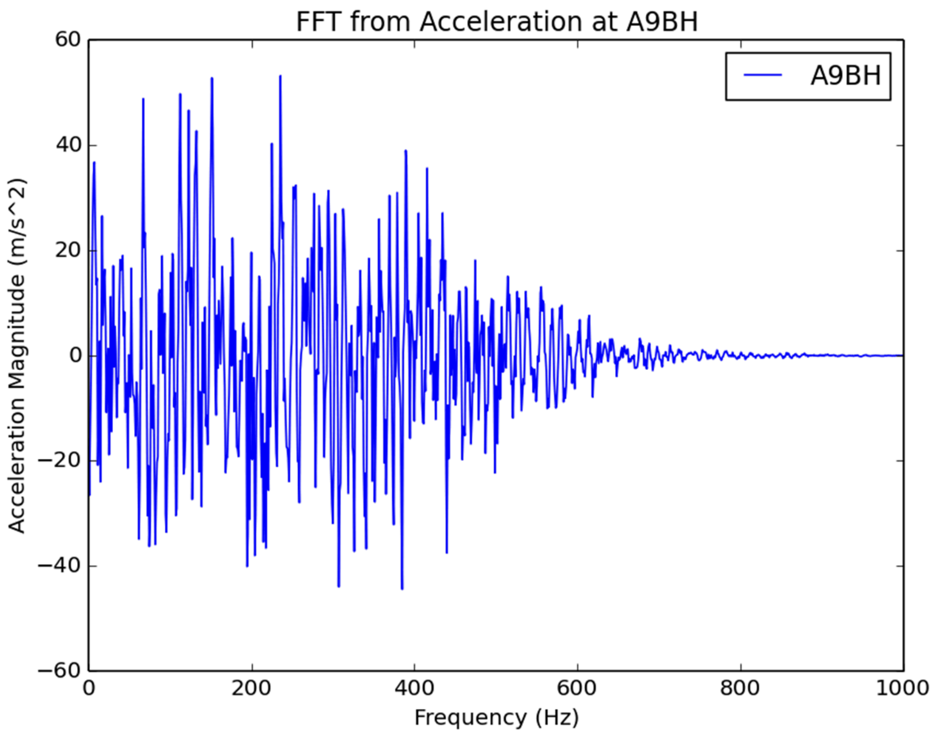

Figure 203: Acceleration Fast Fourier Transform for A9BH

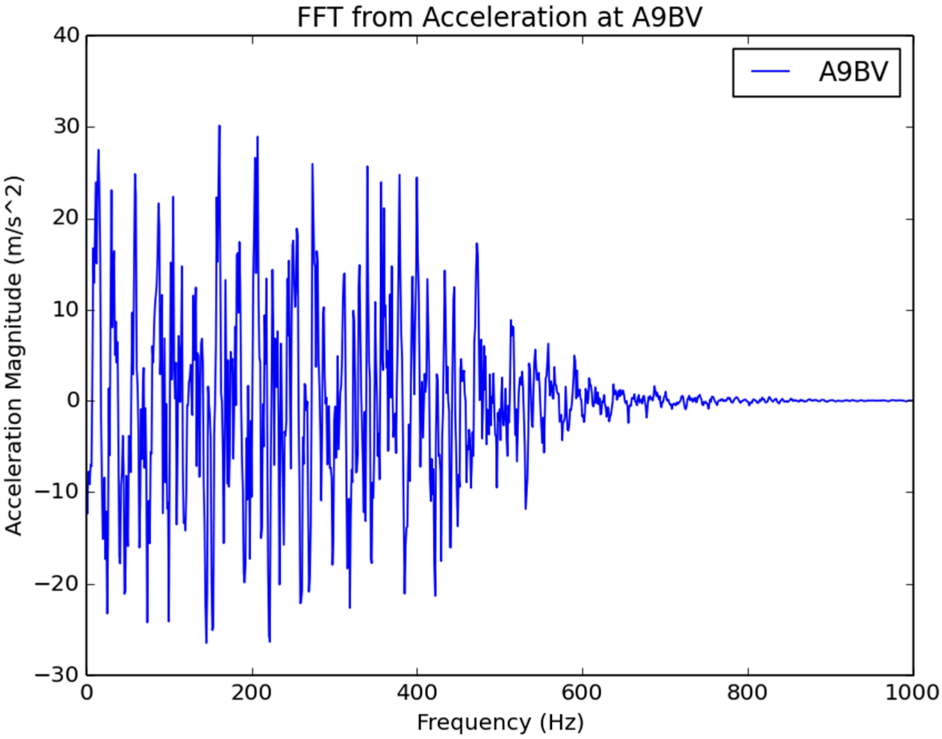

Figure 204: Acceleration Fast Fourier Transform for A9BV

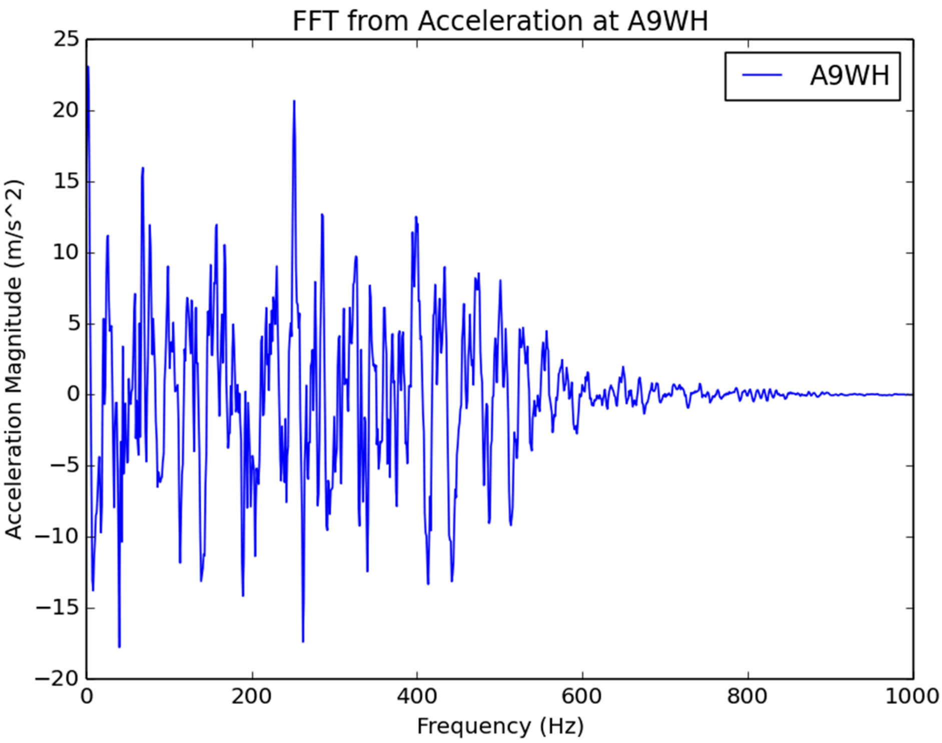

Figure 205: Acceleration Fast Fourier Transform for A9WH

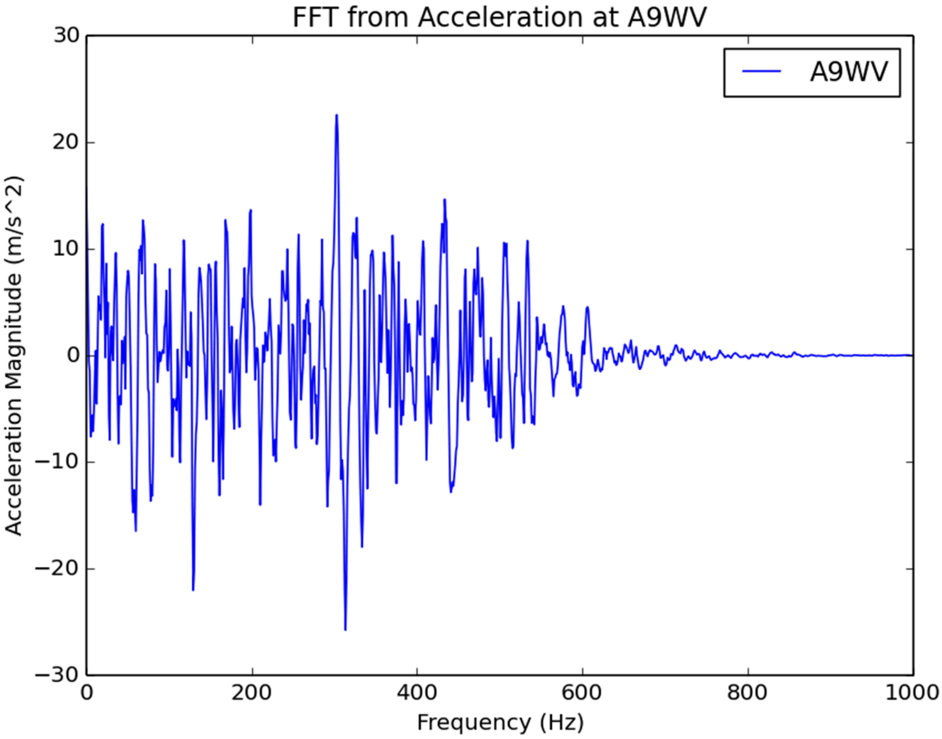

Figure 206: Acceleration Fast Fourier Transform for A9WV

5.3 Pseudo-equipments results

5.3.1 Time histories

5.3.1.1 Displacements

The displacement versus time response for the two beams (welded and bolted) is shown in Figure 207.

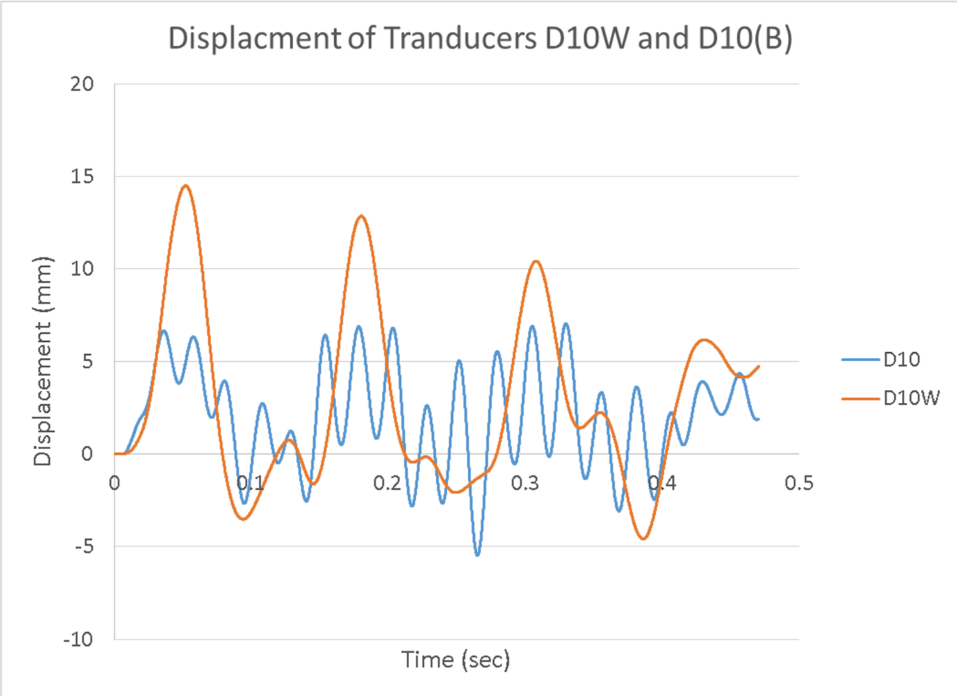

Figure 207: Time displacement history for D10 and D10W

5.3.1.2 Accelerations

The filtered acceleration versus time response data for the two beams for the 170 m/s impact are shown in Figure 208 through Figure 211.

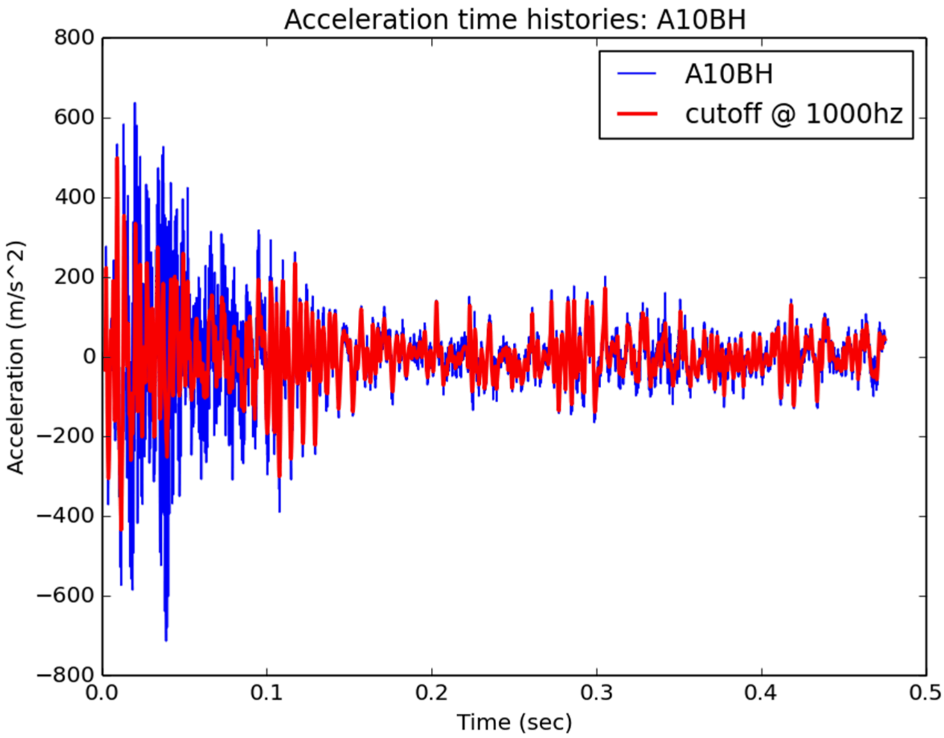

Figure 208: Acceleration versus time for A10BH

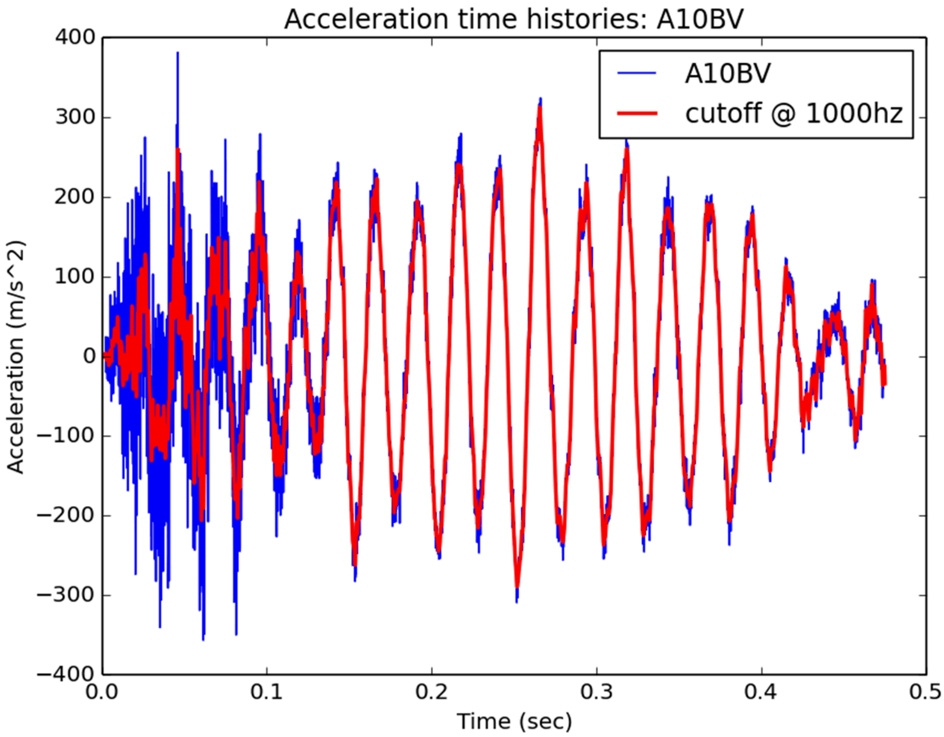

Figure 209: Acceleration versus time for A10BV

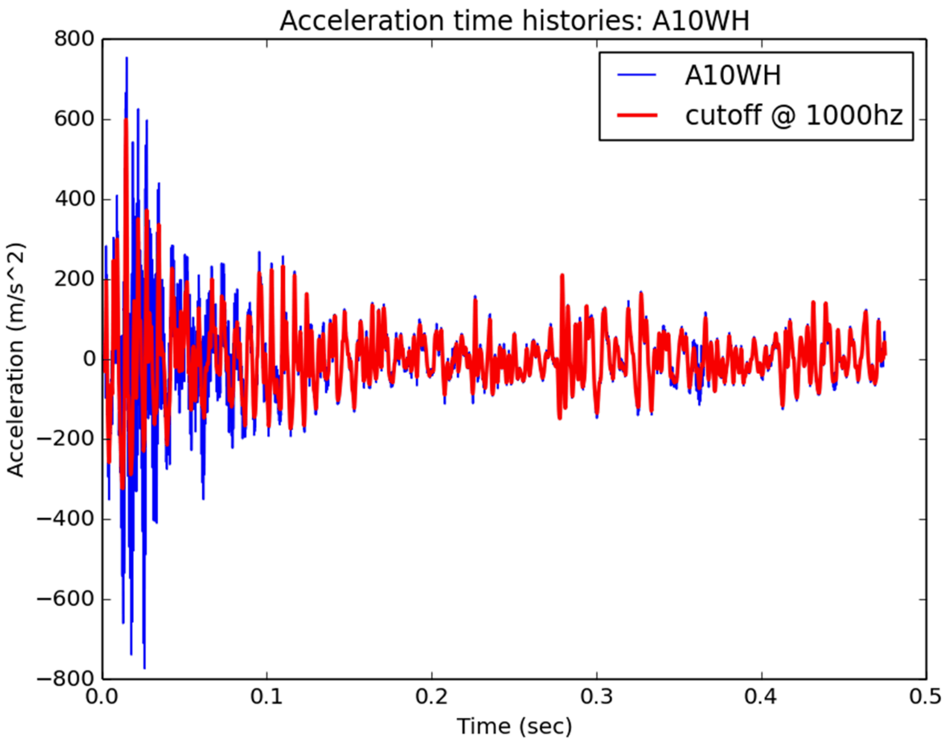

Figure 210: Acceleration versus time for A10WH

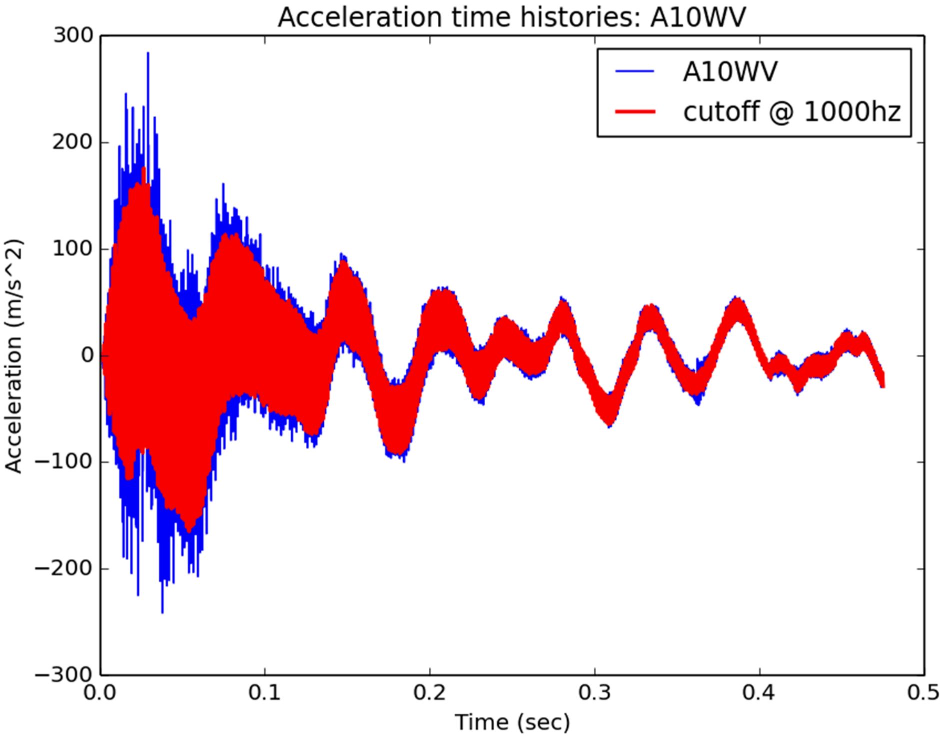

Figure 211: Acceleration versus time for A10WV

5.3.2 Acceleration frequency content analysis

Fast Fourier Transform analysis results for the two beams are shown in Figure 212 through Figure 215.

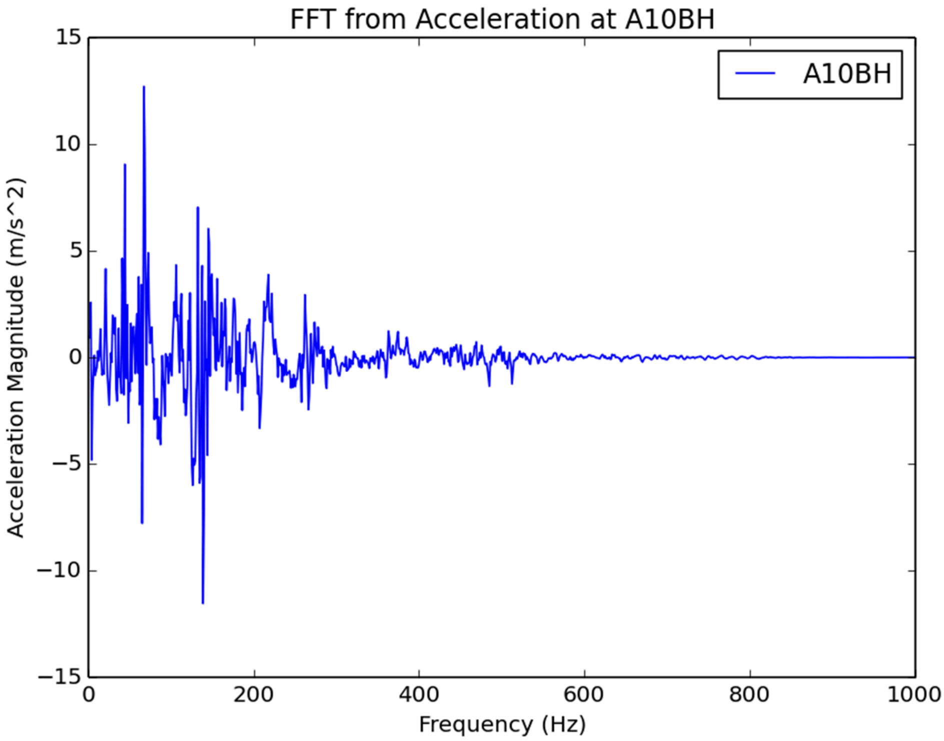

Figure 212: Fast Fourier Transform for A10BH

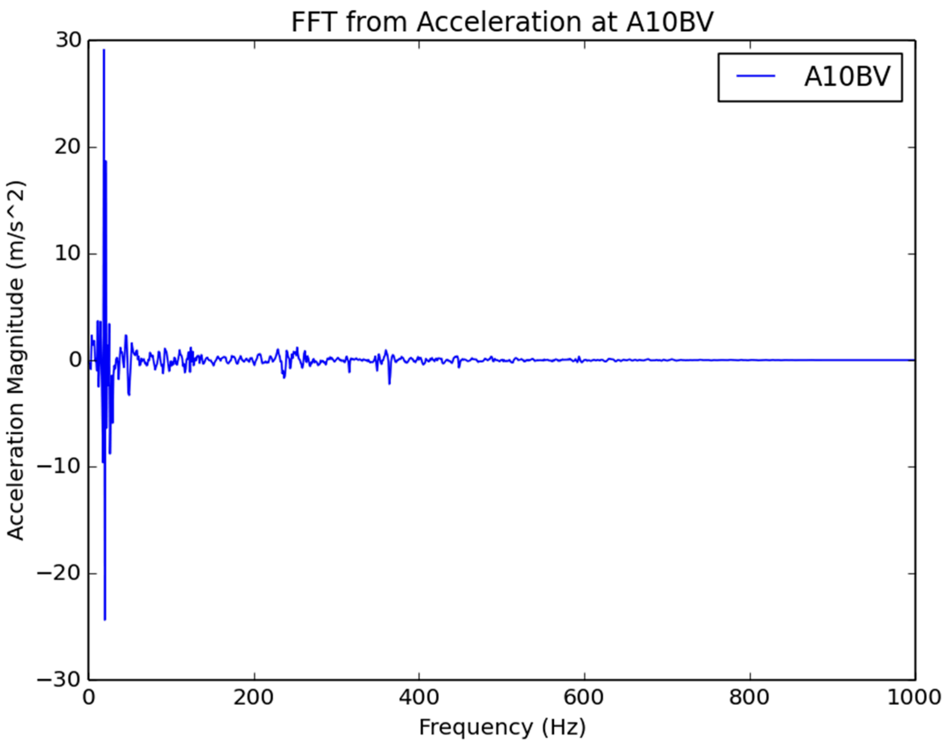

Figure 213: Fast Fourier Transform for A10BV

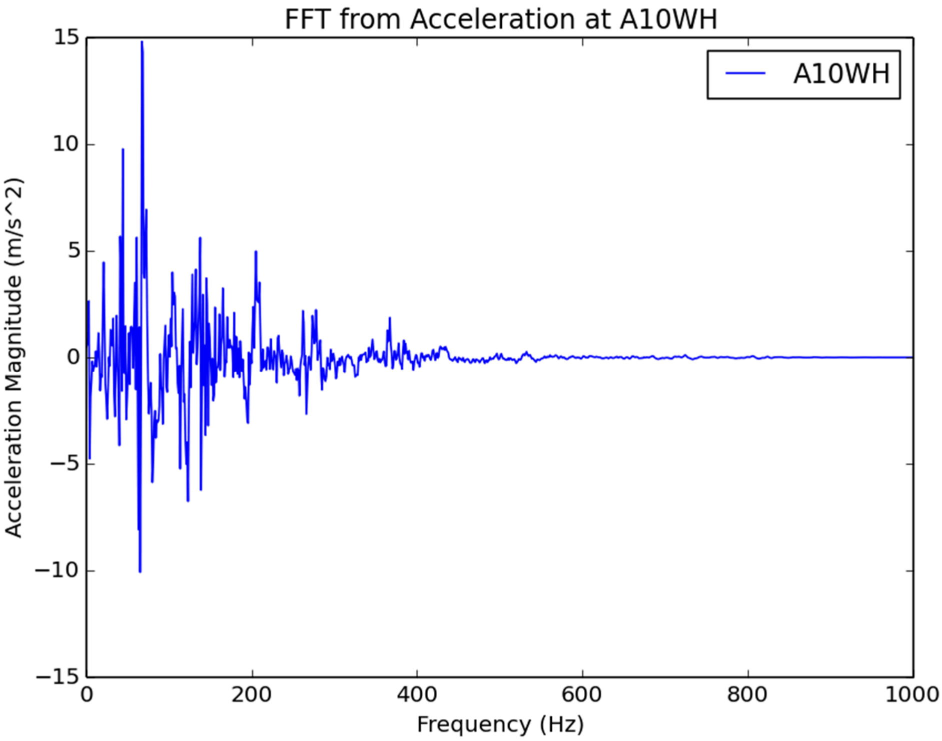

Figure 214: Fast Fourier Transform for A10WH

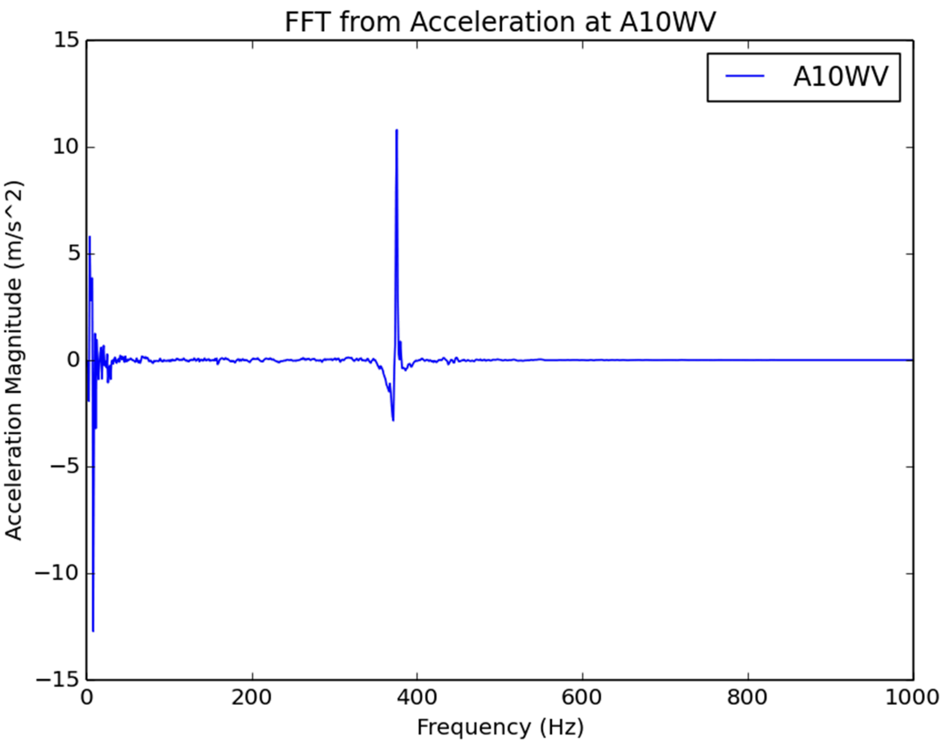

Figure 215: Fast Fourier Transform for A10WV

5.4 IRIS III Vc test conclusions

The 170 m/s missile penetrated the concrete face and caused permanent rebar plastic deformation. The missile may likely pass through the front face, though these simulation results predict rebound of the missile owing to the present non-rigorous treatment of material damage for the rebar elements. Damage accrued primarily on the front face and at corners in the concrete, including any corners where a steel plate was attached. There was a vast difference in behavior between the two pseudo-equipments in both oscillation frequency and amplitude; this could be due to the fact that the I-beam with a welded connection was 100 mm longer than the I-beam with a bolted connection, and the pseudo-equipment masses were both the same. However, there was a more definite similarity between the two I-beams in the 170 m/s simulation than the 90 m/s simulations. Figure 85 and Figure 146 show little similarities between the two I-beams, but Figure 207 shows some similarity most likely due to a more dominant vibration for the entire structure.